

SUPERCritical ADSORPTION TESTING OF POROUS
SILICON, ACTIVATED CARBON, AND ZEOLITE MATERIALS

BRENDAN HARVEY



**SUPERCritical ADSORPTION TESTING OF POROUS SILICON, ACTIVATED
CARBON, AND ZEOLITE MATERIALS**

by

© Brendan Harvey

A thesis submitted to the

School of Graduate Studies in partial fulfillment of the requirements for the degree

of

Master of Engineering (M.Eng.)

Faculty of Engineering and Applied Science

Memorial University of Newfoundland

March 2012

St. John's, Newfoundland

ABSTRACT

The supercritical adsorption of methane gas on porous silicon, activated carbon, and zeolite materials was studied. An apparatus that utilizes the volumetric adsorption measurement technique was designed and constructed to conduct the experiments. Activated carbon materials consisted of Norit RX3 Extra, Zorflex FM30K woven activated carbon cloth, and Zorflex FM10 knitted activated carbon cloth. Zeolite materials consisted of 3A, 4A, 5A, and 13X zeolites. Porous silicon materials consisted of stain etched and electrochemically etched porous films, and stain etched porous powder. All adsorption tests were conducted at room temperature (approximately 298 K) and pressures up to approximately 5 MPa. Overall, the Norit RX3 Extra granulated activated carbon produced the highest excess adsorption and effective storage capacities. Effective storage and delivery capacities of 109 and $90 \frac{\text{stp ml}}{\text{ml}}$ were obtained at a pressure of 3.5 MPa and a temperature of approximately 298 K.

ACKNOWLEDGEMENTS

The current thesis was made possible through the help and contributions of several individuals. Firstly, I would like to thank my supervisors Dr. Todd Andrews and Dr. John Shirokoff for giving me the opportunity to pursue this research endeavor. They have provided me with the academic, mentoring, financial, and overall general support that has enabled me to obtain this accreditation in a most enjoyable manner. I would like to thank my fellow porous silicon team members Jordan Peckham and Lance Parsons for also providing advice, knowledge, and support.

I would like to thank all of my family and friends for their support during this research undertaking. I would also like to give special thanks to my fiancée Celeste England for all of her patience, love, and support.

Technical support was provided by Gordon Whelan, Wayne Holly, and Rodger Guest who facilitated the fabrication and operation of the adsorption testing apparatus. I would also like to thank Dr. Maynard Clouter, Dr. Anand Yethiraj, Dr. Michael Morrow, and Pam King for allowing me to utilize the laboratory facilities required to conduct my research.

Financial support was provided by the Natural Sciences and Engineering Research Council of Canada (NSERC), the Research & Development Corporation of Newfoundland and Labrador (RDC), the Memorial University of Newfoundland Faculty of Engineering and Applied Science, Dr. John Shirokoff, and Dr. Todd Andrews.

Table of Contents

ABSTRACT	ii
ACKNOWLEDGEMENTS	iii
Table of Contents	iv
List of Tables	x
List of Figures	xxv
Abbreviations	xxxvi
Nomenclature	xxxvii
List of Appendices	xli
- 1 - Introduction	1-1
1.1 - Problem Statement	1-1
1.2 - Motivation for Study	1-2
1.3 - Objectives & Scope of Study	1-3
1.4 - Outline	1-3
- 2 - Literature Review	2-5
2.1 - Natural Gas	2-5
2.1.1 - Introduction	2-5
2.1.2 - Storage & Distribution Technologies	2-5
2.1.3 - Uses of Natural Gas	2-6
2.1.4 - Benefits of Using Natural Gas	2-8

2.2 - Adsorption.....	2-8
2.2.1 - Introduction.....	2-8
2.2.2 - History & General Applications.....	2-16
2.2.3 - Adsorption Studies.....	2-18
2.2.4 - Supercritical Adsorption Models.....	2-24
2.3 - Adsorbed Natural Gas.....	2-28
2.3.1 - Introduction.....	2-28
2.3.2 - Advantages of ANG.....	2-28
2.3.3 - Performance Evaluation.....	2-29
2.3.4 - Adsorbent Requirements.....	2-38
2.3.5 - Adsorbent Studies.....	2-44
2.3.6 - Applications & Economics.....	2-47
2.4 - Porous Silicon.....	2-50
2.4.1 - Introduction.....	2-50
2.4.2 - Material Classification.....	2-50
2.4.3 - Applications.....	2-51
- 3 - Experimental Procedures.....	3-53
3.1 - Apparatus.....	3-53
3.1.1 - Introduction.....	3-53
3.1.2 - Volumetric Technique.....	3-54
3.1.3 - Apparatus Description.....	3-55
3.1.4 - Design & Fabrication.....	3-58

3.1.5 - Operation	3-68
3.2 - Sample Adsorption Preparation	3-76
3.2.1 - Volume & Mass Measurements	3-76
3.2.2 - Degassing	3-78
3.2.3 - Sample Containment	3-79
3.2.4 - Dehydrating	3-79
3.3 - Adsorption Isotherm Calculation	3-80
3.3.1 - Introduction	3-80
3.3.2 - Equation of State	3-80
3.3.3 - Isotherm Calculation Methodology	3-83
3.3.4 - Isotherm Data Fitting	3-87
3.3.5 - Experimental Error & Uncertainty	3-89
3.4 - Sample Fabrication Methodology	3-99
3.4.1 - Electrochemical Etching	3-99
3.4.2 - Stain Etching	3-102
3.4.3 - Sample Analysis	3-105
- 4 - Results and Discussion	4-109
4.1 - Introduction	4-109
4.2 - Sample Production Studies	4-109
4.2.1 - Electrochemical Studies	4-110
4.2.2 - Stain Etching Studies	4-110
4.3 - Adsorption Testing	4-127

4.3.1 - Data Presentation.....	4-127
4.3.2 - Modified Isotherm Models	4-128
4.4 - Specific Surface Area Approximation Technique	4-130
4.5 - Adsorption Test Results & Analysis.....	4-132
4.5.1 - Introduction.....	4-132
4.5.2 - Porous Carbon.....	4-133
4.5.3 - Zeolites.....	4-185
4.5.4 - Silicates	4-234
4.5.5 - Porous Silicon.....	4-245
4.5.6 - All Materials.....	4-258
4.6 - Discussion & Literature Comparison.....	4-264
4.6.1 - General Discussion.....	4-264
4.6.2 - Literature Comparison	4-268
4.6.3 - Materials Comparison.....	4-289
- 5 - Conclusions & Recommendations	5-291
5.1 - Conclusions.....	5-291
5.1.1 - Porous Silicon Production.....	5-291
5.1.2 - Adsorption Results.....	5-291
5.1.3 - Summary of Contributions	5-292
5.1.4 - Final Remarks.....	5-293
5.2 - Recommendations	5-293
- 6 - Bibliography	6-295

- 7 - Appendix A1.....	7-311
7.1 - Helium Dead Space Volume Measurement.....	7-311
7.2 - Methane Excess Adsorption & Effective Storage.....	7-314
7.2.1 - Master control program.....	7-314
7.2.2 - Excess Adsorption Function.....	7-329
7.2.3 - Effective Storage Function.....	7-333
7.3 - Methane Excess Adsorption & Effective Storage Cycle.....	7-337
7.3.1 - Master control program.....	7-337
7.3.2 - Excess Desorption Function.....	7-350
7.3.3 - Effective Storage Discharge Function.....	7-353
- 8 - Appendix A2.....	8-358
8.1 - Adsorption Plots.....	8-358
8.1.1 - RX3.....	8-359
8.1.2 - FM30K.....	8-375
8.1.3 - FM10.....	8-389
8.1.4 - 3A Zeolite.....	8-404
8.1.5 - 4A Zeolite.....	8-419
8.1.6 - 5A Zeolite.....	8-426
8.1.7 - 13X Zeolite.....	8-441
8.1.8 - Silica Gel.....	8-456
8.2 - Porous Silicon.....	8-463
8.2.1 - PSIEC_Mix.....	8-463

8.2.2 - PSIEC_Mix_2.....	8-465
8.2.3 - PSIPW_3.....	8-469
8.2.4 - PSIPW_10.....	8-473
8.2.5 - PSIPW_14.....	8-480
8.2.6 - PSIPW_15.....	8-486
8.2.7 - Adsorption Isotherms.....	8-493

List of Tables

Table 2-1: Excess adsorption evaluation parameters.....	2-31
Table 2-2: Excess desorption evaluation parameters.....	2-32
Table 2-3: Excess adsorption effective delivery evaluation parameters.....	2-33
Table 2-4: Effective storage evaluation parameters.....	2-34
Table 2-5: Effective discharge evaluation parameters.....	2-35
Table 2-6: Effective storage effective delivery evaluation parameters.....	2-36
Table 2-7: Summary of the capabilities of various gas storage technologies compared to gasoline.....	2-49
Table 2-8: Pore size classification.....	2-51
Table 2-9: Porous silicon applications and properties.....	2-52
Table 3-1: Gas Properties.....	3-58
Table 3-2: Modified BWR equation of state coefficients.....	3-82
Table 3-3: Gas expansion error.....	3-92
Table 4-1: Electrochemical sample production summary. HF and [C ₂ H ₅ OH] are the pure volumetric percentages for the electrolyte components. I_p is the etching current density, t_{ech} is the total etching time, $P_{r,Opt.}$ is the sample porosity as obtained through optical techniques, and $P_{r,Eq.}$ is the sample porosity as obtained via equation 5-53.....	4-110

Table 4-2: Stain etching study #1 run summary. The electrolyte components are given as the pure volumetric percentage, t_{inc} is reaction incubation time (amount of that passes before the etching reaction starts once the silicon material is exposed to the etchant), and t_{ech} is the total etching reaction time after the incubation period has passed.....	4-113
Table 4-3: Table 4-3: Stain etching study #2 runs summary. $T_{f,Eq.}$ is the porous material layer thickness as obtained via equation 3-55, $P_{r,m}$ is the porous material porosity as obtained through gravimetric techniques (equation 3-50).....	4-115
Table 4-4: Stain etching study #3 runs summary.....	4-116
Table 4-5: Stain etching study #4 runs summary.....	4-117
Table 4-6: Stain etching study #5 runs summary ($T_{f,SEM}$ is the porous material layer thickness as approximated by the use of a SEM)	4-118
Table 4-7: Stain etching study #6 runs summary.....	4-120
Table 4-8: S Stain etching study #7 runs summary. d_p is the silicon particle diameter before etching, $\frac{V_{etch}}{V_{Si_{pw}}}$ is simply the volumetric ratio of etchant to silicon powder	4-122
Table 4-9: Stain etching study #8 runs summary. RXN Strength provides a relative indication of the vigorousness of the KOH etching reaction based on visual observation.....	4-123
Table 4-10: Stain etching study #9 runs summary.....	4-125
Table 4-11: Stain etching study #10 runs summary.....	4-126
Table 4-12: Comparison of specific surface area equation results for zeolites and silicates.....	4-132

Table 4-13: Comparison of specific surface area equation results for carbon materials.

..... 4-132

Table 4-14: Physical properties of activated carbon materials. A_{sm} is the specific surface area, A_{sv} is the available surface area per packed volume, ρ_b is the bulk material density (not packed), ρ_{pak} is the packed material density, m_s is the total sample mass, V_p is the sample packed volume, and ρ_{surf} is the cloth surface density (not packed)..... 4-134

Table 4-15: Norit RX3 Extra - Excess Adsorption Capacities (T \approx 298 K). $\rho_{n_a}^a$ is the excess molar adsorption density, $\rho_{v_a}^a$ is the excess volumetric adsorption density, $\rho_{m_a}^a$ is the excess mass adsorption density, $M_{n_a}^a$ is the excess specific molar adsorption capacity, $M_{v_a}^a$ is the excess specific volumetric adsorption capacity, and $M_{m_a}^a$ is the excess specific mass adsorption capacity..... 4-139

Table 4-16: Zorflex FM30K - Excess Adsorption Capacities (T \approx 298 K). $\rho_{n_a}^a$ is the excess molar adsorption density, $\rho_{v_a}^a$ is the excess volumetric adsorption density, $\rho_{m_a}^a$ is the excess mass adsorption density, $M_{n_a}^a$ is the excess specific molar adsorption capacity, $M_{v_a}^a$ is the excess specific volumetric adsorption capacity, and $M_{m_a}^a$ is the excess specific mass adsorption capacity..... 4-140

Table 4-17: Zorflex FM10 - Excess Adsorption Capacities (T \approx 298 K). $\rho_{n_a}^a$ is the excess molar adsorption density, $\rho_{v_a}^a$ is the excess volumetric adsorption density, $\rho_{m_a}^a$ is the excess mass adsorption density, $M_{n_a}^a$ is the excess specific molar adsorption capacity, $M_{v_a}^a$ is the excess specific volumetric adsorption capacity, and $M_{m_a}^a$ is the excess specific mass adsorption capacity..... 4-140

Table 4-18: Norit RX3 - Excess adsorption capacities during desorption process (T \approx 298 K). $\rho_{n_d}^a$ is the excess molar desorption density, $\rho_{v_d}^a$ is the excess volumetric

desorption density, $\rho_{m_d}^a$ is the excess mass desorption density, $M_{n_d}^a$ is the excess specific molar desorption capacity, $M_{v_d}^a$ is the excess specific volumetric desorption capacity, and $M_{m_d}^a$ is the excess specific mass desorption capacity..... 4-146

Table 4-19: Zorflex FM30K - Excess adsorption capacities during desorption process (T \approx 298 K). $\rho_{n_d}^a$ is the excess molar desorption density, $\rho_{v_d}^a$ is the excess volumetric desorption density, $\rho_{m_d}^a$ is the excess mass desorption density, $M_{n_d}^a$ is the excess specific molar desorption capacity, $M_{v_d}^a$ is the excess specific volumetric desorption capacity, and $M_{m_d}^a$ is the excess specific mass desorption capacity..... 4-146

Table 4-20: Zorflex FM10 - Excess adsorption capacities during desorption process (T \approx 298 K). $\rho_{n_d}^a$ is the excess molar desorption density, $\rho_{v_d}^a$ is the excess volumetric desorption density, $\rho_{m_d}^a$ is the excess mass desorption density, $M_{n_d}^a$ is the excess specific molar desorption capacity, $M_{v_d}^a$ is the excess specific volumetric desorption capacity, and $M_{m_d}^a$ is the excess specific mass desorption capacity..... 4-147

Table 4-21: Norit RX3 - Excess Adsorption - Effective Delivery Capacities (T \approx 298 K). $\rho_{n_e}^a$ is the excess molar delivery density, $\rho_{v_e}^a$ is the excess volumetric delivery density, $\rho_{m_e}^a$ is the excess mass delivery density, $M_{n_e}^a$ is the excess specific molar delivery capacity, $M_{v_e}^a$ is the excess specific volumetric delivery capacity, $M_{m_e}^a$ is the excess specific mass delivery capacity, and R^a is the excess adsorption gas retention.... 4-152

Table 4-22: Zorflex FM30K - Excess Adsorption - Effective Delivery Capacities (T \approx 298 K). $\rho_{n_e}^a$ is the excess molar delivery density, $\rho_{v_e}^a$ is the excess volumetric delivery density, $\rho_{m_e}^a$ is the excess mass delivery density, $M_{n_e}^a$ is the excess specific molar delivery capacity, $M_{v_e}^a$ is the excess specific volumetric delivery capacity, $M_{m_e}^a$ is the excess specific mass delivery capacity, and R^a is the excess adsorption gas retention..... 4-153

Table 4-23: Zorflex FM10 - Excess Adsorption - Effective Delivery Capacities (T ≈ 298 K). $\rho_{n_e}^a$ is the excess molar delivery density, $\rho_{v_e}^a$ is the excess volumetric delivery density, $\rho_{m_e}^a$ is the excess mass delivery density, $M_{n_e}^a$ is the excess specific molar delivery capacity, $M_{v_e}^a$ is the excess specific volumetric delivery capacity, $M_{m_e}^a$ is the excess specific mass delivery capacity, and R^a is the excess adsorption gas retention 4-153

Table 4-24: Norit RX3 - Effective Storage Capacities (T ≈ 298 K). $\rho_{n_a}^s$ is the effective molar storage density, $\rho_{v_a}^s$ is the effective volumetric storage density, $\rho_{m_a}^s$ is the effective mass storage density, $M_{n_a}^s$ effective specific molar storage capacity, $M_{v_a}^s$ is the effective specific volumetric storage capacity, and $M_{m_a}^s$ is the Effective specific mass storage capacity 4-159

Table 4-25: Zorflex FM30K - Effective Storage Capacities (T ≈ 298 K). $\rho_{n_a}^s$ is the effective molar storage density, $\rho_{v_a}^s$ is the effective volumetric storage density, $\rho_{m_a}^s$ is the effective mass storage density, $M_{n_a}^s$ effective specific molar storage capacity, $M_{v_a}^s$ is the effective specific volumetric storage capacity, and $M_{m_a}^s$ is the Effective specific mass storage capacity. 4-159

Table 4-26 : Zorflex FM10 - Effective Storage Capacities (T ≈ 298 K). $\rho_{n_a}^s$ is the effective molar storage density, $\rho_{v_a}^s$ is the effective volumetric storage density, $\rho_{m_a}^s$ is the effective mass storage density, $M_{n_a}^s$ effective specific molar storage capacity, $M_{v_a}^s$ is the effective specific volumetric storage capacity, and $M_{m_a}^s$ is the Effective specific mass storage capacity 4-160

Table 4-27: Norit RX3 - Effective storage capacities during desorption process (T ≈ 298 K). $\rho_{n_d}^s$ is the effective molar discharge density, $\rho_{v_d}^s$ is the effective volumetric discharge density, $\rho_{m_d}^s$ is the effective mass discharge density, $M_{n_d}^s$ is the effective

specific molar discharge capacity, $M_{V_d}^s$ is the effective specific volumetric discharge capacity, and $M_{m_d}^s$ is the effective specific mass discharge capacity 4-165

Table 4-28: Zorflex FM30K - Effective storage capacities during desorption process (T \approx 298 K). $\rho_{n_d}^s$ is the effective molar discharge density, $\rho_{V_d}^s$ is the effective volumetric discharge density, $\rho_{m_d}^s$ is the effective mass discharge density, $M_{n_d}^s$ is the effective specific molar discharge capacity, $M_{V_d}^s$ is the effective specific volumetric discharge capacity, and $M_{m_d}^s$ is the effective specific mass discharge capacity 4-166

Table 4-29 : Zorflex FM10 - Effective storage capacities during desorption process (T \approx 298 K). $\rho_{n_d}^s$ is the effective molar discharge density, $\rho_{V_d}^s$ is the effective volumetric discharge density, $\rho_{m_d}^s$ is the effective mass discharge density, $M_{n_d}^s$ is the effective specific molar discharge capacity, $M_{V_d}^s$ is the effective specific volumetric discharge capacity, and $M_{m_d}^s$ is the effective specific mass discharge capacity 4-166

Table 4-30: Norit RX3 – Effective Storage - Effective Delivery Capacities (T \approx 298 K). $\rho_{n_e}^s$ is the effective molar delivery density, $\rho_{V_e}^s$ is the effective volumetric delivery density, $\rho_{m_e}^s$ is the effective mass delivery density, $M_{n_e}^s$ is the effective specific molar delivery capacity, $M_{V_e}^s$ is the effective specific volumetric delivery capacity, $M_{m_e}^s$ is the effective specific mass delivery capacity, and R^s is the effective adsorption gas retention..... 4-172

Table 4-31: Zorflex FM30K - Effective Storage - Effective Delivery Capacities (T \approx 298 K). $\rho_{n_e}^s$ is the effective molar delivery density, $\rho_{V_e}^s$ is the effective volumetric delivery density, $\rho_{m_e}^s$ is the effective mass delivery density, $M_{n_e}^s$ is the effective specific molar delivery capacity, $M_{V_e}^s$ is the effective specific volumetric delivery capacity, $M_{m_e}^s$ is the effective specific mass delivery capacity, and R^s is the effective adsorption gas retention..... 4-172

Table 4-32 : Zorflex FM10 - Effective Storage - Effective Delivery Capacities (T ≈ 298 K). $\rho_{n_e}^s$ is the effective molar delivery density, $\rho_{V_e}^s$ is the effective volumetric delivery density, $\rho_{m_e}^s$ is the effective mass delivery density, $M_{n_e}^s$ is the effective specific molar delivery capacity, $M_{V_e}^s$ is the effective specific volumetric delivery capacity, $M_{m_e}^s$ is the effective specific mass delivery capacity, and R^s is the effective adsorption gas retention.....	4-173
Table 4-33: Bulk compression component fraction for effective storage of activated carbons.	4-176
Table 4-34: Excess adsorption model isotherm parameter values and fit statistics.....	4-179
Table 4-35: Excess adsorption model isotherm parameter values and fit statistics.....	4-179
Table 4-36: Excess adsorption model isotherm parameter values and fit statistics.....	4-179
Table 4-37: Excess adsorption model isotherm parameter values and fit statistics.....	4-183
Table 4-38: Effective storage model isotherm parameter values and fit statistics.	4-184
Table 4-39: Effective storage model isotherm parameter values and fit statistics.	4-184
Table 4-40: Zeolite materials classification and supplier.	4-185
Table 4-41: Physical properties of zeolite materials. A_{sm} is the specific surface area, A_{sv} is the available surface area per packed volume, ρ_k is the bulk material density (not packed), ρ_{pak} is the packed material density, m_s is the total sample mass, V_p is the sample packed volume, and D_{pore} is the average material pore diameter.....	4-186

Table 4-42: 4A Zeolite - Excess Adsorption Capacities (T ≈ 298 K). $\rho_{n_a}^a$ is the excess molar adsorption density, $\rho_{V_a}^a$ is the excess volumetric adsorption density, $\rho_{m_a}^a$ is the excess mass adsorption density, $M_{n_a}^a$ is the excess specific molar adsorption capacity, $M_{V_a}^a$ is the excess specific volumetric adsorption capacity, and $M_{m_a}^a$ is the excess specific mass adsorption capacity..... 4-194

Table 4-43: 5A Zeolite - Excess Adsorption Capacities (T ≈ 298 K). $\rho_{n_a}^a$ is the excess molar adsorption density, $\rho_{V_a}^a$ is the excess volumetric adsorption density, $\rho_{m_a}^a$ is the excess mass adsorption density, $M_{n_a}^a$ is the excess specific molar adsorption capacity, $M_{V_a}^a$ is the excess specific volumetric adsorption capacity, and $M_{m_a}^a$ is the excess specific mass adsorption capacity..... 4-195

Table 4-44: 13X Zeolite - Excess Adsorption Capacities (T ≈ 298 K). $\rho_{n_a}^a$ is the excess molar adsorption density, $\rho_{V_a}^a$ is the excess volumetric adsorption density, $\rho_{m_a}^a$ is the excess mass adsorption density, $M_{n_a}^a$ is the excess specific molar adsorption capacity, $M_{V_a}^a$ is the excess specific volumetric adsorption capacity, and $M_{m_a}^a$ is the excess specific mass adsorption capacity..... 4-195

Table 4-45: 5A Zeolite - Excess adsorption capacities during desorption process (T ≈ 298 K). $\rho_{n_d}^a$ is the excess molar desorption density, $\rho_{V_d}^a$ is the excess volumetric desorption density, $\rho_{m_d}^a$ is the excess mass desorption density, $M_{n_d}^a$ is the excess specific molar desorption capacity, $M_{V_d}^a$ is the excess specific volumetric desorption capacity, and $M_{m_d}^a$ is the excess specific mass desorption capacity..... 4-199

Table 4-46: 13X Zeolite - Excess adsorption capacities during desorption process (T ≈ 298 K). $\rho_{n_d}^a$ is the excess molar desorption density, $\rho_{V_d}^a$ is the excess volumetric desorption density, $\rho_{m_d}^a$ is the excess mass desorption density, $M_{n_d}^a$ is the excess

specific molar desorption capacity, $M_{V_d}^a$ is the excess specific volumetric desorption capacity, and $M_{m_d}^a$ is the excess specific mass desorption capacity..... 4-200

Table 4-47: 5A Zeolite - Excess Adsorption - Effective Delivery Capacities (T \approx 298 K). $\rho_{n_e}^a$ is the excess molar delivery density, $\rho_{V_e}^a$ is the excess volumetric delivery density, $\rho_{m_e}^a$ is the excess mass delivery density, $M_{n_e}^a$ is the excess specific molar delivery capacity, $M_{V_e}^a$ is the excess specific volumetric delivery capacity, $M_{m_e}^a$ is the excess specific mass delivery capacity, and R^a is the excess adsorption gas retention..... 4-204

Table 4-48: 13X Zeolite - Excess Adsorption - Effective Delivery Capacities (T \approx 298 K). $\rho_{n_e}^a$ is the excess molar delivery density, $\rho_{V_e}^a$ is the excess volumetric delivery density, $\rho_{m_e}^a$ is the excess mass delivery density, $M_{n_e}^a$ is the excess specific molar delivery capacity, $M_{V_e}^a$ is the excess specific volumetric delivery capacity, $M_{m_e}^a$ is the excess specific mass delivery capacity, and R^a is the excess adsorption gas retention 4-204

Table 4-49: 4A Zeolite - Effective Storage Capacities (T \approx 298 K). $\rho_{n_a}^s$ is the effective molar storage density, $\rho_{V_a}^s$ is the effective volumetric storage density, $\rho_{m_a}^s$ is the effective mass storage density, $M_{n_a}^s$ effective specific molar storage capacity, $M_{V_a}^s$ is the effective specific volumetric storage capacity, and $M_{m_a}^s$ is the effective specific mass storage capacity 4-212

Table 4-50: 5A Zeolite - Effective Storage Capacities (T \approx 298 K). $\rho_{n_a}^s$ is the effective molar storage density, $\rho_{V_a}^s$ is the effective volumetric storage density, $\rho_{m_a}^s$ is the effective mass storage density, $M_{n_a}^s$ effective specific molar storage capacity, $M_{V_a}^s$ is the effective specific volumetric storage capacity, and $M_{m_a}^s$ is the effective specific mass storage capacity 4-212

Table 4-51: 13X Zeolite - Effective Storage Capacities ($T \approx 298$ K). $\rho_{n_a}^s$ is the effective molar storage density, $\rho_{v_a}^s$ is the effective volumetric storage density, $\rho_{m_a}^s$ is the effective mass storage density, $M_{n_a}^s$ effective specific molar storage capacity, $M_{v_a}^s$ is the effective specific volumetric storage capacity, and $M_{m_a}^s$ is the effective specific mass storage capacity 4-213

Table 4-52: 5A Zeolite - Effective storage capacities during desorption process ($T \approx 298$ K). $\rho_{n_d}^s$ is the effective molar discharge density, $\rho_{v_d}^s$ is the effective volumetric discharge density, $\rho_{m_d}^s$ is the effective mass discharge density, $M_{n_d}^s$ is the effective specific molar discharge capacity, $M_{v_d}^s$ is the effective specific volumetric discharge capacity, and $M_{m_d}^s$ is the effective specific mass discharge capacity 4-217

Table 4-53: 13X Zeolite - Effective storage capacities during desorption process ($T \approx 298$ K). $\rho_{n_d}^s$ is the effective molar discharge density, $\rho_{v_d}^s$ is the effective volumetric discharge density, $\rho_{m_d}^s$ is the effective mass discharge density, $M_{n_d}^s$ is the effective specific molar discharge capacity, $M_{v_d}^s$ is the effective specific volumetric discharge capacity, and $M_{m_d}^s$ is the effective specific mass discharge capacity 4-217

Table 4-54: 5A Zeolite - Effective Storage - Effective Delivery Capacities ($T \approx 298$ K). $\rho_{n_e}^s$ is the effective molar delivery density, $\rho_{v_e}^s$ is the effective volumetric delivery density, $\rho_{m_e}^s$ is the effective mass delivery density, $M_{n_e}^s$ is the effective specific molar delivery capacity, $M_{v_e}^s$ is the effective specific volumetric delivery capacity, $M_{m_e}^s$ is the effective specific mass delivery capacity, and R^s is the effective adsorption gas retention 4-221

Table 4-55: 13X Zeolite - Effective Storage - Effective Delivery Capacities ($T \approx 298$ K). $\rho_{n_e}^s$ is the effective molar delivery density, $\rho_{v_e}^s$ is the effective volumetric delivery density, $\rho_{m_e}^s$ is the effective mass delivery density, $M_{n_e}^s$ is the effective specific molar delivery capacity, $M_{v_e}^s$ is the effective specific volumetric delivery capacity, $M_{m_e}^s$ is the

effective specific mass delivery capacity, and R^S is the effective adsorption gas retention.....	4-222
Table 4-56: Bulk compression component fraction for effective storage of zeolites....	4-225
Table 4-57: Excess adsorption model isotherm parameter values and fit statistics.....	4-228
Table 4-58: Excess adsorption model isotherm parameter values and fit statistics.....	4-228
Table 4-59: Excess adsorption model isotherm parameter values and fit statistics.....	4-228
Table 4-60: Effective storage model isotherm parameter values and fit statistics.	4-232
Table 4-61: Effective storage model isotherm parameter values and fit statistics.	4-233
Table 4-62: Effective storage model isotherm parameter values and fit statistics.	4-233
Table 4-63: Physical Properties - Silica Gel. A_{sm} is the specific surface area, A_{sv} is the available surface area per packed volume, ρ_b is the bulk material density (not packed), ρ_{pak} is the packed material density, m_s is the total sample mass, and V_p is the sample packed volume.....	4-235
Table 4-64: Silica Gel - Excess Adsorption Capacities (T \approx 298 K). $\rho_{n_a}^a$ is the excess molar adsorption density, $\rho_{V_a}^a$ is the excess volumetric adsorption density, $\rho_{m_a}^a$ is the excess mass adsorption density, $M_{n_a}^a$ is the excess specific molar adsorption capacity, $M_{V_a}^a$ is the excess specific volumetric adsorption capacity, and $M_{m_a}^a$ is the excess specific mass adsorption capacity.....	4-237

Table 4-65: Silica Gel - Effective Storage Capacities (T \approx 298 K). $\rho_{n_a}^s$ is the effective molar storage density, $\rho_{V_a}^s$ is the effective volumetric storage density, $\rho_{m_a}^s$ is the effective mass storage density, $M_{n_a}^s$ effective specific molar storage capacity, $M_{V_a}^s$ is the effective specific volumetric storage capacity, and $M_{m_a}^s$ is the Effective specific mass storage capacity 4-240

Table 4-66: Excess adsorption model isotherm parameter values and fit statistics..... 4-242

Table 4-67: Effective storage model isotherm parameter values and fit statistics.4-244

Table 4-68: Physical properties of porous silicon powder samples. m_s is the sample mass, d_p is the average particle size, V_p is the sample packed volume, ρ_{pak} is the sample packing density, and V_d is the sample dead space volume 4-249

Table 4-69: Bulk compression component fraction for effective storage of zeolites.... 4-257

Table 4-70: Excess adsorption capacity summary for carbon materials (CH₄ - P = 3.5MPa - T \approx 298K). A_{sp} is the specific surface area, CH₄ is the absolute excess molar adsorption capacity, $\rho_{n_a}^a$ is the excess molar adsorption density, $\rho_{V_a}^a$ is the excess volumetric adsorption density, $\rho_{m_a}^a$ is the excess mass adsorption density, $M_{n_a}^a$ is the excess specific molar adsorption capacity, $M_{V_a}^a$ is the excess specific volumetric adsorption capacity, $M_{m_a}^a$ is the excess specific mass adsorption capacity, n_e^a is the absolute excess molar delivery capacity, $\rho_{n_e}^a$ is the excess molar delivery density, $\rho_{V_e}^a$ is the excess volumetric delivery density, $\rho_{m_e}^a$ is the excess mass delivery density, $M_{n_e}^a$ is the excess specific molar delivery capacity, $M_{V_e}^a$ is the excess specific volumetric delivery capacity, $M_{m_e}^a$ is the excess specific mass delivery capacity, and R^a is the excess adsorption gas retention 4-269

Table 4-71: Excess adsorption values for materials similar to the Norit RX3 Extra found in the literature. A_{sp} is the specific surface area, $M_{n_a}^a$ is the excess specific molar adsorption capacity, and $M_{m_a}^a$ is the excess specific mass adsorption capacity..... 4-270

Table 4-72: Excess adsorption values for materials similar to the Zorflex FM30K & FM10 found in the literature. A_{sp} is the specific surface area, $M_{n_a}^a$ is the excess specific molar adsorption capacity, and $M_{m_a}^a$ is the excess specific mass adsorption capacity..... 4-271

Table 4-73: Additional carbon material excess adsorption results. A_{sp} is the specific surface area, $M_{n_a}^a$ is the excess specific molar adsorption capacity, and $M_{m_a}^a$ is the excess specific mass adsorption capacity..... 4-272

Table 4-74: Effective storage capacity summary for carbon materials ($CH_4 - P = 3.5MPa - T \approx 298K$). n_a^s is the absolute effective molar storage capacity, $\rho_{n_a}^s$ is the effective molar storage density, $\rho_{V_a}^s$ is the effective volumetric storage density, $\rho_{m_a}^s$ is the effective mass storage density, $M_{n_a}^s$ effective specific molar storage capacity, $M_{V_a}^s$ is the effective specific volumetric storage capacity, $M_{m_a}^s$ is the effective specific mass storage capacity. n_e^s is the absolute effective molar delivery capacity, $\rho_{n_e}^s$ is the effective molar delivery density, $\rho_{V_e}^s$ is the effective volumetric delivery density, $\rho_{m_e}^s$ is the effective mass delivery density, $M_{n_e}^s$ is the effective specific molar delivery capacity, $M_{V_e}^s$ is the effective specific volumetric delivery capacity, $M_{m_e}^s$ is the effective specific mass delivery capacity, and R^s is the effective storage gas retention..... 4-276

Table 4-75: Effective storage values for materials similar to the Norit RX3 Extra found in the literature. A_{sp} is the specific surface area, $\rho_{V_a}^s$ is the effective volumetric storage density, $\rho_{V_e}^s$ is the effective volumetric delivery density, $M_{n_a}^s$ is the effective specific mass storage capacity, and R^s is the effective storage gas retention..... 4-277

Table 4-76: Effective storage values for materials similar to the Zorflex FM30K & FM10 found in the literature. A_{sp} is the specific surface area, $\rho_{V_a}^s$ is the effective volumetric storage density, $\rho_{V_e}^s$ is the effective volumetric delivery density, $M_{m_a}^s$ is the effective specific mass storage capacity, and R^s is the effective storage gas retention..... 4-278

Table 4-77: Additional carbon material excess adsorption results. A_{sp} is the specific surface area, $\rho_{V_a}^s$ is the effective volumetric storage density, $\rho_{V_e}^s$ is the effective volumetric delivery density, $M_{m_a}^s$ is the effective specific mass storage capacity, and R^s is the effective storage gas retention..... 4-279

Table 4-78: Excess adsorption capacity summary for zeolite materials ($CH_4 - P = 3.5MPa - T \approx 298K$). A_{sp} is the specific surface area, n_a^a is the absolute excess molar adsorption capacity, $\rho_{n_a}^a$ is the excess molar adsorption density, $\rho_{V_a}^a$ is the excess volumetric adsorption density, $\rho_{m_a}^a$ is the excess mass adsorption density, $M_{n_a}^a$ is the excess specific molar adsorption capacity, $M_{V_a}^a$ is the excess specific volumetric adsorption capacity, $M_{m_a}^a$ is the excess specific mass adsorption capacity, n_e^a is the absolute excess molar delivery capacity, $\rho_{n_e}^a$ is the excess molar delivery density, $\rho_{V_e}^a$ is the excess volumetric delivery density, $\rho_{m_e}^a$ is the excess mass delivery density, $M_{n_e}^a$ is the excess specific molar delivery capacity, $M_{V_e}^a$ is the excess specific volumetric delivery capacity, $M_{m_e}^a$ is the excess specific mass delivery capacity, and R^a is the excess adsorption gas retention 4-282

Table 4-79: Excess adsorption values for zeolite materials found in the literature. A_{sp} is the specific surface area, $M_{n_a}^a$ is the excess specific molar adsorption capacity, and $M_{m_a}^a$ is the excess specific mass adsorption capacity 4-283

Table 4-80: Effective storage capacity summary for zeolite materials ($CH_4 - P = 3.5MPa - T \approx 298K$). n_a^s is the absolute effective molar storage capacity, $\rho_{n_a}^s$ is the

effective molar storage density, $\rho_{V_a}^s$ is the effective volumetric storage density, $\rho_{m_a}^s$ is the effective mass storage density, $M_{n_a}^s$ effective specific molar storage capacity, $M_{V_a}^s$ is the effective specific volumetric storage capacity, $M_{m_a}^s$ is the effective specific mass storage capacity. n_e^s is the absolute effective molar delivery capacity, $\rho_{n_e}^s$ is the effective molar delivery density, $\rho_{V_e}^s$ is the Effective volumetric delivery density, $\rho_{m_e}^s$ is the effective mass delivery density, $M_{n_e}^s$ is the effective specific molar delivery capacity, $M_{V_e}^s$ is the effective specific volumetric delivery capacity, $M_{m_e}^s$ is the effective specific mass delivery capacity, and R^s is the effective storage gas retention..... 4-285

Table 4-81: Effective storage values for zeolite materials found in the literature. A_{sp} is the specific surface area, and $\rho_{V_a}^s$ is the effective volumetric storage density..... 4-286

Table 4-82: Summary of excess adsorption and storage capacity for silica gel (CH_4 - P = 3.5MPa - T \approx 298K). A_{sp} is the specific surface area, n_a^a is the absolute excess molar adsorption capacity, $\rho_{n_a}^a$ is the excess molar adsorption density, $\rho_{V_a}^a$ is the excess volumetric adsorption density, $\rho_{m_a}^a$ is the excess mass adsorption density, $M_{n_a}^a$ is the excess specific molar adsorption capacity, $M_{V_a}^a$ is the excess specific volumetric adsorption capacity, $M_{m_a}^a$ is the excess specific mass adsorption capacity, $\rho_{n_a}^s$ is the effective molar storage density, $\rho_{V_a}^s$ is the effective volumetric storage density, $\rho_{m_a}^s$ is the effective mass storage density, $M_{n_a}^s$ effective specific molar storage capacity, $M_{V_a}^s$ is the effective specific volumetric storage capacity, $M_{m_a}^s$ is the effective specific mass storage capacity, and R^s is the effective storage gas retention. 4-287

Table 4-83: Excess adsorption values for various silica gel materials found in the literature. A_{sp} is the specific surface area, $M_{n_a}^a$ is the excess specific molar adsorption capacity, and $M_{m_a}^a$ is the excess specific mass adsorption capacity..... 4-288

List of Figures

Figure 2-1: Pictorial illustration of adsorption terms.....	2-10
Figure 2-2: Absolute & excess adsorption phase identification.....	2-14
Figure 2-3: Excess adsorption isotherms with and without maxima.....	2-20
Figure 2-4: Isotherms depicting gas retention properties of two adsorbents.....	2-40
Figure 3-1: Apparatus Schematic.....	3-56
Figure 3-2: Volumetric adsorption setup.....	3-63
Figure 3-3: Isometric drawing of supply vessel.....	3-66
Figure 3-4: Isometric drawing of sample vessel.....	3-67
Figure 3-5: Finite Element Analysis of supply & sample vessels.....	3-68
Figure 3-6: Apparatus sectional identification schematic.....	3-69
Figure 3-7: Sample vessel volume values obtained via gas expansion.....	3-71
Figure 3-8: Adjusted sample vessel volume values obtained via gas expansion.....	3-71
Figure 3-9: Supply vessel steady state error.....	3-94
Figure 3-10: Sample vessel steady state error.....	3-94
Figure 3-11: Gas expansion process error.....	3-95
Figure 3-12: Wave transit illustration.....	3-96
Figure 3-13: Temperature control pressure error.....	3-98
Figure 3-14: Temperature control temperature error.....	3-98

Figure 3-15: Disassembled electrochemical etching cell	3-101
Figure 3-16: Assembled electrochemical etching cell.....	3-101
Figure 3-17: Cross-sectional SEM of stain etched wafer.	3-108
Figure 4-1: Stain etched sample viewed under ultraviolet light.....	4-119
Figure 4-2: Stain etched film curvature.	4-121
Figure 4-3: SEM of stain etched sample with curvature.....	4-121
Figure 4-4: Pictorial representation of superimposing absolute adsorption and bulk gas compression to obtain effective storage.....	4-129
Figure 4-5: Specific surface area and specific moles adsorbed at 3.5 MPa and 298 K for various adsorbent materials found in the literature.	4-131
Figure 4-6: Norit RX3 - Excess Volumetric Adsorption Capacity.....	4-135
Figure 4-7: Norit RX3 - Specific Excess Molar Adsorption Capacity.....	4-135
Figure 4-8: Norit RX3 - Specific Excess Mass Adsorption Capacity.....	4-136
Figure 4-9: Zorflex FM30K - Excess Volumetric Adsorption Capacity.....	4-136
Figure 4-10: Zorflex FM30K - Specific Excess Molar Adsorption Capacity.	4-137
Figure 4-11: Zorflex FM30K - Specific Excess Mass Adsorption Capacity.....	4-137
Figure 4-12: Zorflex FM10 - Excess Volumetric Adsorption Capacity.....	4-138
Figure 4-13: Zorflex FM10 - Specific Excess Molar Adsorption Capacity.	4-138
Figure 4-14: Zorflex FM10 - Specific Excess Mass Adsorption Capacity.....	4-139

Figure 4-15: Norit RX3 - Excess Volumetric Adsorption/Desorption Cycle.....	4-141
Figure 4-16: Norit RX3 - Specific Excess Molar Adsorption/Desorption Cycle.....	4-142
Figure 4-17: Norit RX3 - Specific Excess Mass Adsorption/Desorption Cycle.	4-142
Figure 4-18: Zorflex FM30K - Excess Volumetric Adsorption/Desorption Cycle...	4-143
Figure 4-19: Zorflex FM30K - Specific Excess Molar Adsorption/Desorption Cycle.....	4-143
Figure 4-20: Zorflex FM30K - Specific Excess Mass Adsorption/Desorption Cycle.	4-144
Figure 4-21: Zorflex FM10 - Excess Volumetric Adsorption/Desorption Cycle.....	4-144
Figure 4-22: Zorflex FM10 - Specific Excess Molar Adsorption/Desorption Cycle.	4-145
Figure 4-23: Zorflex FM10 - Specific Excess Mass Adsorption/Desorption Cycle.	4-145
Figure 4-24: Norit RX3 - Excess Volumetric Delivery Capacity.	4-148
Figure 4-25: Norit RX3 - Specific Excess Molar Delivery Capacity.....	4-148
Figure 4-26: Norit RX3 - Specific Excess Mass Delivery Capacity.....	4-149
Figure 4-27: Zorflex FM30K - Specific Excess Molar Delivery Capacity.....	4-149
Figure 4-28: Zorflex FM30K - Specific Excess Mass Delivery Capacity.....	4-150
Figure 4-29: Zorflex FM30K - Excess Volumetric Delivery Capacity.....	4-150
Figure 4-30: Zorflex FM10 - Excess Volumetric Delivery Capacity.....	4-151
Figure 4-31: Zorflex FM10 - Specific Excess Molar Delivery Capacity.....	4-151

Figure 4-32: Zorflex FM10 - Specific Excess Mass Delivery Capacity.....	4-152
Figure 4-33: Norit RX3 - Effective Volumetric Storage Capacity.....	4-154
Figure 4-34: Norit RX3 – Specific Effective Molar Storage Capacity.....	4-155
Figure 4-35: Norit RX3 – Specific Effective Mass Storage Capacity.	4-155
Figure 4-36: Zorflex FM30K – Specific Effective Molar Storage Capacity.....	4-156
Figure 4-37: Zorflex FM30K – Specific Effective Mass Storage Capacity.	4-156
Figure 4-38: Zorflex FM30K - Effective Volumetric Storage Capacity.....	4-157
Figure 4-39: Zorflex FM10 - Effective Volumetric Storage Capacity.	4-157
Figure 4-40: Zorflex FM10 – Specific Effective Molar Storage Capacity.....	4-158
Figure 4-41: Zorflex FM10 – Specific Effective Mass Storage Capacity.	4-158
Figure 4-42: Norit RX3 - Effective Volumetric Storage Charge/Discharge Cycle. ...	4-161
Figure 4-43: Norit RX3 - Specific Effective Molar Charge/Discharge Cycle.....	4-161
Figure 4-44: Norit RX3 - Specific Effective Mass Charge/Discharge Cycle.....	4-162
Figure 4-45: Zorflex FM30K - Effective Volumetric Storage Charge/Discharge Cycle. 4-162	
Figure 4-46: Zorflex FM30K - Specific Effective Molar Charge/Discharge Cycle....	4-163
Figure 4-47: Zorflex FM30K - Specific Effective Mass Charge/Discharge Cycle.	4-163
Figure 4-48: Zorflex FM10 - Effective Volumetric Storage Charge/Discharge Cycle. ...	4-164

Figure 4-49: Zorflex FM10 - Specific Effective Molar Charge/Discharge Cycle.....	4-164
Figure 4-50: Zorflex FM10 - Specific Effective Mass Charge/Discharge Cycle.	4-165
Figure 4-51: Norit RX3 - Effective Volumetric Delivery Capacity.....	4-167
Figure 4-52: Norit RX3 - Specific Effective Molar Delivery Capacity.....	4-168
Figure 4-53: Norit RX3 - Specific Effective Mass Delivery Capacity.....	4-168
Figure 4-54: Zorflex FM30K - Effective Volumetric Delivery Capacity.....	4-169
Figure 4-55: Zorflex FM30K - Specific Effective Molar Delivery Capacity.....	4-169
Figure 4-56: Zorflex FM30K - Specific Effective Mass Delivery Capacity.	4-170
Figure 4-57: Zorflex FM10 - Effective Volumetric Delivery Capacity.....	4-170
Figure 4-58: Zorflex FM10 - Specific Effective Molar Delivery Capacity.....	4-171
Figure 4-59: Zorflex FM10 - Specific Effective Mass Delivery Capacity.	4-171
Figure 4-60: Norit RX3 - Absolute excess adsorption isotherm model fits.....	4-177
Figure 4-61: Zorflex FM30K - Absolute excess adsorption isotherm model fits....	4-178
Figure 4-62: Zorflex FM10 - Absolute excess adsorption isotherm model fits.....	4-178
Figure 4-63: Norit RX3 - Absolute effective storage isotherm model fits.....	4-180
Figure 4-64: Norit RX3 - Absolute effective storage modified isotherm model fits.....	4-181
Figure 4-65: Zorflex FM30K - Absolute effective storage isotherm model fits.....	4-181

Figure 4-66: Zorflex FM30K - Absolute effective storage modified isotherm model fits.	4-182
Figure 4-67: Zorflex FM10 - Absolute effective storage isotherm model fits.....	4-182
Figure 4-68: Zorflex FM10 - Absolute effective storage modified isotherm model fits.	4-183
Figure 4-69: 3A Zeolite - Absolute Excess Molar Adsorption Capacity.	4-188
Figure 4-70: 3A Zeolite - Specific Excess Molar Adsorption Capacity.....	4-188
Figure 4-71: 3A Zeolite - Absolute Excess Molar Adsorption Capacity (N ₂).....	4-189
Figure 4-72: 3A Zeolite - Specific Excess Molar Adsorption Capacity (N ₂).....	4-189
Figure 4-73: 4A Zeolite - Excess Volumetric Adsorption Capacity.....	4-190
Figure 4-74: 4A Zeolite - Specific Excess Molar Adsorption Capacity.....	4-190
Figure 4-75: 4A Zeolite - Specific Excess Mass Adsorption Capacity.....	4-191
Figure 4-76: 5A Zeolite - Excess Volumetric Adsorption Capacity.....	4-191
Figure 4-77: 5A Zeolite - Specific Excess Molar Adsorption Capacity.....	4-192
Figure 4-78: 5A Zeolite - Specific Excess Mass Adsorption Capacity.....	4-192
Figure 4-79: 13X Zeolite - Excess Volumetric Adsorption Capacity.	4-193
Figure 4-80: 13X Zeolite - Specific Excess Molar Adsorption Capacity.....	4-193
Figure 4-81: 13X Zeolite - Specific Excess Mass Adsorption Capacity.....	4-194
Figure 4-82: 5A Zeolite - Excess Volumetric Adsorption/Desorption Cycle.	4-196

Figure 4-83: 5A Zeolite - Specific Excess Molar Adsorption/Desorption Cycle.....	4-197
Figure 4-84: 5A Zeolite - Specific Excess Mass Adsorption/Desorption Cycle.....	4-197
Figure 4-85: 13X Zeolite - Excess Volumetric Adsorption/Desorption Cycle.....	4-198
Figure 4-86: 13X Zeolite - Specific Excess Molar Adsorption/Desorption Cycle....	4-198
Figure 4-87: 13X Zeolite - Specific Excess Mass Adsorption/Desorption Cycle.....	4-199
Figure 4-88: 5A Zeolite - Excess Volumetric Delivery Capacity.	4-201
Figure 4-89: 5A Zeolite - Specific Excess Molar Delivery Capacity.	4-201
Figure 4-90: 5A Zeolite - Specific Excess Mass Delivery Capacity.....	4-202
Figure 4-91: 13X Zeolite - Specific Excess Molar Delivery Capacity.....	4-202
Figure 4-92: 13X Zeolite - Specific Excess Mass Delivery Capacity.....	4-203
Figure 4-93: 13X Zeolite - Excess Volumetric Delivery Capacity.....	4-203
Figure 4-94: 3A Zeolite - Effective Volumetric Storage Capacity.....	4-205
Figure 4-95: 3A Zeolite - Specific Effective Molar Storage Capacity.....	4-206
Figure 4-96: 3A Zeolite - Effective Volumetric Storage Capacity (N ₂).....	4-206
Figure 4-97: 3A Zeolite - Specific Effective Molar Charge/Discharge Cycle (N ₂)...	4-207
Figure 4-98: 4A Zeolite - Specific Effective Mass Storage Capacity.....	4-207
Figure 4-99: 4A Zeolite - Effective Volumetric Storage Capacity.....	4-208
Figure 4-100: 4A Zeolite - Specific Effective Molar Storage Capacity.....	4-208
Figure 4-101: 5A Zeolite - Effective Volumetric Storage Capacity.	4-209

Figure 4-102: 5A Zeolite – Specific Effective Molar Storage Capacity.....	4-209
Figure 4-103: 5A Zeolite – Specific Effective Mass Storage Capacity.	4-210
Figure 4-104: 13X Zeolite - Effective Volumetric Storage Capacity.	4-210
Figure 4-105: 13X Zeolite – Specific Effective Molar Storage Capacity.	4-211
Figure 4-106: 13X Zeolite – Specific Effective Mass Storage Capacity.....	4-211
Figure 4-107: 5A Zeolite - Effective Volumetric Storage Charge/Discharge Cycle.	4-214
Figure 4-108: 5A Zeolite - Specific Effective Molar Charge/Discharge Cycle.....	4-214
Figure 4-109: 5A Zeolite - Specific Effective Mass Charge/Discharge Cycle.	4-215
Figure 4-110: 13X Zeolite - Effective Volumetric Storage Charge/Discharge Cycle.....	4-215
Figure 4-111: 13X Zeolite - Specific Effective Molar Charge/Discharge Cycle.	4-216
Figure 4-112: 13X Zeolite - Specific Effective Mass Charge/Discharge Cycle ($T \approx 298$ K).....	4-216
Figure 4-113: 5A Zeolite - Effective Volumetric Delivery Capacity.....	4-218
Figure 4-114: 5A Zeolite - Specific Effective Molar Delivery Capacity.....	4-219
Figure 4-115: 5A Zeolite - Specific Effective Mass Delivery Capacity.	4-219
Figure 4-116: 13X Zeolite - Specific Effective Molar Delivery Capacity.	4-220
Figure 4-117: 13X Zeolite - Specific Effective Mass Delivery Capacity.....	4-220
Figure 4-118: 13X Zeolite - Effective Volumetric Delivery Capacity.	4-221

Figure 4-119: 4A Zeolite - Absolute excess adsorption isotherm model fits.....	4-226
Figure 4-120: 5A Zeolite - Absolute excess adsorption isotherm model fits.....	4-227
Figure 4-121: 13X Zeolite - Absolute excess adsorption isotherm model fits.....	4-227
Figure 4-122: 4A Zeolite - Absolute effective storage isotherm model fits.....	4-229
Figure 4-123: 4A Zeolite - Absolute effective storage modified isotherm model fits... 4-	230
Figure 4-124: 5A Zeolite - Absolute effective storage isotherm model fits.....	4-230
Figure 4-125: 5A Zeolite - Absolute effective storage modified isotherm model fits... 4-	231
Figure 4-126: 13X Zeolite - Absolute effective storage isotherm model fits.....	4-231
Figure 4-127: 13X Zeolite - Absolute effective storage modified isotherm model fits. 4-	232
Figure 4-128: Silica Gel - Excess Volumetric Adsorption Capacity.	4-236
Figure 4-129: Silica Gel - Specific Excess Molar Adsorption Capacity.....	4-236
Figure 4-130: Silica Gel - Specific Excess Mass Adsorption Capacity.	4-237
Figure 4-131: Silica Gel - Effective Volumetric Storage Capacity.....	4-238
Figure 4-132: Silica Gel - Specific Effective Molar Storage Capacity.....	4-239
Figure 4-133: Silica Gel - Specific Effective Mass Storage Capacity.....	4-239
Figure 4-134: Silica Gel - Absolute excess adsorption isotherm model fits.....	4-242
Figure 4-135: Silica Gel - Absolute effective storage isotherm model fits.....	4-243

Figure 4-136: Silica Gel- Absolute effective storage modified isotherm model fits.....	4-244
Figure 4-137: Electrochemical PSi- Absolute Excess Molar Adsorption Capacity.	4-246
Figure 4-138: Electrochemical PSi - Absolute Excess Molar Adsorption Capacity.	4-247
Figure 4-139: Electrochemical PSi - Excess Volumetric Adsorption Capacity.....	4-248
Figure 4-140: PSiPW3 - Absolute Excess Molar Adsorption Capacity.	4-250
Figure 4-141: PSiPW10 - Absolute Excess Molar Adsorption Capacity.....	4-251
Figure 4-142: PSiPW14 - Absolute Excess Molar Adsorption Capacity.....	4-251
Figure 4-143: PSiPW15 - Absolute Excess Molar Adsorption Capacity.....	4-252
Figure 4-144: PSiPW3 - Absolute Effective Molar Storage Capacity.....	4-253
Figure 4-145: PSiPW10 - Effective Absolute Molar Storage Capacity.....	4-253
Figure 4-146: PSiPW10 - Effective Volumetric Storage Capacity.	4-254
Figure 4-147: PSiPW14 - Effective Absolute Molar Storage Capacity.....	4-254
Figure 4-148: PSiPW14 - Effective Volumetric Storage Capacity.	4-255
Figure 4-149: PSiPW15 - Effective Absolute Molar Storage Capacity.....	4-255
Figure 4-150: PSiPW15 - Effective Volumetric Storage Capacity.	4-256
Figure 4-151: Combined Materials - Excess Volumetric Adsorption Capacity.....	4-259
Figure 4-152: Combined Isotherms - Specific Excess Mass Adsorption Capacity.	4-259

Figure 4-153: Combined Isotherms - Effective Volumetric Storage Capacity.....	4-260
Figure 4-154: Combined Isotherms - Specific Effective Mass Storage Capacity. ...	4-261
Figure 4-155: Combined Isotherms - Specific Effective Mass Delivery Capacity....	4-262
Figure 4-156: ANG/CNG Effective Storage Density Ratio for Norit RX3 Extra.....	4-267
Figure 4-157: Comparison of specific mass adsorption capacity and specific surface area for carbon materials.	4-272
Figure 4-158: Comparison of effective volumetric storage capacity and specific surface area for carbon materials.	4-279
Figure 4-159: Comparison of specific mass adsorption capacity and specific surface area for zeolite materials.	4-284
Figure 4-160: Comparison of specific mass adsorption capacity and specific surface area for silica gel.	4-288

Abbreviations

ACC	Activated Carbon Cloth	LED	Light Emmiting Diode
ACF	Activated Carbon Fiber	SOI	Silicon On Insulator
ANG	Adsorbed Natural Gas	SSE	Sum of the Squares of the Error
CNG	Compressed Natural Gas	R_{adj}^2	Adjusted R-Squared
DOE	Department of Energy	RMSE	Root Mean Square of the Error
FEA	Finite Element Analysis	PSi	Porous Silicon
GAC	Granulated Activated Carbon		
IUPAC	International Union of Pure and Applied Chemistry		
LNG	Liquefied Natural Gas		
SEM	Scanning Electron Microscope		
STP	Standard Temperature & Pressure		

Nomenclature

n_a^a	Absolute excess molar adsorption capacity	n_d^a	Absolute excess molar desorption capacity
V_a^a	Absolute excess volumetric adsorption capacity	V_d^a	Absolute excess volumetric desorption capacity
m_a^a	Absolute excess mass adsorption capacity	m_d^a	Absolute excess mass desorption capacity
$\rho_{n_a}^a$	Excess molar adsorption density	$\rho_{n_d}^a$	Excess molar desorption density
$\rho_{V_a}^a$	Excess volumetric adsorption density	$\rho_{V_d}^a$	Excess volumetric desorption density
$\rho_{m_a}^a$	Excess mass adsorption density	$\rho_{m_d}^a$	Excess mass desorption density
$M_{n_a}^a$	Excess specific molar adsorption capacity	$M_{n_d}^a$	Excess specific molar desorption capacity
$M_{V_a}^a$	Excess specific volumetric adsorption capacity	$M_{V_d}^a$	Excess specific volumetric desorption capacity
$M_{m_a}^a$	Excess specific mass adsorption capacity	$M_{m_d}^a$	Excess specific mass desorption capacity
n_e^a	Absolute excess molar delivery capacity	n_a^s	Absolute effective molar storage capacity
V_e^a	Absolute excess volumetric delivery capacity	V_a^s	Absolute effective volumetric storage capacity
m_e^a	Absolute excess mass delivery capacity	m_a^s	Absolute effective mass storage capacity
$\rho_{n_a}^a$	Excess molar delivery density	$\rho_{n_a}^s$	Effective molar storage density
$\rho_{V_e}^a$	Excess volumetric delivery density	$\rho_{V_a}^s$	Effective volumetric storage density
$\rho_{m_e}^a$	Excess mass delivery density	$\rho_{m_a}^s$	Effective mass storage density
$M_{n_e}^a$	Excess specific molar delivery capacity	$M_{n_a}^s$	Effective specific molar storage capacity
$M_{V_e}^a$	Excess specific volumetric	$M_{V_a}^s$	Effective specific volumetric

	delivery capacity		storage capacity
$M_{m_e}^a$	Excess specific mass delivery capacity	$M_{m_a}^s$	Effective specific mass storage capacity
R^a	Excess adsorption retention	n_e^s	Absolute effective molar delivery capacity
n_d^s	Absolute effective molar discharge capacity	V_e^s	Absolute effective volumetric delivery capacity
V_d^s	Absolute effective volumetric discharge capacity	m_e^s	Absolute effective mass delivery capacity
m_d^s	Absolute effective mass desorption capacity	$\rho_{n_e}^s$	Effective molar delivery density
$\rho_{n_d}^s$	Effective molar discharge density	$\rho_{V_e}^s$	Effective volumetric delivery density
$\rho_{V_d}^s$	Effective volumetric discharge density	$\rho_{m_e}^s$	Effective mass delivery density
$\rho_{m_d}^s$	Effective mass discharge density	$M_{n_e}^s$	Effective specific molar delivery capacity
$M_{n_d}^s$	Effective specific molar discharge capacity	$M_{V_e}^s$	Effective specific volumetric delivery capacity
$M_{V_d}^s$	Effective specific volumetric discharge capacity	$M_{m_e}^s$	Effective specific mass delivery capacity
$M_{m_d}^s$	Effective specific mass discharge capacity	R^s	Effective adsorption retention
ρ_g	Equivalent gas storage density	ρ_{stp}	Density of gas at STP conditions
ΔH_c°	Heat of combustion	E_{Gas}	Gasoline energy equivalency
M_M	Molar mass	T_{crit}	Critical temperature
P_{crit}	Critical pressure	ρ_{liq}	Liquid density
V_o	Material pore volume	D_k	Kinetic molecular diameter
D_p	Average material pore diameter	V_s	Sample volume

P_r	Material porosity	V_a	Allotted pore volume
N_p	Number of material pore present	L_c	Thickness of an adsorbed layer
A_{tot}	Total material internal surface area	$n_{p,t}$	Number of moles in free fluid phase
$N_{m,t}$	Total number of molecules contained by a material	$N_{m,a}$	Number of molecules in the adsorbed phase
$N_{m,p}$	Number of molecules in the free fluid phase	N_A	Avogadro's number
A_m	Cross-sectional area of a molecule	$n_{m,t}$	Maximum number of moles stored
$n_{1,i}$	Initial process supply vessel moles	$n_{1,f}$	Final process supply vessel moles
$n_{2,i}$	Initial process sample vessel moles	$n_{2,f}$	Final process sample vessel moles
Z	Gas compressibility	Z_{avg}	Average process gas compressibility
R	Universal gas constant	V_d	Sample dead volume
V_p	Sample packed volume	V_{sys}	Volume of sample vessel with sample container loaded
V_{mes}	Sample vessel volume when sample is loaded	n_{exs}	Excess moles adsorbed
n_{sys}	Total moles in entire system	V_{blk}	Bulk gas phase volume

n_{abs}	Absolute moles adsorbed	ρ_{blk}	Bulk gas molar density
n_{eff}	Moles effectively stored	θ_b	Brewster angle
τ	Porous film thickness	A	Etched film area
m_1	Sample mass prior to etching process	m_2	Sample mass after etching process
m_3	Sample mass after porous volume removed	I_p	Electrochemical etching current density
t_{ech}	Total sample etching time	$P_{r,opt.}$	Porosity obtained via optical methods
t_{inc}	Stain etching reaction incubation time	$P_{r,Eq.}$	Porosity obtained via mass and geometry
$T_{f,Eq.}$	Porous film thickness obtained from empirical modes	$P_{r,m}$	Porosity obtained via mass only
$T_{f,SEM.}$	Porous film thickness obtained from SEM measurements	d_p	Average material particle diameter
t_{KOH}	Time for a porous film removal reaction to complete	A_{sm}	Specific surface area
A_{sv}	Volumetric surface area	ρ_{pak}	Material packing density
m_s	Sample mass		

List of Appendices

Appendix A1 – MATLAB Isotherm Calculation Programs.....	7-311
Appendix A2 – Adsorption Plots.....	8-358

- 1 - Introduction

1.1 - Problem Statement

The world's demand for energy is increasing at an exponential rate. Thus, conventional energy sources continuously struggle to maintain sufficient supply despite facing permanent depletion of natural resources. Environmental concerns coupled with the instability of current energy markets have stimulated growth and research into alternative energy sources and utilization methods. One area in particular which is gaining much attention is alternative natural gas technologies. Natural gas is the cleanest of all the fossil fuels and is thus rapidly growing as an alternative energy source. When compared with coal and oil, it burns cleaner, more efficiently, and with lower levels of potentially harmful by-products that are released into the atmosphere. Natural gas currently supplies almost 60% of the energy contributions made by oil and its usage is continuously growing (U.S. Department of Energy, 2011). Currently, relatively few proven gas reserves are being developed and utilized to their full potential. The main reason for this underutilization is economics. The economics of a natural gas project is mainly determined by the developed gas quantity (reserves and production rates), the operational and capital expenses associated with the storage and transportation technology, and the capital costs necessary to meet gas processing requirements. Current conventional methods for the bulk transport of natural gas (liquefied natural gas & pipeline) require multi-billion dollar investments in complex, long-term engineering projects, and as a result only the largest gas resources are developed. While a significant amount may not necessarily be commercially recoverable, there are proven gas storage and transportation technologies such as adsorbed natural gas which may produce economical solutions to commercialize and utilize some of this natural gas.

1.2 - Motivation for Study

Adsorbed natural gas (ANG) provides many benefits compared to conventional natural gas technologies and thus may facilitate the future production of currently uneconomical gas reserves. ANG may also stimulate natural gas utilization in previously foreign commercial areas such as the automotive industry. The ability to store appreciable volumes of gas at relatively low pressures while having low energy, material, and capital requirements, makes ANG an appealing technology. Although the concept of ANG may seem like a viable solution for many of the problems impeding increased natural gas usage, facets particular of the technology have thus far prevented its wide spread utilization acceptance in industry. In particular, obtaining an adsorbent material that is capable of storing large amounts of gas at low pressures while still being relatively inexpensive to produce remains the problem at hand.

Studies investigating the viability of ANG for industrial use have mainly utilized porous carbon adsorbents due to the high material availability. These adsorbent materials can be produced to achieve relatively high levels of performance but their production costs most often exceed the increased storage benefits obtained. Thus, the widespread use of ANG is dependent on producing a new low cost high performance adsorbent material. It is suspected that a porous silicon based material can be engineered for such an application. Porous silicon has many attributes that potentially offer numerous advantages over more traditional adsorbent materials. For example, it has a very high internal surface area which is essential for high adsorption volumes. Unlike porous carbons, the pore size, porosity, and morphology of porous silicon can be accurately adjusted over a wide range to maximize adsorption quantities. The raw materials required for the production of porous silicon is readily available and relatively inexpensive, and the required processing technology is currently being utilized in industry.

1.3 - Objectives & Scope of Study

The main purpose of this research endeavor is to investigate the suitability of utilizing porous silicon as a medium for the storage of natural gas. The objectives of the study are to identify the material parameters that will allow for maximum gas adsorption, the production parameters required to establish these material parameters, and the overall suitability of the material to be an ANG adsorbent based on a number of performance evaluation criteria. The anticipated success of the material to be utilized by industry will be evaluated based on current standards set forth by porous carbon materials. In addition to the porous silicon materials, activated carbon and zeolite materials that have not been previously studied are also investigated as potential ANG adsorbents.

The scope of this study involves the design and construction of a suitable gas adsorption testing apparatus which is also capable of serving as a prototype ANG containment system; obtain optimal material production parameters through experimental studies, determine the material properties which will produce maximum gas adsorption and desorption quantities, and determine whether the material is truly suitable for industrial use.

1.4 - Outline

In this section the objectives, motivation, and scope of the study were introduced. The second chapter contains background information on natural gas, adsorption in porous materials, ANG, and porous silicon. A review of work that has been done in the area of adsorption of supercritical methane on porous materials, and materials studied for use as ANG adsorbents is also presented. Chapter three provides an account of the experimental methodology used. It provides a detailed description of the design, construction, and operation of the gas adsorption testing apparatus. It explains how the adsorption isotherms are obtained from the available testing information and the sources of error and uncertainty in the adsorption measurement process. It also presents the sample production methods and required adsorption test

preparations. Chapter four presents the results of the sample production experiments and adsorption tests. The performance of the materials are compared to one another and with results found in the literature. An empirical method of approximating a material's specific surface area and a method of modifying standard isotherm models to describe effective storage is also presented. Chapter five provides conclusions and recommendations that have been established based on the research conducted.

- 2 - Literature Review

2.1 - Natural Gas

2.1.1 - Introduction

Natural gas is a naturally occurring gaseous fossil fuel that is typically found in gas fields, oil fields, and coal beds. World natural gas reserves are currently estimated at over 6000 trillion cubic feet, approximately 70% of which is in the Eastern Europe and Middle Eastern regions (U.S. Department of Energy, 2011). Offshore Newfoundland & Labrador has a modest portion of these gas reserves with latest estimates quoting approximately 10.85 trillion cubic feet (Canada-Newfoundland and Labrador Offshore Petroleum Board, 2011). Natural gas is colorless, odourless, and less dense than air when in its pure form. It consists mostly of methane although impurities such as CO₂, H₂O, H₂S, N₂, O₂ and larger hydrocarbons are often present when in its raw unprocessed form. Processed natural gas contains very little to relatively none of these impurities due to safety and combustion performance reasons.

2.1.2 - Storage & Distribution Technologies

Current conventional methods of transporting natural gas are through the use of pipeline or liquefied natural gas (LNG). Pipeline is considered the most primitive method of transporting natural gas but it is also the most versatile. Pipeline may be used to transport gas in virtually any stage of the production to consumer usage process. Pipeline transport networks are established in industrial, commercial, and residential areas and they may be placed above or below ground, or on the bottom of bodies of water. Pipeline networks are capable of very high transport rates and have very little operational expenses. However, the installation of pipeline networks often requires very large capital investments. Thus, pipeline is typically only economical for gas projects involving large quantities and high transportation rates over long periods of time.

The common alternative to pipeline is liquefied natural gas. LNG is a more advanced method of transporting natural gas which involves cooling the gas at atmospheric pressure to approximately 112 K to establish and maintain a liquid state. The liquefied natural gas is then loaded into insulated cryogenic vessels and transported to its destination. LNG is typically only used for the marine transport of natural gas. This involves using massive tanker ships specially designed for LNG storage. However, systems have been developed to transport LNG via roadway with specially designed tank trailers that can be transported with standard cargo trucks (Chart Ferro, 2011). Due to the large amounts of processing and specialized equipment required, LNG is a very expensive gas transport technology compared to that utilized for other fossil fuels. It is typically only used in situations where transport distances are too long to justify the use of pipeline.

Alternative methods have been developed to transport and store natural gas in a more economical manner compared to the more conventional methods previously described. The most popular of these alternative technologies is compressed natural gas (CNG). Compressed natural gas is simply natural gas that is stored in pressure vessels as a compressed supercritical fluid at ambient temperatures and pressures between 20 to 25 MPa (Cardenas, Lagoven, & Pilehvari, 1996). Systems have been developed to transport compressed natural gas in both the marine and land based contexts (Chart Ferro, 2011). However, to date very few have been utilized in industry. CNG transport densities are lower than that of LNG, and transport rates are lower than pipeline. However, the lower capital and material requirements generally allows CNG to be much more cost effective when dealing with smaller gas quantities and shorter transport distances (Economides, Kai, & Subero, 2005).

2.1.3 - Uses of Natural Gas

Natural gas is becoming increasingly integrated into society and is emerging as a primary source of clean energy. It has a large variety and number of uses in the industrial, commercial, and residential sectors making it a very flexible, highly

applicable, and thus very important energy source. Typical industrial uses include waste treatment and incineration, metals preheating (particularly for iron and steel), drying and dehumidification, glass melting, food processing, fuelling industrial boilers, and as a feedstock for the manufacturing of a large number of chemicals and products (Natural Gas Supply Association, 2010). This sector represents almost half of the total usage of natural gas (Natural Gas Supply Association, 2010). Current common residential uses mainly consist of heating, air conditioning, and cooking. However, other uses currently growing in popularity consist of electricity generation and fuel for internal combustion engines (Natural Gas Supply Association, 2010). Commercial uses of natural gas are very similar to residential usage but on a much larger scale.

Another sector in which natural gas is becoming increasingly popular is the transportation sector. Natural gas has the potential of being an alternative fuel for vehicular internal combustion engines. It is estimated that there currently exists over five million natural gas vehicles worldwide and this number is steadily increasing (Russell, 2011). This growth is mainly due to government policies and pressure to reduce energy consumption and increase environmentally friendly energy utilization methods. Although virtually any system that utilizes an internal combustion engine can be modified to consume natural gas, widespread utilization of this technology is relatively low due to current natural gas storage methods. Current methods for small volume storage of natural gas consist only of CNG. However, low storage densities coupled with higher storage tank requirements make this method less appealing for many applications. However, adsorbed natural gas has the potential of making this area more appealing due to increased storage densities at lower pressures, and lower storage vessel material requirements (Burchell, Cook, Komodromos, Quinn, & Ragan, 1999; Sun, Jarvi, Conopask, & Satyapal, 2001).

2.1.4 - Benefits of Using Natural Gas

Natural gas has a number of advantages when compared to other fossil fuel energy sources. Perhaps the most important of which is its environmental benefits. Natural gas burns cleaner and more efficiently than any other fossil fuel and is almost free of harmful contaminants, thus making it an environmentally friendly alternative energy source (Cardenas et al, 1996). Being the cleanest fossil fuel, combustion of natural gas produces mostly carbon dioxide and water vapor. Harmful by-products such as sulphur dioxide, nitrogen oxides, and carbon monoxide are produced but their relative concentrations are very low compared to all other fossil fuels (Natural Gas Supply Association, 2010). Compared to diesel, the utilization of natural gas by automobiles can reduce air toxins such as benzene by up to 100%, smog-forming volatile organic compounds by up to 92%, sulphur dioxide by up to 83%, carbon monoxide by up to 40%, carbon dioxide by up to 25%, nitrogen oxide by up to 10%, and particulate matter by well over 90% (Lozano et al., 2002).

Another important aspect of natural gas is that market trends regarding supply, demand, and consumer cost are much more stable than other fossil fuels such as oil (Natural Gas Supply Association, 2010). Estimated world reserves are also larger than that of oil or coal, thus making natural gas the logical fuel for the future (U.S. Department of Energy, 2011).

2.2 - Adsorption

2.2.1 - Introduction

Adsorption can be defined as the sticking of atoms, ions, or molecules of a fluid to a solid surface (Keller, Staudt, & Siegen, 2005). It results in the effective increase in the density of a fluid in the vicinity of solid-fluid interface (Rouquerol, Rouquerol, & Sing, 1999). Adsorption is caused by the existence of a force field at the surface of a solid, which reduces the potential energy of a fluid molecule below that of the ambient fluid phase causing an attraction (Karge & Weitkamp, 2008). Interaction forces between

an adsorbent material surface and gas molecules cause the molecules to effectively "stick" to the adsorbent surface. For low to moderate fluid pressures, adsorption allows gas molecules to be packed at much higher densities compared to that of the free gaseous phase at the same pressure. Therefore, when a fixed volume is filled with an adsorbent material the gas capacity of that volume will then be greater than if the volume had contained only compressed gas for a given pressure. This is simply due to the presence of the high density adsorbed phase.

Adsorption always occurs to some degree whenever a solid surface is exposed to fluid particles (both gas and liquid) (Rouquerol et al., 1999). However, only materials having microstructures that create relatively large accessible internal surface areas are capable of adsorbing any significant amount of fluid molecules. The fluid free to adsorb is known as the Adsorptive, while the fluid already adsorbed is known as the Adsorbate. The solid material on which adsorption occurs is known as the Adsorbent. Figure 2-1 displayed below gives a pictorial representation of these definitions. During adsorption, adsorbate molecules form a film over the adsorbent material that may consist of a single or multiple layers of atoms or molecules. Molecules may subsequently detach from the surface of the adsorbent and return to the immediate fluid phase. This phenomenon is known as desorption. During fluid-adsorbent interaction, adsorption and desorption may occur simultaneously. When the rate of adsorption equals that of desorption, kinetic adsorption equilibrium is established. For highly porous materials such as activated carbons and zeolites, this diffusion may remain entirely internal (no mass transfer from adsorbent to surroundings or vice versa) (Keller et al., 2005).

In general, adsorption can be considered to be a surface interaction phenomenon and should not be confused with the term absorption which refers to the incorporation of matter (molecules, atoms, ions, etc.) into a host bulk phase. Unlike adsorption, absorption involves molecules being taken up or contained by a host volume instead of the host surface.

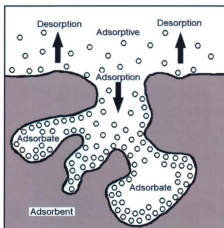


Figure 2-1: Pictorial illustration of adsorption terms.

2.2.1.1 - Physical and Chemical Adsorption

Adsorption is classified into two main categories: physical adsorption and chemical adsorption. The type of adsorption that occurs simply depends on the nature of the adsorbent surface potential. Physical adsorption occurs when adsorption potentials on the surface of the adsorbent overcomes the kinetic and thermal energy of fluid molecules. Molecules are then held in a localized region close to the material surface where the attraction and repulsion forces between the molecule and surface are equal. Since the energy of an adsorbed molecule is always reduced, adsorption is an exothermic process. Physical adsorption potentials are created by net dispersion and repulsion forces caused by Van der Waals forces or dipole-dipole interactions (Rouquerol et al., 1999). Due to the nature of these forces, potentials are relatively weak and the adsorption process is completely reversible. Physical adsorption is generally favoured under lower temperatures and increased pressures, while desorption is favoured under increased temperatures and lower pressures. Physical adsorption is further classified as being either subcritical or supercritical. Subcritical adsorption refers to the adsorption of a subcritical fluid, while supercritical

adsorption refers to the adsorption of a supercritical fluid. A supercritical fluid is one whose pressure and temperature are above its critical pressure and temperature. A subcritical fluid is one whose pressure and temperature are below its critical pressure and temperature.

Chemical adsorption involves the formation of chemical bonds at the fluid-solid interface. The formation of a chemical bond through electron transfer or electron sharing between the solid and fluid particle essentially produces new chemical species. Thus, adsorption potentials associated with chemical adsorption are much stronger than that of physical adsorption. It is a non-reversible process since desorption may only occur if the adsorbate-adsorbent bonds are broken by adding another chemical species with a higher reaction potential (Keller et al., 2005).

2.2.1.2 - Subcritical Adsorption

Subcritical adsorption is the most popular form of physical adsorption reported in the literature. This is no doubt due to its usefulness and utility in classifying porous materials. It was popularized by Irving Langmuir and Stephen Brunauer, Paul Emmett, and Edward Teller who developed semi-empirical models to quantify physical aspects of porous materials such as surface area, pore size, porosity, etc. (Brunauer, Emmett, & Teller, 1938; Langmuir, 1916). Since gases involved in subcritical adsorption are in the subcritical phase region, adsorption can occur until fluid pressures cause gas condensate to form in the pores of an adsorbent. Depending on the adsorbent microstructure, single or multiple layers of adsorbate may form on pore walls with increasing pressure until condensate densities are achieved (Brunauer, Emmett, & Teller, 1938). This is known as multilayer adsorption.

2.2.1.3 - Supercritical Adsorption

Supercritical adsorption most often refers to the adsorption of gases at standard ambient temperature or higher, since nearly all gases are in a supercritical state at these temperatures. Methane for example has a critical temperature of 190.4 K and a

critical pressure of 4.6 MPa. Since the gas is in a semi-supercritical state at ambient conditions, it is impossible for it to condense with the application of pressure alone. Thus, unlike subcritical adsorption, condensate formation cannot occur during the adsorption of a supercritical gas.

Another implication that arises from supercritical adsorption is that it is thought to be limited to mono-layer coverage (Zhou, 2009). This is believed to be due to fluid molecules having an energy state that is too high to be significantly affected by adsorption potentials beyond one molecular layer (Zhou, 2009). Because of these properties, supercritical adsorption cannot achieve the molecular packing that is achieved by subcritical adsorption. However, some authors disagree that supercritical adsorption is constrained to monolayer coverage and believe that up to three adsorbed layers are possible in small micropores (Do & Do, 2003). Experiments have been conducted with mesoporous adsorbents that prove multilayer adsorption is not present when above critical temperatures, and that multilayers formed by gases below their critical temperature will reduce to a monolayer upon transition into the critical state region (Schneider, Grunwaldt, & Baiker, 2004; Zhou, Zhou, Bai, & Yang, 2002). However, it is well known that smaller pores have increased adsorption affinities due to the overlapping of adsorption potentials created by pore curvature, while larger pores have decreased potentials due to the lack of adsorption potential overlap (Do & Do, 2003). It is also known that micropores are typically filled with molecules solely in the adsorbed phase (Do & Do, 2003). Thus, it may simply be the case that supercritical multilayer adsorption is not possible with mesoporous and macroporous materials due to decreased adsorption potentials; and microporous materials that have adequate adsorption potentials are comprised of pores that are too small to facilitate the number of molecules required to form multiple well-defined layers.

2.2.1.4 - Excess Adsorption

Excess adsorption provides a means of establishing a relative comparison of the adsorption affinity and thermodynamic properties of different materials. The definition of excess adsorption arises from the Gibbs free energy concept and more specifically, the Gibbs interfacial thermodynamics regarding how the phase dividing surface is defined (Talu & Myers, 2001). The phase dividing surface is an imaginary discrete surface that separates and partially defines two different thermodynamic phases. An adsorbent system can be defined as the sum of the absolute adsorbed phase volume and the bulk pressure phase volume, which are contained by an overall constant adsorbent system volume (essentially the true material pore volume). A problem arises with specifying the phase volume boundary surface for the adsorbed phase and bulk fluid phase interface. Since the two phases are not separated by any abrupt measureable change in thermodynamic conditions, the phase boundary cannot be determined through direct measurement and can only be approximated.

Since the exact geometry of a material's porous structure is essentially always unknown, the adsorbed phase volume cannot be specified. Thus, the bulk phase volume must be determined in order to describe the adsorption process. The bulk fluid phase volume can either be specified by some known physical properties such as through the porosity of a crystalline substance of known volume, or it must be determined by some indirect method such as inert gas expansion. By expanding an inert gas such as helium into a porous material, the bulk gas phase volume can be determined which then allows for the calculation of the overall system volume. However, specifying the phase boundary in this manner leads to an inherent error since the true boundary location will overlap that established from the gas expansion. Because the bulk fluid and adsorbed phases are said to be homogeneous, densities across each phase remain constant. Thus, the error can be specified as the apparent decrease in the adsorbed phase density due to the overlapping of the true and measured phase volumes. Figure 2-2 presented below depicts this phenomenon, where the level of shading provides a relative measure of the density of each phase.

The first subfigure shows the true adsorbent system with a clear distinction between the bulk gas and adsorbed phases. The second subfigure shows the specified bulk phase volume which essentially includes the whole pore volume. The third subfigure shows the true adsorbed phase density. The fourth subfigure shows the measured adsorbed phase density, which is simply the difference between the true adsorbent system phase shown in subfigure one with the specified bulk gas phase shown in subfigure two. Notice that the density of the calculated adsorbed phase is less than the true adsorbed phase density. Excess adsorption is thus the apparent molecular quantity of gas that constitutes this calculated adsorbed phase, while the absolute adsorption is the actual molecular quantity of gas that is located in the adsorbed phase volume.

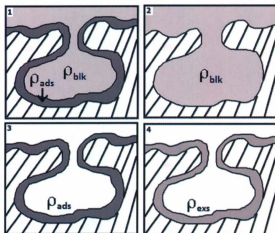


Figure 2-2: Absolute & excess adsorption phase identification.

Excess adsorption is the quantity measured during all adsorption experiments. It is given by the following equation:

Eq. 2-1

$$n_{exs} = n_{sys} - V_{blk} \rho_{blk}$$

where n_{exs} is the excess moles of gas adsorbed, n_{sys} is the total number of moles of gas measured to be in the system, V_{blk} is the volume of the bulk gas phase, and ρ_{blk} is the bulk gas molar density.

One feature that arises from the properties of excess adsorption is that adsorption isotherms may display decreasing and even negative adsorption quantities with increasing pressures. This occurs when the maximum adsorption capacity has been attained but the bulk gas density continues to increase through the application of pressure. If the bulk gas density becomes greater than the adsorbed phase density, negative excess adsorption values will be obtained. Subcritical isotherm models can be applied to these isotherms only up to the point where the slope changes sign.

As previously stated, the absolute adsorption is the actual or true amount of molecules contained in the adsorbed phase. It can be approximated by adding back the bulk gas phase density that was subtracted from the adsorbed phase, and approximating the adsorbed phase volume. Thus, absolute adsorption is defined as the excess adsorption plus the amount of gas contained in the adsorbed volume at the bulk gas density. It is given by the following equation:

Eq. 2-2

$$n_{abs} = n_{exs} + \rho_{blk} V_{ads} = n_{sys} + \rho_{bulk} (V_{ads} - V_{blk})$$

where V_{ads} is the volume of the adsorbed phase.

Unlike excess adsorption, absolute adsorption isotherms do not have a distinct maximum and are monotonically increasing functions that are asymptotic to some limiting value which represents the maximum amount that can be adsorbed by a material. Thus, commonly used subcritical isotherm models such as the Langmuir adsorption model can be applied over all conditions (Choi et al., 2003; Delavar et al., 2010; Zhou & Zhou, 2000).

2.2.1.5 - Effective Storage

Effective storage is a measure of the total amount of gas that is stored by a material in the combined adsorbed and bulk phases. Unlike excess adsorption, effective storage uses the volume that corresponds to the external sample surface boundary which is commonly referred to as the packed volume. This allows for both the absolute adsorbed phase and bulk gas phases to be accounted for. The effective storage can be represented by:

$$n_{eff} = n_{exs} + n_{blk} \quad \text{Eq. 2-3}$$

The effective storage of a material allows one to evaluate a material in terms of its true storage potential and its physical packing density. Since the volume of a sample is dependent on its packing density, materials having higher packing densities generally have better storage performance. This is important since it is possible that a material may have very good excess adsorption characteristics but cannot achieve high enough packing densities to achieve target effective storage levels. For engineering applications regarding the gas storage capabilities of a material, effective storage should always be used although it is very seldom reported in literature.

2.2.2 - History & General Applications

Adsorption has long been studied by scientists with first reports dating back as far as 1777 (Fontana, 1777; Scheele, 1780). However, the term adsorption did not appear until 1881 when it was introduced by Kayser (Kayser, 1881). One of the first reports of adsorption was by Fontana who had noted that freshly calcined charcoal was able to take up several times its own volume of various gases when cooled under mercury (Gregg & Sing, 1982). In the same year, Scheele also recorded that air expelled from charcoal during heating was taken up again upon cooling (Gregg & Sing, 1982).

Since the days of Fontana and Scheele, the adsorption of fluids on porous materials has been extensively studied, and thus a very large number of fluid-material

combinations have been documented. The results of these studies have allowed adsorption to be applied to many of today's modern industrial processes. Historical industrial applications of adsorption mainly included the removal of impurities found in air and water (Ullmann's Encyclopedia of Industrial Chemistry, 2001; Meunier, 1998). Today however, the development of an increased number of adsorbent materials coupled with the advancement in understanding of adsorption processes has allowed adsorption to be utilized in many industries such as the chemical, biochemical, processing, and petroleum industries. Perhaps the most popular modern use of adsorption is for the purification and separation of gas and liquid mixtures (Notaro, Ackley, & Smolarek, 1999; Ruthven, 1984; Yang, 1997). Some common applications of liquid phase adsorption include water treatment and purification, metal recovery, chemical purification, and chemical species separation. Some common gas phase adsorption applications include gas purification, specific chemical species separation, vapour separation, and solvent recovery. Relatively new applications of adsorption that involve energetic processes include air conditioning, refrigeration, and heat pump systems (Meunier, 1998; Suzuki, 1990; Vasiliev, 2001). Adsorption measurements are often undertaken in many academic and industrial laboratories to classify and characterize porous materials (Rouquerol et al., 1999). This is the most common use of adsorption in the academic community.

Another relatively new application of adsorption which is currently underutilized in industry is the storage of combustible gases such as natural gas and hydrogen. These gases can be stored in pressure vessels while in an adsorbed phase creating high densities at relatively low pressures. This application is becoming an increasingly attractive alternative to conventional natural gas storage methods such as CNG and LNG due to its cost and safety benefits (Crittenden & Thomas, 1998). A spin-off to this technology which has been introduced very recently is the storage of sludge digestion gas (biogas) by adsorbent materials (Himeno, Komatsu, & Fujita, 2005). Since biogas is becoming an increasing problem with regards to greenhouse gas emissions, this application of adsorption may prove to be an effective way of reducing air pollution.

2.2.3 - Adsorption Studies

To date, there have been a very large number of studies reported on the adsorption of gasses by porous materials. As previously stated, adsorption experiments conducted on charcoal were among the first reported, dating back as far as 1777 (Fontana, 1777). Today nearly all porous materials thought to possess high internal surface areas have been studied and classified through adsorption techniques. Some of the most common materials studied purely to investigate their gas storage properties include carbonaceous materials such as activated powders, activated fibers, granulated activated carbon, carbon nanotubes, coals, metal oxides, silica powders and gels, smectites and venticulites, pillared clays, molecular sieves, metal organic frameworks, covalent organic frameworks and zeolites (Rouquerol et al., 1999; Sun et al., 2009).

2.2.3.1 - Porous Activated Carbons

Activated carbon is the general term used to describe a class of carbonaceous materials that have been processed to make them very porous. These materials are typically composed of micropores and mesopores, and have porosities on the order of 75%. The processing often gives the material very large internal surface areas making them very good for adsorption applications. Surface areas typically range from 800 to 1700 m²/g but it can be produced to have areas in excess of 3000 m²/g (Lozano-Castello, Cazorla-Amoros, & Linares-Solano, 2002; Manocha, 2003; Menon & Komarneni, 1998). They are formed by pyrolysis of carbonaceous materials such as coconut shells, coal, peat, lignite, or wood followed by an activation process which typically involves exposure to steam or carbon dioxide at temperatures between 700 and 1000 °C (Alcañiz-Monge & Illán-Gómez, 2008; Patrick, 1995). This activation forms a network of pores with a broad size distribution from micropores to macropores. The average pore size and distribution can be modified by varying parameters during the activation process (Patrick, 1995).

Porous activated carbons are a very important material component for many of today's industrial processes and their use can be dated back thousands of years. For example, the use of charcoal by the Egyptians to purify water for medicinal purposes can be dated back to 2000 BC (Manocha, 2003). Many of today's common industrial uses for activated carbons include treatment of potable and waste water, solvent recovery, air purification, catalyst support, chemical separation, and gas storage (Manocha, 2003).

Activated carbons and carbonaceous materials in general have received more attention than any other material in the area of supercritical adsorption. This is no doubt due to these materials being considered the most promising candidates for use as a natural gas storage medium. For example, many studies have been conducted on the adsorption of supercritical methane on porous activated carbon powders (Lozano et al., 2002; David, 2002; Delavar, Ghoreyshi, Jahanshahi, & Irannejad, 2010; Frere & Weireld, 2002; Himeno et al., 2005; Li, Ming, & Yaping, 2000; Ming, Anzhong, Xuesheng, & Rongshun, 2004; Salem, Braeuer, Szombathely et al., 1998; Wang, French, Kandadai, & Chua, 2010; Xiao-dong et al., 2002; Zhou, Chen, Li, Sun, & Zhou, 2000; Zhou, Liu, Su, Sun, & Zhou, 2010), granulated activated carbons (Belmabkhout, De Weireld, & Frere, 2004; Choi, Choi, Lee, Lee, & Kim, 2003; Himeno et al., 2005; Malbrunot et al., 1998; Salehi, Taghikhani, Ghotbi, Nemat Lay, & Shojaei, 2007), and activated carbon fibers (Lozano et al., 2002; Himeno et al., 2005; Miyawaki & Kanedo, 2001; Y. Sun et al., 2009). Numerous studies have also been conducted using methane and various types of coal (Siemons & Busch, 2007; Yongjun, 1999; Yongjuni et al., 2010). Since these investigations are often purely scientific in nature, few results or application relevant engineering data are presented except for excess adsorption and possibly desorption isotherm plots. These plots typically provide the specific molar amounts adsorbed for a given adsorption pressure.

Typically, supercritical adsorption studies are conducted at or slightly above standard ambient temperature, and at moderate pressures of up to approximately 10 MPa (David, 2002; Delavar et al., 2010; Frere & Weireld, 2002; Himeno et al., 2005; Li et

al., 2000; Xiao-dong et al., 2002; Zhou & Zhou, 2000). Results generally consist of excess adsorption isotherms that exhibit clear maxima and decreasing excess adsorption values. Many excess adsorption studies have been conducted using relatively low pressures of up to approximately 5 MPa and at or slightly above standard ambient temperature (Belmabkhout et al., 2004; Choi et al., 2003; Wang et al., 2010). Isotherms obtained from these works closely resemble that of the IUPAC Type-I isotherm. No maxima were present since temperatures were moderate and pressures were relatively low. High-pressure adsorption studies of methane on activated carbon have also been reported (Malbrunot et al., 1998; Ming et al., 2004; Salem, Braeuer, Szombathely et al., 1998). Results generally contain excess adsorption isotherms that exhibit clear maxima and decreasing excess adsorption values. One study in particular used super high pressures of up to 650 MPa (Malbrunot et al., 1998). Excess adsorption isotherms with clear maxima and decreasing slopes which extend to produce negative excess adsorption values were obtained. Figure 2-3 depicts two typical excess isotherms; one containing a distinct maximum with decreasing values extending into the negative region, and the other containing no maxima and no decreasing values.

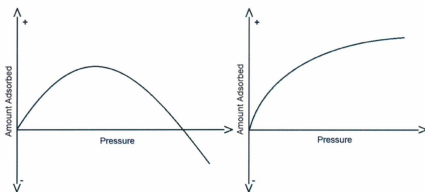


Figure 2-3: Excess adsorption isotherms with and without maxima.

The supercritical adsorption of methane on other less conventional carbonaceous materials has also been studied in some detail. Some of these materials include carbon molecular sieves, multiwalled carbon nanotubes, activated carbon paper, carbon black, and carbon polymers (Busch, Krooss, Gensterblum, Van Bergen, & Pagnier, 2003; David, 2002; Fitzgerald et al., 2005; Goodman et al., 2004; Krooss et al., 2002; Moffat & Weale, 1955; Murata & Kaneko, 2000; Sun et al., 2009; Yongjun, 1999; Yongjuni et al., 2010). Excess adsorption isotherms obtained from these studies were found to resemble those of conventional carbons. However, these materials were found to adsorb much smaller quantities of gas compared to most other conventional carbons.

2.2.3.2 - Zeolites

Zeolites are a class of crystalline solids with well-defined cage like structures. They typically contain silicon, aluminum, oxygen, and a variety of metallic ions in their framework, and have a microporous structure (Ackley, Rege, & Saxena, 2003). Over 200 different zeolite frameworks are known and are used to construct thousands of different chemical compounds. In fact, over 40 occur naturally as minerals and are extensively mined in many parts of the world. Others are synthetic and are made commercially for specific purposes, or produced by research scientists trying to understand more about their chemistry. Because of their unique porous properties, zeolites are used in a variety of applications. Major uses are in petrochemical cracking, selective chemical removal, liquid and gas purification, process catalysts, detergents, health supplements, and in the separation and removal of gases and solvents (Ackley et al., 2003).

Zeolites have long been considered excellent candidates for the adsorptive storage of methane gas because of their inherent ability to adsorb a wide variety of compounds. Thus, a number of studies have been conducted measuring the excess adsorption of supercritical methane on a variety of zeolites. Studies have been conducted using Linde 5A zeolite and 13X zeolite at high pressures of up to approximately 18 MPa and

at standard ambient temperatures, producing excess adsorption isotherms with distinct maxima (Wakasugi, Ozawa, & Yoshtsada, 1981). Studies conducted using 13X zeolite at low to moderate pressures of up to 5 MPa and temperatures between 298 and 323 K produced monotonic isotherms with no distinct maxima (Cavenati, Grande, & Rodrigues, 2004). These isotherms were found to resemble that of IUPAC Type-I isotherms. Low pressure adsorption tests using 13X zeolite at low pressures of up to 3.5 MPa at standard ambient temperature produced similar results (Sun et al., 2009). Other studies involving supercritical methane adsorption on ETS-10 zeolite, microporous organic zeolite, H-mordenite zeolite, CaX zeolite, MCM41 zeolite, 4A zeolite, and 5A zeolite have also been reported and were found to produce similar results (Al-Baghli & Loughlin, 2005; Sun et al., 2009; Tedesco, Erra, & Brunelli, 2010; Triebe, Tezel, & Khulbe, 1996).

2.2.3.3 - Other Materials

In addition to carbonaceous materials and zeolites, a variety of other porous materials have been studied to determine supercritical methane adsorption quantities and isotherms. Some of these materials include silica gels, adsorption resins, metal organic frameworks, polymers, and molecular sieves (Belmabkhout et al., 2004; Salem et al., 1998; Senkovska & Kaskel, 2008; Sun et al., 2009).

Studies are sometimes conducted using a wide variety of materials under identical conditions to directly compare adsorption performance results between different material classes. Once such study involved the adsorption of supercritical methane on sixteen different materials at low pressures of up to 3.5 MPa and at standard ambient temperature (Sun et al., 2009). The materials consisted of multiwalled carbon nanotube, zeolites (13X, MCM41), silica gel, adsorption resin (H103), activated carbon fibers (ACF1, ACF2), carbon mesoporous molecular sieve (CMK-3), hyper-cross-linked polymer network (ML-L), activated carbons (AC-BY0, AC-LM1, AC-BY1, AC-BY2, ACLM3), metal organic framework (PCN-14), and activated carbon paper (ACP). From a direction comparison of the results it was found that adsorbed

quantities increased linearly with respect to specific internal surface area regardless of the adsorbent material type being tested. A similar study using different forms of activated carbon also revealed a linear relationship between storage capacity and micropore volume (Zouadi, Gabouze, Bradai, & Dahmane, 1999). A review of studies conducted at 298 K and 3.45 MPa with methane on a large number of materials including carbons, zeolites, and silica gels also reported a linear relationship between adsorbed amount and specific surface area (Menon & Komarneni, 1998). These reports suggest that supercritical adsorption is limited to monolayer coverage regardless of the increased adsorption potentials that may be possessed by a material.

2.2.3.4 - Porous Silicon

To date there have been no reports of studies conducted on the adsorption of supercritical gases on porous silicon for the purpose of determining excess adsorption isotherms or gas storage quantities. However, there have been reports on the adsorption of supercritical gases on porous silicon for other applications, and the adsorption of subcritical gases for material characterization purposes.

Most all adsorption studies on porous silicon have been subcritical experiments conducted solely to characterize the material in terms of pore size, pore distribution, internal surface area, and pore volume (Bjorklund, Zangoie, & Arwin, 1997; Bomchil, Herino, Barla, & Pfister, 1983; Cisneros, Pfeiffer, & Wang, 2010; Dolino, Bellet, & Faivre, 1996; Jarvis, Barnes, Badalyan, Pendleton, & Prestidge, 2008; Salonen, Björkqvist, & Laine, 2000; Vashpanov, Son, Kwack, & Shin, 2008). Many of these studies have in turn been used to help establish the effect of varying fabrication parameters on the resulting porous silicon microstructure (Coasne, Grosman, Ortega, & Simon, 2005; Dolino et al., 1996; Foll et al., 2002).

Currently, all supercritical adsorption studies involving porous silicon have been for applications other than determining gas storage quantities. The most commonly

reported application is gas sensing. There have been a fairly large number of reports regarding the adsorption of gases such as N_2 , O_2 , H_2S , H_2 , and Ozone for the development of gas sensors (Arwin, Wang, & Jansson, 2003; Galeazzo, Peres, Santos, Peixoto, & Ramirez-Fernandez, 2003; Jalkanena, Tuuraa, Mäkilä, & Salonen, 2010; Mkhitarian, Shatveryan, & Aroutiounian, 2007; Skryshevsky, Zinchuk, Benilov, Milovanov, & Tretyak, 2006; Solntsev, Litovchenko, Gorbanyuk, & Evtukh, 2008; Valladares, Valladares, Valladares, & Calles, 2007; Vashpanov, Jung, & Kwack, 2011; Zouadi et al., 1999). These studies did not measure isotherms or adsorbed gas quantities, but rather an electrical voltage change or shifts in the optical reflectance spectrum due to the adsorption of a gas on the material. Other adsorption studies have involved the development of a hydrogen fuel cell through hydrogen gas adsorption, and the adsorption of biological compounds such as proteins and plant viruses (Arwin, Gavutis, & Gustafsson, 2000; Cisneros, Peiffer, & Wang, 2010; Vashpanov et al., 2008).

2.2.4 - Supercritical Adsorption Models

2.2.4.1 - Introduction

Adsorption models are mathematical models that are developed to gain information about adsorbent materials from adsorption isotherms. They are developed through theoretical considerations, empirical data, or a combination of both. Information typically obtained from adsorption models consists of internal surface area, average pore size, pore size distribution, total pore volume, and porosity.

To date, there have been relatively few generally accepted theoretical or empirical models developed to describe excess supercritical adsorption. Unlike subcritical adsorption, supercritical adsorption does not have a well-defined upper boundary condition such as a saturation vapour pressure, and supercritical adsorption isotherms are not monotonic functions if adsorption pressures are significantly higher than the adsorbate critical pressure. Thus, it is much more difficult to

determine functions that can provide the geometrical properties of an adsorbent based on theoretical considerations. Supercritical adsorption has therefore been primarily used to analyze the performance of a material with regards to a specific application such as gas storage or filtering, instead of material classification. This is in contrast to subcritical adsorption models which are mainly used to characterize porous materials.

2.2.4.2 - Models

There have been a large number of attempts to develop supercritical adsorption models. However, relatively few of these models have thus far been widely accepted or adopted. Most attempts to develop models were made by either modifying subcritical models with the addition of a quasi-quantity such as a quasi-saturation vapor pressure (Amankwah & Schwarz, 1995; Do & Do, 2003; Murata & Kaneko, 2000; Ozawa, Kusumi, & Ogino, 1976; Kaneko & Murata, 1997), utilizing pure mathematical functions such as the Ono-Kondo equation (Aranovich & Donohue, 1996; Aranovich & Donohue, 1997; Benard & Chahine, 1997), or by using molecular simulations such as Density Functional Theory (Al-Muhtaseb & Ritter, 1998; Amankwah & Schwarz, 1995; Aranovich & Donahue, 1996; Benard & Chahine, 1997; Chen et al., 1997; Do & Wang, 1998; Dobruskin, 1998; Jensen & Seaton, 1996; Jiang, Zollweg, & Gubbins, 1994; Kaneko, Shimizu, & Suzuki, 1992; Kaneko & Murata, 1997; Malbrunot et al., 1992; Murata & Kaneko, 2000; Neimark & Ravikovitch, 1998; Rolniak & Kobayashi, 1980; Shethna & Bhatia, 1994; Sosin & Quinn, 1995; Subramanian, Pyada, & Lira, 1995; Ustinov, Do, Herbst, Staudt, & Harting, 2002), the Grand Canonical Monte Carlo method (Cracknell, Gordon, & Gubbins, 1993; Kaneko, Shimizu, & Suzuki, 1992; Kaneko, Cracknell, & Nicholson, 1994; Tan, 1990), or the Elliott-Suresh-Donohue method (Soule, Smith, Yang, & Lira, 2001).

The development of supercritical adsorption models through the modification of subcritical models by the addition of a quasi-quantity such as a quasi-saturation vapor pressure has been reported with mixed success. It has generally been found

that attempts to use modified subcritical equations to model excess supercritical adsorption fail when isotherms exhibit maxima since the modified functions are monotonic and the isotherms are not (Tedesco et al., 2010). However, it has been found that modified subcritical equations such as the Langmuir equation can generally be applied to absolute supercritical adsorption isotherms with good success since these isotherms always increase monotonically with pressure (Do & Do, 2003). Excess adsorption isotherms obtained from the supercritical adsorption of methane on powdered and granulated activated carbon have been successfully fitted using modified Freundlich and Langmuir equations, since fluid pressures were not high enough for isotherms to exhibit maxima (Choi et al., 2003; Delavar et al., 2010; Zhou & Zhou, 2000). Similar studies have successfully utilized the Toth and modified Dubinin-Astakhov equations for isotherm fitting (Akkimaradi, Prasad, Dutta, Saha, & Srinivasan, 2009; Himeno et al., 2005; Malbrunot, Vidal, & Vermesse, 1997; Wang et al., 2010). The Toth and multisite Langmuir equations have also been utilized to model adsorption isotherms of methane on 13X zeolite (Cavenati et al., 2004). One study which involved methane adsorption on four different granulated activated carbons at standard ambient temperature and pressures of up to 3.5 MPa successfully utilized a large number of isotherm equations (Salehi et al., 2007). Since pressures were low and temperatures moderate, excess adsorption isotherms did not contain maxima and were thus modeled using the Langmuir, Freundlich, Unilan, Toth, Sips, Jovanovich, Dubinin-Radushkevich, Dubinin-Stoeckli, Dubinin-Radushkevich-Astakhov, and two-term Theory of Volume Filling of Micropores (TVFM) equations. It was found that all isotherm equations produced good fits to experimental data, but the TVFM was found to be the most accurate. This was thought to be because the TVFM equation is essentially two Dubinin-Radushkevich equations combined, which can simultaneously describe two pore filling mechanisms. The results of this study suggests that essentially all subcritical adsorption models can be utilized to model supercritical adsorption isotherms if no maxima are present.

Modeling supercritical adsorption using a purely mathematical approach such as Lattice Theory has also been found to give results with mixed success (Al-Asheh & Al-Emadi, 2009). However, unlike the method of modifying subcritical models, no conditions have been determined to accurately predict when the method will fail. The Ono-Kondo equation has generally obtained good results. It has been successfully used to model a variety of gas-adsorbent combinations such as the adsorption of methane, carbon dioxide, and nitrogen on activated carbon, graphite, and coal (Aranovich & Donohue, 1996; Donohue & Aranovich, 1998; Yongjuni et al., 2010).

The simulation approach has been generally found to give good modeling results. For example, the Grand Canonical Monte Carlo method and the Density Functional Theory have been used to simulate the excess adsorption isotherms of methane and nitrogen on porous activated carbon, molecular sieves, and zeolites with good success (Salem, Braeuer, Szombathely et al., 1998). The Elliott-Suresh-Donohue method has also been used to simulate the excess adsorption isotherms for a variety of gases such as methane, nitrogen, and propane on different activated carbons (Soule et al., 2001).

Other modeling methods have also been used to model excess supercritical isotherms such as the Simplified Local Density Model (Chen et al., 1997; Rangarajan, Lira, & Subramanian, 1995; Subramanian, Pyada, & Lira, 1995), isotherm fitting using proportional adsorption phase volumes (Murata & Kaneko, 2000; Zhou & Zhou, 2000; Zhou et al., 2000), isotherm transformations (Zhou & Zhou, 1996; Zhou & Zhou, 1998; Zhou et al., 2000), and the adsorption potential theory approach (Fischer, Bohn, Korner, & Findenegg, 1986; Kim, Holste, Hall, & Slattery, 1993; Nguyen & Do, 1999). Adsorption potential theory for example has been successfully used to analyze the adsorption of methane on activated carbon at high pressures (Ming et al., 2004).

2.3 - Adsorbed Natural Gas

2.3.1 - Introduction

Adsorbed natural gas is a gas storage technology in which natural gas is stored in an adsorbed phase by a porous adsorbent material at room temperature and relatively low pressures. Typically the gas is stored at pressures of approximately 3.5 to 4 MPa since most adsorbents reach maximum adsorption capacity at these pressures (Lozano-Castello et al., 2002). Adsorbed natural gas has emerged in the industrial scene relatively recently compared to other more conventional gas storage technologies such as compressed natural gas and liquefied natural gas. However, it has been extensively studied and is very well understood. In fact, devices have been developed to store natural gas in an adsorbed state since the 1950's (Spangler, 1953).

2.3.2 - Advantages of ANG

To date no adsorbent materials have been identified that would allow ANG to attain the densities possessed by LNG and high pressure CNG (greater than 25 MPa). However, it does provide the ability to produce moderate gas densities at relatively low pressures and ambient temperatures. Thus, gas storage by physical adsorption has multiple advantages over more conventional methods such as LNG and pipeline, and less conventional methods such as CNG. For example, because ANG does not require cooling or high compression, the infrastructure required to facilitate gas processing and loading would have significantly lower capital and operating costs compared to CNG and LNG. Since ANG storage pressures are relatively low, storage vessels can be constructed from inexpensive materials and can consist of non-cylindrical shapes. This would allow tanks to be tailored for specific applications to occupy the least amount of valuable space, which is especially beneficial for retrofitting applications where space is limited such as natural gas vehicle conversions. The reduced storage pressures associated with ANG also create a much higher level of safety compared to that of CNG. Even at pressures equivalent to CNG,

ANG is inherently safer despite the higher gas inventory due to the nature of adsorption and fluid flow through porous media. Yet another benefit of the low pressure requirements of ANG is that it can be better utilized in residential applications. For example, a low pressure ANG storage tank can be filled with natural gas from a domestic pipeline using a small single-stage compressor. A low-pressure ANG home filling system would therefore be relatively inexpensive and reliable enough to place ANG use within the reach of many consumers.

With respect to small scale storage and transportation, ANG also has none of the problems that are currently associated with the use of LNG and CNG. For example, LNG is not considered viable in this area since it is a cryogenic fuel. LNG requires specialized insulated vessels, and the facilities required to liquefy and store the gas are extremely expensive. Thus, the requirements of LNG are simply too demanding for it to be utilized for small storage applications such as natural gas vehicles. CNG is a more viable option compared to LNG, although it is far from being ideal. Due to the high pressures associated with CNG, high strength, high cost, non-conformable cylinders are required for storage (Mat, Zakaria, & Paou, 2006). These high pressures also create the need for expensive multi-stage compressors since gas supply pipelines operate at very low pressures. This in turn causes CNG loading facilities to be very expensive (Mat et al., 2006).

2.3.3 - Performance Evaluation

The performance of an ANG adsorbent is typically evaluated with respect to both its excess adsorption and effective storage performance. The excess adsorption is the excess amount of gas adsorbed by a material, and can be expressed in terms of mass, moles, and volumes of gas if taken at standard temperature & pressure (STP). The excess adsorption of a material allows one to obtain a relative sense of the pure adsorption affinity of a material. The effective storage of a material is simply the amount of gas that a material can effectively hold. It includes both the gas bound by adsorption, and the gas located inside the material porous volume in the bulk gas

phase. It can also be expressed in terms of mass, moles, and STP volumes. The effective storage of a material allows one to obtain the overall storage potential and efficiency of a material. For measuring either excess adsorption or effective storage, isotherms are constructed to display the adsorption or storage capacity, the desorption or discharge retention capacity, and the effective delivery capacity. The adsorption or storage capacity isotherm is most commonly used to describe a material. It simply displays the amount of gas adsorbed or effectively stored for a given pressure. The desorption or discharge retention capacity isotherm represents the amount of gas remaining adsorbed or effectively stored for a given pressure when discharging to atmospheric conditions. Typically the adsorption or storage capacity isotherm and subsequent discharge capacity are plotted together as a charge/discharge cycle plot. The effective delivery isotherm represents the amount of gas that can be effectively delivered for a given pressure if discharged to atmospheric conditions. It is calculated from the excess adsorption and desorption, or the effective storage and discharge isotherms as follows:

$$n_e(P) = n_a(P) - n_d(P_{atm}) \quad \text{Eq. 2-4}$$

where n_e is the effective delivery capacity, n_a is the excess adsorption or effective storage capacity, and n_d is the excess desorption or discharge capacity.

In general, effective deliverability isotherms are the most useful plots when describing the performance of an adsorbent that is subject to charge and discharge storage cycles.

For each of the general isotherm types, plots are constructed representing the isotherms in various unit parameters. A total of nine unit parameters are used to represent each isotherm type. These parameters are summarized below in Tables 2-1 through 2-6.

Table 2-1: Excess adsorption evaluation parameters.

Parameter	Units	Name	Parameter Description
n_a^a	(mmol)	Absolute excess molar adsorption capacity	Absolute number of excess moles adsorbed
V_a^a	(STP cm ³)	Absolute excess volumetric adsorption capacity	Absolute amount of excess volumes of STP gas adsorbed
m_a^a	(mg)	Absolute excess mass adsorption capacity	Absolute amount of excess mass adsorbed
$\rho_{n_a}^a = \frac{n_a^a}{V_d}$	$\left(\frac{\text{mmol}}{\text{cm}^3}\right)$	Excess molar adsorption density	Excess moles adsorbed per sample dead space volume
$\rho_{V_a}^a = \frac{V_a^a}{V_d}$	$\left(\frac{\text{STP cm}^3}{\text{cm}^3}\right)$	Excess volumetric adsorption density	Excess STP volumes adsorbed per sample dead space volume
$\rho_{m_a}^a = \frac{m_a^a}{V_d}$	$\left(\frac{\text{mg}}{\text{cm}^3}\right)$	Excess mass adsorption density	Excess mass adsorbed per sample dead space volume
$M_{n_a}^a = \frac{n_a^a}{M_s}$	$\left(\frac{\text{mmol}}{\text{g}}\right)$	Excess specific molar adsorption capacity	Excess moles adsorbed per sample mass
$M_{V_a}^a = \frac{V_a^a}{M_s}$	$\left(\frac{\text{STP cm}^3}{\text{g}}\right)$	Excess specific volumetric adsorption capacity	Excess STP volumes adsorbed per sample mass
$M_{m_a}^a = \frac{m_a^a}{M_s}$	$\left(\frac{\text{mg}}{\text{g}}\right)$	Excess specific mass adsorption capacity	Excess mass adsorbed per sample mass

Table 2-2: Excess desorption evaluation parameters.

Parameter	Name	Parameter Description
n_d^a	Absolute excess molar desorption capacity	Absolute number of excess moles remaining adsorbed when desorbing
V_d^a	Absolute excess volumetric desorption capacity	Absolute amount of excess volumes of STP gas remaining adsorbed when desorbing
m_d^a	Absolute excess mass desorption capacity	Absolute amount of excess mass remaining adsorbed when desorbing
$\rho_{n_d}^a = \frac{n_d^a}{V_d}$	Excess molar desorption density	Excess moles remaining adsorbed when desorbing per sample dead space volume
$\rho_{V_d}^a = \frac{V_d^a}{V_d}$	Excess volumetric desorption density	Excess STP volumes remaining adsorbed when desorbing per sample dead space volume
$\rho_{m_d}^a = \frac{m_d^a}{V_d}$	Excess mass desorption density	Excess mass remaining adsorbed when desorbing per sample dead space volume
$M_{n_d}^a = \frac{n_d^a}{M_s}$	Excess specific molar desorption capacity	Excess moles remaining adsorbed when desorbing per sample mass
$M_{V_d}^a = \frac{V_d^a}{M_s}$	Excess specific volumetric desorption capacity	Excess STP volumes remaining adsorbed when desorbing per sample mass
$M_{m_d}^a = \frac{m_d^a}{M_s}$	Excess specific mass desorption capacity	Excess mass remaining adsorbed when desorbing per sample mass

Table 2-3: Excess adsorption effective delivery evaluation parameters.

Parameter	Name	Parameter Description
n_e^a	Absolute excess molar delivery capacity	Absolute number of excess moles deliverable when discharging from a given pressure to atmospheric pressure
V_e^a	Absolute excess volumetric delivery capacity	Absolute amount of excess volumes of STP gas deliverable when discharging from a given pressure to atmospheric pressure
m_e^a	Absolute excess mass delivery capacity	Absolute amount of excess mass deliverable when discharging from a given pressure to atmospheric pressure
$\rho_{n_e}^a = \frac{n_e^a}{V_d}$	Excess molar delivery density	Excess moles deliverable per sample dead space volume when discharging from a given pressure to atmospheric pressure
$\rho_{V_e}^a = \frac{V_e^a}{V_d}$	Excess volumetric delivery density	Excess STP volumes deliverable per sample dead space volume when discharging from a given pressure to atmospheric pressure
$\rho_{m_e}^a = \frac{m_e^a}{V_d}$	Excess mass delivery density	Excess mass deliverable per sample dead space volume when discharging from a given pressure to atmospheric pressure
$M_{n_e}^a = \frac{n_e^a}{M_s}$	Excess specific molar delivery capacity	Excess moles deliverable per sample mass when discharging from a given pressure to atmospheric pressure
$M_{V_e}^a = \frac{V_e^a}{M_s}$	Excess specific volumetric delivery capacity	Excess STP volumes deliverable per sample mass when discharging from a given pressure to atmospheric pressure
$M_{m_e}^a = \frac{m_e^a}{M_s}$	Excess specific mass delivery capacity	Excess mass deliverable per sample mass when discharging from a given pressure to atmospheric pressure
R^a	Excess adsorption retention	Percent gas that would be retained if discharging from a given pressure to atmospheric conditions

Table 2-4: Effective storage evaluation parameters.

Parameter	Name	Parameter Description
n_a^s	Absolute effective molar storage capacity	Absolute number of moles effectively stored
V_a^s	Absolute effective volumetric storage capacity	Absolute amount of volumes of STP gas effectively stored
m_a^s	Absolute effective mass storage capacity	Absolute amount of mass effectively stored
$\rho_{n_a}^s = \frac{n_a^s}{V_p}$	Effective molar storage density	Number of moles effectively stored per sample packed volume
$\rho_{V_a}^s = \frac{V_a^s}{V_p}$	Effective volumetric storage density	STP volumes effectively stored per sample packed volume
$\rho_{m_a}^s = \frac{m_a^s}{V_p}$	Effective mass storage density	Mass effectively stored per sample packed volume
$M_{n_a}^s = \frac{n_a^s}{M_s}$	Effective specific molar storage capacity	Number of moles effectively stored per sample mass
$M_{V_a}^s = \frac{V_a^s}{M_s}$	Effective specific volumetric storage capacity	STP volumes effectively stored per sample mass
$M_{m_a}^s = \frac{m_a^s}{M_s}$	Effective specific mass storage capacity	Mass effectively stored per sample mass

Table 2-5: Effective discharge evaluation parameters.

Parameter	Name	Parameter Description
n_d^s	Absolute effective molar discharge capacity	Absolute number of moles effectively remaining stored when desorbing
V_d^s	Absolute effective volumetric discharge capacity	Absolute amount of STP volumes of gas effectively remaining stored when desorbing
m_d^s	Absolute effective mass desorption capacity	Absolute amount of mass effectively remaining stored when desorbing
$\rho_{n_d}^s = \frac{n_d^s}{V_p}$	Effective molar discharge density	Number moles effectively remaining stored when desorbing per sample packed volume
$\rho_{V_d}^s = \frac{V_d^s}{V_p}$	Effective volumetric discharge density	STP volumes effectively remaining stored when desorbing per sample packed volume
$\rho_{m_d}^s = \frac{m_d^s}{V_p}$	Effective mass discharge density	Mass effectively remaining stored when desorbing per sample packed volume
$M_{n_d}^s = \frac{n_d^s}{M_s}$	Effective specific molar discharge capacity	Number of moles effectively remaining stored when desorbing per sample mass
$M_{V_d}^s = \frac{V_d^s}{M_s}$	Effective specific volumetric discharge capacity	STP volumes effectively remaining stored when desorbing per sample mass
$M_{m_d}^s = \frac{m_d^s}{M_s}$	Effective specific mass discharge capacity	Mass effectively remaining stored when desorbing per sample mass

Table 2-6: Effective storage effective delivery evaluation parameters.

Parameter	Name	Parameter Description
n_e^s	Absolute effective molar delivery capacity	Absolute number of effectively stored moles deliverable when discharging from a given pressure to atmospheric pressure
V_e^s	Absolute effective volumetric delivery capacity	Absolute amount of effectively stored STP gas volumes deliverable when discharging from a given pressure to atmospheric pressure
m_e^s	Absolute effective mass delivery capacity	Absolute amount of effectively stored mass deliverable when discharging from a given pressure to atmospheric pressure
$\rho_{n_e}^s = \frac{n_e^s}{V_p}$	Effective molar delivery density	Effectively stored moles deliverable per sample packed volume when discharging from a given pressure to atmospheric pressure
$\rho_{V_e}^s = \frac{V_e^s}{V_p}$	Effective volumetric delivery density	Effectively stored STP volumes deliverable per sample packed volume when discharging from a given pressure to atmospheric pressure
$\rho_{m_e}^s = \frac{m_e^s}{V_p}$	Effective mass delivery density	Effectively stored mass deliverable per sample packed volume when discharging from a given pressure to atmospheric pressure
$M_{n_e}^s = \frac{n_e^s}{M_s}$	Effective specific molar delivery capacity	Effectively stored moles deliverable per sample mass when discharging from a given pressure to atmospheric pressure
$M_{V_e}^s = \frac{V_e^s}{M_s}$	Effective specific volumetric delivery capacity	Effectively stored STP volumes deliverable per sample mass when discharging from a given pressure to atmospheric pressure
$M_{m_e}^s = \frac{m_e^s}{M_e}$	Effective specific mass delivery capacity	Effectively stored mass deliverable per sample mass when discharging from a given pressure to atmospheric pressure
R^s	Effective adsorption retention	Percent gas that would be retained if discharging from a given pressure to atmospheric conditions

Out of the above listed evaluation parameters, only a few are commonly reported in the literature. However, all of the parameters are useful for evaluating different performance aspects of an adsorbent material. For excess adsorption the common parameters are the excess specific molar adsorption capacity ($M_{n_a}^a$), and the excess

specific mass adsorption capacity ($M_{n_a}^a$). For effective storage the parameters are the effective volumetric storage density ($\rho_{v_a}^s$) (also known as the effective volumetric storage capacity), the effective specific mass storage capacity ($M_{n_a}^s$), and the effective volumetric delivery density ($\rho_{v_e}^s$) (also known as the effective volumetric delivery capacity).

Since storage capacity is defined as the amount adsorbed or stored by a virgin adsorbent with the process starting point taken at a high vacuum pressure, some amount of gas will remain adsorbed when the pressure is reduced from the maximum operating pressure to atmospheric pressure. This is referred to as gas retention (R^a or R^s) and is expressed as a percentage of the maximum adsorption or storage capacity.

It should be noted that all volumetric capacities are expressed in terms of volumes of gas at STP conditions, where STP is taken to be 293.15 K and 101,325 Pa. It is important to define the exact conditions that are assumed to constitute standard conditions since multiple definitions exist and currently no one definition is accepted worldwide. For example, the International Union of Physics and Chemistry (IUPAC) definition of standard conditions corresponds to a temperature and pressure of 273.15 K and 100,000 Pa. The National Institute of Standards and Technology (NIST) definition corresponds to a temperature of 293.15 K and pressure of 101,325 Pa. The International Standard Metric Conditions (ISMC) for natural gas and similar fluids is 288.15 K and 101,325 Pa; while the imperial or U.S. customary definition is 288.71 K and 101,325 Pa. Due to the large number of differing definitions, it is often very difficult to compare results found in literature with certainty since most authors do not state exactly which conditions are being used. For example, the volumetric capacity of a material ($\frac{V_{STP}}{V_P}$) will have a larger value if using the IUPAC definition when compared to the ISMC or imperial definitions. These variations in conditions will produce a variation in storage capacity values of approximately 6%. Thus, any

volumetric storage values reported in literature without clear definition of the STP conditions assumed can be considered to have a relative uncertainty of at least 6%.

2.3.4 - Adsorbent Requirements

In order for a material to be considered a viable ANG adsorbent it must first meet a number of general requirements (Lozano et al., 2002; Menon & Komarneni, 1998). These requirements are:

- 1) High Storage Capacity and Deliverability
- 2) Low Gas Retention
- 3) Microporous Structure
- 4) High Adsorbent Packing Density
- 5) Low Heat of Adsorption
- 6) High Mass Transfer Rates and Diffusivity
- 7) Hydrophobicity
- 8) Low Cyclic Deterioration
- 9) Inexpensive

2.3.4.1 - Storage Capacity and Deliverability

High storage capacities and high gas deliverability are the most essential requirements for any ANG adsorbent. In order for a potential adsorbent to be viable it must be capable of storing and delivering gas quantities typically achieved by CNG. Current industry targets for gas deliverability have been set by the United States Department of Energy (U.S. D.O.E). In 1993, the U.S. D.O.E. defined the minimum ANG volumetric deliverability for a successful adsorbent as $150 \frac{\text{stp ml}}{\text{ml}}$ at 3.5 MPa and 298 K (Duren, Sarkisov, Yaghi, & Snurr, 2004). In the year 2000 this value was changed to $180 \frac{\text{stp ml}}{\text{ml}}$ at 3.5 MPa and 298 K to obtain an effective storage density comparable to CNG at 25 MPa and 298K.

A wide variety of adsorbent materials have been studied which offer a wide range of volumetric storage densities. Volumetric storage densities as low as $43 \frac{\text{stp ml}}{\text{ml}}$ and as high as $230 \frac{\text{stp ml}}{\text{ml}}$ have been reported in literature (Al-Asheh & Al-Emadi, 2009; Ma et al., 2008). However, volumetric storage densities between 100 and $200 \frac{\text{stp ml}}{\text{ml}}$ are more typical. It should be noted that gas deliverability is much more important than gas storage capacity for evaluating adsorbent performance. This is simply because a material that has a very high storage capacity may still have an overall poor performance from an ANG application standpoint if it has a low gas delivery capacity. Deliverability capacities ranging from $62 \frac{\text{stp ml}}{\text{ml}}$ to $150 \frac{\text{stp ml}}{\text{ml}}$ have been reported (Menon & Komarneni, 1998; Sun et al., 2001). However, values in the vicinity of $100 \frac{\text{stp ml}}{\text{ml}}$ to $140 \frac{\text{stp ml}}{\text{ml}}$ are more typical for higher performing adsorbents (Biloe, Goetz, & Guillot, 2002; Lozano et al., 2002; Matranga, Myers, & Glandt, 1992; Menon & Komarneni, 1998; Zhou, 2010).

2.3.4.2 - Gas Retention

As opposed to compression storage, adsorption is highly nonlinear with respect to fluid pressures. Materials with high adsorption affinities tend to have steep isotherms with the majority of the adsorption occurring at low pressures. As a consequence, a significant amount of gas may remain in storage when the pressure attains its minimum operating value. Therefore, an adsorbent material that has a very high storage capacity may not be a good ANG adsorbent material if it has a very high adsorption affinity at very low pressures. Carbon adsorbents for example typically retain anywhere from 10% to 30% of their maximum volumetric storage capacity when discharged to atmospheric pressure (Sun et al., 2001; Wegrzyn, 1996). However, retentions as high as 50% have been reported (Alcaniz-Monge, Casa-Lillo, Cazorla-Amoros, & Linares-Solano, 1997). It is thought that this gas retention is caused by increased adsorption potentials created by small micropores (Sun et al., 2001). Figure 2-4 shown below illustrates this concept. Two adsorbent materials

(*ANG-1* & *ANG-2*) are capable of storing the same amount of gas at the maximum operating pressure (V_{max} @ P_{max}). Adsorbent *ANG-1* has a much higher adsorption affinity than *ANG-2* and therefore the majority of its adsorption takes place at lower pressures. However, upon discharging to atmospheric pressure it is clear that the first adsorbent (*ANG-1*) retains much more gas (V_{res-1}) than the second adsorbent ($V_{res-1} > V_{res-2}$). Therefore, the second adsorbent (*ANG-2*) would be much better suited to ANG use since it will have a higher overall gas deliverability.

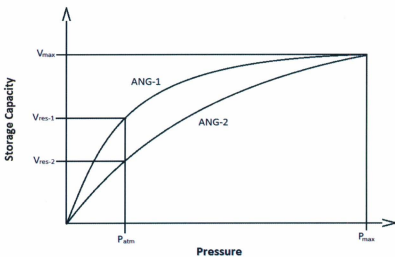


Figure 2-4: Isotherms depicting gas retention properties of two adsorbents.

2.3.4.3 - Microporous Structure

The problem of high gas retention can be alleviated by optimal pore sizing since it has been found that pore size directly affects an adsorbent's overall adsorption affinity (Lozano et al., 2002; Salehi et al., 2007). In general, smaller pore sizes leads to increased adsorption potentials due to overlapping field potentials which in turn increases the overall adsorption affinity of a material. However, smaller pore sizes also increase internal surface area, which is essential for high storage capacities.

Thus, there exists an optimal pore size which will produce maximum storage capacities while minimizing gas retention. Results of experimentation and simulation suggest that microporous materials should have pore sizes no smaller than 0.8 nm (Lozano et al., 2002). Results of other studies conducted on granular activated carbon suggest that a pore size of 1.14 nm would be optimal since it would create the high surface areas needed for high storage capacities and produce lower adsorption affinities to minimize gas retention (Salehi et al., 2007).

2.3.4.4 - Adsorbent Packing Density

One important property of adsorbents which greatly affects gas storage capacity is the adsorbent packing density. Adsorbent materials do not have continuous microstructures but are composed of small continuous porous particles packed together. Typically the space between neighboring particles is much larger than the particle pore size. This volume is essentially wasted since it is very inefficient at adsorbing gas due to reduced adsorption potentials. Reducing the space by increasing particle packing density places more adsorption-capable pores in the adsorbent volume domain and effectively increases the storage efficiency of the space created between neighboring particles. This ultimately leads to higher storage capacities (Mat et al., 2006).

2.3.4.5 - Heat of Adsorption

Minimal thermal effects during the adsorption and desorption process is another desirable property of an ANG adsorbent. Since adsorption is an exothermic process, significant amounts of heat can be generated during the process (Bastos-Neto, Torres, Azevedo, & Cavalcante, 2005). This in turn increases the temperature of the adsorptive gas which in turn degrades its ability to adsorb. The amount of thermal energy dissipated during adsorption is known as the latent heat of adsorption. Latent heat of adsorption values of approximately 12 to 17 kJ/mole are typical for methane storage on activated carbon (Biloea, Goetza, & Mauran, 2001; Mota & Lyubchik,

2008). Studies suggest that adsorbents having a high heat capacity and low heat of methane adsorption produce a much lower temperature rise during adsorption and a much lower temperature fall during desorption (Mat et al., 2006). This ultimately results in better storage and deliverability capacities. Good heat conduction is also a favorable characteristic of adsorbents since it has been found that better storage and deliverability capacities can be obtained during isothermal conditions (Mat et al., 2006).

2.3.4.6 - Mass Transfer and Diffusivity

The ability to diffuse and transfer gas at reasonable rates is an absolute necessity for a successful ANG adsorbent. The viability of ANG to be utilized in industry greatly depends on gas storage rates. Predicting storage rates is often difficult since it depends on a large number of factors such as the material porosity and pore interconnectivity, charging fluid pressure and temperature, storage vessel size and shape, and the number and distribution of gas diffusion points (Bastos-Neto et al., 2005). Studies have shown that there is a tradeoff between filling times, storage capacity, and deliverability. It has been found that with higher filling rates lower storage capacities are obtained. It has also been found that higher discharging rates typically cause inefficient gas delivery (Mat et al., 2006).

2.3.4.7 - Hydrophobic Properties

Another desirable characteristic of an ANG adsorbent is that it should be very hydrophobic. Adsorbents that are not hydrophobic such as zeolites and silica gel greatly deteriorate in performance over time due to the adsorption of water vapour (Menon & Komarneni, 1998). However, studies have been conducted utilizing wet adsorbents that have achieved significantly higher storage capacities due to the formation of hydrates inside the adsorbent pores. Hydrate formation effectively increases the stored gas density and the overall volumetric storage capacity of an adsorbent. Wet storage studies utilizing activated carbons, silica gels, and molecular

sieves have been reported with good results (Al-Asheh & Al-Emadi, 2009; Kang & Lee, 2010; Zhou et al., 2010). Storage capacities were generally found to increase significantly, while thermal effects associated with high adsorption and desorption rates were decreased by tenfold in some cases. However, hydrate formation was also found to require temperatures at approximately 275 K and in some instances the process required up to 1.5 months to attain equilibrium (Al-Asheh & Al-Emadi, 2009). Both of these aspects would no doubt cause substantial problems if this technology was to be used by industry.

2.3.4.8 - Cyclic Loading & Deterioration

One important aspect of an ANG material that is surprisingly seldom studied and reported is cyclic performance. Under cyclic operation, adsorbent performance deteriorates due to the gradual onset of damage to the material microstructure caused by pressure differentials and fluid flow through the material during operation (Mat et al., 2006). This deterioration will eventually require the replacement of the adsorbent material. Another cyclic performance issue that is often not studied is performance deterioration resulting from the use of natural gas. Since natural gas is composed mostly of methane, nearly all adsorption studies reported in literature utilize methane instead of natural gas for convenience. However, studies that have been conducted with natural gas have found that impurities commonly found in the gas typically remain adsorbed after discharging (Wegrzyn, 1996). Thus, with each successive charge and discharge, the storage capacity of the material is reduced by the residual impurities. However, this deterioration can be somewhat prevented by installing a sacrificial adsorbent dedicated to adsorbing the impurities while letting the hydrocarbons pass through (Wegrzyn, 1996). This adsorbent is often referred to as a guard bed. The guard also serves as a filter to prevent any particulate adsorbent material from leaving the storage vessel during discharge.

2.3.4.9 - Material Cost

The success of ANG as a lucrative commercial storage technology will ultimately depend on the final cost of the adsorbent material. Regardless of how well an adsorbent performs, it will not be industrially viable if it is too expensive for the end user. In fact, materials have been developed that perform very well but are not expected to be currently viable since bulk production costs would be high (Bari, Mohammed, & Shuaab, 2008; Ma et al., 2008; Zhou, 2010). It has been suggested that an adsorbent should cost no more than 10 \$/kg in order for ANG to be considered a viable natural gas storage option (Menon & Komarneni, 1998).

2.3.5 - Adsorbent Studies

2.3.5.1 - Porous Carbons

A wide variety of porous materials have been studied for their suitability as an ANG adsorbent. However, thus far activated carbon has been the only material seriously considered as a potential solution and has dominated this particular field of study. Therefore, almost all performance benchmarks established by ANG for commercial applications have been through the use of activated carbons (Lozano et al., 2002). This is mainly because activated carbons have relatively low production costs and offer high adsorption capacities compared to other non-carbonaceous materials. Internal surface areas of up to 4057 m²/g have been reported, although areas closer to 1500 m²/g are more typical (Menon & Komarneni, 1998). One of the features of activated carbons that many see as being a major benefit is that they can be obtained from scrap or recycled materials. However, these carbons typically offer poor performance with storage capacities being less than 100 $\frac{\text{STP ml}}{\text{ml}}$. Such materials include scrap tires, bituminous coals, olive oil waste, rice husks, and palm shells (Balathanigaimani et al., 2006; Solara et al., 2008; Sun, Brady, Rood, & Lehmann, 1997). In fact, some of the best and worst performing ANG adsorbents reported have been activated carbons (Menon & Komarneni, 1998; Sun et al., 1997). This is because

a wide variety of pore sizes and pore distributions are achievable depending on the starting organic material and the activation process used. Although some carbons are capable of achieving high storage and deliverability capacities, the majority of them that have been reported in literature fall short of the deliverability capacity of $180 \frac{\text{STP ml}}{\text{ml}}$ set by the United States Department of Energy (Alcaniz-Monge et al., 1997; Balathanigaimani et al., 2006; Biloe et al., 2002; Lozano et al., 2002; Lozano-Castello et al., 2002; Mat et al., 2006; Solara et al., 2008; Sun et al., 1997; Sun et al., 2001). Thus far, one of the highest performing carbons reported had a volumetric storage capacity of $202 \frac{\text{STP ml}}{\text{ml}}$ at 4.1 MPa and was produced from Australian lignite (Chaffee, 1990).

Relatively new high density carbons materials such as activated carbon fibres have been found to outperform more conventional carbons such as powdered and granulated activated carbon. These carbons may prove to be a solution to the inadequate storage and deliverability capacities found with most conventional carbons (Menon & Komarneni, 1998). Activated carbon fibers have the benefit of much higher packing densities and a microstructure consisting mostly of micropores (Alcaniz-Monge et al., 1997). It has been proposed that surface areas as high as $6000 \text{ m}^2/\text{g}$ are attainable with these carbons. However, they have significantly higher production costs compared to more conventional carbons. In general it has been found that increasing the storage capacity of activated carbons increase their costs exponentially (Menon & Komarneni, 1998).

Simulation studies suggest that the theoretical maximum effective volumetric storage capacity is between 209 and $220 \frac{\text{STP ml}}{\text{ml}}$, and the maximum deliverability is approximately $195 \frac{\text{STP ml}}{\text{ml}}$ for activated carbons (D. Lozano et al., 2002; Matranga et al., 1992; Menon & Komarneni, 1998). However, considering the fact that activated carbons usually retain anywhere from 10% to 30% of their maximum storage capacity; it appears that an activated carbon material would be required to reach its theoretical maximum in order to achieve the D.O.E. deliverability target of $180 \frac{\text{STP ml}}{\text{ml}}$

at 3.5 MPa (Sun et al., 2001; Wegrzyn, 1996). Thus, after many years of research and development it appears that activated carbons may not be able to fulfill the requirements of a successful ANG adsorbent as defined by the U.S. D.O.E. This is in contrast to the expectations of many who have investigated this class of materials. However, to date carbonaceous materials are the only class of materials being utilized by industry for ANG to any extent.

2.3.5.2 - Zeolites

Due the inability of carbon materials to produce adequate volumetric storage and delivery capacities, researchers have turned their attention to other porous materials. One such material class that has been extensively studied is the zeolites. Some of the earliest works conducted on adsorbents for ANG storage systems began with zeolites (Munson & Clifton, 1971). Zeolites have been found to have high packing densities compared to other adsorbent materials such as activated carbons. However, they typically have lower micropore volumes and thus typically have lower storage capacities (Lozano et al., 2002). It has actually been suggested that accessible internal surfaces areas greater than $1000 \text{ m}^2/\text{g}$ are not attainable even with synthetic zeolites (Menon & Komarneni, 1998). Most zeolites have volumetric storage capacities below $100 \frac{\text{STP ml}}{\text{ml}}$ and are therefore generally not considered as being suitable ANG adsorbents (Al-Asheh & Al-Emadi, 2009; Menon & Komarneni, 1998; Zhou, 2010). In addition, zeolites have been found to be very hydrophilic and can lose their adsorption capacity for methane with time due to preferential moisture adsorption (Menon & Komarneni, 1998).

2.3.5.3 - Metal Organic Frameworks

Another class of materials that has been receiving much attention lately is the Metal Organic Frameworks (MOF). MOFs are porous polymeric materials consisting of metal ions or clusters linked together by organic bridging ligands to form three-dimensional framework structures like "crystal sponges". The versatile metal joints

and organic linkers, large surface areas, and tunable pore sizes make MOF compounds highly attractive for storing methane gas (Zhou, 2010). MOFs having internal surface areas in excess of 4500 m²/g have been reported (Saha & Deng, 2010). They have also obtained some of the highest methane storage capacities to date. Typical volumetric storage capacities have been reported to range from 155 to 240 $\frac{\text{STP ml}}{\text{ml}}$ (Duren et al., 2004; Zhou, 2010). Most MOF materials are reported to have storage capacities above 200 $\frac{\text{STP ml}}{\text{ml}}$ (Jensen & Seaton, 1996; Ma et al., 2008; Senkovska & Kaskel, 2008). It is clear that MOFs possess the ability to be successful ANG adsorbents in terms of storage capacity. However, more research is needed to address the other important areas required such as gas deliverability and production costs.

2.3.5.4 - Other Materials

Many other porous materials have been studied as potential ANG adsorbents. Some of these materials include carbon and zeolite molecular sieves (Akkimaradi et al., 2009; Al-Asheh & Al-Emadi, 2009; Jensen & Seaton, 1996; Ma et al., 2008; Senkovska & Kaskel, 2008), silica gels (Bari et al., 2008; Menon & Komarneni, 1998; Ventura, Hum, Narang, 1992), organic gels (Menon & Komarneni, 1998; Ventura, Hum, Narang, 1992), and alumina (Li, Yan, Xin, 1993; Ding, Ozawa, Yamazaki, Watanuki, Ogino, 1988). However, these materials have thus far all fallen very short of the U.S. D.O.E deliverability target of 180 $\frac{\text{STP ml}}{\text{ml}}$.

2.3.6 - Applications & Economics

ANG may fulfill a wide number of applications in both the midstream and downstream areas of petroleum-utilizing industry. In the midstream sector, ANG may provide solutions to develop currently uneconomical gas reserves through the transport of natural gas via sea or road. Since ANG requires low capital and moderate operational resources, it may prove to be a solution for situations in which gas quantities are too small for the economical use of LNG or Pipeline. Such situations

would typically include projects with smaller gas reserves, lower production rates, and relatively short gas transport distances. Essentially ANG should fulfill all of the expectations of CNG but with reduced resource requirements. The potential downstream applications of ANG consist of a replacement fuel source for almost any system in which combustion or internal combustion engines are utilized. Perhaps the most widely advocated application is small-scale on-board fuel storage for natural gas vehicles such as motorcycles, cars, buses, trains, and ships. Other potential applications include large-scale gas storage, capture of natural gas emissions such as coal bed methane, and biogas storage.

Although current ANG adsorbents have yet to reach the suggested performance standards required to obtain a prominent position in industry, a number of companies are utilizing the technology. For example, MichCon has already commercialized an ANG storage system for fork lifts and welding equipment which utilizes a carbon adsorbent (Menon & Komarneni, 1998). G-Tec has also commercialized a similar system to supply natural gas for welding equipment (G-Tec, 2011). Germanischer Lloyd has developed an integrated ANG storage system for light and heavy duty natural gas vehicles such as scooters and trucks (Germanischer Lloyd Industrial Services, 2011). Angstore Technologies Ltd. also offers a similar system for the conversion of natural gas vehicles, as well as conformable ANG tanks for automotive use (Angstore Technologies Ltd., 2011).

As previously mentioned, one of the most prominent applications of ANG is its use as a vehicular fuel. However, in order for natural gas to be a successful replacement to gasoline it must be comparable in terms of energy density. Natural gas when stored at ambient conditions offers a very low energy density compared to other fossil fuels such as gasoline. In fact, the energy density of natural gas at STP conditions is only 0.12% of that of gasoline. Thus, the onboard storage of natural gas at STP conditions is clearly not a viable option. LNG has volumetric density of about 600 times greater than natural gas at STP conditions. This produces an energy density of approximately 66% to that of gasoline. However, as previously discussed LNG is not practical for

small scale storage and transportation since it is a cryogenic fuel. CNG typically offers a volumetric density of approximately 230 times greater than natural gas at STP conditions. This produces an energy density of approximately 25% to that of gasoline. However, because of the high pressures associated with CNG, cylinders are not conformable and thus occupy valuable cargo or trunk space (Mat et al., 2006). ANG is capable of a wide range of volumetric storage densities. At a volumetric density of 200 times that of STP natural gas, ANG offers an energy density of approximately 22% of that of gasoline. This makes ANG appealing because at a pressure of only 3.5 MPa it is capable of producing energy densities obtained with CNG at 20 MPa. Also, CNG operating at 3.5 MPa is only capable of producing 18% of the energy density obtained with ANG. According to the United States Department of Energy, an energy density of approximately 20% of gasoline is required for ANG to be a viable alternative to gasoline (Duren et al., 2004). Table 2-7 shown below gives a summary of the gas storage densities typically obtained with ANG, CNG, and LNG (Lozano et al., 2002). Where ρ_g is the stored gas density, $\frac{\rho_g}{\rho_{stp}}$ represents the STP storage ratio, ΔH_c° is the heat of combustion, and E_{Gas} is the energy content relative to gasoline.

Table 2-7: Summary of the capabilities of various gas storage technologies compared to gasoline.

	T (K)	P (MPa)	ρ_g ($\frac{g}{ml}$)	$\frac{\rho_g}{\rho_{stp}}$	ΔH_c° ($\frac{MJ}{L}$)	E_{Gas} (%)
LNG	113	0.1	0.4	600	23	66
CNG	298	20	0.15	230	8.8	25
CNG	298	3.5	0.0234	36	1.35	4
ANG	298	3.5	0.13	200	7.48	22
STP Gas	298	0.1	0.0065	1	0.038	0.11

2.4 - Porous Silicon

2.4.1 - Introduction

Porous silicon is crystalline silicon with a porous network located throughout its microstructure. It is produced by the electrochemical etching or stain etching of doped crystalline silicon in an HF-based electrolyte. During the etching process, pores are formed throughout the material-fluid interface and extend into the material creating a porous microstructure. These pores allow the material to have very high internal surface areas. Ratios as high as $1000 \text{ m}^2/\text{cm}^3$ have been reported, although values of approximately $500 \text{ m}^2/\text{cm}^3$ are more typical (Monuko du, 2007). Porous silicon can be produced by using both n-type and p-type silicon, although the resulting microstructure for each is often quite different from one another (Zhang, 2004).

Porous silicon was discovered in 1956 by Uhlir while performing electropolishing experiments on silicon wafers using an electrolyte containing hydrofluoric acid (HF) (Pérez, 2007). However it wasn't until the 1990 when Leigh Canham published his results on red-luminescence from porous silicon did the material gain much attention. Since then the optical properties of porous silicon have become a very intense area of research with applications focusing around silicon-based optoelectronic devices (Pérez, 2007).

2.4.2 - Material Classification

Porous silicon is typically classified by its pore size and porosity. Porosity is defined as the fraction of void space within the porous silicon layer. It can be easily determined by weight measurements or optical reflectance techniques (Peckham, 2011). IUPAC guidelines define the range of pore sizes used to characterize porous silicon. These ranges are given below in Table 2-8 (Sing, 1985). These size classifications give rise to the three general forms of porous silicon: microporous, mesoporous, and macroporous.

Table 2-8: Pore size classification.

Pore Width (nm)	Classification
≤ 2	Microporous
2 - 50	Mesoporous
> 50	Macroporous

2.4.3 - Applications

Porous silicon is constantly gaining attention in the scientific and engineering communities due to the large number of unique properties it possesses. An increasing number of potential applications are being identified because of these geometrical, chemical, biological, electrical, mechanical, acoustic, and optical properties. Some application areas include optoelectrics (Bisi, Stefano, & Pavesi, 2000), microelectronics and micromachining (Foll et al., 2002), biotechnology (Lehmann, 2002), energy storage and conversion (Aravamudhan et al., 2005; Jiang, 2007), chemical sensing (Foucaran, 1997), and nano-explosives (Monuko du, 2007). Table 2-9 displays some of the key properties and roles of porous silicon for various applications (Bisi, Stefano, & Pavesi, 2000).

One potential application area which has yet to be studied is the use of porous silicon as medium to store natural gas. It is believed that porous silicon may excel in this area because it has many benefits compared to other materials currently being studied for use as ANG adsorbents such as porous carbons, zeolites, and metal organic frameworks. Some of these beneficial areas include: very high internal surface areas, highly variable material morphologies, the ability to produce fully microporous material structures, simplistic production methods, high material availability, relatively low material cost, and the ability to accurately control the final material properties during the production process. Each of these areas is considered essential for a suitable ANG adsorbent. Thus, based on the current research information available on porous silicon, the material does present itself as being a strong candidate for an industrially viable ANG adsorbent.

Table 2-9: Porous silicon applications and properties.

Application Area	Role of PS	Key Property
Optoelectronics	LED	Efficient electroluminescence
	Waveguide	Tunability of refractive index
	Meld emitter	Hot carrier emission
	Optical memory	Non-linear properties
Micro-optics	Fabry-Perot filters	Refractive index modulation
	Photonic band gap structures	Regular macropore array
	All optical switching	Highly non-linear properties
Energy Conversion	Antireflection coatings	Low refractive index
	Photo-electrochemical cells	Photo-corrosion cells
Environmental Monitoring	Gas sensing	Ambient sensitive properties
Microelectronics	Micro-capacitor	High specific surface area
	Insulator layer	High resistance
	Low-k material	Electrical properties
Wafer Technology	Buffer layer in heteroepitaxy	Variable lattice parameter
	SOI wafers	High etch selectivity
Micromachining	Thick sacrificial layer	Highly controllable etching parameters
Biotechnology	Tissue bonding	Tunable chemical reactivity
	Biosensors	Enzyme immobilization

- 3 - Experimental Procedures

3.1 - Apparatus

3.1.1 - Introduction

The adsorption of supercritical fluids by porous materials can be measured using a variety of different techniques. The most common adsorption measurement methods are the volumetric technique and the gravimetric technique since these are the most versatile and simplistic in nature. Both of the methods measure excess adsorption and produce equivalent results. However, the volumetric testing technique is the method most commonly reported in the literature. Other less conventional techniques include oscillometry and impedance spectroscopy (Keller et al., 2005). The volumetric method was utilized for all adsorption experiments presented in this thesis and will be discussed in more detail in subsequent sections.

Due to the relative simplicity of the methods employed to measure adsorption, experimenters typically design and construct their own apparatus to meet specific requirements. Many of these apparatus designs have been presented in detail in the literature (Hammond, Tompsett, Auerbach, & Conner, 2007; Keller et al., 2005; Wang, Wei, & Wang, 2006). Automated commercial adsorption testing apparatus are also available such as the ASAP-200 (Micromeritics Corporation), Autosorb (Quantachrome Corporation), Omnisorb (Beckman Coulter) and Sorptomatic (Carlo Erba Instruments). Utilization of some of these devices has also been reported in literature but to a much less degree compared to custom apparatus. This is likely due to their high cost compared to constructing one's own apparatus. The apparatus utilized for all tests presented in this thesis was designed and constructed specifically for the supercritical adsorption testing of porous materials.

3.1.2 - Volumetric Technique

The volumetric technique of measuring gas adsorption is based on determining adsorbed gas quantities from the measurement of gas pressures and temperatures in fixed known volumes. It involves sending known molar quantities of gas into a known volume containing an adsorbent specimen. Once the gas has been delivered, its final pressure and temperature are measured. This gives the apparent gas quantity located in the sample volume. Since the gas quantity sent to, and the apparent quantity remaining in the sample volume are both known, the adsorbed molar quantity is simply the difference between these two quantities. The adsorbed gas will simply appear to be missing gas since it does not effectively contribute to the bulk gas pressure inside the pressure vessel which contains the adsorbent sample. This method is often referred to as the "BET volumetric method" (named after Brunauer, Emmett, and Teller) since it was the type of measurement originally made by Brunauer, Emmett, and Teller (Emmett & Brunauer, 1934) and was described by Emmett (Emmett, 1942) when conducting the first subcritical adsorption measurements. However, this technique is used for both subcritical and supercritical adsorption experiments.

The volumetric technique can be employed by using either the discrete or continuous methods. The discrete method is a dosing approach where specific-sized gas doses are sent to a sample vessel and measurements are taken after the system is allowed to reach complete equilibrium. The main disadvantages of this method are the dosing requirement, inability to measure adsorption rates, compound errors based on inaccurate dosing volumes, and low isotherm resolution (Rouquerol et al., 1999). The continuous method is a rate dosing approach where a large gas dose (large enough to bring the sample chamber to the desired final equilibrium pressure) is sent continuously to a sample vessel at a rate that maintains quasi-equilibrium. Measurements are taken and recorded continuously throughout the experimental process by a computer using any desired time interval. The continuous method has the benefit of being able to produce high resolution isotherms, and the apparatus

requires very little attention to operate once a test has started. Typical expansion rates are on the order of 25 to 100 STP/cm³. The continuous method of adsorption measurement was used for all tests presented in this thesis. Data for the adsorption experiments conducted were recorded continuously at a rate of 0.3 Hz or approximately one measurement every 3.3 s.

The volumetric technique is the most commonly utilized method since it offers many benefits over other approaches. One of the major benefits is the increased measurement accuracy compared to other methods (Belmabkhout et al., 2004; Choi et al., 2003; Malbrunot et al., 1998). Other benefits include a decreased operational cost, increased simplicity which allows for the design and construction of custom measurement apparatus without the requirement of specialized and costly equipment, and operation of such an apparatus is very straight-forward.

3.1.3 - Apparatus Description

3.1.3.1 - General Description

A schematic of the apparatus utilized to conduct the adsorption experiments presented in this thesis is shown below in Figure 3-1. As previously stated, the apparatus was designed to conduct supercritical excess adsorption experiments using the continuous volumetric technique. Electronic sensors and a computer were incorporated to minimize the operational requirements for the user and to enhance the overall process measurement resolution. The apparatus consists of a supply vessel, sample vessel, vacuum pump, gas supply tanks, pressure and temperature sensors, manual high pressure control valves, high pressure tubing and fittings, a data acquisition module, and a personal computer.

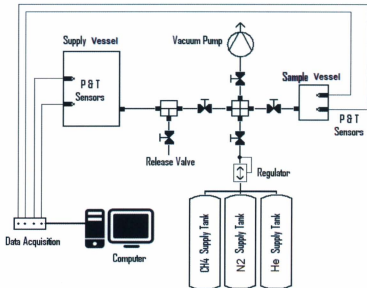


Figure 3-1: Apparatus Schematic.

3.1.3.2 - Supply & Sample Vessels

The supply and sample vessels were designed and constructed specifically to meet the requirements of the anticipated testing conditions. The supply vessel consists of a cylinder-like pressure vessel with the pressure and temperature sensors and gas line located along the axial section in the radial direction. The sample vessel consists of a cylinder-like pressure vessel with an o-ring sealed detachable top for sample loading. The pressure and temperature sensors and the gas line are also located along the axial section in the radial direction.

3.1.3.3 - Pressure & Temperature Sensors

Pressure and temperature sensors are located in both the supply and sample vessels. The pressure sensors consist of high accuracy micro-machined silicon pressure transducers (PX409) with a 1/4 national pipe thread tapered fitting (NPT), and were

obtained from Omega Engineering. The voltage output is 0 to 10 V which linearly corresponds to an absolute pressure range of 0 to 1000 psi. Temperature sensors consist of type E thermocouple pipe plug probes with a 1/8 NPT fitting. The pressure and temperature sensors are connected to a universal serial bus (USB) data acquisition module (OMB-DAQ-54) which is then interfaced to a personal computer where the sensor values can be recorded continuously over a specified time interval.

3.1.3.4 - Data Acquisition System

The data acquisition module is required to convert the pressure and sensor reading values into a form that is recognizable by a computer. More specifically, it converts the analog voltage signals to a digital signal which can be interpreted by a computer. The converted sensor signals are sent in real-time to Microsoft Excel where they can be viewed and manipulated. Using calibration data supplied by the sensor manufacturer, the digital voltage signals are then converted into the required pressure (Pa) and temperature (K) values.

3.1.3.5 - Vacuum Pump

The vacuum pump used consists of a belt driven dual stage rotary vane pump capable of achieving absolute pressures as low as 0.01 Pa. The vacuum pump is used to evacuate gas from the apparatus as well as remove any residual gas molecules that may have been adsorbed by a sample while at atmospheric conditions before an adsorption test is conducted.

3.1.3.6 - Valves & Supply Lines

All valves, line splitting blocks, and gas line tubing are constructed out of stainless steel and have a pressure rating in excess of 200 MPa.

3.1.3.7 - Testing Gas

Gases used for the adsorption testing process include methane, helium, and nitrogen. The gases were supplied by Air Liquide and are of high purity, although no universally accepted definition of what constitutes a high purity gas currently exists (Whitlock, 2000). The helium and nitrogen gas used were industrial grade with a 99.9 % purity rating, while the methane gas used had a purity rating of 99.995 %. The physical properties for each of the gases used are displayed in Table 3-1 below. T_{crit} and P_{crit} are the critical temperature and pressure respectively, ρ_{liq} is the density of liquefied gas and ρ_{STP} is the gas density at STP conditions. D_k is the effective kinetic diameter of a fluid molecule in the gaseous phase.

Table 3-1: Gas Properties.

	Methane (CH ₄)	Helium (He)	Nitrogen (N ₂)
M_M ($\frac{g}{mol}$)	16.04	4.00	28.01
T_{crit} (K)	190.3	5	126
P_{crit} (MPa)	4.60	0.23	3.3999
ρ_{liq} ($\frac{g}{cm^3}$)	0.423	0.125	0.809
ρ_{STP} ($\frac{g}{cm^3}$)	0.68×10^{-3}	0.17×10^{-3}	1.16×10^{-3}
D_k (nm)	0.38	0.27	0.37

3.1.4 - Design & Fabrication

3.1.4.1 - Vessel Volume Sizing

The first step in the apparatus design process was to determine appropriate volumes for the supply and sample vessels. This step was required to ensure that pressure changes caused by the adsorption process would be significant enough to be measured with acceptable accuracy. Evaluation parameters were chosen based on a

number of constraints and operational conditions. These constraints and requirements were as follows:

- 1) The supply chamber should not exceed a pressure 6 MPa while the final pressure of the apparatus should be at least 4 MPa at the end of the adsorption process.
- 2) The ratio of the pressure change resulting from the adsorption process and that resulting entirely from the volumetric expansion should be maximized.
- 3) The supply chamber must be evacuated no more than twice when conducting the reverse expansion to atmospheric pressure which is required for the desorption measurement process.

A simple theoretical model was constructed to approximate the amount of gas that may be adsorbed by a porous silicon sample during a typical adsorption experiment. The model involved taking a sample of known volume and porosity and assuming the free space was composed entirely of spherical non-interconnected pores of a constant chosen size. By specifying the size of the pores, the total surface area available for adsorption can then be calculated. Using this surface area in conjunction with the cross-sectional area of a methane molecule, the total maximum number of molecules which can be adsorbed can then be estimated. Applying multilayer adsorption simply involves reducing the effective radius of each pore by the thickness of the adsorbed layer and recalculating the available surface area using this new effective pore size. It was assumed that the adsorption process was limited to two layers in thickness. However, it was later found that this assumption may be incorrect as some researchers argue that supercritical adsorption is limited to monolayer coverage. The following model parameter values were either assumed or obtained from the literature (Atkins & Paula 2009; Bisi, Stefano, & Pavesi, 2000; Canham, 2006).

- 1) The volume of a sample was assumed to be at least 1 cm^3
- 2) The sample porosity was taken to be on the order of 60 to 70%
- 3) The sample specific surface area was assumed to be $500 \frac{\text{m}^2}{\text{cm}^3}$

- 4) The cross-sectional area of a methane molecule was taken as $0.16 \frac{\text{nm}^2}{\text{molecule}}$
- 5) The thickness of the adsorbed layer was assumed to be the longest length in the methane unit cell which is 0.25 nm.

Some general assumptions made in order to construct the model were as follows:

- 1) All pores are of the same volume and have a spherical geometry
- 2) Pores are not interconnected
- 3) There is no space between adjacent adsorbed molecules
- 4) The remaining volume of the pore (after adsorption has taken place) is filled with fluid at the applied bulk pressure
- 5) The adsorption process occurs at a temperature of 293 K
- 6) Gas quantities are approximated using the ideal gas law where applicable

The volume of each pore is assumed to be spherical. Thus the volume of each pore is given by:

$$V_o = \pi \frac{D_p^3}{6} \quad \text{Eq. 3-1}$$

where D_p is the average pore diameter.

The maximum volume allotted to empty pore space is:

$$V_a = V_s P_r \quad \text{Eq. 3-2}$$

where V_s is the total sample volume, and P_r is the sample porosity.

Combining equations 3-1 & 3-2 we get the theoretical maximum number of pores in the material which is given by:

Eq. 3-3

$$N_p = \frac{V_a}{V_o} = \frac{6V_S P_r}{\pi D_p^3}$$

For multilayer adsorption, the effective pore diameter for each pore made available to the adsorbate due to the presence of an adsorption layer is given by:

Eq. 3-4

$$D_{i,p} = (D_p - 2L_c(i - 1))$$

where $D_{i,p}$ is the effective pore diameter, L_c is the adsorbed layer thickness, and i is the i^{th} layer number.

Thus the adsorption area available at the i^{th} layer for each pore is:

Eq. 3-5

$$A_{i,p} = \pi (D_p - 2L_c(i - 1))^2$$

The pore volume available for bulk pressure storage after the i^{th} layer is adsorbed is given by:

Eq. 3-6

$$V_{i,p} = \frac{\pi}{6} (D_p - 2L_c(i))^3$$

Thus, the total area made available for adsorption is:

Eq. 3-7

$$A_{tot} = N_p \sum_{i=1}^n A_{i,p} = \frac{V_S P_r}{D_p^3} \sum_{i=1}^n (D_p - 2L_c(i - 1))^2$$

The total number of moles of gas inside the material pores in the free fluid phase ($n_{p,t}$) is given by the ideal gas law:

Eq. 3-8

$$n_{p,t} = \sum_{i=1}^n \frac{P V_{i,p}}{Z R T}$$

where P is the gas pressure, $V_{i,p}$ is the gas volume, Z is the gas compressibility factor, R is the universal gas constant, and T is the gas temperature.

The total number of molecules effectively contained by the porous material is the number of molecules in the adsorbed phase $N_{m,a}$, plus the number in the free fluid phase within the material pores $N_{m,p}$:

Eq. 3-9

$$N_{m,t} = N_{m,a} + N_{m,p}$$

where

Eq. 3-10

$$N_{m,a} = \frac{A_{tot}}{A_m} = \frac{V_S P_r}{A_m D_p^3} \sum_{i=1}^n (D_p - 2L_c(i-1))^2$$

and

Eq. 3-11

$$N_{m,p} = n_{p,t} N_A = \frac{P V_{i,p} N_A}{Z R T} = \frac{P N_A \pi}{R T Z 6} (D_p - 2L_c(i))^3$$

where N_A is Avogadro's number and A_m is the cross-sectional area of a methane molecule.

Substitution of 3-10 and 3-11 into 3-9 gives the maximum number of moles of gas stored by a sample:

$$n_{m,t} = \frac{6 V_S P_r}{N_A A_m D_p^3} \sum_{i=1}^n (D_p - 2Lc(i-1))^2 + \frac{P V_S P_r}{Z R T D_p^3} \sum_{i=1}^n (D_p - 2Lc(i-1))^3 \quad \text{Eq. 3-12}$$

Using equation 3-12 the expected pressure change due to adsorption by a sample can now be estimated for a given supply vessel volume V_1 and given sample vessel volume V_2 . Below, Figure 3-2 depicts the volumetric adsorption setup.

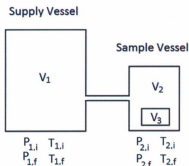


Figure 3-2: Volumetric adsorption setup.

By recognizing that the amount of gas present in the system remains constant, the following equation can be written which relates the initial and final conditions in each volume:

$$n_{1,i} = n_{1,f} - n_{2,i} + n_{2,f} + n_3 \quad \text{Eq. 3-13}$$

where $n_{1,i}$ and $n_{1,f}$ are the initial and final number of moles of gas located in the supply vessel; $n_{2,i}$ and $n_{2,f}$ is the initial and final number of moles of gas located in the sample vessel; and n_3 is the number of moles stored by the adsorbent that does not contribute to the bulk gas pressure in sample volume (V_2). Since the sample vessel is degassed, the number of moles of gas initially present in this volume can be assumed to be zero ($n_{2,i} \approx 0$).

Applying the ideal gas law to equation 3-13 gives:

Eq. 3-14

$$\frac{(P_{1,i} V_1)}{Z_{1,i} R T_{1,i}} = \frac{(P_{1,f} V_1)}{Z_{1,f} R T_{1,f}} + \frac{(P_{2,f} (V_2 - V_3))}{Z_{2,f} R T_{2,f}} + n_3$$

Assuming a constant temperature throughout the process and using an average compressibility factor that was approximated based on the expected overall pressure range during the adsorption process (0 to 3.5 MPa) gives:

Eq. 3-15

$$(P_{1,i} V_1) = (P_{1,f} V_1) + (P_{2,f} (V_2 - V_3)) + n_3 R T Z_{avg}$$

The total pressure change in the supply vessel is therefore given by:

Eq. 3-16

$$\Delta P_{1,tot} = \frac{(P_{2,f} (V_2 - V_3))}{V_1} + \frac{(n_3 R T Z_{avg})}{V_1}$$

where the pressure change in the supply vessel solely due to adsorption is given by:

Eq. 3-17

$$\Delta P_{1,ads} = P_{1,i} - \frac{Z_{avg} (n_{1,i} - n_3) R T}{V_1}$$

and the pressure change in the supply vessel solely due to volumetric expansion is given by:

Eq. 3-18

$$\Delta P_{vol} = P_{1,i} - \frac{Z_{avg} (n_{1,i} - n_{2,f}) R T}{(V_1 + V_2 - V_3)}$$

The volumes of the supply and sample vessels were chosen such that $\frac{\Delta P_{1,ads}}{\Delta P_{vol}}$ was maximized and ΔP_{vol} was minimized while adhering to the constraints previously

listed. This analysis resulted in theoretical volumes for the supply and sample vessels of 500 cm³ and 50 cm³ respectively.

3.1.4.2 - Supply Vessel

The supply vessel consists of a 4 inch diameter, 7 inch long tubular pressure vessel composed of a 316 stainless steel metal alloy. It was fabricated by hollowing a section of solid bar stock, and welding an end cap to complete the enclosure. The vessel was designed to have a volumetric capacity of 500 cm³. However, volume measurements of the vessel made by water volume filling revealed that the volume of the vessel was actually 482.4 cm³. The difference between the theoretical and actual volumes can be attributed to molten metal burn through during the welding of the end cap to the main vessel body, and tolerances used in the machining process. The volume of the vessel was later further reduced by adding aluminum beads and steel balls to enhance the adsorption process measuring sensitivity. Holes required to facilitate the pressure and temperature sensors, and gas supply line, are located at equal distances along the radial direction and are offset along the axial direction to minimize stress concentration. Figure 3-3 displays an isometric drawing of the supply chamber and end cap.

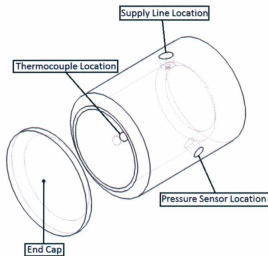


Figure 3-3: Isometric drawing of supply vessel.

3.1.4.3 - Sample Vessel

The sample chamber consists of a 3 inch diameter, 1.75 inch long tubular pressure vessel, and like the supply vessel it is also composed of a 316 stainless steel metal alloy. Unlike the supply vessel, the sample vessel was required to have a removable portion to enable the loading and unloading of test samples. To seal the chamber, a flange type flat-faced o-ring seal design was utilized. The chamber top is secured using eight high strength hex head cap screws. Holes required to facilitate the pressure and temperature sensors, and gas supply line, are located at equal distances along the radial direction and are offset along the axial direction to minimize stress concentration. The internal volume of the sample chamber was designed to be 50 cm³, however factors such as sample container volume and sample dead space volume were not taken into consideration during the design phase. The actual effective volume of the vessel is approximately 32.5 cm³, which was obtained through

helium and methane gas expansion tests. Figure 3-4 displays an isometric drawing of the sample vessel and top.

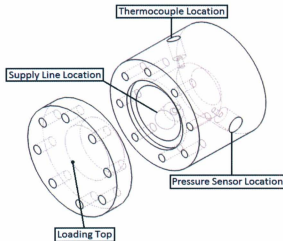


Figure 3-4: Isometric drawing of sample vessel.

3.1.4.4 - Drafting & Analysis

The supply and sample vessels were drafted and modeled using the Solid Works 2009 software package. Finite Element Analysis (FEA) was conducted on the vessel models to ensure safety requirements were met. Static pressure tests were conducted using an internal pressure of 10 MPa. This resulted in a minimum factor of safety of 1.85 for the supply vessel and 4.65 for the sample vessel. However, operational pressures rarely exceed 5 MPa which would produce a factor of safety of 3.95 for the supply vessel and 9.94 for the sample vessel. Figure 3-5 displays the factor of safety plots for both vessels which is essentially a stress distribution plot.

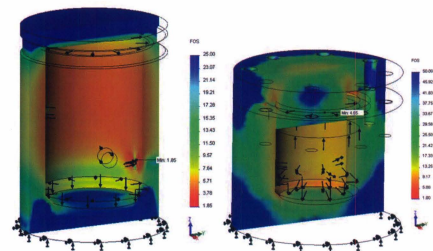


Figure 3-5: Finite Element Analysis of supply & sample vessels.

3.1.5 - Operation

3.1.5.1 - Sectional Volume Determination

In order to employ the volumetric technique of adsorption measurement, the volume of all sections of the apparatus must be known. Figure 3-6 displays a schematic of the apparatus with its various sections identified. The volumes of the supply vessel and valves located in section S1 were calculated through water volume filling. A burette with a measuring uncertainty of ± 0.02 ml was used to fill the volumes with water to determine their volumetric capacity. After each filling, the supply vessel was emptied and heated to approximately 300 °C using a hotplate to remove any remaining water. Valves were cleared of any water by running compressed helium through them. A total of eight measurements were made for the supply vessel, giving a total volume of 482.8 ± 0.3 ml. The volume of the 3-way line was also determined using water filling. The volume occupied by the thermocouple in the supply chamber was calculated by measuring the protruding portion of the thermocouple using a caliper. The pressure

sensor does not protrude into the supply chamber volume and thus its volume does not need to be accounted for. The volume of the tubing was calculated by taking length and internal diameter measurements using a caliper. The total section S1 volume was thus calculated to be 483.6 ± 0.3 ml. This volume was later reduced to 325.0 ± 0.3 ml by adding aluminum beads and steel balls of known volume to increase gas measurement accuracy during expansion from section S1. With the volume of section S1 known, the volume of the remaining apparatus sections can be obtained from gas expansions.

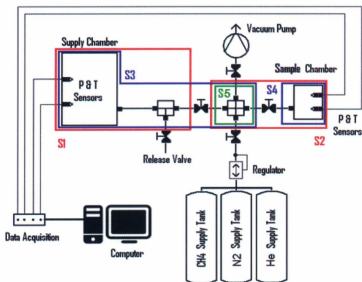


Figure 3-6: Apparatus sectional identification schematic.

The volume of section S2 was obtained by expanding gas from section S1 to the remainder of the apparatus volume. A total of 42 helium expansions were conducted to obtain a S2 section volume of 37.23 ± 0.08 ml. The use of a standard-sized sample container was later employed which required the expansion measurements to be conducted again. Prior to this, samples were not contained using any additional

container located inside the sample vessel. A total of 15 helium expansions were conducted to obtain a S2 section volume of 32.21 ± 0.08 ml. Expansion measurements were also conducted using methane and nitrogen gas. A total of 17 methane expansions were conducted, giving a volume of 32.5 ± 0.1 ml. A total of 10 nitrogen gas expansions were also conducted giving a volume of 31.0 ± 0.1 ml. Although methane and nitrogen gas will adsorb on the internal walls of the sample vessel, surface areas are too small to produce any significant amount of error in the volume measurements. Differences between the volume values obtained with each gas are thought to be due to inaccuracies in the equations of state utilized. For example, using the Van der Waals equation of state to describe methane gas expansions produces an average volume of 32.98 ml; a difference of 0.45 ml between that and the value obtained while using the Modified-BWR equation of state. It was assumed that the equation of state used for methane (Modified-BWR) produced the most accurate values since this equation is of much higher order and contains many more fitting parameters which were determined through experimentation based on a chosen pressure range. Thus, the final apparatus sectional volume values were obtained through the use of methane gas. Further details regarding the equations of state utilized are discussed in Section 3.1.2. Differences in volume measurements obtained from the different gases were used as correction factors when conducting sample dead space volume measurements. Since helium is required for sample dead space measurements, general expansion deviations between it and the gas used for the adsorption process would have to be corrected. For example, adsorption tests using methane would require a correction by adding 0.31 ml to the sample dead space volume obtained by helium. Adsorption tests conducted using nitrogen would require subtracting 1.22 ml from the sample dead space volume obtained by helium. These correction values are simply the differences between the volume values obtained with methane and that of the adsorption testing gas. Failure to correct the volume difference would result in increased error in adsorption measurements since the sample volume would be incorrect with respect to the adsorbate being used.

Figures 3-7 and 3-8 show the volume expansion values obtained with each gas for section S2 before and after adjusting the values.

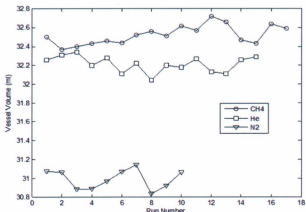


Figure 3-7: Sample vessel volume values obtained via gas expansion.

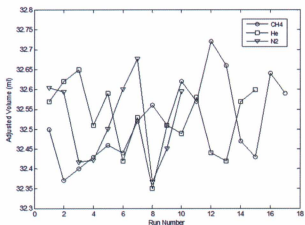


Figure 3-8: Adjusted sample vessel volume values obtained via gas expansion.

The volume of section S5 was obtained by expanding methane gas from section S1 into section S5. The combined volumes of sections S1 and S5 define section S3. A total

of 12 expansions were conducted giving a total section S5 volume of 1.7 ± 0.1 ml. Using the volume values of sections S1, S2, and S3, the volume of section S4 was then calculated to be 30.9 ± 0.1 ml. The volume of section S4 which includes the sample chamber is required in order to conduct a desorption test.

3.1.5.2 - Operational Test Procedures

3.1.5.2.1 - Sectional Volume Determination Procedure

To determine the volume of the sample chamber and connecting tubing using a gas expansion, the procedure is as follows:

- 1) Fill the supply vessel with the appropriate gas. Random expansion pressures should be chosen in the adsorption testing range (0 - 5 MPa).
- 2) Isolate the supply vessel and evacuate the remaining apparatus volume.
- 3) Expand the gas from the supply vessel into the sample vessel until equilibrium is established.
- 4) Calculate the volume of the sample chamber based on the initial and final conditions of the system (details presented in Section 3.3).

The same procedure is also used for determining sample volumes for calculating excess adsorption isotherms.

3.1.5.3 - Adsorption Test Procedures

The testing procedure for conducting an adsorption test is as follows:

- 1) The apparatus is opened to atmospheric conditions.
- 2) A sample is placed inside the sample vessel and the vessel top is secured in place.
- 3) The sample vessel is isolated and the supply vessel is filled with an adequate amount of adsorbate.
- 4) The supply vessel is isolated and the remaining apparatus is evacuated using the vacuum pump.

- 5) Once each vessel has reached equilibrium, the gas located in the supply vessel is expanded into the sample vessel at the desired expansion rate.
- 6) Pressure and temperature measurements are taken continuously throughout the expansion process in the supply and sample vessels.
- 7) The adsorption process is complete when the pressure and temperature inside the supply and sample vessels are equal and remain constant.
- 8) The amount adsorbed is calculated by comparing the amount of gas present in the sample vessel, to the amount of gas that should be in the sample chamber according to the conditions in the supply vessel.

3.1.5.4 - Desorption Test Procedure

The desorption test procedure is essentially the same as the adsorption procedure but in reverse. The procedure for conducting a desorption test is as follows:

- 1) Upon completion of the adsorption process, the sample chamber is isolated from the rest of the apparatus.
- 2) The supply vessel and remaining apparatus is then evacuated using the vacuum pump.
- 3) The gas located in the sample vessel is expanded into the supply vessel at the desired rate until the two vessels reach an equilibrium state.
- 4) Pressure and temperature measurements are taken continuously throughout the expansion process in the supply and sample vessels to calculate the amount of gas desorbed.

In order to conduct a desorption test to atmospheric pressure, the desorption procedure must be conducted twice. That is, upon reaching equilibrium after the first desorption expansion, the supply vessel is evacuated again and another expansion is performed. This step is required because the pressures inside the sample vessel will still be above atmospheric conditions upon completion of the first desorption expansion. Thus, in order to obtain desorption values for pressure values

corresponding to atmospheric conditions and below, the test must be conducted again using the final pressure of the first desorption expansion as the initial pressure for the second desorption expansion.

3.1.5.5 - Trouble Shooting & Modification

Upon constructing the apparatus, a number of problems were encountered which prevented the apparatus from producing accurate test results. These problems were gas leaks, inadequate temperature control, and difficulty in setting the gas expansion rate.

3.1.5.5.1 - Leak Test

Initial operational tests of the apparatus revealed leaks were present in the system when pressurized to the maximum operating pressure. Using a helium leak detector, vacuum pressure and high positive pressure leak tests were conducted on the apparatus. Tests indicated that the leaks were originating from the temperature sensors. Further investigation revealed that the incorrect thermocouple had been specified by the product supplier. Replacement of the thermocouples with the correct ones remedied the leak problem.

3.1.5.5.2 - Temperature Control

Another problem that presented itself was the sensitivity of the apparatus to changes in the temperature of surrounding environment. Relatively quick uncontrollable temperature changes in the environment combined with uneven heating or cooling of the apparatus sections produced increased error in the adsorption measurements. For example, since the environment surrounding the testing apparatus (laboratory room) is fairly small, running the vacuum pump and other heat emitting devices such as a hot plate for extended periods of time causes an increase in the temperature of the apparatus and surrounding environment. Halting operation of the pump prior to starting an adsorption test will cause the temperature to decrease during the testing

process. This change can be much larger and can occur faster if the surrounding environment is opened to another environment which has a lower temperature (opening door between lab room and hallway). A good solution to the problem would have been to insulate and isolate the apparatus from its surroundings and utilize a temperature control system to maintain a constant temperature in the region closely surrounding the apparatus. Although this particular solution was not employed, the problem was greatly alleviated by covering the entire apparatus with multiple layers of insulating cloth to prevent any sudden heat transfer between it and its surroundings.

3.1.5.5.3 - Gas Expansion Rate Control

Increased expansion rates often result in increased measurement error during the adsorption process due to the compressibility of the gas flow when passing through the regulating valve, and an increased event time delay between the two measurement locations in the apparatus. Also, high expansion rates prevent the adsorption process from proceeding in a quasi-equilibrium fashion which would also produce measuring error. During the adsorption process, expansion of the gas is controlled by a manual high pressure valve. However, the valve used was too responsive when opening to accurately achieve the small flow rates required. To attain these flow rates the valve had to be delicately tapped open rather than assigning any measurable turn by hand. Since it was practically impossible to assign specific expansion rates, rates often varied between tests. Deviations in the isotherms for different runs with a given sample are in part due to this issue. Typically, expansion rates were on the order of 50 to 200 $\frac{\text{STP cm}^3}{\text{hr}}$. Expansion rates in this range were essentially the minimum attainable with the expansion control valve used. However, rates were generally low enough to allow a quasi-equilibrium process and prevent the occurrence of any considerable error. A solution to the problem would be to install a sensitive needle control valve to adjust the flow rate.

3.2 - Sample Adsorption Preparation

3.2.1 - Volume & Mass Measurements

Prior to testing a sample, various volume and mass measurements are required in order to obtain the performance characteristics of the sample material. The sample dead space volume and packed volume are used to establish the volumetric performance, while the mass of the sample allows one to establish the mass storage performance of the adsorbent material.

3.2.1.1 - Dead Space Volume

In order to determine the excess amount adsorbed by a material, the dead space volume must be determined. It is essentially the dense structural volume of an adsorbent material where no gas molecules can be located. To determine the dead space volume, the sample is subject to a helium expansion test. Helium gas expansion is the standard method for determining the dead space volume of a material since the gas is inert and does not adsorb in any measureable amount at pressures below 10 MPa (Malbrunot et al., 1997). This approach measures essentially all the volume that is accessible to an adsorbate gas. The dead space volume is obtained as follows:

$$V_d = V_{sys} - V_{mes}$$

Eq. 3-19

where V_d is the dead space volume, V_{sys} is the volume of the sample vessel and sample holding container without a sample present, and V_{mes} is the measured volume of the sample vessel when the sample is loaded. Note that V_{mes} is also the bulk gas phase volume V_{blk} . For each test sample, an average of three dead space volume measurements was used.

3.2.1.2 - Packed Volume

The packed volume is the overall external boundary volume of an adsorbent material if it were packed into a vessel of some arbitrary volume. It is used to calculate the

effective storage of a material and when specifying the overall volumetric performance of an adsorbent via the parameters $\frac{V_{ads}}{V_p}$, $\frac{m_{ads}}{V_p}$, $\frac{n_{ads}}{V_p}$, where V_p is the sample packed volume. Adsorption quantities obtained while using the packed volume are also referred to as effective storage densities. Since the sample testing containers had a volume of approximately 10 ml, sample packed volumes were limited to a maximum value of 10 ml.

Depending on the nature of the sample, the packing volume may be measured by a variety of methods. Since the effective storage performance is largely dependent on the material packing density, the packing density of the materials were maximized to ensure optimal performance was obtained. For materials consisting of a powdered or granulated form, the packing density was typically taken as the maximum natural packing density. The maximum natural packing density is simply the maximum density achievable without the application of any external compressive force. To achieve this density the sample was subject to a vibratory disturbance while located in a 10 ml graduated cylinder. The volume is measured when successive disturbances fail to reduce the sample volume any more. Typically, sample material is added to the measuring volume until a packed volume of 10 ml is obtained. For the case of carbon cloth, the material was wrapped to form a 10 ml cylindrical plug while applying a maximum tensile force to ensure a high wrapping/packing efficiency.

For the case of structurally continuous materials such as electrochemically etched porous silicon produced on silicon wafers, the packing volume can be obtained from measuring the etched area and calculating the theoretical thickness based on etching models found in literature, or through direct measurement using devices such as a scanning electron microscope (SEM) (Lehmann, 2002). For these types of materials, the dead space volume can be calculated by using the packed volume in conjunction with the material porosity instead of using the gas expansion method. The dead space volume would then be given by:

$$V_d = (1 - P_r)V_p$$

For the case of structurally discontinuous materials such as powders, an overall material porosity that includes the sample packing density can be obtained from the dead space volume and packing volume as follows:

$$P_r = \frac{V_d}{V_p}$$

3.2.1.3 - Mass

To determine the mass performance of an adsorbent, its mass prior to adsorption must be known. Sample mass measurements were obtained using a microbalance which has a repeatability accuracy of ± 0.00002 g. An average of three mass measurements was used for each sample.

3.2.2 - Degassing

Prior to conducting an adsorption test, the sample must be degassed. Degassing involves removing any molecules that may be adsorbed during exposure of the material to atmospheric conditions. This is done by subjecting the sample to a vacuum and sometimes applying heat simultaneously. Failure to degas a sample would result in an error in the maximum measurable amount of gas that can be adsorbed since the residual adsorbed gases will constitute an immeasurable portion of the material's total adsorption capacity. This would produce false performance characteristics which would always be lower than the true values. All samples presented in this thesis were degassed by subjecting them to a vacuum only since the apparatus was not equipped with heating capabilities. Samples were subject to degassing for a period of approximately 3 hours prior to conducting a test. Although it is commonly found in literature that samples are degassed for upwards of 12 hours, experimentation revealed that no measurable change occurred in the total amount

of gas adsorbed for a given sample once degassing times surpassed approximately 3 hours. In actuality, one needs only to wait until the minimum vacuum pressure of the system is attained. Once this point is reached, the passing of time will not remove any more molecules provided sufficient time is allowed for the diffusion of the initially detached molecules when reaching the minimum pressure.

3.2.3 - Sample Containment

Samples were contained using specialized plastic sample containers. The containers are composed of high density polyethylene and consist of a fully hollow cylindrical body with snap-rings that fit on each end. The rings are used to secure the top and bottom of the container which consists of thin polypropylene films. A clear polypropylene film is secured to the bottom of the container which allows for sample viewing, and an opaque microporous polypropylene film is secured to the top of the container to allow for pressure equalization while preventing the loss of any particulate material to the surrounding sample vessel. The containers have a maximum volume of 10 ml.

3.2.4 - Dehydrating

Some materials tested such as the Zeolites and Silica Gels are desiccants, which mean they will adsorb water from their surrounding environment. This water occupies valuable pore space and should be removed before conducting an adsorption experiment. Samples were exposed to temperatures in the range of 120 to 200 °C in glass vials open to atmospheric conditions for a minimum of 48 hours to remove any adsorbed moisture. Samples were placed in the testing apparatus immediately following removal from the heat source to prevent the readsorption of any moisture onto the material surface and bulk porous volume.

3.3 - Adsorption Isotherm Calculation

3.3.1 - Introduction

Adsorption isotherms are plots depicting the amount of fluid adsorbed with respect to the applied bulk gas pressure at a given constant temperature. For our purposes, the area of supercritical adsorption can be divided into the following categories: Excess Adsorption, Absolute Adsorption, and Effective Storage. For engineering applications, excess adsorption and effective storage are the most commonly utilized forms. Both forms are significantly different although they produce results of equal value.

3.3.2 - Equation of State

3.3.2.1 - Introduction

An equation of state can be generally defined as a thermodynamic equation describing the state of matter under a given set of physical conditions. More specifically, it relates state variables such as pressure, temperature, and specific volume to the physical state of matter in a system. Equations of state are very useful in describing the properties of fluids, fluid mixtures, and solids. There are a reasonably large number of equations developed for both pure substances and substance mixtures. Most equations are of a general form and can be applied to many different substances. These equations simply require the determination of constants that are characteristic of the particular substance. Some common equations of state that can be utilized to describe methane, helium, and nitrogen are the Ideal Gas Law, Van der Waals, Redlich-Kwong, Berthelot, Modified Berthelot, Dieterici, Clausius, Virial Expansion, Peng and Robinson, Wohl, Beattie-Bridgeman, Benedict-Webb-Rubin (BWR), and the Modified Benedict-Webb-Rubin (MBWR) (Graham & Szczepanski, 1982; Schamp, Mason, Richardson, & Altman, 1954; Sievers & Schulz, 1980). Although each of the equations listed are rather general in nature, they do exhibit differing amounts of accuracy in different state variable regions. Thus, no one

equation can be considered best for all state variable regions. Often the choice of which equation to be used is based on a combination of the desired accuracy and the ease of use.

3.3.2.2 - Methane

All experiments conducted using methane gas were described using a 32 term Modified Benedict-Webb-Rubin (MBWR) equation of state. The equation was developed by Graham Saville and Richard Szczepanski for pure methane, and each of the 32 fitting terms contained in the equation was determined through physical experimentation (Graham & Szczepanski, 1982). This equation is very accurate over a wide range of state variables and was thus considered the most appropriate for the experiments conducted for this thesis. The equation is as follows:

Eq. 3-22

$$\begin{aligned}
 P = & \rho R T + (\rho^2) \left(A1 T + A2 (T^{0.5}) + A3 + \frac{A4}{T} + \frac{A5}{T^2} \right) \\
 & + (\rho^3) \left(A6 T + A7 + \frac{A8}{T} + \frac{A9}{T^2} \right) + (\rho^4) \left(A10 T + A11 + \frac{A12}{T} \right) \\
 & + (\rho^5) A13 + (\rho^6) \left(\frac{A14}{T} + \frac{A15}{T^2} \right) + (\rho^7) \frac{A16}{T} + (\rho^8) \left(\frac{A17}{T} + \frac{A18}{T^2} \right) \\
 & + (\rho^9) \frac{A19}{T^2} \\
 & + (\rho^3) e^{(-\gamma(\rho^2))} \left(\left(\frac{A20}{T^2} + \frac{A21}{T^3} \right) + (\rho^2) \left(\frac{A22}{T^2} + \frac{A23}{T^4} \right) \right) \\
 & + (\rho^4) \left(\frac{A24}{T^2} + \frac{A25}{T^3} \right) + (\rho^6) \left(\frac{A26}{T^2} + \frac{A27}{T^4} \right) + (\rho^8) \left(\frac{A28}{T^2} + \frac{A29}{T^3} \right) \\
 & + (\rho^{10}) \left(\frac{A30}{T^2} + \frac{A31}{T^3} + \frac{A32}{T^4} \right)
 \end{aligned}$$

where P is the gas pressure, T is the gas temperature, ρ is the molar density, R is the universal gas constant, and the coefficients $A1$ through $A32$ and γ are empirical fitting parameters.

Table 3-2 displayed below gives the values for each of the equation constants.

Table 3-2: Modified BWR equation of state coefficients.

Modified BWR Coefficients							
A1	8.98E-05	A10	2.03E-13	A19	-4.97E-29	A28	2.05E-34
A2	1.89E-02	A11	-8.83E-11	A20	4.27E-01	A29	4.06E-32
A3	-5.07E-01	A12	2.70E-07	A21	-1.25E+02	A30	-8.73E-43
A4	2.42E+01	A13	1.63E-14	A22	-1.02E-08	A31	-3.82E-41
A5	-2.76E+03	A14	-9.66E-16	A23	7.89E-05	A32	5.33E-40
A6	6.68E-09	A15	-4.98E-14	A24	-3.75E-18	γ	9.70E-09
A7	6.60E-06	A16	3.88E-20	A25	1.27E-15	R	8.314
A8	-4.75E-03	A17	-4.47E-25	A26	-2.36E-25		
A9	9.42E-01	A18	2.81E-23	A27	-1.23E-21		

Since pressure and temperature are the measured independent variables during an adsorption experiment, the molar density is the unknown that must be determined. However, since the above equation cannot be solved in terms of ρ using analytical methods, numerical techniques such as the Newton-Raphson method must be employed.

3.3.2.3 - Helium & Nitrogen

All experiments conducted using helium or nitrogen gas are described using the Redlich-Kwong equation of state. The equation is as follows:

$$p = \frac{RT}{\frac{1}{\rho} - b} - \frac{a\rho}{\sqrt{T}(\frac{1}{\rho} + b)} \quad \text{Eq. 3-23}$$

where

$$a = \frac{0.42748 R^2 T_c^2}{P_c} \quad \text{Eq. 3-24}$$

and

$$b = \frac{0.08662 R T_c}{P_c}$$

and T_c and P_c are the critical temperature of the gas being described.

As with the Modified BWR equation, the Redlich-Kwong equation must also be solved using numerical techniques and with the aid of a numerical software package such as MATLAB. Further details regarding the utilization of the equations of state are presented in the next section.

3.3.3 - Isotherm Calculation Methodology

3.3.3.1 - Isotherm Calculation Procedure

The calculations required to obtain the adsorption data and plot the adsorption isotherms were completed using the MATLAB software package. The raw sensor data points are recorded in Microsoft Excel during the experiment process. The data is then transferred to MATLAB where it is manipulated to produce the adsorption data and isotherm plots. A program was written in MATLAB to automate the manipulation and calculation process. The code for the program is located in appendix A1. Automating the calculation procedure was necessary since the large number of data points recorded during a test would be very time consuming to analyze manually. Typically, anywhere from 10,000 to 15,000 test points are recorded for each sensor during a test. Thus, the isotherms constructed from the data have a very high resolution.

As previously mentioned, the bulk gas density in each of the gas vessels is calculated by using the Newton-Raphson method to numerically solve the appropriate equation of state. The Newton-Raphson equation is written as:

Eq. 3-26

$$x_{i+1} = x_n - \frac{f(x_i)}{f'(x_i)}$$

Solving Newton's equation requires an iterative procedure where convergence is established when the difference between successive x_i values falls below some specified error value. In this case, the error value was specified to be 0.001% when solving the respective equation of state. The iterative procedure was conducted by the MATLAB program previously mentioned.

Newton's method can be applied to the equations of state by substituting the independent variable x with the molar gas density ρ , and setting the function $f(x_i)$ as the appropriate equation of state.

Eq. 3-27

$$x_i = \rho_i$$

Eq. 3-28

$$f(x_i) = f_{EOS}(\rho_i, P, T)$$

Using the Mathematica software suite, the derivatives of each of the equations of state were calculated. The functions and their first derivatives are shown below for both the Redlich-Kwong and Modified BWR equations.

The Redlich-Kwong equation of state function and its first derivative is given as:

Eq. 3-29

$$f_{RK} = -p + \frac{RT}{\frac{1}{\rho} - b} - \frac{a\rho}{\sqrt{T}(\frac{1}{\rho} + b)}$$

Eq. 3-30

$$f'_{RK} = -\frac{a}{\sqrt{T}(b + \frac{1}{\rho})} - \frac{RT}{(-b + \frac{1}{\rho})^2 \rho^2} - \frac{a}{\sqrt{T}(b + \frac{1}{\rho})^2 \rho}$$

The Modified BWR equation of state function and its first derivative is given as:

Eq. 3-31

$$\begin{aligned}
 f_{MBWR} = & -P + \rho RT + (\rho^2)(A1T + A2(T^{0.5}) + A3 + \frac{A4}{T} + \frac{A5}{T^2}) + (\rho^3)(A6T + A7 \\
 & + \frac{A8}{T} + \frac{A9}{T^2}) + (\rho^4)(A10T + A11 + \frac{A12}{T}) + (\rho^5)A13 + (\rho^6)(\frac{A14}{T} \\
 & + \frac{A15}{T^2}) + (\rho^7)\frac{A16}{T} + (\rho^8)(\frac{A17}{T} + \frac{A18}{T^2}) + (\rho^9)\frac{A19}{T^2} \\
 & + (\rho^3)e^{(-\gamma^*(\rho^2))}(\frac{A20}{T^2} + \frac{A21}{T^3}) + (\rho^2)(\frac{A22}{T^2} + \frac{A23}{T^4}) + (\rho^4)(\frac{A24}{T^2} + \frac{A25}{T^3}) \\
 & + (\rho^6)(\frac{A26}{T^2} + \frac{A27}{T^4}) + (\rho^8)(\frac{A28}{T^2} + \frac{A29}{T^3}) + (\rho^{10})(\frac{A30}{T^2} + \frac{A31}{T^3} + \frac{A32}{T^4})
 \end{aligned}$$

Eq. 3-32

$$\begin{aligned}
 f'_{MBWR} = & \frac{1}{e^{\gamma\rho^2}} 3\rho^2(\frac{21A}{T^3} + \frac{20A}{T^2} + \rho^6(\frac{27A}{T^4} + \frac{26A}{T^2}) + \rho^2(\frac{23A}{T^4} + \frac{22A}{T^2}) + \rho^8(\frac{29A}{T^3} + \frac{28A}{T^2}) \\
 & + \rho^4(\frac{25A}{T^3} + \frac{24A}{T^2}) + \rho^{10}(\frac{32A}{T^4} + \frac{31A}{T^3} + \frac{30A}{T^2})) - \frac{1}{e^{\gamma\rho^2}} 2\gamma\rho^4 \text{Log}[e](\frac{21A}{T^3} \\
 & + \frac{20A}{T^2} + \rho^6(\frac{27A}{T^4} + \frac{26A}{T^2}) + \rho^2(\frac{23A}{T^4} + \frac{22A}{T^2}) + \rho^8(\frac{29A}{T^3} + \frac{28A}{T^2}) + \rho^4(\frac{25A}{T^3} \\
 & + \frac{24A}{T^2}) + \rho^{10}(\frac{32A}{T^4} + \frac{31A}{T^3} + \frac{30A}{T^2})) + \frac{1}{e^{\gamma\rho^2}} \rho^3(6\rho^5(\frac{27A}{T^4} + \frac{26A}{T^2}) \\
 & + 2\rho(\frac{23A}{T^4} + \frac{22A}{T^2}) + 8\rho^7(\frac{29A}{T^3} + \frac{28A}{T^2}) + 4\rho^3(\frac{25A}{T^3} + \frac{24A}{T^2}) + 10\rho^9(\frac{32A}{T^4} \\
 & + \frac{31A}{T^3} + \frac{30A}{T^2})) + \frac{171A\rho^8}{T^2} + 8\rho^7(\frac{18A}{T^2} + \frac{17A}{T}) + 6\rho^5(\frac{15A}{T^2} + \frac{14A}{T}) \\
 & + 3\rho^2(\frac{9A}{T^2} + 6AT + \frac{8A}{T} + 7A) + 2\rho(2AT^{0.5} + \frac{5A}{T^2} + AT + \frac{4A}{T} + 3A) \\
 & + \frac{112A\rho^6}{T} + 4\rho^3(10AT + \frac{12A}{T} + 11A) + 65A\rho^4 + RT
 \end{aligned}$$

Using the convergent values obtained from Newton's method, the number of moles of gas present in a vessel of arbitrary volume is given by:

Eq. 3-33

$$n_i = \rho_i V$$

By realizing that any gas adsorbed will appear as missing gas if only measuring pressure and temperature; the number of moles of gas adsorbed can be determined

by a molar balance between the initial conditions and the conditions at any measurement point i taken at any time thereafter.

$$n_{a,i} = n_{1,1} + n_{2,1} - n_{1,i} - n_{2,i} \quad \text{Eq. 3-34}$$

The volume of gas adsorbed when taken at standard conditions is approximated using the ideal gas law. The mass adsorbed is simply the product of the moles adsorbed and the gas molar mass.

$$V_{STP,i} = \frac{n_{a,i} R T_{STP}}{P_{STP}} \quad \text{Eq. 3-35}$$

$$m_{a,i} = n_{a,i} M_M \quad \text{Eq. 3-36}$$

3.3.3.2 - Volume Determination Calculation Procedure

Since the equations of state utilized could not be solved analytically for an unknown vessel volume, a numerical approach was required. Thus, calculating the volume of an apparatus section or sample dead space using the volume expansion procedure discussed earlier is conducted as follows.

A specified range of volume values is chosen for the unknown vessel, sample, or apparatus section volume. The total number of moles of gas present in the system is then calculated for each of the volume values in the specified range. By recognizing that during a volume expansion no gas should appear as missing, a molar balance can be used to define an error equation. The equation will produce zero if the correct volume is used, otherwise it will be either positive or negative. The error equation is as follows:

$$f_{err,i} = n_{1,i} + n_{2,i} - n_{1,i} - n_{2,i}$$

For each volume value, the error equation is applied to obtain the error for each measurement point. The overall error for each volume value is found by taking the sum of the squares of the error values. Using MATLAB, minimization analysis was applied to the set of the sum of squares values to obtain the minimum error value and the volume that corresponds to it. This volume is then taken as the true vessel or sample volume.

$$SS_{err,j} = \sum_{i=1}^n (f_{err,i})^2$$

3.3.4 - Isotherm Data Fitting

3.3.4.1 - Introduction

Isotherm models were used to describe the adsorption data obtained from the experiments. The MATLAB software package was utilized to obtain the fitting parameter values for the isotherm models that allowed them to describe the data most accurately. The isotherm models utilized are discussed below.

3.3.4.2 - Theoretical Isotherm Models

The Freundlich equation was developed in 1906 by Herbert Freundlich and was the first isotherm model (Freundlich, 1906). It is an entirely empirical model which relates the concentration of a fluid in the bulk fluid phase to the concentration of that fluid in the adsorbed phase. Although the equation was originally developed for subcritical adsorption, it can be applied to supercritical excess adsorption isotherms provided adsorption pressures are low enough for the isotherms to remain monotonic (Choi et al., 2003; Delavar et al., 2010; Zhou & Zhou, 2000). The Freundlich equation is given by:

Eq. 3-39

$$n_{ads} = n_{max} a P^{(1/b)}$$

where n_{max} is the predicted maximum molar quantity that can be adsorbed on a monolayer of adsorbent, P is the applied bulk fluid pressure, and a and b are empirical constants for a given adsorbent/adsorbate system.

The Langmuir model was developed by Irving Langmuir in 1916 (Langmuir, 1916). It is a relatively simple model that assumes a thermodynamic equilibrium to predict the fraction of an adsorbent surface covered by an adsorbate as a function of fluid pressure or concentration. This equation was also developed to describe subcritical adsorption but is valid for supercritical adsorption if the isotherm remains monotonic (Choi et al., 2003; Delavar et al., 2010; Zhou & Zhou, 2000). The Langmuir equation is given by:

Eq. 3-40

$$n_{ads} = n_{max} \frac{bP}{1 + bP}$$

where b is the Langmuir adsorption equilibrium constant.

In 1971 the Toth model was proposed as a generalization of the Langmuir model (Toth, 1971). Toth's model was developed to account for deviations found when using the Langmuir equation to model experimental adsorption data. These deviations were considered to be due to heterogeneities in the adsorbent materials studied. The Toth model generally produces better data correlations than either the Langmuir or Freundlich models. The Toth model is commonly used for heterogeneous adsorbents such as activated carbon because it correctly predicts adsorption behavior at both low and high pressures, and the equation is also of a simple form (Himeno et al., 2005). The Toth equation is given by:

$$n_{ads} = n_{max} \frac{P}{(b + Pa)^{\frac{1}{a}}}$$

where b is an equilibrium constant, and a is a parameter that indicates the heterogeneity of an adsorbent.

3.3.5 - Experimental Error & Uncertainty

Multiple errors or uncertainties were found to be associated with the measuring of an adsorption process using the constructed apparatus. These uncertainties were the minimum calculated error associated with a single adsorption value, the experimentally determined short-term steady state noise error, and the experimentally determined error associated with the expansion process itself.

Two general types of uncertainty were found to be present in the adsorption measurement process. These were a calculated uncertainty, and an experimentally determined measurement uncertainty. The calculated uncertainties were obtained using the propagation of errors technique. The general equation for calculating uncertainty via the propagation of errors method for n number of interacting variables each having an uncertainty value is as follows:

$$\varepsilon_x = \sqrt{\varepsilon_{x_1}^2 + \varepsilon_{x_{i+1}}^2 + \dots + \varepsilon_{x_n}^2}$$

The uncertainty ε can be represented by δ when determining absolute error values, and σ when determining relative uncertainties.

The relationship between the absolute and relative errors is as follows:

$$\sigma_{x_i} = \frac{\varepsilon_{x_i}}{x_i}$$

Experimentally determined measurement errors were determined by calculating the standard deviation. The standard deviation is an absolute error and is given by:

$$\delta_{SD} = \sqrt{\frac{1}{n-1} \sum_{i=1}^n (x_i - \bar{x})^2}$$

3.3.5.1 - Single Point Measurement Uncertainty

The single point measurement uncertainty refers to the calculated minimum uncertainty associated with a single adsorption point measurement. It is dependent on the pressure measurement uncertainty, temperature measurement uncertainty, and the volume measurement uncertainties associated with both the supply and sample vessels. It also depends on the uncertainty in the sample dead space volume. Thus, the total calculated uncertainty associated with a single adsorption is given by the following functional form:

$$\varepsilon_{pt} = f_{pt}(\varepsilon_{P_1}, \varepsilon_{P_2}, \varepsilon_{T_1}, \varepsilon_{T_2}, \varepsilon_{V_1}, \varepsilon_{V_2}, \varepsilon_{V_{dead}})$$

where ε can be either the absolute uncertainty (δ) or the relative uncertainty (σ).

The relative uncertainty values for the pressure and temperature sensors ($\sigma_{P_1}, \sigma_{P_2}, \sigma_{T_1}, \sigma_{T_2}$) were provided by the sensor manufacturer, the uncertainty values for the supply vessel and the sample dead space volume were determined experimentally, while the uncertainty associated with the sample vessel volume was determined by combining calculation and experimentally determined values.

3.3.5.1.1 - Pressure & Temperature Measurement Uncertainty

The relative uncertainty in the pressure and temperature sensor values was given as 0.08 % and 0.5 % respectively. A maximum testing pressure value of 6 MPa and a maximum temperature value of 298 K were chosen to calculate the maximum expected absolute error for the sensors. This produced uncertainty values of ± 4800 Pa and ± 1.5 K.

3.3.5.1.2 - Supply Vessel Volume Uncertainty

The uncertainty of the sample vessel volume was determined by taking the standard deviation of the volume values obtained from the eight water filling tests conducted, and combining it with the measurement uncertainty of the burette which was provided by the manufacturer. The standard deviation of the water filling tests was found to be ± 0.26 ml, while the burette measurement uncertainty was given as ± 0.02 ml. Combining the two uncertainties as per equation 3-42 produced absolute and relative uncertainties of ± 0.26 ml and 0.06 % respectively.

3.3.5.1.3 - Sample vessel Volume Uncertainty

The uncertainty associated with the sample vessel volume is the combination of the minimum calculated error as obtained through the propagation of errors method, and the experimentally determined uncertainty as obtained through calculating the standard deviation of the gas expansion volume values. This can be represented as:

$$\epsilon_{V_2} = \sqrt{\epsilon_{V_{2,clc}}^2 + \epsilon_{V_{2,SD}}^2}$$

Eq. 3-46

The ideal gas law was used to approximate the molar amounts since the actual equations of state used were large and complex. Solving the system molar balance equation (Eq. 3-34) for V_2 and applying the propagation of errors technique produces the following equation:

$$\varepsilon_{V_2ctc} = \sqrt{2\varepsilon_{V_1}^2 + 2\varepsilon_p^2 + 2\varepsilon_T^2}$$

Applying the standard deviation equation to the experimental data sets for the expansion of methane, helium, and nitrogen gas gives the absolute and relative uncertainties. Table 3-3 displayed below gives the error values obtained for each gas.

Table 3-3: Gas expansion error.

	δ_{SD} (\pm ml)	σ_{SD} (%)
CH ₄	0.1	0.31
He	0.08	0.26
N ₂	0.1	0.32

Combining the experimental uncertainties produced an average absolute uncertainty of $\delta_{SD} = \pm 0.1$ ml and relative uncertainty of $\sigma_{SD} = 0.3$ %.

Combining equations 3-46 and 3-47, and substituting the appropriate values gives a total absolute and relative uncertainty of $\delta_{V_2} \pm 0.2$ ml and $\sigma_{V_2} = 0.78$ % for the sample vessel volume.

3.3.5.1.4 - Sample Dead Space Volume Uncertainty

The uncertainty associated with determining the sample dead space volume is equal to that obtained when determining the sample vessel volume. This is because the same procedure is used for determining both volumes. The only difference between the two procedures is that when calculating the dead space volume a sample is present inside the sample vessel instead of the vessel being empty, thus no adsorption occurs. The actual sample dead space is therefore taken as the difference between the empty sample vessel volume and the populated sample vessel volume. The absolute and relative uncertainties present when determining the dead space volume is thus $\delta_{V_s} \pm 0.2$ ml and $\sigma_{V_s} = 0.78$ % respectively.

3.3.5.1.5 - Total Single Point Measurement Uncertainty

The theoretical minimum error for a single adsorption value is the combined result of the uncertainty in the pressure, temperature, and vessel volume measurements. It is given by the following equation:

$$\varepsilon_{pt} = 2 \sqrt{\varepsilon_{V_1}^2 + \varepsilon_p^2 + \varepsilon_T^2 + \varepsilon_{V_2}^2 + \varepsilon_{V_{dead}}^2}$$

Eq. 3-48

Substituting the appropriate parameter (δ or σ) into the above equation along with its respective value produces a maximum expected absolute uncertainty of $\delta_{pt} \pm 0.96$ mmol, and a relative uncertainty of $\sigma_{pt} = 1.3\%$

3.3.5.2 - Short-Term Steady State Uncertainty

The short-term steady state uncertainty arises from signal noise on the pressure and temperature sensors and/or the data acquisition system. This noise creates a variation in the sensor values with time when subject to steady state conditions. These variations tend to be periodic in nature. It is suspected that this noise is due to electrical interference.

Tests were conducted in which the system was brought to an equilibrium state at various pressures found when conducting an adsorption test. The standard deviation of the fluctuating values was taken as a measure of the uncertainty. The maximum steady state error associated with measuring the number of moles of gas present was found to be $\delta_{st} \pm 0.2$ mmol and $\sigma_{st} = 0.27\%$. Plots depicting the steady state error for the number of moles of gas in the supply and sample vessels are shown below.

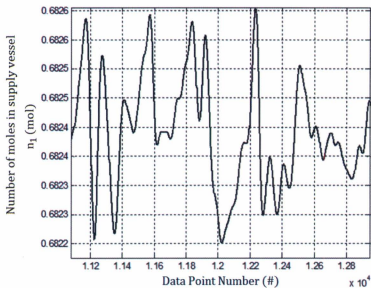


Figure 3-9: Supply vessel steady state error.

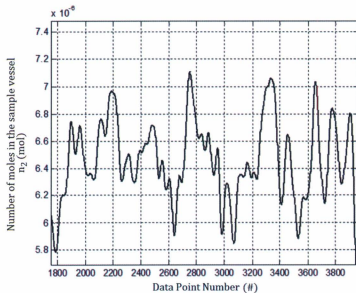


Figure 3-10: Sample vessel steady state error.

3.3.5.3 - Gas Expansion Error

The gas expansion error is the adsorption measurement error found when expanding gas at average rates equal to that used when conducting an adsorption test. Multiple tests were conducted where methane gas was expanded from the supply vessel to the empty sample vessel at different rates. The number of moles of gas adsorbed was calculated for each expansion. A plot of the number of moles of gas adsorbed for each expansion test conducted is shown below. Note that adsorption values would remain approximately zero throughout the process if no error was present.

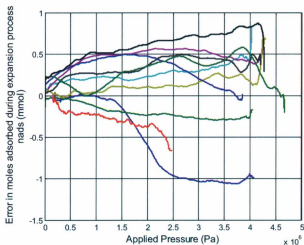


Figure 3-11: Gas expansion process error.

It is thought that the error is the result of an event transit-time difference between the supply vessel and sample vessel sensors. Figure 3-12 shown below provides a simplified schematic that depicts the process.

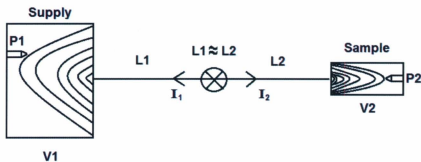


Figure 3-12: Wave transit illustration.

Information (I) in the form of pressure disturbance waves that are caused by the control valve transit away from the valve in opposite directions towards their respective vessel. The velocity (v_f) of a pressure wave in a fluid medium is dependent on the fluid density. The distance from the control valve to either vessel (L) is approximately equal. Since the pressure in the supply vessel is much larger than that in the sample vessel ($P_1 \gg P_2$), the density in the supply is also much greater ($\rho_1 \gg \rho_2$). Therefore, the velocity of the pressure wave travelling towards the supply vessel sensor is greater than that for the sample vessel. Thus, if an event such as a pressure disturbance was created by the control valve and was to be measured by both pressure sensors taking readings simultaneously at a fixed rate; the information would be measured by the supply vessel sensor before it reaches the sample vessel sensor. This produces an error since adsorption is said to occur if some amount of gas was measured to have left the supply vessel but that same amount was not measured to have arrived in the sample vessel. Normally, this type of error would reach steady state at a relatively low value. However, the control valve used did not maintain a constant flow rate during the adsorption process. Typically the flow rate would increase during the first quarter of the testing process, decrease during the last quarter, and remain approximately constant during the middle portion of the test. Since the flow rate is continuously changing, the pressure disturbances continue to

occur and have a compounding effect on the measured error causing it to increase as the test progresses. This trend can be observed in the plot of the expansion error runs shown above in Figure 3-11. In general, the expansion error increases as the average expansion rate for the process increases.

The total error for the expansion process was taken as the standard deviation of the adsorption error values for each of the test runs. An absolute uncertainty of $\delta_{\text{exp}} \pm 0.62$ mmol and a relative uncertainty of $\sigma_{\text{te}} = 0.83$ % were obtained.

3.3.5.4 - Temperature Control Error

Another error associated with the measurement process is caused by uneven heat transfer between the system and surroundings. Since the surrounding environment was subject to uncontrollable temperature fluctuations, heat is transferred between the system and its environment during the course of an adsorption test. Thus, the temperature of the gas in the supply and sample vessels may differ and also change at different rates throughout a test. Since temperatures could not be kept at constant values, adsorption values presented by isotherm plots were said to occur at the overall average temperature in the supply and sample vessels throughout a test. This error is essentially impossible to predict for a given test since the fluctuations in the environmental temperatures are unpredictable. Below are plots of the temperature change and corresponding pressure change for the supply vessel at steady state conditions over a period of 24 hours.

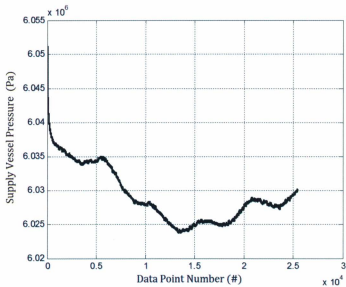


Figure 3-13: Temperature control pressure error.

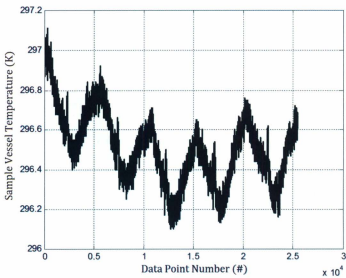


Figure 3-14: Temperature control temperature error.

3.3.5.5 - Total Adsorption Measurement Uncertainty

The total uncertainty for an adsorption value presented by an isotherm plot is thus the combination of all the uncertainty values presented above. The total uncertainty or error for the process can therefore be represented by the following equation:

$$\epsilon_{tot} = \sqrt{\epsilon_{pt}^2 + \epsilon_{st}^2 + \epsilon_{exp}^2}$$

Eq. 3-49

where ϵ_{pt} is the uncertainty associated with a single adsorption value, ϵ_{st} is the short-term steady state error, and ϵ_{exp} is the error associated with the expansion process.

Substituting the appropriate value into the above equation produces an overall total absolute uncertainty of $\delta_{tot} \pm 1.2$ mmol and a relative uncertainty of $\sigma_{tot} = 1.6\%$.

3.4 - Sample Fabrication Methodology

3.4.1 - Electrochemical Etching

3.4.1.1 - Explanation

Porous silicon is typically produced by electrochemical anodization of doped crystalline silicon in an aqueous hydrofluoric acid (HF) based electrolyte. The overall dissolution process is controlled by either the anodic current or potential. Constant current is typically preferable since it allows for better control of porosity, thickness, and reproducibility from run to run (Canham, 2006). Anodization parameters which affect the production process include anodic current density or potential, electrolyte concentration, doping element type and concentration, illumination, temperature, and dissolution duration. Characteristics of the produced porous silicon such as pore size, porosity, and morphology are strongly dependent on these anodization parameters. Thus, careful control and variation of the parameters allows one to accurately adjust the final material properties (Lehmann, 2002).

There are various types of electrolytes and fabrication cells that can be utilized to produce porous silicon. Aqueous electrolytes such as ethanol (C_2H_5OH) and hydrofluoric acid (HF) are most commonly used for the electrochemical production of silicon (Lehmann, 2002). However, for some applications organic electrolytes such as Acetonitrile and HF or Dimethylformamide and HF are used (Rieger & Kohl, 1995). Due to the hydrophobic character of a clean silicon surface, surfactants such as ethanol are usually added to the aqueous electrolyte to increase surface wettability. The addition of ethanol prevents hydrogen bubbles that are produced during the anodization process from sticking to the material surface (Lehmann, 2002).

Figures 3-15 and 3-16 depict the fabrication cell used to produce porous silicon. Metal contact is made on the back-side of the wafer and is sealed so that only the front side of the sample is exposed to the electrolyte. The silicon wafer then serves as the anode while the cathode is located in the electrolyte and is typically made of platinum wire. The cell body itself is generally made of a highly acid-resistant polymer such as Teflon. Using this type of cell leads to porous silicon layers of good uniformity and offers a good control of the final material thickness and porosity (Canham, 2006).

Lightly doped (p^-) or highly doped (p^+) p-type and n-type silicon can be used. Lightly doped p-type silicon generally tends to produce microporous silicon, while highly doped p-type silicon generally produces mesoporous silicon. All porous silicon samples produced via electrochemical etching presented in this thesis utilized lightly doped (p^-) p-type silicon with resistivity values ranging from 2.5 – 4.0 Ωcm .

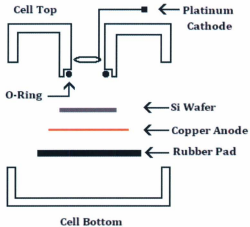


Figure 3-15: Disassembled electrochemical etching cell.

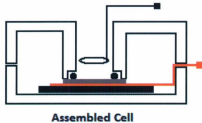


Figure 3-16: Assembled electrochemical etching cell.

3.4.1.2 - General Production Procedure

The general procedure for producing porous silicon films via the electrochemical method is as follows: Samples are first cleaved into approximately 2 x 2 cm square sections from larger wafers. Prior to etching, samples are immersed in a 49% volumetric HF solution for approximately 60 s, then removed, rinsed with water, and finally dried. This removes any native oxides located on the surface of the sample. The electrolyte is mixed to the desired component proportions using 49% HF and 100% ethanol. The sample is then loaded into an etching cell and the electrolyte is added. A

constant current is then passed through the cell via copper and platinum electrodes for the desired period of time. Typically samples are etched in darkness to prevent any photochemical etching from occurring. Upon completion of the etching, the sample is removed from the etching cell, rinsed with water, and dried with paper towel. The sample is then placed in pentane for approximately 60 s. The pentane helps prevent structural cracking during drying since it has a lower surface tension than water (Lehmann, 2002). Finally, the sample is dried in ambient air and stored at room conditions until testing is required.

3.4.2 - Stain Etching

3.4.2.1 - Explanation

Another method in which porous silicon may be produced is through chemical stain etching of doped crystalline silicon, typically in a mixture of hydrofluoric acid (HF), nitric acid (HNO_3), and water. The first reports of porous silicon in literature were formed via stain etching (Turner, 1958; Turner, 1960). However the relationship between etching parameters and final material characteristics is much less understood and less documented compared to electrochemical etching (Vazsonyi et al., 2001). Etching parameters which affect the final material characteristics include etchant chemical composition and concentration, mechanical agitation of the etchant such as stirring or sonication, illumination, material doping element and concentration, temperature, etching time, and the addition of any incubation time reducing agents such as NaNO_2 . A very diverse range of values for these factors have been reported in literature for producing porous silicon in this method (Dimova-Malinovska, Sendova-Vassileva, Tzenov, & Kamenova, 1997; Fathauer, George, Ksendzov, & Vasquez, 1991; Litvinenko et al., 2010; Parbukov et al., 2001; Shih et al., 1992; Vazsonyi et al., 2001; Winton, Russell, & Gronsky, 1997). It has been observed that a period of time is often required for the etching reaction to start once the silicon becomes exposed to the etchant. This time period is known as the incubation time and can typically range anywhere from 60 to 800 s (Dimova-Malinovska et al., 1997).

The production of porous silicon via stain etching is very attractive because of its simplicity; it does not require any specialized etching cell or external power source. Since an applied directed current flow is not required, stain etching can essentially produce porous silicon on any crystalline silicon surface exposed to the etchant. This in turn allows for the production of very large etched areas with great ease. Although this method is considered much easier than the electrochemical etching technique, it is employed much less frequently by scientists since porous silicon produced in this manner has been found to have non-uniform etch profiles, extremely thin porous layers, and lower quantum yields of photoluminescence (Foll et al., 2002; Shih et al., 1992; Vazsonyi et al., 2001). Although stain etched films are generally very thin, large volumes of porous silicon can be produced by exposing large areas of silicon to the etchant. The simplest way in which to do this is through the use of silicon powder. This approach is considered optimal since reducing the particle volume results in a larger surface area to volume ratio. For example, a typical silicon wafer having a diameter of 10 cm and thickness of 500 μm would have a surface area available to etching of approximately 80 cm^2 , while the same wafer formed into a powder having an average particle size of 63 μm would have a surface area available to etching of approximately 3700 cm^2 . This feature makes stain etching much more appealing for applications such as gas adsorption testing where large volumes of porous material are required.

3.4.2.2 - General Production Procedure

3.4.2.2.1 - Porous Films

The general procedure for producing porous silicon films via stain etching is very straightforward. The procedure is essentially the same as that used when electrochemical etching except no external power source is used. The etching cell used for electrochemical etching is also used except no platinum cathode or copper anode back contact is present. This type of cell was used since it exposes a known silicon surface area to the etchant, which later greatly aids in the analysis of the

sample. Etchant compositions used were obtained from 49 % HF and 70 % HNO₃ volumetric solutions.

3.4.2.2.2 - Porous Powder

The procedure for producing doped silicon powder is as follows: A mortar and pestle was used to grind silicon wafers into particles. Using a mini-sieve set, the particles were sorted into size ranges. The particle size ranges used were: 250-177 μm , 88-63 μm , and 63-37 μm . The majority of the silicon powder produced and tested was in the 63-37 μm size range since the ratio of surface area to volume increases with decreasing radius for a spherical particle. After sorting, the powder was washed to remove any super fine silicon powder that would completely dissolve during the stain etching process. The silicon powder was then dried at temperature of 120 °C using a hot plate.

The procedure for stain etching porous silicon powder is as follows: The chemical etchant components are first mixed in the desired proportions. The doped silicon powder is added to the etching reaction vessel and the etchant is then added. The powder is added to the etching reaction vessel first since adding it after the etchant causes a large amount of powder to remain suspended on the etchant surface. After the desired amount of etching time has passed, the silicon powder is filtered from the etchant and rinsed with water. The now porous powder is then dried at 120 °C for 2 to 3 days to ensure all water is removed from material pores. Unlike the etching of wafers, silicon powder does not undergo immersion in an HF solution prior to etching. The powder is also not immersed in pentane after etching since any cracks formed in the porous microstructure during drying would essentially produce smaller substructures in the material. This would further increase surface area of the material provided it remains wholly intact beyond the desired size range.

3.4.3 - Sample Analysis

Electrochemically etched and stain etched porous silicon films are typically analyzed and characterized in terms of their porosity and thickness. The porosity and thickness of a sample allows one to obtain an approximation of the specific surface area, volume, and overall surface area. Studies have been conducted that relate porous silicon porosity to its specific surface area for different formation conditions (Vazsonyi et al., 2001). Porosities in the area of 50 to 60 % are most desirable since they generally produce the highest specific surface areas. The thickness of a film, along with its etched outer surface area allows one to obtain the total volume of porous material formed in a crystalline medium. This, in combination with the porosity, allows one to calculate the total sample area.

3.4.3.1.1 - Porosity

The porosity of an electrochemically etched sample can be found by a number of methods. The first method is a gravimetric approach which is also destructive to the porous material. It involves measuring the mass of a sample before and after etching, and after the porous silicon material has been removed from the crystalline silicon substrate. Mass measurements were made by taking an average of three values using a microbalance. Potassium Hydroxide (KOH) in the form of an aqueous 1 % mass solution is used to etch the porous silicon from the crystalline substrate. The equation for porosity is as follows:

$$P_r = \frac{m_1 - m_2}{m_1 - m_3} \quad \text{Eq. 3-50}$$

where m_1 the sample is mass prior to etching, m_2 is the sample mass after etching, and m_3 is the sample mass after etching in KOH. The mass measuring method is only used when necessary since the porous silicon film is completely destroyed in the process and the sample can no longer be used for further testing.

The second method of obtaining porosity is using an optical approach (Peckham, 2011). Using a monochromatic light source and a light intensity meter, the Brewster angle of the porous silicon film can be determined. The light is reflected off a porous silicon sample and its intensity is measured. The Brewster angle (θ_b) is obtained by measuring the reflectance intensity as a function of the angle of incidence. Using the Brewster angle, the refractive index can be calculated by:

$$n = \tan \theta_b \quad \text{Eq. 3-51}$$

The Bruggeman effective medium model can then be utilized to calculate the porosity P_r of the sample material. The Bruggeman model is given by (Bruggeman, 1935):

$$P_r = 1 - \frac{(1 - n^2)(h^2 + 2n^2)}{3n^2(1 - h^2)} \quad \text{Eq. 3-52}$$

where n is the measured refractive index, and h is the refractive index of crystalline silicon at $\lambda = 532$ nm (the wavelength of the laser light used in the reflectance measurements).

Comparisons of the mass porosity to the optical porosity for a number of samples revealed that this method is not well suited to stain etched films. This is thought to be due to the large variation in properties across the film which is an inherent property of using the stain etching approach. The optical method is a nondestructive process and is thus generally preferred over the mass measurement method.

Another approach for approximating the porosity is through the measurement of the etched film area A , porous film thickness τ , and the mass removed during etching. By directly measuring the etched area and mass removed, and calculating the film thickness using equation 3-57, the porosity can then be calculated as follows:

$$P_r = 1 - \frac{\rho_{Si} \frac{m_1 - m_2}{A \tau}}{\rho_{Si}}$$

where ρ_{Si} is the density of crystalline silicon, m_1 is the sample mass prior to etching, m_2 is the sample mass after etching, A is the etched surface area, and τ is the average porous film thickness.

3.4.3.1.2 - Thickness

The thickness of a porous silicon film can be determined by a number of ways depending on how it was fabricated. For electrochemically etched silicon, the following equation was utilized to determine the porous film thickness (Lehmann, 2002):

$$\frac{d\tau}{dt} = 1.05 J^{0.89}$$

where τ is the porous film thickness given in micrometers, J is the formation current density specified in $\frac{\text{mA}}{\text{cm}^2}$, and t is the etching time specified in minutes.

An alternative approach is to measure the film thickness directly using by cross-sectioning a sample and viewing it with a scanning electron microscope (SEM). However, this method typically does not work very well for microporous films since the pores are typically too small for the resolving power of the SEM to decipher the difference between the porous layer and the crystalline substrate. Numerous attempts were made to determine the thickness of stain etched films but none were considered successful. Figure 3-17 shows a cross sectional SEM of a stain etched film.

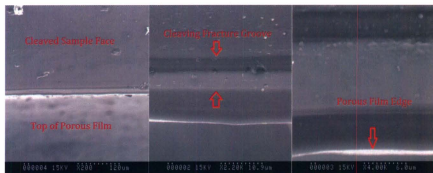


Figure 3-17: Cross-sectional SEM of stain etched wafer.

The thickness of stain etched films cannot be determined by either of the above methods, since no general etching rate equations have been established and typically stain films are microporous. To obtain an approximation of stain film thickness, a combination of mass measurement and direct measurement was utilized. By measuring the mass of the porous layer and the etched surface area, the film thickness can be approximated using the following equation:

$$\tau = \frac{m_2 - m_3}{\rho_{St} A (1 - P_r)} \quad \text{Eq. 3-55}$$

The etched surface area was found by using a caliper to measure the sample area that would be exposed to the etchant.

The above method can be applied to both stain and electrochemically etched porous films.

- 4 - Results and Discussion

4.1 - Introduction

This chapter presents the results of adsorption tests conducted on activated carbon, zeolite, porous silicon, and silicate materials using methane and nitrogen gas. Each of the materials are evaluated relative to one another, and compared with results found in the literature. All tests were performed at room temperature which was approximately 298 K. Adsorption isotherms were fitted using Langmuir, Freundlich, and Toth isotherm models. A new method of modifying isotherm models to better describe effective storage isotherms is presented. A new technique of approximating the specific surface area of a porous material is also presented. Finally, a brief economic analysis of the top performing materials is provided to analyze the viability of using such materials as a gasoline replacement for internal combustion engines.

This chapter also presents the results and details of the experimental production studies that were conducted to produce porous silicon samples for adsorption testing. The samples consisted of porous silicon films formed on crystalline silicon wafers via electrochemical etching or stain etching, and porous silicon powders formed via stain etching of crystalline silicon powder. A number of experimental studies were conducted in which production parameters were strategically varied in an effort to produce porous silicon capable of adsorbing methane gas.

4.2 - Sample Production Studies

The sample production studies are a series of experiments that were conducted to produce porous silicon samples for adsorption testing. The studies are grouped into two classes, which consist of electrochemical etching and stain etching. However, the majority of studies conducted utilized stain etching as the method of production. The details of the production studies are presented below.

4.2.1 - Electrochemical Studies

Only one electrochemical study was conducted before it was realized that sample material volumes produced were too small to facilitate any measureable amount of gas adsorption. Porous film volumes were on the order of 0.025 cm^3 , which would only have a surface area of approximately 12.5 m^2 . A total of three samples were produced during the study. The fabrication parameters and porosity results for the samples produced are displayed below in Table 4-1. From the sample analysis results we can see good agreement between the porosity values obtained through the optical and mass geometry methods.

Table 4-1: Electrochemical sample production summary. [HF] and $[\text{C}_2\text{H}_5\text{OH}]$ are the pure volumetric percentages for the electrolyte components. I_p is the etching current density, t_{ech} is the total etching time, $P_{r,opt.}$ is the sample porosity as obtained through optical techniques, and $P_{r,Eq.}$ is the sample porosity as obtained via equation 5-53.

Sample	[HF] (%)	$[\text{C}_2\text{H}_5\text{OH}]$ (%)	I_p ($\frac{\text{mA}}{\text{cm}^2}$)	t_{ech} (s)	$P_{r,opt.}$ $\pm 5\%$	$P_{r,Eq.}$ $\pm 5\%$
3.11#1	45	8.2	5	1800	65	59
3.12#1	35	28.6	10	3600	72	69
3.12#2	35	28.6	10	3600	68	70

4.2.2 - Stain Etching Studies

4.2.2.1 - Introduction

The purpose of the stain etching studies was to determine the effect of etchant composition and other contributing factors on the formation of stain etched porous silicon films. Unlike electrochemically etched silicon, no information has been presented in the literature regarding the stain etching of silicon to produce porous films having thicknesses on the order of 5 to 10 μm . Thus, experimentation was required to determine the fabrication parameter values that would produce this

result. These experiments were conducted using crystalline silicon wafers so the resulting stain etched films could be analyzed more easily. The results of the wafer studies were then used to stain etch crystalline Si powder. The production parameters studied are as follows:

- The pure volumetric fraction of HF & HNO₃.
- The mass concentration of any incubation reducing agents such as NaNO₂.
- The volumetric fraction of any surfactants such as C₂H₅OH & CH₃COOH.
- Doping level of the crystalline silicon used (p⁺ or p⁻).
- Total etching time after the incubation period has ceased.

Due to the lack of information regarding factor value starting points, the large number of contributing factors, and the high sensitivity of the etching process to those factors; statistical experimental design techniques such as Design of Experiments were deemed inappropriate. Experiments were therefore conducted in a series of blocks or studies where the results of each study were used to determine parameter values to be used in subsequent studies. For each block of experiments, one or more factors were held constant while others were varied to determine their effect. The porous films produced were evaluated in terms of their thickness and porosity. A number of samples were also evaluated by subjecting the porous materials to a destructive etching process using a KOH solution. The etching process was utilized to indicate whether a microporous or mesoporous material had been produced (mesoporous materials do not produce visible etching reactions).

A total of ten stain etching studies were conducted. Studies 1 to 6 were conducted using p⁺ or p⁻ crystalline silicon wafers, while the remaining studies were conducted using mainly p⁺ crystalline silicon powder and wafers. For each of the etching studies presented, a clear description of the purpose, production parameter values, and experimental results is briefly discussed. The experimental studies are further discussed below.

4.2.2.2 - Study Results Summary

Based on the studies conducted, it was determined that larger ratios of HF to HNO_3 produced porous silicon with more desirable properties such as thicker films and lower porosities. More specifically, a pure component volumetric ratio of 400:1 HF: HNO_3 mixed from 49% HF and 70% HNO_3 volumetric solutions produced the best results (thicker films and porosities between 50 % and 60 %) for stain etching films. A higher volumetric ratio of 1200:1 HF: HNO_3 was found to produce the best results (as established through KOH etching experiments) for stain etching silicon powder. Stain etched films formed on p^+ silicon were generally much thicker than that for p^- silicon. p^+ film thicknesses generally ranged from 2 to 5 μm , while p^- films are typically less than 1 μm . Due to the small pore volumes present in the produced materials (microporous), film thicknesses could not be established through the use of an SEM since resolutions were not sufficient to allow any distinction to be made between the porous and nonporous material interface. Thus, film thicknesses had to be approximated through the use of equation 3-55 instead. It was found that reactions having a much lower driving potential acting over longer time periods produced thicker films with lower porosities. Etching times on the order of 600 s to 900 s were found to produce the thickest films, and was usually enough time for the etching reaction to stop due to the depletion of HNO_3 in the etchant solution. Lower ratios of HF to HNO_3 produced more vigorous reactions which often led to electropolishing. The stain etching process is believed to be a self-limiting process where the properties arising from the porous material layer formation cause the etching reaction to increasingly favor electropolishing instead of porous material formation. As porous material thicknesses increase, the etching reaction tends to favor destruction of the outermost porous material surface due to a decreased ability to replace the depleted etchant with fresh etchant at the advancing porous material face since the process requires fluid diffusion through the porous material layer. This feature was observed during the stain etching experiments by the somewhat periodic formation, destruction, and reformation of porous material films during an etching

process. This causes stain etched films to have a very limited thickness, which is relatively thin compared to that obtained through electrochemical etching. Due to physical properties of the etching process, stain etching generally produces non-uniform films which are not well suited to optical experimentation. Stain etching crystalline silicon powder instead of wafers created an additional set of variables that needed to be accounted for, such as the problem of bubbles sticking to silicon particles during the etching process. The addition of acetic acid (CH_3COOH) to the etchant solution seemed to help alleviate this problem. A 99% volumetric solution of CH_3COOH was used to produce an etching solution with a 15% pure volumetric component fraction of the acid.

4.2.2.3 - Study #1

4.2.2.3.1 - Experiment Details

The purpose of the first study was to successfully produce porous silicon using etching compositions commonly found in the literature; and determine the effect that adding $\text{C}_2\text{H}_5\text{OH}$ & NaNO_2 had on the etching of p^+ and p^- type silicon. Extended etching times were used in an attempt to produce thicker stains films. The parameter values used are shown in Table 4-2 below.

Table 4-2: Stain etching study #1 run summary. The electrolyte components are given as the pure volumetric percentage, t_{inc} is reaction incubation time (amount of that passes before the etching reaction starts once the silicon material is exposed to the etchant), and t_{ech} is the total etching reaction time after the incubation period has passed.

Sample	Doping p^+, p^-	$[\text{C}_2\text{H}_5\text{OH}]$ (%)	$[\text{HF}]$ (%)	$[\text{HNO}_3]$ (%)	t_{inc} (s)	t_{ech} (s)
3.20#1	p^-	0	28.5	43.0	0	900
4.16#1	p^+	0	28.5	43.0	0	900
4.16#2	p^+	15	24.5	36.0	0	900
4.16#3	p^+	0	5.4	71.2	360	2340
4.16#5	p^+	0	11.1	55.6	15	900

4.2.2.3.2 - Results

All samples were severely electro-polished which most likely means that etching times and/or acidic component concentrations were too high. Most samples were subject to seemingly mild reactions but still had significant mass removal. One wafer sample etched completely through the material volume due to severe electropolishing. Due to the high concentrations of the acidic etchant components, no incubation times were observed and thus no experiments were conducted while using NaNO_2 as was originally intended. The addition of the surfactant $\text{C}_2\text{H}_5\text{OH}$ to the etchant component HNO_3 produced a violent reaction. Thus, unlike electrochemical etching, $\text{C}_2\text{H}_5\text{OH}$ cannot be used as a surfactant for stain etching. All samples were also subject to a significant amount of bubbles sticking on the silicon surface during etching.

4.2.2.4 - Study #2

4.2.2.4.1 - Experiment Details

The purpose of this study was to determine the effect of varying the etchant composition on the formation of porous silicon on p^+ silicon. Pure component volume percentage constraints were chosen based on the results of study #1 and reports found in literature. Using these constraints, a 3-part mixture D-optimal design was utilized to determine the factor values to be used. The required number of runs and component percentages were calculated by the Design Expert statistical software package. A D-optimal design was used since it allows for the modeling of mixtures while also minimizing the number of experimental runs required to achieve an accurate statistical model. The D-optimal process is used to select the optimal combination of experiments out of all possible designs. This selection process depends on a set of given criteria and is solved by a computer algorithm. The design table for the study is shown below.

Table 4-3: Stain etching study #2 runs summary. $T_{f,Eq}$ is the porous material layer thickness as obtained via equation 3-55, $P_{r,m}$ is the porous material porosity as obtained through gravimetric techniques (equation 3-50).

Sample	Doping P ⁺ , P ⁻	[HF] (%)	[HNO ₃] (%)	[H ₂ O] (%)	t_{inc} (s)	t_{ech} (s)	$T_{f,Eq}$ ± 0.5 μm	$P_{r,m}$ ± 10%
4.17#1	P ⁺	2.0	20.0	78.0	570	180	1.2	87
4.17#2	P ⁺	20.0	2.0	78.0	270	180	1.3	47
4.17#3	P ⁺	14.8	10.3	74.9	120	180	4.0	77
4.17#5	P ⁺	2.0	4.0	94.0	60	180	1.4	85
4.17#6	P ⁺	20.0	20.0	60.0	0	-	-	-

4.2.2.4.2 - Results

All etching reactions with the exception of sample 4.17#6 were subject to incubation times. The reaction for 4.17#5 did not start after 45 minutes so NaNO₂ was added to the etchant at a mass concentration of 5 g/L in order to start the reaction. The relatively low porosity of sample 4.17#2 suggests that a large ratio HF to HNO₃ may produce the most desirable results since higher material surface areas are generally achieved for decreasing porosities with porous silicon up to approximately 50 %, at which point it decreases. Sample 4.17#3 produced a large calculated thickness; however it is suspected that the high value may be an error caused by electropolishing during the etching process. Sample 4.17#6 was subject a very strong reaction which electropolished the material instead of forming a porous structure. Because some of the initially chosen parameter values did not produce measurable results, no statistical model could be constructed. All samples were also subject to bubbles sticking on the silicon surface and thus formed non-uniform films. Since sample 4.17#2 seemed to possess the most favorable properties, its etching parameters were studied more closely in the following studies.

4.2.2.5 - Study #3

4.2.2.5.1 - Experiment Details

The purpose of this study was to determine the effect of etching time while using the composition in Study #2 Run #2, the effect of increasing the concentration of HF, and the effect that varying the mass concentration of NaNO_2 has on the etching process. Unlike Study #1 and Study #2, samples were not subject to a HF dip prior to etching, nor were they dipped in pentane after etching for this study and all remaining studies. This procedure modification was implemented to allow the etching process to more closely resemble that used to make porous silicon powder. The design table for the study is shown below.

Table 4-4: Stain etching study #3 runs summary.

Sample	Doping p^+, p^-	[HF] (%)	[HNO_3] (%)	[H_2O] (%)	[NaNO_2] (g/L)	t_{inc} (s)	t_{etch} (s)	$T_{f,Eq}$ $\pm 0.5 \mu\text{m}$	$P_{r,m}$ $\pm 10\%$
4.16#4	p^+	20.0	2.0	78.0	2.5	-	900	1.5	69
4.17#4	p^+	20.0	2.0	78.0	5.0	90	300	3.6	69
4.17#8	p^+	45.0	2.0	53.0	0.0	0	120	-	-
3.20#2	p^-	45.0	2.0	53.0	0.0	0	120	-	-
3.20#4	p^-	45.0	2.0	53.0	0.0	0	90	-	-

4.2.2.5.2 - Results

The reactions for samples 4.16#4 & 4.17#4 did not proceed as expected since they were subject to large incubation times. The reaction for sample 4.16#4 did not start after 45 minutes. Drops of HNO_3 were then added directly to the etching cell until the reaction started, but the sample still did not etch completely over the available surface area. This suggests that by not exposing samples to HF prior to etching, higher etchant component concentrations (HF and HNO_3) are required and incubation times are generally increased. Increasing the ratio of HF to HNO_3 produced strong reactions with no incubation times. Very fine bubbles were produced and bubble

sticking was not as evident. Samples 3.20#2 and 3.20#4 produced films which exhibited optical interference with visible light suggesting a thin microporous structure was present. Based on these results it was decided to conduct further studies using composition ratios of 10 to 25 [HF]/[HNO₃].

4.2.2.6 - Study #4

4.2.2.6.1 - Experiment Details

The purpose of this study was to determine the effect of varying the concentration of HF on the etching process of p⁻ silicon. Since the results of study #3 indicated that not immersing samples in HF prior to etching had a significant effect on the etching process, information obtained from studies 1 and 2 cannot be applied to the production of porous silicon powder. The design table for the study is shown below.

Table 4-5: Stain etching study #4 runs summary.

Sample	Doping p ⁺ , p ⁻	[HF] (%)	[HNO ₃] (%)	[H ₂ O] (%)	t _{inc} (s)	t _{etch} (s)	T _{f,Eq.} ±0.5 μm	P _{r,m} ± 10%
3.20#3	p ⁻	49.0	-	51.0	-	500	0.5	82
3.20#6	p ⁻	49.0	-	51.0	-	500	0.4	80
3.20#7	p ⁻	35.0	2.0	63.0	120	300	4.9	99
3.20#5	p ⁻	37.5	2.0	60.5	30	500	22.7	99
4.17#10	p ⁺	37.5	2.0	60.5	15	500	7.9	85
3.20#8	p ⁻	48.5	1.0	50.0	60	500	15.4	97

4.2.2.6.2 - Results

The reactions for samples 3.20#3 and 3.20#6 did not start after approximately 35 minutes using the initially chosen concentrations (30% HF and 2% HNO₃). The electrolyte was emptied from the cells and a 49% HF solution was re-added to the cells. Upon adding the HF to the etching cell an etching reaction started before any amount of HNO₃ could be added. This was caused by HNO₃ that had remained when the electrolyte was initially removed since the cell had not been washed down. This

suggests that only a tiny amount of HNO_3 is required to start an etching reaction if HF concentrations are high. Both samples formed visibly purple films. Sample 3.20#7 formed a rough grey film suggesting electropolishing, while samples 3.20#5 and 3.20#8 also electropolished to an even greater degree. This is also evident from the calculated thickness and mass porosity values. It was found that increasing the ratio of HF to HNO_3 while maintaining high concentrations of HF produced the most desirable results. Sample 4.17#10 formed a black film which visibly resembled those formed via electrochemical etching. Based on the results it also appears that p^- type silicon is much more susceptible to electropolishing than p^+ type silicon.

4.2.2.7 - Study #5

4.2.2.7.1 - Experiment Details

The purpose of this study was to examine the effect of high $[\text{HF}] / [\text{HNO}_3]$ ratios and time on the etching of p^+ type and p^- type silicon. The ratio of $[\text{HF}] / [\text{HNO}_3]$ was varied by changing the HF component only. Based on the previous studies it is evident that lowering the HNO_3 concentration produces the best results. Thus, the volume of HNO_3 was held constant at its minimum measureable value. This value corresponds to one drop of liquid when ejected from a 1 ml syringe, which produces a volume of approximately 0.025 ml. The design table for the study is shown below.

Table 4-6: Stain etching study #5 runs summary ($T_{f,SEM}$ is the porous material layer thickness as approximated by the use of a SEM).

Sample	Doping p^+, p^-	$\frac{[\text{HF}]}{[\text{HNO}_3]}$	t_{inc} (s)	t_{ech} (s)	$P_{r,m}$ $\pm 10\%$	$P_{r,OpL}$ $\pm 5\%$	$T_{f,Eq.}$ $\pm 0.5 \mu\text{m}$	$T_{f,SEM}$ $\pm 0.1 \mu\text{m}$
4.17#9	p^+	400	15	300	37	101	4.1	2.6
4.17#11	p^+	600	25	900	31	98	3.4	2.8
4.18#1	p^+	400	15	600	46	112	3.6	-
3.20#9	p^-	400	15	300	89	66	1.1	-
3.20#11	p^-	320	15	300	89	88	1.6	-
3.20#10	p^-	320	15	600	77	88	2.3	-

4.2.2.7.2 - Results

All p^+ type silicon samples formed black porous films, while the p^- type silicon formed porous films that exhibited thin film visible light interference. These samples were also often electropolished to some degree around the outer edges of the film area. The samples were etched in KOH to obtain porosity values and provide a relative measure of film thickness. It was assumed that longer KOH etching times meant thicker and possibly less porous films are present. In general, the p^+ type samples etched much longer with a more vigorous reaction. All samples luminesced when viewed under ultraviolet light. Figure 4-1 shows sample 4.18#1 under normal light and ultraviolet light. The luminescence gives an indication that the material is microporous. From the results it appears that p^+ type silicon may be better suited for producing thick stain etched porous films. Thus, the remainder of the studies will be conducted using p^+ type silicon only.



Figure 4-1: Stain etched sample viewed under ultraviolet light.

From the porosity values obtained from the mass and optical measurements, we can verify that the optical method is not well suited for stain etched films as previously stated. This is simply due to a non-uniform film which is indicated in Figure 4-1 by the dark spots on the film when viewed under ultraviolet light.

4.2.2.8 - Study #6

4.2.2.8.1 - Experiment Details

The purpose of this study was to examine the effect of high $[HF] / [HNO_3]$ ratios, and time on the stain etching of p^+ type silicon. Some of the experimental parameters used when conducting Study #5 were used again to give an indication of the reproducibility error associated with the production process. The design table for the study is shown below.

Table 4-7: Stain etching study #6 runs summary.

Sample	Doping p^+, p^-	$\frac{[HF]}{[HNO_3]}$	t_{inc} (s)	t_{etch} (s)	$P_{r,m}$ $\pm 10\%$	$T_{f,Eq}$ $\pm 0.5 \mu m$	$T_{f,SEM}$ $\pm 0.1 \mu m$
4.18#3	p^+	400	20	300	28	2.3	1.6
4.18#4	p^+	400	20	600	49	4.1	2.6
4.18#5	p^+	400	15	600	29	3.1	2.1
4.18#2	p^+	400	30	900	44	4.2	2.7
4.18#6	p^+	600	30	900	26	2.5	0.9
4.18#7	p^+	320	10	300	39	3.2	1.6
4.18#8	p^+	680	35	900	28	2.9	3.3
4.18#9	p^+	320	10	900	63	5.3	3.3

4.2.2.8.2 - Results

All samples formed black porous silicon films without any evidence of electropolishing. Cross-sectional SEM measurements were taken of the samples upon removal of their porous films to confirm the calculated porous layer thickness. However, it was found that the results did not agree with those obtained through calculation. The results obtained via SEM were considered to be less accurate due to the geometry of the porous films and the method in which the measurements were carried out. The film thickness was measured by taking the distance from the sample face to the bottom of the previously porous material volume. During the etching process the material located along the etchant-cell boundary etches at a different rate

causing curvature in the actual film shape. Since the SEM used did not have any accurate means of aligning the sample surface plane to the device coordinate frame, measurements had to be taken from only one image which included both points of measure. Thus, SEM measurements were required to be taken along this curved area which produces error in the thickness values. Note that all SEM measurements are less than the calculated values. Figure 4-2 shown below illustrates this problem. An SEM image taken from a sample also shows this curvature in Figure 4-3. Attempts were also made to measure the film thickness by taking cross-sectional SEM measurements with the porous film intact. However, maximum magnifications obtained by the SEM were insufficient to establish the boundary between the microporous film and the crystalline substrate volumes. The calculated method however is also somewhat incorrect as it assumes a cylindrical porous volume with no curvature. Thus, the calculated value only provides an average film thickness. This method will also produce inaccurate results if any electropolishing takes place during the etching process.



Figure 4-2: Stain etched film curvature.



Figure 4-3: SEM of stain etched sample with curvature.

4.2.2.9 - Study #7

4.2.2.9.1 - Experiment Details

The purpose of this study was to attempt to produce porous silicon powder using the most suitable conditions established from the results of Study #6. Some of the experimental parameters used when conducting Study #6 were used again in this study. The design table for the study is shown below.

Table 4-8: Stain etching study #7 runs summary. d_p is the silicon particle diameter before etching, $\frac{V_{etch}}{V_{Si_{pw}}}$ is simply the volumetric ratio of etchant to silicon powder.

Sample	d_p (μm)	Doping p^+, p^-	$\frac{[\text{HF}]}{[\text{HNO}_3]}$	$\frac{V_{etch}}{V_{Si_{pw}}}$	t_{inc} (s)	t_{ech} (s)	$P_{r,m}$ $\pm 10\%$	$T_{f,Eq.}$ $\pm 0.5 \mu\text{m}$	$T_{f,SEM}$ $\pm 0.1 \mu\text{m}$
PSiPW_3	63-37	p^+	364	16.7	0	600	-	-	-
4.18#10	-	p^+	400	-	17	900	48	4.3	2.9
4.18#11	-	p^+	400	-	23	600	27	3.1	2.1
4.18#12	-	p^+	400	-	33	900	41	4.1	2.5

4.2.2.9.2 - Results

The silicon powder produced a moderate reaction with no incubation time. During the etching process, bubbles would stick to the particles causing them to clump and rise to the etchant surface. The powder and etchant mixture also developed a foam-like consistency. No visible evidence such as a color change was present to suggest that porous silicon had formed. However, etching of small amounts of the powder in KOH produced strong reactions which suggest that a microporous or mesoporous material was present. Similar amounts of the starting crystalline powder were also placed in KOH for a comparison and no etching reaction occurred. This further suggests that porous silicon powder was created.

4.2.2.10 - Study #8

4.2.2.10.1 - Experiment Details

The purpose of this experiment was to determine whether the volumetric ratio of electrolyte to silicon powder had any effect on the formation of porous silicon via stain etching. Since the surface area exposed to the etchant is much greater when stain etching silicon powder compared to silicon wafers, it was speculated that components of the etchant may be depleted before the desired etching time is reached. The etching time was also varied to determine its effect on the process. To establish a relative sense of which conditions produced the highest volume of porous silicon, 0.5 g of each powder sample was etched in KOH while measuring the total etching time and the approximate reaction strength. Samples yielding longer etching times with more vigorous reactions were considered to have higher amounts of porous silicon. The design table for the study is shown below.

Table 4-9: Stain etching study #8 runs summary. RXN Strength provides a relative indication of the vigorosity of the KOH etching reaction based on visual observation.

Sample	d_p (μm)	Doping p^+, p^-	$\frac{[\text{HF}]}{[\text{HNO}_3]}$	$\frac{V_{etch}}{V_{SiPW}}$	t_{inc} (s)	t_{ech} (s)	t_{KOH} (s)	RXN Strength
PSiPW_4	63 - 37	p^+	400	25	10	300	1200	*
PSiPW_5	63 - 37	p^+	400	25	10	600	1500	**
PSiPW_6	63 - 37	p^+	400	75	10	300	1080	***
PSiPW_7	63 - 37	p^+	400	75	8	600	600	*****
PSiPW_8	63 - 37	p^+	1200	75	12	600	1440	****
PSiPW_9	63 - 37	p^-	1200	75	11	600	360	***

4.2.2.10.2 - Results

All samples were subject to etching reactions of moderate strength compared to those from previous studies. The powders were generally etched until some or most all of the particles were small enough that gas bubbles resulting from the reaction carried the particles to the surface of the KOH where they remained due to their

inability to overcome the fluid surface tension. This phenomenon provides a relative indication of the particle volume that was converted into porous silicon during production process. From analysis of the etching times, apparent reaction strengths, and amounts of particulate silicon located on the etchant surface after the reactions had ceased, it was determined that the conditions used to produce sample PSiPW_8 were the most optimum. PSiPW_8 was subject to a long and vigorous reaction, and produced much more matter that floated up and remained on the fluid surface than any of the other samples. Analysis of the results suggest that varying the volume ratio of etchant to silicon powder had an effect since samples produced with high volume ratios tended to have much more vigorous reactions. It is also evident that increasing sample etching times had a significant positive effect, since samples etched for longer times during production generally etched for longer periods of time in KOH. From the results of PSiPW_9 it is evident that stain etched p^- silicon does not produce porous material layers as thick as those obtained when using p^+ silicon. From the porosity and thickness results of PSiPW_8 it appears that the best general conditions for stain etching silicon powder is to reduce the concentration of HNO_3 while using enough electrolyte to prevent significant concentration changes during the etching process, and using extended etching times. This conclusion was also reached but to a lesser extent from the results of study #5.

In order to ensure that the etching process that occurred was the result of the presence of porous silicon, pre-etched doped crystalline silicon powder was added to the KOH for extended periods of time. However, no visible reaction occurred. Based on this result, it was concluded that the stain etched silicon powder must be in fact porous; and that the increased etching times and reaction strengths found for the powder are an indication that the material is most likely microporous.

4.2.2.11 - Study #9

4.2.2.11.1 - Experiment Details

The purpose of this study was to determine the effect of adding acetic acid (CH_3COOH) on the stain etching of porous silicon. It was established in a previous study (study #1) that the use of $\text{C}_2\text{H}_5\text{OH}$ as a surfactant is not suitable for stain etching since it reacts violently with HNO_3 . During the stain etching of silicon powder, bubbles would stick to the particles causing them to clump and be lifted to the top of the etchant surface. Also, areas covered by a gas bubble are unable to etch since the etchant cannot access the silicon surface. In an attempt to alleviate this problem, an acid-based surfactant was used. Previous reports on the use of CH_3COOH for stain etching has been presented in the literature (Foll et al., 2002; Jenkins, 1977; Shih et al., 1992). The design table for the study is shown below.

Table 4-10: Stain etching study #9 runs summary.

Sample	d_p (μm)	Doping p^+, p^-	$\frac{[\text{HF}]}{[\text{HNO}_3]}$	CH_3COOH (%)	$\frac{V_{etch}}{V_{Si_{pw}}}$	t_{inc} (s)	t_{ech} (s)
4.20#1	-	p^+	380	5	-	13	600
4.20#2	-	p^+	360	10	-	20	600
PSiPW_11	63 - 37	p^+	1200	15	75	2	300
PSiPW_12	88 - 63	p^+	1200	15	75	4	600
PSiPW_13	500-177	p^+	1200	15	75	5	600

4.2.2.11.2 - Results

The addition of CH_3COOH clearly caused a reduction in the amount of bubbles sticking to the silicon surface during etching for the silicon wafers; and also reduced powder clumping and material lifting for the silicon powder. Etching of sample PSiPW_11 in KOH however did not produce any noticeably different results compared to sample PSiPW_8 produced in study #8. Samples PSiPW_12 & PSiPW_13 were not

subject to particle lifting and no foam like consistency was present. Sample PSiPW_13 formed visibly black porous films on some of the larger particles.

4.2.2.12 - Study #10

4.2.2.12.1 - Experiment Details

The purpose of this study was to produce a large quantity of porous silicon for adsorption testing using the most promising etching parameters obtained from the previous studies. Also, samples produced in study #9 were to be briefly etched in 49% HF solution since it had been found that prolonged exposure of porous silicon to atmospheric conditions prevented the porous silicon samples from being etched by KOH. It was suspected that this may be due to the formation of oxides on the porous silicon surface which cannot be sufficiently removed by KOH. Samples 4.20#1 and 4.20#2 had been heated to 100°C for 48 hours to accelerate the oxide formation process. Prior to etching in HF solution, the samples were placed in a aqueous 1% mass solution of KOH to confirm that a sufficient amount oxide had formed to prevent etching. The design table for the study is shown below.

Table 4-11: Stain etching study #10 runs summary.

Sample	d_p (μm)	Doping p^+, p^-	$\frac{[\text{HF}]}{[\text{HNO}_3]}$	CH_3COOH (%)	$\frac{V_{etch}}{V_{Si_{pw}}}$	t_{Inc} (s)	t_{etch} (s)
PSiPW_15	63 - 37	p^+	400	15	-	0	600
PSiPW_16	88 - 63	p^+	400	15	-	0	600
4.20#1	-	p^+	∞	-	-	-	60
4.20#2	-	p^+	∞	-	-	-	30

4.2.2.12.2 - Results

The silicon powder etched as expected. However, during the filtering process the filter paper used broke and sample PSiPW_16 was completely lost. Upon completion of the oxide removal etch, the wafer samples were placed in a 1% solution of KOH and

immediately the porous layer etched away. This confirms the etch inhibition due to surface oxides as previously speculated. It is thought that this process of removing oxides from the porous silicon pore surfaces may also be an effective method of enlarging pore sizes.

4.3 - Adsorption Testing

4.3.1 - Data Presentation

For each material three types of plots are presented in order to describe the adsorption. These plots consist of an adsorption isotherm, an adsorption-desorption cycle isotherm, and an effective delivery capacity isotherm. These isotherms are used to represent both the excess adsorption and effective storage of a material. The adsorption tests used to construct the plots were performed at pressures from approximately 0 MPa up to anywhere between 3.5 to 6 MPa and at room temperature, which was found to vary anywhere from 296 to 298 K.

The adsorption isotherm plots consist of three isotherms superimposed to illustrate reproducibility error and sensitivity to temperature variation between test runs. The adsorption-desorption cycle isotherm depicts the adsorption phase and desorption phase of the process cycle. It should be noted that the desorption portion of the isotherm does not depict the amount of gas delivered but rather the amount of gas remaining adsorbed for a given discharge pressure. The desorption tests were conducted from the maximum adsorption pressure attained during the cycle test, to slightly less than atmospheric pressure. Only materials having relatively high adsorption values were subject to an adsorption-desorption cycle test.

For each of the plot types (adsorption, adsorption-desorption cycle, and effective delivery), plots were generated for each of the performance unit parameters defined in Section 2.3.3. However, due to the large number of plots generated only plots using the most popular performance parameters are presented in this chapter. The remaining plots are located in Appendix A2.

In addition to the presented plots, tables are also provided with corresponding data values for various pressures spanning the adsorption test range. Percentage gas retention values are also given which gives the percentage of gas that would be retained for a given adsorption pressure if discharging to atmospheric conditions. For tested materials that have already been reported in the literature, the excess adsorption results were used as a comparison and to confirm the accuracy of the constructed testing apparatus.

4.3.2 - Modified Isotherm Models

As described previously in chapter 3, isotherm models such as the Langmuir, Toth, and Freundlich equations were developed to describe excess and or absolute adsorption only. Thus, application of these models to effective storage isotherms often results in very poor data fits. It was therefore deemed necessary to modify the models to better describe effective storage isotherms. The effective storage of a material can be thought of as the superposition of the absolute adsorption and bulk gas compression storage. The absolute adsorption can be modeled using standard isotherms models such as the Langmuir and Toth models. The bulk gas compression storage can be modeled using an appropriate equation of state for the gas. Thus, a successful modified isotherm model would simply need to encompass two of these facets; a standard isotherm model to account for the absolute adsorption, and an equation of state to model the bulk gas compression storage. For the sake of simplicity, the equation of state is represented by a linear term which would imply using the ideal gas law since it is a first order equation. Therefore, all standard isotherm models used are subject to a general modification which involves the addition of a linear term. The linear term is given by cP , where P is the bulk gas pressure and c is an empirical constant. Figure 4-4 provides a pictorial representation of the superposition of the absolute adsorption with bulk gas compression to obtain effective storage isotherms. It should be noted that the modified isotherm models have been developed entirely for data fitting purposes and hence likely do not reveal any fundamental information regarding the properties of the adsorbent material.

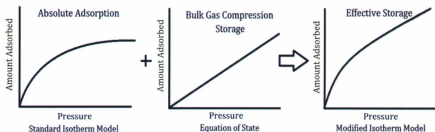


Figure 4-4: Pictorial representation of superimposing absolute adsorption and bulk gas compression to obtain effective storage.

The modified isotherm models are presented below. For each of the materials tested, the original and modified models are applied to the effective storage isotherms to allow a direct comparison and depiction of the increased accuracy obtained when using the modified models.

The Modified Freundlich equation is given by:

$$n_{store} = n_{max} a P^{\left(\frac{1}{b}\right)} + c P \quad \text{Eq. 4-1}$$

where n_{max} is the predicted maximum amount that can be adsorbed on a monolayer of adsorbent, P is applied bulk fluid pressure, and a , b , and c are empirical constants for a given adsorbent/adsorbate system.

The Modified Langmuir equation is given by:

$$n_{store} = n_{max} \frac{bP}{1 + bP} + c P \quad \text{Eq. 4-2}$$

where b is the Langmuir adsorption equilibrium constant, and c is an empirical constant that accounts for the bulk gas storage due solely to compression.

The Modified Toth equation is given by:

$$n_{store} = n_{max} \frac{P}{(b + P^a)^{\frac{1}{a}}} + c P \quad \text{Eq. 4-3}$$

where b is an equilibrium constant, a is a parameter that indicates the heterogeneity of an adsorbent, and c is an empirical constant.

Note that all model isotherm fitting was conducted using the MATLAB mathematical software package in which a nonlinear least squares fitting method was employed. The sum of the squares of the error (SSE), adjusted R-squared values (R_{adj}^2), and the root mean square of the error ($RMSE$) is also presented along with the isotherm model fitting parameter values.

4.4 - Specific Surface Area Approximation Technique

The following method is proposed as a technique for approximating the specific surface area of a material based on the specific excess adsorption of the material. Past publications have suggested that a linear relationship exists between the specific surface area of a material and its specific excess adsorption regardless of the type of adsorbent tested (Sun et al., 2009; Yongjuni et al., 2010). An extensive literature review was conducted to obtain adsorption data that is representative of all types of adsorbents such as porous carbons, zeolites, and silicates. Adsorption points were taken at 3.5 MPa and 298 K since it was the mostly commonly reported adsorption state found in the literature. The specific surface areas used were obtained using the BET method. Figure 4-5 shown below displays a plot of the obtained data which depicts the relationship between specific surface area and specific excess adsorption. Most of the data used to construct the plot is displayed below in Section 4.6.2.

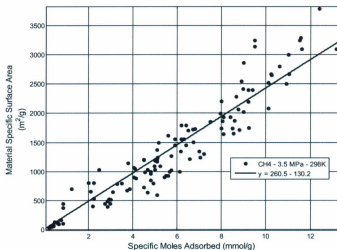


Figure 4-5: Specific surface area and specific moles adsorbed at 3.5 MPa and 298 K for various adsorbent materials found in the literature.

It is clear from the plot that a linear relationship exists. An adjusted R-squared value of 0.90 was obtained indicating a good data correlation. Based on the fit, the following linear equation was obtained:

Eq. 4-4

$$A_{sm} = 243 \frac{n_{ads}}{m_s}$$

The specific surface area of any material can thus be approximated by applying the above empirical equation to the experimental adsorption data obtained at 3.5 MPa and 298 K. Since the tested materials already had specific surface areas obtained via the BET method, the equation was applied to each of these materials to verify its accuracy. BET values used for the 4A Zeolite, 5A Zeolite, and Silica Gel were obtained by taking an average of values found in the literature. Surface areas for the remaining materials were provided by the material manufacturers. Some deviation between the

values reported by the equation and that previously established can be attributed to the fact that most adsorption tests were conducted at temperatures anywhere between 296 and 298 K. Also, it should be noted that relatively large variations in material surface area values can be realized from the use of the BET method, which is evident by the surface area ranges presented in the tables below. The values obtained for the tested materials are summarized in the Tables 4-12 and 4-13 below.

Table 4-12: Comparison of specific surface area equation results for zeolites and silicates.

	3A Zeolite	4A Zeolite	5A Zeolite	13X Zeolite	Silica Gel
$A_{BET} \left(\frac{m^2}{g}\right)$	-	300 - 400	400 - 500	500 - 600	300 - 500
$A_{EQ} \left(\frac{m^2}{g}\right)$	-	109	627	569	259

Table 4-13: Comparison of specific surface area equation results for carbon materials.

	RX3 Extra	FM10	FM30K
$A_{BET} \left(\frac{m^2}{g}\right)$	1370	1000 - 2000	1000 - 2000
$A_{EQ} \left(\frac{m^2}{g}\right)$	1445	940	1349

From the results displayed above in Tables 4-12 and 4-13 it is clear that the equation is an accurate approximation for most all of the materials, since values obtained via the constructed equation are relatively close to those provided by the material suppliers.

4.5 - Adsorption Test Results & Analysis

4.5.1 - Introduction

Below the results of the adsorption and adsorption/desorption cycle tests are presented for the carbon, zeolite, porous silicon, and silicate materials.

4.5.2 - Porous Carbon

4.5.2.1 - Introduction

Two forms of porous carbons were tested. These were granulated activated carbon (GAC), and activated carbon cloth (ACC). The GAC tested consisted of Norit RX3 Extra and was obtained courtesy of Norit Americas Inc. The ACC consisted of Zorflex cloth, and was provided by Chemviron Carbon. Two forms of Zorflex activated cloth were tested; a woven form (FM10) and a knitted form (FM30K). The adsorption test results for each of the carbon materials are presented in the following sections.

4.5.2.2 - Material Properties

The physical properties for each of the activated carbon materials are presented below in Table 4-14. Prior to testing, the RX3 GAC was powdered using a mortar and pestle to maximize its packing density. The natural packing density of the material was found to be $0.36 \frac{\text{g}}{\text{cm}^3}$. The powdered material achieved packing densities of approximately $0.57 \frac{\text{g}}{\text{cm}^3}$, which represents an increase of 58 %.

Table 4-14: Physical properties of activated carbon materials. A_{sm} is the specific surface area, A_{sv} is the available surface area per packed volume, ρ_b is the bulk material density (not packed), ρ_{pak} is the packed material density, m_s is the total sample mass, V_p is the sample packed volume, and ρ_{surf} is the cloth surface density (not packed).

	Norit RX3 Extra		Zorflex FM30K	Zorflex FM10
m_s (g)	2.28	m_s (g)	2.26	2.71
A_{sm} ($\frac{m^2}{g}$)	1370	A_{sm} ($\frac{m^2}{g}$)	1000 - 2000	1000 - 2000
A_{sv} ($\frac{m^2}{cm^3}$)	781	A_{sv} ($\frac{m^2}{cm^3}$)	473 - 946	383 - 766
ρ_b ($\frac{g}{cm^2}$)	0.38	ρ_{surf} ($\frac{g}{m^2}$)	110	120
ρ_{pak} ($\frac{g}{cm^2}$)	0.57	ρ_{pak} ($\frac{g}{cm^2}$)	0.47	0.6
V_p (cm^3)	8.8	V_p (cm^3)	9.5	9.5
Cost ($\frac{\$}{kg}$)	5.91	Cost ($\frac{\$}{kg}$)	263.60	220
Cost ($\frac{\$}{L}$)	3.37	Cost ($\frac{\$}{L}$)	124.70	85
		Cost ($\frac{\$}{m^2}$)	30.00	27

4.5.2.3 - Results

4.5.2.3.1 - Excess Adsorption

Excess Adsorption

Isotherm plots for the excess adsorption of methane gas on the Norit RX3 Extra GAC, Zorflex FM30K knitted ACC, and Zorflex FM10 woven ACC expressed in various commonly used evaluation unit parameters are presented below in Figures 4-6 through 4-14. The excess adsorption capacities displayed by the isotherm plots have been tabulated and are displayed for each of the materials below in Tables 4-15 to 4-17. Excess adsorption isotherm plots measured in other less commonly used performance units are presented in Appendix A2.

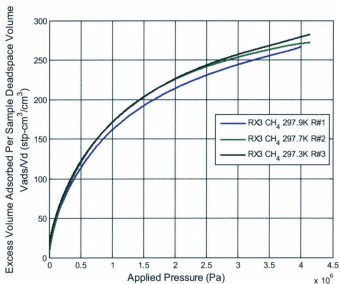


Figure 4-6: Norit RX3 - Excess Volumetric Adsorption Capacity.

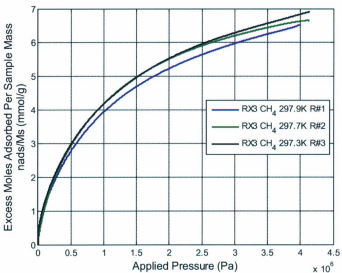


Figure 4-7: Norit RX3 - Specific Excess Molar Adsorption Capacity.

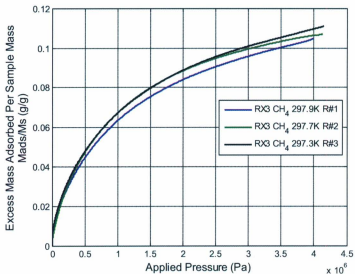


Figure 4-8: Norit RX3 - Specific Excess Mass Adsorption Capacity.

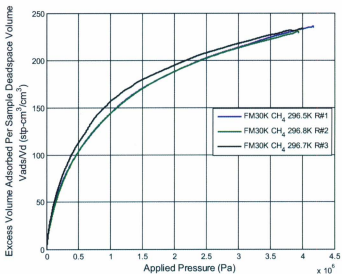


Figure 4-9: Zorflex FM30K - Excess Volumetric Adsorption Capacity.

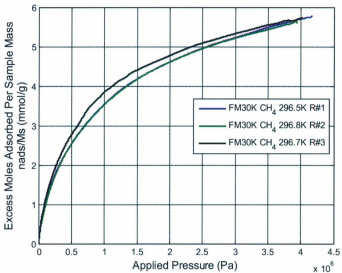


Figure 4-10: Zorflex FM30K - Specific Excess Molar Adsorption Capacity.

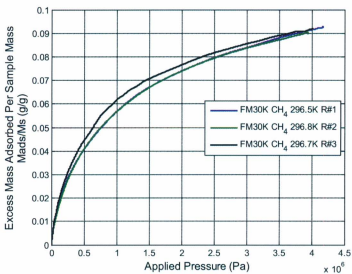


Figure 4-11: Zorflex FM30K - Specific Excess Mass Adsorption Capacity.

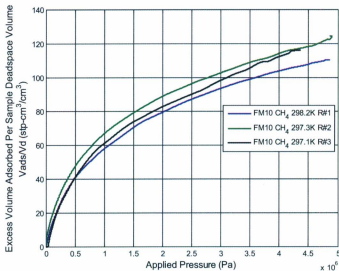


Figure 4-12: Zorflex FM10 - Excess Volumetric Adsorption Capacity.

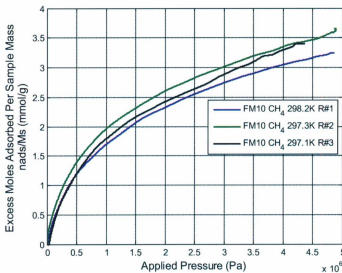


Figure 4-13: Zorflex FM10 - Specific Excess Molar Adsorption Capacity.

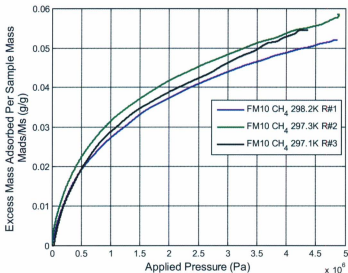


Figure 4-14: Zorflex FM10 – Specific Excess Mass Adsorption Capacity.

Table 4-15: Norit RX3 Extra - Excess Adsorption Capacities ($T \approx 298$ K). $\rho_{n_a}^a$ is the excess molar adsorption density, $\rho_{V_a}^a$ is the excess volumetric adsorption density, $\rho_{m_a}^a$ is the excess mass adsorption density, $M_{n_a}^a$ is the excess specific molar adsorption capacity, $M_{V_a}^a$ is the excess specific volumetric adsorption capacity, and $M_{m_a}^a$ is the excess specific mass adsorption capacity.

P	$\rho_{n_a}^a$	$\rho_{V_a}^a$	$\rho_{m_a}^a$	$M_{n_a}^a$	$M_{V_a}^a$	$M_{m_a}^a$
± 0.01	± 0.6	± 14	± 9	± 0.3	± 6	± 4
MPa	mmol/ml	ml/ml	mg/ml	mmol/g	ml/g	mg/g
1.00	8.5	206	137	3.9	83	62
2.00	11.2	270	179	5.1	110	82
3.00	12.5	302	201	5.7	124	92
3.50	13.1	315	210	5.9	130	96
4.00	13.4	324	215	6.1	135	98
4.50	13.7	330	220	6.2	150	100
5.00	13.8	333	222	6.3	152	101
5.50	14.0	338	225	6.4	154	103
5.88	14.3	343	229	6.5	156	104

Table 4-16: Zorflex FM30K - Excess Adsorption Capacities ($T \approx 298$ K). $\rho_{n_a}^a$ is the excess molar adsorption density, $\rho_{V_a}^a$ is the excess volumetric adsorption density, $\rho_{m_a}^a$ is the excess mass adsorption density, $M_{n_a}^a$ is the excess specific molar adsorption capacity, $M_{V_a}^a$ is the excess specific volumetric adsorption capacity, and $M_{m_a}^a$ is the excess specific mass adsorption capacity.

P ± 0.01 MPa	$\rho_{n_a}^a$ ± 0.5 mmol/ml	$\rho_{V_a}^a$ ± 13 ml/ml	$\rho_{m_a}^a$ ± 9 mg/ml	$M_{n_a}^a$ ± 0.3 mmol/g	$M_{V_a}^a$ ± 6 ml/g	$M_{m_a}^a$ ± 4 mg/g
1.00	5.9	141	95	2.8	68	45
2.00	7.7	187	124	3.7	89	59
3.00	8.7	210	140	4.2	101	67
3.50	9.0	217	145	4.3	104	69
4.00	9.3	224	149	4.4	107	71
4.50	9.6	231	154	4.6	111	74
4.96	9.8	237	157	4.7	113	75

Table 4-17: Zorflex FM10 - Excess Adsorption Capacities ($T \approx 298$ K). $\rho_{n_a}^a$ is the excess molar adsorption density, $\rho_{V_a}^a$ is the excess volumetric adsorption density, $\rho_{m_a}^a$ is the excess mass adsorption density, $M_{n_a}^a$ is the excess specific molar adsorption capacity, $M_{V_a}^a$ is the excess specific volumetric adsorption capacity, and $M_{m_a}^a$ is the excess specific mass adsorption capacity.

P ± 0.01 MPa	$\rho_{n_a}^a$ ± 0.4 mmol/ml	$\rho_{V_a}^a$ ± 11 ml/ml	$\rho_{m_a}^a$ ± 7 mg/ml	$M_{n_a}^a$ ± 0.3 mmol/g	$M_{V_a}^a$ ± 8 ml/g	$M_{m_a}^a$ ± 5 mg/g
1.00	3.4	83	55	2.4	59	39
2.00	4.5	109	72	3.2	77	51
3.00	5.2	126	84	3.7	89	59
3.50	5.5	132	88	3.9	93	62
4.00	5.7	138	92	4.1	98	65
4.50	6.0	145	96	4.2	103	68
5.00	6.2	151	100	4.4	107	71
5.47	6.5	158	105	4.6	112	74

Adsorption/Desorption Cycle

Isotherm plots of an excess adsorption-desorption cycle for each of the carbon materials expressed in various commonly used evaluation unit parameters are presented below in Figures 4-15 to 4-23. Tables 4-18 through 4-20 displayed below provides values for the excess amounts of gas remaining adsorbed for various discharge pressures for each of the materials.

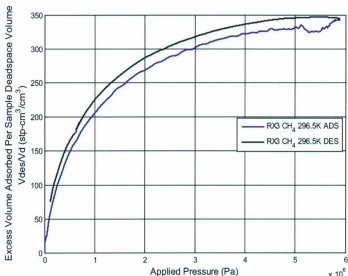


Figure 4-15: Norit RX3 - Excess Volumetric Adsorption/Desorption Cycle.

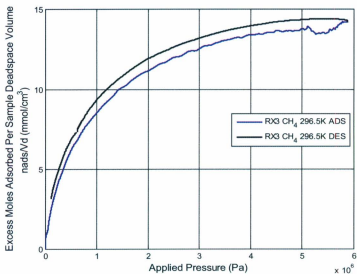


Figure 4-16: Norit RX3 - Specific Excess Molar Adsorption/Desorption Cycle.

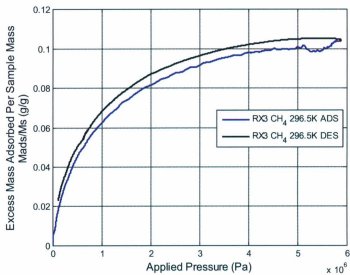


Figure 4-17: Norit RX3 - Specific Excess Mass Adsorption/Desorption Cycle.

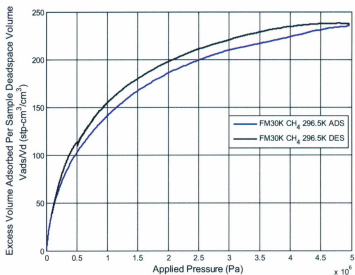


Figure 4-18: Zorflex FM30K - Excess Volumetric Adsorption/Desorption Cycle.

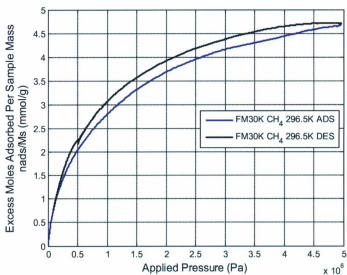


Figure 4-19: Zorflex FM30K - Specific Excess Molar Adsorption/Desorption Cycle.

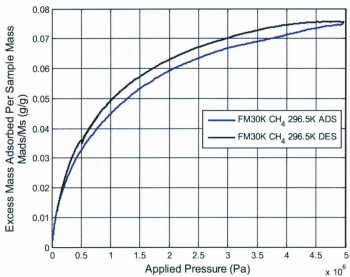


Figure 4-20: Zorflex FM30K - Specific Excess Mass Adsorption/Desorption Cycle.

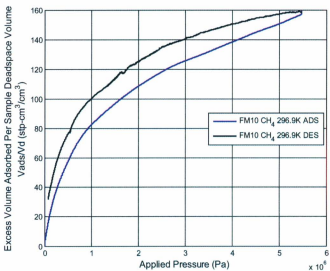


Figure 4-21: Zorflex FM10 - Excess Volumetric Adsorption/Desorption Cycle.

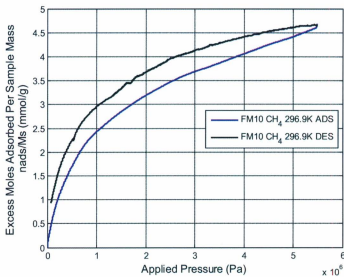


Figure 4-22: Zorflex FM10 - Specific Excess Molar Adsorption/Desorption Cycle.

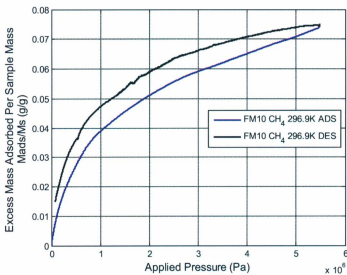


Figure 4-23: Zorflex FM10 - Specific Excess Mass Adsorption/Desorption Cycle.

Table 4-18: Norit RX3 - Excess adsorption capacities during desorption process ($T \approx 298$ K). $\rho_{n_d}^a$ is the excess molar desorption density, $\rho_{V_d}^a$ is the excess volumetric desorption density, $\rho_{m_d}^a$ is the excess mass desorption density, $M_{n_d}^a$ is the excess specific molar desorption capacity, $M_{V_d}^a$ is the excess specific volumetric desorption capacity, and $M_{m_d}^a$ is the excess specific mass desorption capacity.

P	$\rho_{n_d}^a$	$\rho_{V_d}^a$	$\rho_{m_d}^a$	$M_{n_d}^a$	$M_{V_d}^a$	$M_{m_d}^a$
± 0.01	± 0.6	± 14	± 9	± 0.3	± 6	± 4
MPa	mmol/ml	ml/ml	mg/ml	mmol/g	ml/g	mg/g
atm	2.8	71	46	1.3	32	21
1.00	9.4	226	151	4.3	103	69
2.00	12.0	288	192	5.4	131	87
3.00	13.2	319	212	6.0	145	97
3.50	13.7	329	219	6.2	150	100
4.00	14.0	337	224	6.4	153	102
4.50	14.2	343	228	6.5	156	104
5.00	14.4	346	230	6.5	157	105
5.50	14.4	347	231	6.6	158	105
5.88	14.3	343	229	6.5	156	104

Table 4-19: Zorflex FM30K - Excess adsorption capacities during desorption process ($T \approx 298$ K). $\rho_{n_d}^a$ is the excess molar desorption density, $\rho_{V_d}^a$ is the excess volumetric desorption density, $\rho_{m_d}^a$ is the excess mass desorption density, $M_{n_d}^a$ is the excess specific molar desorption capacity, $M_{V_d}^a$ is the excess specific volumetric desorption capacity, and $M_{m_d}^a$ is the excess specific mass desorption capacity.

P	$\rho_{n_d}^a$	$\rho_{V_d}^a$	$\rho_{m_d}^a$	$M_{n_d}^a$	$M_{V_d}^a$	$M_{m_d}^a$
± 0.01	± 0.5	± 13	± 9	± 0.3	± 6	± 4
MPa	mmol/ml	ml/ml	mg/ml	mmol/g	ml/g	mg/g
atm	1.7	42	28	0.8	20	14
1.00	6.5	156	103	3.1	75	49
2.00	8.2	198	132	3.9	95	63
3.00	9.1	221	147	4.4	106	70
3.50	9.5	229	152	4.5	109	73
4.00	9.7	234	156	4.6	112	75
4.50	9.9	238	158	4.7	114	76
4.96	9.8	237	157	4.7	113	75

Table 4-20: Zorflex FM10 - Excess adsorption capacities during desorption process ($T \approx 298$ K). $\rho_{n,d}^a$ is the excess molar desorption density, $\rho_{V,d}^a$ is the excess volumetric desorption density, $\rho_{m,d}^a$ is the excess mass desorption density, $M_{n,d}^a$ is the excess specific molar desorption capacity, $M_{V,d}^a$ is the excess specific volumetric desorption capacity, and $M_{m,d}^a$ is the excess specific mass desorption capacity.

P	$\rho_{n,d}^a$	$\rho_{V,d}^a$	$\rho_{m,d}^a$	$M_{n,d}^a$	$M_{V,d}^a$	$M_{m,d}^a$
± 0.01	± 0.4	± 11	± 7	± 0.3	± 8	± 5
MPa	mmol/ml	ml/ml	mg/ml	mmol/g	ml/g	mg/g
atm	1.5	37	24	1.1	26	17
1.00	4.2	101	67	3.0	71	48
2.00	5.2	125	83	3.7	89	59
3.00	5.8	141	94	4.1	100	66
3.50	6.1	146	97	4.3	103	69
4.00	6.2	150	100	4.4	107	71
4.50	6.4	154	103	4.5	109	73
5.00	6.5	157	105	4.6	111	74
5.47	6.5	158	105	4.6	112	74

Effective Delivery

Isotherm plots for the excess amounts of gas that are effectively deliverable for each of the carbon materials tested expressed in various commonly used unit parameters are presented below in Figures 4-24 to 4-32. Tables 4-21 through 4-23 displayed below provide values for the excess amounts effectively deliverable, along with the gas retention values for each of the materials.

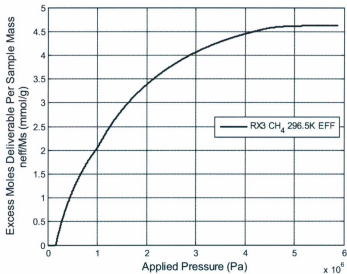


Figure 4-24: Norit RX3 - Excess Volumetric Delivery Capacity.

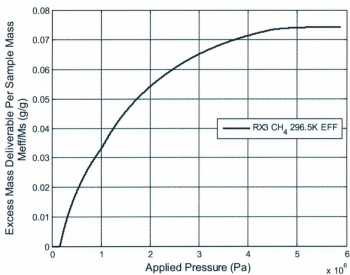


Figure 4-25: Norit RX3 - Specific Excess Molar Delivery Capacity.

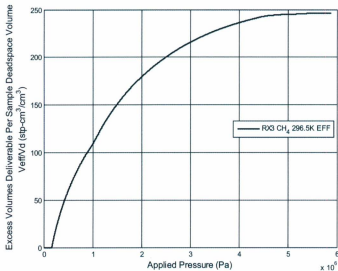


Figure 4-26: Norit RX3 - Specific Excess Mass Delivery Capacity.

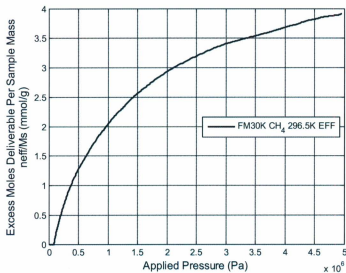


Figure 4-27: Zorflex FM30K - Specific Excess Molar Delivery Capacity.

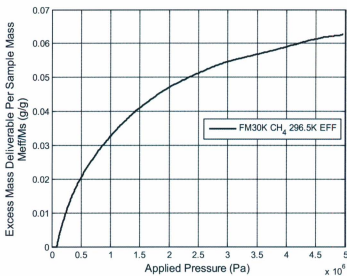


Figure 4-28: Zorflex FM30K - Specific Excess Mass Delivery Capacity.

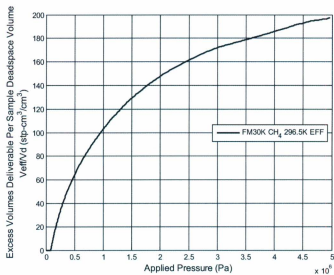


Figure 4-29: Zorflex FM30K - Excess Volumetric Delivery Capacity.

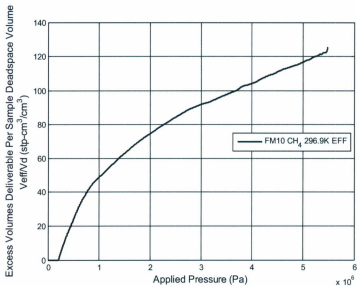


Figure 4-30: Zorflex FM10 - Excess Volumetric Delivery Capacity.

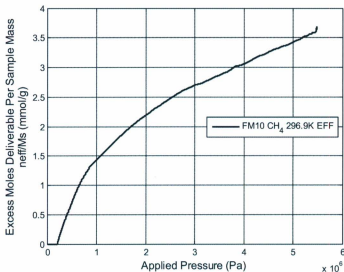


Figure 4-31: Zorflex FM10 - Specific Excess Molar Delivery Capacity.

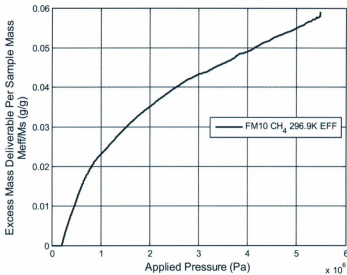


Figure 4-32: Zorflex FM10 - Specific Excess Mass Delivery Capacity.

Table 4-21: Norit RX3 - Excess Adsorption - Effective Delivery Capacities ($T \approx 298$ K). $\rho_{n_e}^a$ is the excess molar delivery density, $\rho_{V_e}^a$ is the excess volumetric delivery density, $\rho_{m_e}^a$ is the excess mass delivery density, $M_{n_e}^a$ is the excess specific molar delivery capacity, $M_{V_e}^a$ is the excess specific volumetric delivery capacity, $M_{m_e}^a$ is the excess specific mass delivery capacity, and R^a is the excess adsorption gas retention.

P	$\rho_{n_e}^a$	$\rho_{V_e}^a$	$\rho_{m_e}^a$	$M_{n_e}^a$	$M_{V_e}^a$	$M_{m_e}^a$	R^a
± 0.01	± 0.6	± 14	± 9	± 0.3	± 6	± 4	(%)
MPa	mmol/ml	ml/ml	mg/ml	mmol/g	ml/g	mg/g	
1.00	5.7	135	91	2.6	51	41	33
2.00	8.4	199	133	3.8	77	61	25
3.00	9.7	232	155	4.4	92	71	23
3.50	10.2	245	164	4.7	98	75	22
4.00	10.6	253	169	4.8	103	77	21
4.50	10.9	260	174	4.9	118	79	21
5.00	11.0	263	175	5.0	120	80	20
5.50	11.2	268	179	5.1	122	82	20
5.88	11.5	273	183	5.2	124	83	20

Table 4-22: Zorflex FM30K - Excess Adsorption - Effective Delivery Capacities ($T \approx 298$ K). $\rho_{n_e}^a$ is the excess molar delivery density, $\rho_{V_e}^a$ is the excess volumetric delivery density, $\rho_{m_e}^a$ is the excess mass delivery density, $M_{n_e}^a$ is the excess specific molar delivery capacity, $M_{V_e}^a$ is the excess specific volumetric delivery capacity, $M_{m_e}^a$ is the excess specific mass delivery capacity, and R^a is the excess adsorption gas retention.

P ± 0.01 MPa	$\rho_{n_e}^a$ ± 0.5 mmol/ml	$\rho_{V_e}^a$ ± 13 ml/ml	$\rho_{m_e}^a$ ± 9 mg/ml	$M_{n_e}^a$ ± 0.3 mmol/g	$M_{V_e}^a$ ± 6 ml/g	$M_{m_e}^a$ ± 4 mg/g	R^a (%)
1.00	4.1	100	66	2.0	48	32	42
2.00	6.0	145	95	2.9	69	46	29
3.00	7.0	168	111	3.3	81	53	25
3.50	7.3	175	116	3.5	84	56	24
4.00	7.6	182	121	3.6	87	58	23
4.50	7.9	189	126	3.8	91	60	22
4.96	8.1	195	129	3.9	93	62	22

Table 4-23: Zorflex FM10 - Excess Adsorption - Effective Delivery Capacities ($T \approx 298$ K). $\rho_{n_e}^a$ is the excess molar delivery density, $\rho_{V_e}^a$ is the excess volumetric delivery density, $\rho_{m_e}^a$ is the excess mass delivery density, $M_{n_e}^a$ is the excess specific molar delivery capacity, $M_{V_e}^a$ is the excess specific volumetric delivery capacity, $M_{m_e}^a$ is the excess specific mass delivery capacity, and R^a is the excess adsorption gas retention.

P ± 0.01 MPa	$\rho_{n_e}^a$ ± 0.4 mmol/ml	$\rho_{V_e}^a$ ± 11 ml/ml	$\rho_{m_e}^a$ ± 7 mg/ml	$M_{n_e}^a$ ± 0.3 mmol/g	$M_{V_e}^a$ ± 8 ml/g	$M_{m_e}^a$ ± 5 mg/g	R^a (%)
1.00	1.9	46	31	1.4	33	22	44
2.00	3.0	72	48	2.1	51	34	34
3.00	3.7	89	59	2.6	63	42	29
3.50	3.9	95	63	2.8	67	45	28
4.00	4.2	102	67	3.0	72	48	26
4.50	4.5	108	72	3.2	77	51	25
5.00	4.7	114	76	3.3	81	54	24
5.47	5.0	121	81	3.6	86	57	23

4.5.2.3.2 - Effective Storage

Effective Storage

Isotherm plots of the effective storage of methane by the RX3 Extra, FM30K, and FM10 materials expressed in various commonly used evaluation unit parameters are presented below in Figures 4-33 through 4-41. The effective storage capacities displayed by the isotherm plots have been tabulated and are displayed for each of the materials below in Tables 4-24 to 4-26. Effective storage isotherm plots measured in other less commonly used performance units are presented in Appendix A2.

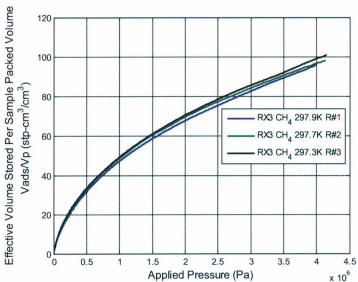


Figure 4-33: Norit RX3 - Effective Volumetric Storage Capacity.

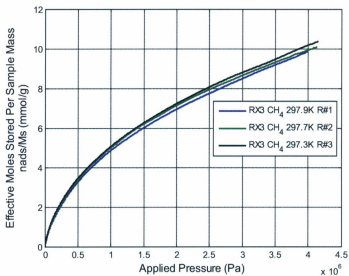


Figure 4-34: Norit RX3 - Specific Effective Molar Storage Capacity.

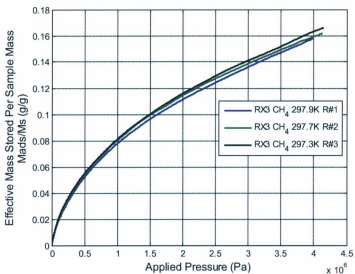


Figure 4-35: Norit RX3 - Specific Effective Mass Storage Capacity.

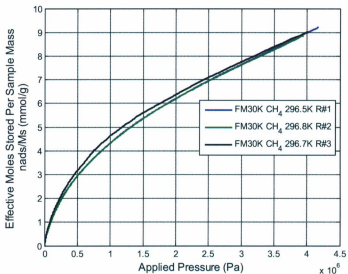


Figure 4-36: Zorflex FM30K – Specific Effective Molar Storage Capacity.

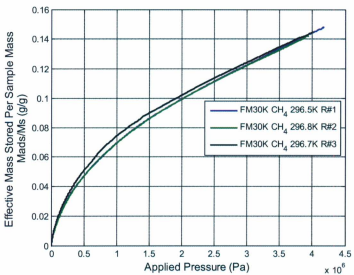


Figure 4-37: Zorflex FM30K – Specific Effective Mass Storage Capacity.

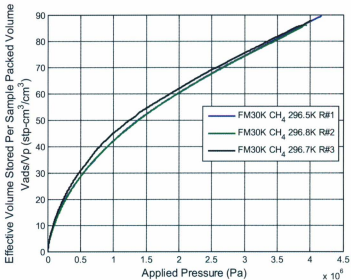


Figure 4-38: Zorflex FM30K - Effective Volumetric Storage Capacity.

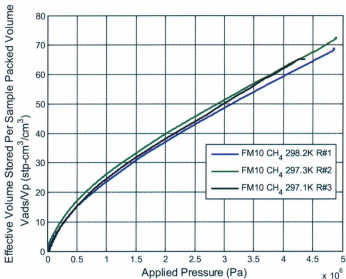


Figure 4-39: Zorflex FM10 - Effective Volumetric Storage Capacity.

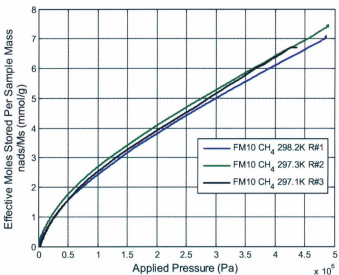


Figure 4-40: Zorflex FM10 – Specific Effective Molar Storage Capacity.

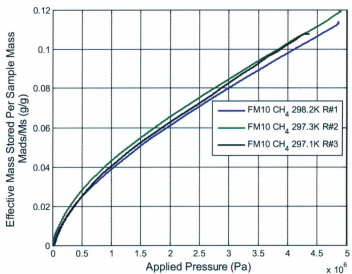


Figure 4-41: Zorflex FM10 – Specific Effective Mass Storage Capacity.

Table 4-24: Norit RX3 - Effective Storage Capacities ($T \approx 298$ K). $\rho_{n_a}^s$ is the effective molar storage density, $\rho_{V_a}^s$ is the effective volumetric storage density, $\rho_{m_a}^s$ is the effective mass storage density, $M_{n_a}^s$ effective specific molar storage capacity, $M_{V_a}^s$ is the effective specific volumetric storage capacity, and $M_{m_a}^s$ is the Effective specific mass storage capacity.

P	$\rho_{n_a}^s$	$\rho_{V_a}^s$	$\rho_{m_a}^s$	$M_{n_a}^s$	$M_{V_a}^s$	$M_{m_a}^s$
± 0.01	± 0.1	± 4	± 2.3	± 0.3	± 6	± 4
MPa	mmol/ml	ml/ml	mg/ml	mmol/g	ml/g	mg/g
1.00	2.5	61	41	4.4	106	71
2.00	3.5	85	57	6.2	149	99
3.00	4.2	101	67	7.4	178	118
3.50	4.5	109	72	7.9	191	127
4.00	4.8	115	76	8.4	202	134
4.50	5.0	121	80	8.8	212	141
5.00	5.2	126	84	9.2	221	147
5.50	5.4	131	87	9.5	230	153
5.88	5.7	137	91	9.9	239	159

Table 4-25: Zorflex FM30K - Effective Storage Capacities ($T \approx 298$ K). $\rho_{n_a}^s$ is the effective molar storage density, $\rho_{V_a}^s$ is the effective volumetric storage density, $\rho_{m_a}^s$ is the effective mass storage density, $M_{n_a}^s$ effective specific molar storage capacity, $M_{V_a}^s$ is the effective specific volumetric storage capacity, and $M_{m_a}^s$ is the Effective specific mass storage capacity.

P	$\rho_{n_a}^s$	$\rho_{V_a}^s$	$\rho_{m_a}^s$	$M_{n_a}^s$	$M_{V_a}^s$	$M_{m_a}^s$
± 0.01	± 0.1	± 3	± 2	± 0.3	± 6	± 4
MPa	mmol/ml	ml/ml	mg/ml	mmol/g	ml/g	mg/g
1.00	1.7	42	28	3.5	84	56
2.00	2.5	60	40	5.0	121	80
3.00	3.1	74	49	6.1	148	98
3.50	3.3	80	53	6.6	160	106
4.00	3.5	86	57	7.1	172	114
4.50	3.8	91	61	7.6	184	122
4.96	4.0	97	65	8.1	195	130

Table 4-26 : Zorflex FM10 - Effective Storage Capacities ($T \approx 298 \text{ K}$). $\rho_{n_a}^s$ is the effective molar storage density, $\rho_{V_a}^s$ is the effective volumetric storage density, $\rho_{m_a}^s$ is the effective mass storage density, $M_{n_a}^s$ effective specific molar storage capacity, $M_{V_a}^s$ is the effective specific volumetric storage capacity, and $M_{m_a}^s$ is the Effective specific mass storage capacity.

P ± 0.01 MPa	$\rho_{n_a}^s$ ± 0.1 mmol/ml	$\rho_{V_a}^s$ ± 3 ml/ml	$\rho_{m_a}^s$ ± 2 mg/ml	$M_{n_a}^s$ ± 0.3 mmol/g	$M_{V_a}^s$ ± 8 ml/g	$M_{m_a}^s$ ± 5 mg/g
1.00	1.3	31	21	3.2	77	51
2.00	1.9	46	30	4.7	114	75
3.00	2.4	58	39	6.0	145	96
3.50	2.6	64	42	6.6	159	105
4.00	2.9	70	46	7.2	173	115
4.50	3.1	76	50	7.8	187	125
5.00	3.4	81	54	8.4	202	134
5.47	3.6	87	58	9.0	216	144

Adsorption/Desorption Cycle

Isotherm plots of an effective storage adsorption-desorption cycle for each of the carbon materials tested expressed in various commonly used evaluation unit parameters are presented below in Figures 4-42 to 4-50. Tables 4-27 through 4-29 displayed below provide values for the effectively stored amounts of gas remaining adsorbed for various discharge pressures for each of the materials.

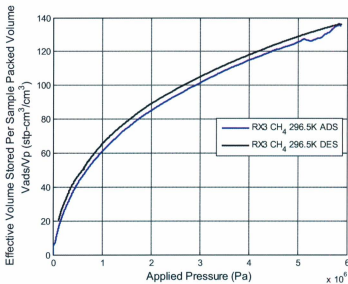


Figure 4-42: Norit RX3 - Effective Volumetric Storage Charge/Discharge Cycle.

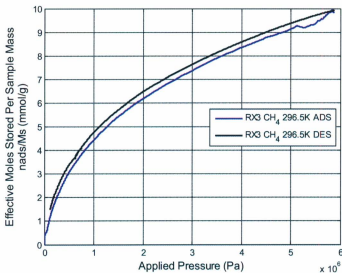


Figure 4-43: Norit RX3 - Specific Effective Molar Charge/Discharge Cycle.

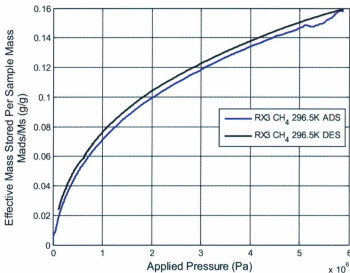


Figure 4-44: Norit RX3 - Specific Effective Mass Charge/Discharge Cycle.

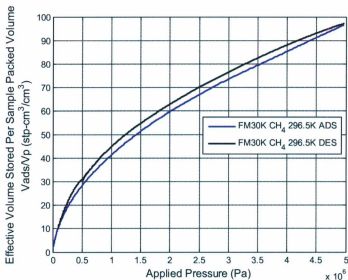


Figure 4-45: Zorflex FM30K - Effective Volumetric Storage Charge/Discharge Cycle.

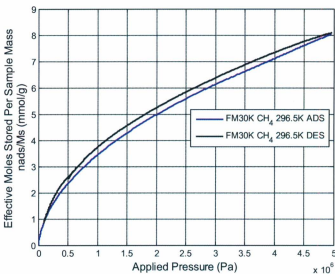


Figure 4-46: Zorflex FM30K - Specific Effective Molar Charge/Discharge Cycle.

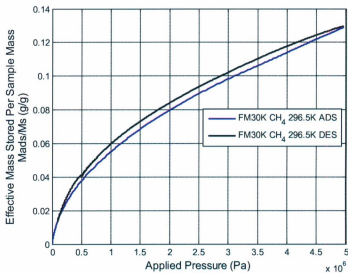


Figure 4-47: Zorflex FM30K - Specific Effective Mass Charge/Discharge Cycle.

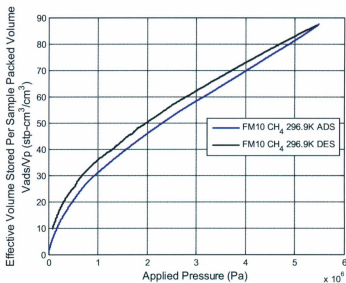


Figure 4-48: Zorflex FM10 - Effective Volumetric Storage Charge/Discharge Cycle.

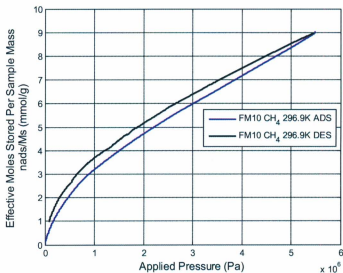


Figure 4-49: Zorflex FM10 - Specific Effective Molar Charge/Discharge Cycle.

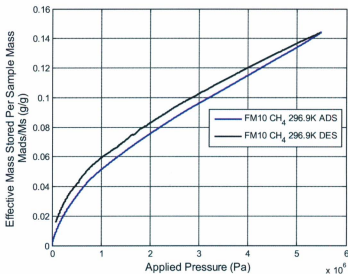


Figure 4-50: Zorflex FM10 - Specific Effective Mass Charge/Discharge Cycle.

Table 4-27: Norit RX3 - Effective storage capacities during desorption process ($T \approx 298$ K). $\rho_{n_d}^s$ is the effective molar discharge density, $\rho_{V_d}^s$ is the effective volumetric discharge density, $\rho_{m_d}^s$ is the effective mass discharge density, $M_{n_d}^s$ is the effective specific molar discharge capacity, $M_{V_d}^s$ is the effective specific volumetric discharge capacity, and $M_{m_d}^s$ is the effective specific mass discharge capacity.

P	$\rho_{n_d}^s$	$\rho_{V_d}^s$	$\rho_{m_d}^s$	$M_{n_d}^s$	$M_{V_d}^s$	$M_{m_d}^s$
± 0.01	± 0.1	± 4	± 2.3	± 0.3	± 6	± 4
MPa	mmol/ml	ml/ml	mg/ml	mmol/g	ml/g	mg/g
atm	0.8	18	13	1.3	32	22
1.00	2.7	66	44	4.8	115	76
2.00	3.7	89	59	6.5	157	104
3.00	4.4	105	70	7.7	185	123
3.50	4.6	112	74	8.1	197	131
4.00	4.9	118	78	8.6	207	138
4.50	5.1	124	82	9.0	217	145
5.00	5.4	129	86	9.4	226	151
5.50	5.5	134	88	9.7	235	154
5.88	5.7	137	91	9.9	239	159

Table 4-28: Zorflex FM30K - Effective storage capacities during desorption process ($T \approx 298$ K). $\rho_{n,d}^s$ is the effective molar discharge density, $\rho_{V,d}^s$ is the effective volumetric discharge density, $\rho_{m,d}^s$ is the effective mass discharge density, $M_{n,d}^s$ is the effective specific molar discharge capacity, $M_{V,d}^s$ is the effective specific volumetric discharge capacity, and $M_{m,d}^s$ is the effective specific mass discharge capacity.

P ± 0.01 MPa	$\rho_{n,d}^s$ ± 0.1 mmol/ml	$\rho_{V,d}^s$ ± 3 ml/ml	$\rho_{m,d}^s$ ± 2 mg/ml	$M_{n,d}^s$ ± 0.3 mmol/g	$M_{V,d}^s$ ± 5 ml/g	$M_{m,d}^s$ ± 6 ml/g
atm	11	7	0.9	22	20	15
1.00	45	30	3.8	91	75	60
2.00	63	42	5.3	127	95	84
3.00	77	51	6.4	154	106	102
3.50	83	55	6.9	166	109	110
4.00	88	59	7.3	177	112	118
4.50	93	62	7.8	187	114	125
4.96	97	65	8.1	195	114	130

Table 4-29 : Zorflex FM10 - Effective storage capacities during desorption process ($T \approx 298$ K). $\rho_{n,d}^s$ is the effective molar discharge density, $\rho_{V,d}^s$ is the effective volumetric discharge density, $\rho_{m,d}^s$ is the effective mass discharge density, $M_{n,d}^s$ is the effective specific molar discharge capacity, $M_{V,d}^s$ is the effective specific volumetric discharge capacity, and $M_{m,d}^s$ is the effective specific mass discharge capacity.

P ± 0.01 MPa	$\rho_{n,d}^s$ ± 0.1 mmol/ml	$\rho_{V,d}^s$ ± 3 ml/ml	$\rho_{m,d}^s$ ± 2 mg/ml	$M_{n,d}^s$ ± 0.3 mmol/g	$M_{V,d}^s$ ± 8 ml/g	$M_{m,d}^s$ ± 5 mg/g
atm	0.5	11	7	1.1	27	18
1.00	1.5	36	24	3.7	89	59
2.00	2.1	50	33	5.2	125	83
3.00	2.6	62	41	6.4	155	103
3.50	2.8	68	45	7.0	168	112
4.00	3.0	73	49	7.5	181	120
4.50	3.2	78	52	8.0	194	129
5.00	3.4	83	55	8.5	206	137
5.47	0.5	11	7	1.1	27	18

Effective Delivery

Isotherm plots for the effectively stored amounts of gas that are effectively deliverable for each of the carbon materials expressed in various commonly used unit parameters are presented below in Figures 4-51 to 4-59. Tables 4-30 through 4-32 displayed below provide values for the effectively stored amounts that are effectively deliverable, along with the gas retention values for each of the materials.

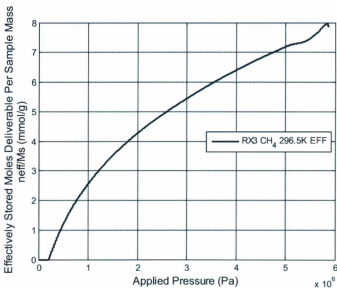


Figure 4-51: Norit RX3 - Effective Volumetric Delivery Capacity.

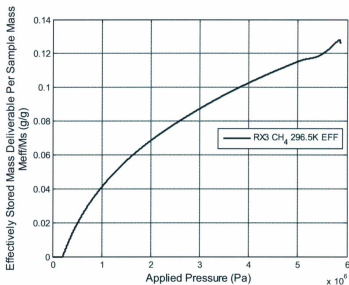


Figure 4-52: Norit RX3 - Specific Effective Molar Delivery Capacity.

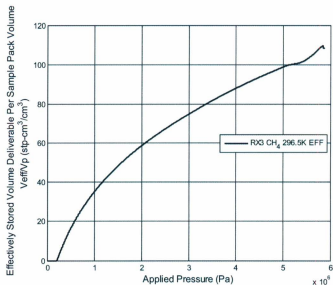


Figure 4-53: Norit RX3 - Specific Effective Mass Delivery Capacity.

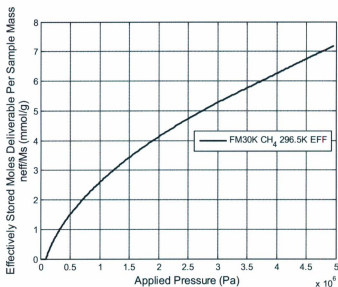


Figure 4-54: Zorflex FM30K - Effective Volumetric Delivery Capacity.

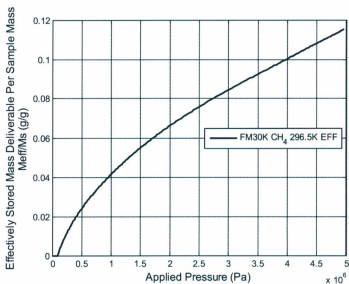


Figure 4-55: Zorflex FM30K - Specific Effective Molar Delivery Capacity.

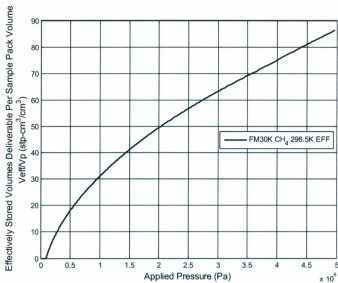


Figure 4-56: Zorflex FM30K - Specific Effective Mass Delivery Capacity.

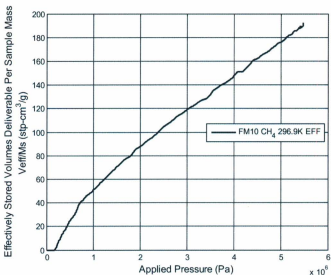


Figure 4-57: Zorflex FM10 - Effective Volumetric Delivery Capacity.

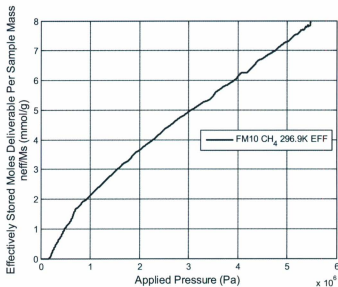


Figure 4-58: Zorflex FM10 - Specific Effective Molar Delivery Capacity.

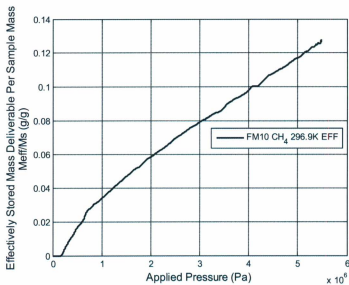


Figure 4-59: Zorflex FM10 - Specific Effective Mass Delivery Capacity.

Table 4-30: Norit RX3 - Effective Storage - Effective Delivery Capacities ($T \approx 298$ K). $\rho_{n_e}^s$ is the effective molar delivery density, $\rho_{V_e}^s$ is the effective volumetric delivery density, $\rho_{m_e}^s$ is the effective mass delivery density, $M_{n_e}^s$ is the effective specific molar delivery capacity, $M_{V_e}^s$ is the effective specific volumetric delivery capacity, $M_{m_e}^s$ is the effective specific mass delivery capacity, and R^s is the effective adsorption gas retention.

P ± 0.01 MPa	$\rho_{n_e}^s$ ± 0.1 mmol/ml	$\rho_{V_e}^s$ ± 4 ml/ml	$\rho_{m_e}^s$ ± 2.3 mg/ml	$M_{n_e}^s$ ± 0.3 mmol/g	$M_{V_e}^s$ ± 6 ml/g	$M_{m_e}^s$ ± 4 mg/g	R^s (%)
1.00	1.8	42	28	3.1	74	49	30
2.00	2.8	67	44	4.9	117	77	21
3.00	3.4	83	55	6.0	146	96	18
3.50	3.7	90	60	6.6	158	104	17
4.00	4.0	96	64	7.0	169	112	16
4.50	4.2	102	68	7.5	179	119	15
5.00	4.5	107	71	7.8	188	124	15
5.50	4.7	113	74	8.2	198	131	14
5.88	4.9	118	78	8.6	207	137	13

Table 4-31: Zorflex FM30K - Effective Storage - Effective Delivery Capacities ($T \approx 298$ K). $\rho_{n_e}^s$ is the effective molar delivery density, $\rho_{V_e}^s$ is the effective volumetric delivery density, $\rho_{m_e}^s$ is the effective mass delivery density, $M_{n_e}^s$ is the effective specific molar delivery capacity, $M_{V_e}^s$ is the effective specific volumetric delivery capacity, $M_{m_e}^s$ is the effective specific mass delivery capacity, and R^s is the effective adsorption gas retention.

P ± 0.01 MPa	$\rho_{n_e}^s$ ± 0.1 mmol/ml	$\rho_{V_e}^s$ ± 3 ml/ml	$\rho_{m_e}^s$ ± 2 mg/ml	$M_{n_e}^s$ ± 0.3 mmol/g	$M_{V_e}^s$ ± 6 ml/g	$M_{m_e}^s$ ± 4 mg/g	R^s (%)
1.00	1.3	31	20	2.5	61	41	26
2.00	2.0	49	32	4.1	98	65	18
3.00	2.6	63	41	5.2	126	83	15
3.50	2.8	68	45	5.7	138	91	14
4.00	3.1	74	49	6.2	150	99	13
4.50	3.3	80	53	6.7	162	107	12
4.96	3.6	86	57	7.2	173	115	11

Table 4-32 : Zorflex FM10 - Effective Storage - Effective Delivery Capacities ($T \approx 298$ K). $\rho_{n_e}^s$ is the effective molar delivery density, $\rho_{V_e}^s$ is the effective volumetric delivery density, $\rho_{m_e}^s$ is the effective mass delivery density, $M_{n_e}^s$ is the effective specific molar delivery capacity, $M_{V_e}^s$ is the effective specific volumetric delivery capacity, $M_{m_e}^s$ is the effective specific mass delivery capacity, and R^s is the effective adsorption gas retention.

P ± 0.01 MPa	$\rho_{n_e}^s$ ± 0.1 mmol/ml	$\rho_{V_e}^s$ ± 3 ml/ml	$\rho_{m_e}^s$ ± 2 mg/ml	$M_{n_e}^s$ ± 0.3 mmol/g	$M_{V_e}^s$ ± 8 ml/g	$M_{m_e}^s$ ± 5 mg/g	R^s (%)
1.00	0.8	20	13	2.1	50	33	36
2.00	1.4	35	23	3.6	86	57	24
3.00	2.0	47	31	4.9	117	78	19
3.50	2.2	53	35	5.4	131	87	17
4.00	2.4	59	39	6.0	145	97	16
4.50	2.7	64	43	6.6	160	106	15
5.00	2.9	70	47	7.2	174	116	14
5.47	3.2	76	51	7.8	189	126	13

4.5.2.4 - Analysis

4.5.2.4.1 - Excess Adsorption

From the excess adsorption isotherms for the RX3 Extra displayed in Figures 4-6 through 4-8, it is clear that there is deviation between the isotherms obtained from the different test runs. However, these deviations can be attributed to the different temperatures present during the tests. It is evident that the lowest temperature isotherm produces the highest adsorption values, and the highest temperature isotherm produces the lowest adsorption values as one would expect since increasing temperatures decrease a material's adsorption capacity. Overall there is a relatively low reproducibility error for the tests.

It is evident from the excess adsorption/desorption cycle plots displayed above in Figures 4-15 through 4-17 for the RX3 Extra that some hysteresis is present, although its effect is relatively small. This is a desired property for adsorbent materials, as it will ultimately lead to higher delivery capacities since gas retention will be reduced.

The slight deviation of the adsorption plots from expected values (based on the general plot trend) between pressures of approximately 5 to 6 MPa is due to a minor electrical malfunction of the apparatus that occurred during the test.

Based on the excess adsorption isotherms displayed in Figures 4-9 through 4-11 for the Zorflex FM30K, it is evident that there is a slight deviation between isotherms obtained from the different test runs conducted. Since temperature variations between the runs are small and all of the plots merge to a common final value, the deviation in the isotherm values can be attributed to differences in gas expansion rates during testing. Overall there is a relatively low reproducibility error for the tests. In fact, the first and second test runs produce nearly identical values.

It is again clear that some hysteresis is present for the Zorflex FM30K based on the excess adsorption/desorption plots displayed in Figures 4-18 through 4-20. However, its effect is insignificant. The slight discontinuity in the desorption isotherms at approximately 0.5 MPa is due to the desorption process having to be conducted in two independent desorption steps. The discontinuity is made more evident when the desorption process is subject to temperature changes, and/or there is large a difference in the expansion rate between the sub processes. Note that all of the excess adsorbed gas is effectively desorbed upon discharging to atmospheric conditions. Thus, the presence of the hysteresis does not contribute to the overall gas retention values. However, a gas retention value of 24% was obtained at 3.5 MPa (see Table 4-22), which is relatively high for activated carbon cloth materials. This essentially means that 24% of the material's total adsorption capacity is obtained at pressures less than atmospheric.

From the excess adsorption isotherms for the Zorflex FM10 displayed in Figures 4-12 through 4-14, it is clear that there is a significant deviation between isotherms obtained from different test runs. At the final adsorption test pressure there is a difference of approximately 8% between the first and second runs. However, the majority of this deviation is most likely due to the difference in adsorption testing

temperatures, which is approximately 1 K. Differences in the average gas expansion rates for the different test runs would also contribute to this observed deviation. Overall, there is a moderate reproducibility error between test runs when compared to the other materials tested.

Based on the excess adsorption/desorption plots displayed in Figures 4-21 through 4-23 it is clear that hysteresis is very significant for the Zorflex FM10. Note that unlike the Zorflex FM30K cloth, all the adsorbed gas is not returned at atmospheric pressure. This produces significant gas retention values which are on the order of 28 % (see Table 4-23), when discharging from a pressure of 3.5 MPa to atmospheric conditions.

4.5.2.4.2 - Effective Storage

From the effective storage plots presented above in Figures 4-33 through 4-41, it is evident that significantly larger amounts of gas are effectively stored compared to the excess adsorption amounts obtained for each of the carbon materials tested. For example, at a pressure of 3.5 MPa an excess adsorption value of $96 \frac{\text{mg}}{\text{g}}$ and an effective storage value of $127 \frac{\text{mg}}{\text{g}}$ were obtained for the RX3 Extra. This represents a storage increase of approximately 32 %. The FM30K produced a storage increase of 54 % ($69 \frac{\text{mg}}{\text{g}}$ to $106 \frac{\text{mg}}{\text{g}}$), while the FM10 produced a storage increase of 69 % ($62 \frac{\text{mg}}{\text{g}}$ to $105 \frac{\text{mg}}{\text{g}}$). It is also evident that deviations between runs are much less significant than that found with excess adsorption. This indicates that the adsorption process is much more temperature sensitive than the gas compression process.

For each of the materials a rough calculation can be performed to determine the percentage of the effective storage capacity that can be attributed to the bulk gas compressive storage. This can be determined by comparing the theoretical bulk gas compression values with the effective storage values reported by the isotherm plots. The theoretical bulk gas compression storage can be obtained by approximating the

material's pore volume as the difference between the sample powder pack volume and the sample dead space volume; and then applying the ideal gas law to determine the amount of gas that could be stored in this volume at a given pressure. Calculations are performed at a pressure of 3.5 MPa for each of the samples.

For the RX3 Extra it was determined that the effective storage if no adsorption had taken place would be approximately $2.5 \frac{\text{mmol}}{\text{g}}$. Since a value of approximately $9 \frac{\text{mmol}}{\text{g}}$ was obtained, $6.5 \frac{\text{mmol}}{\text{g}}$ would have been adsorbed which is in agreement with the results displayed by Figure 4-7. Thus, the compression process accounts for approximately 28 % of the material's effective storage.

The results of the bulk compression component analysis for each of the activated carbon materials studied is presented below in Table 4-33.

Table 4-33: Bulk compression component fraction for effective storage of activated carbons.

Material	Theoretical Effective Storage Without Adsorption	Effective Storage Value Obtained	Bulk Compression Component of Effective Storage
Norit RX3	$2.5 \frac{\text{mmol}}{\text{g}}$	$9 \frac{\text{mmol}}{\text{g}}$	28 %
Zorflex FM30K	$2.8 \frac{\text{mmol}}{\text{g}}$	$8.3 \frac{\text{mmol}}{\text{g}}$	34 %
Zorflex FM10	$2.6 \frac{\text{mmol}}{\text{g}}$	$5.8 \frac{\text{mmol}}{\text{g}}$	45 %

From the effective adsorption/desorption cycle plots displayed for the materials in Figures 4-15 through 4-23, it is evident that hysteresis is again present but its effect is much less significant than that for excess adsorption. Since the amount of hysteresis present in the plots is greatly reduced, gas retention values are also greatly reduced when compared to excess adsorption. For example, the RX3 Extra was found to have a gas retention value of 17 % when discharging from 3.5 MPa. The Zorflex FM30K and

FM10 materials were found to have gas retention values of 14 % and 17 % respectively.

4.5.2.4.3 - Model Isotherm Fits

Absolute excess amounts and effectively stored amounts were successfully described by the Langmuir, Freundlich, and Toth isotherm models for each of the activated carbon materials. The modified versions of these models were also applied to the effective storage isotherms.

Excess Adsorption

Figures 4-60 to 4-62 presented below show fits of the isotherm models for the absolute excess adsorption isotherms of the RX3 Extra, Zorflex FM30K, and Zorflex FM10 materials. The isotherm model parameter values and fit statistics are shown below in Tables 4-34 through 4-36.

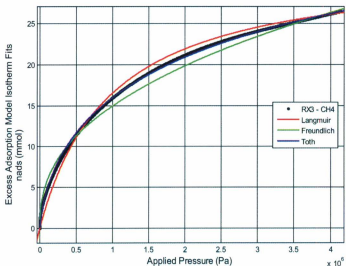


Figure 4-60: Norit RX3 - Absolute excess adsorption isotherm model fits.

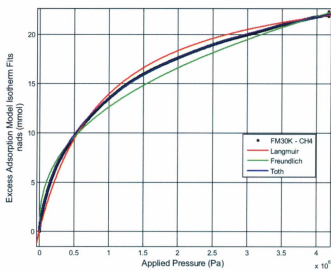


Figure 4-61: Zorflex FM30K - Absolute excess adsorption isotherm model fits.

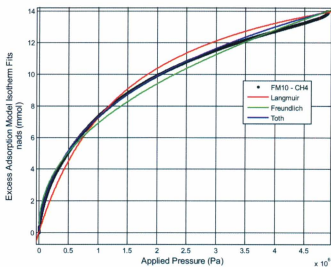


Figure 4-62: Zorflex FM10 - Absolute excess adsorption isotherm model fits.

Table 4-34: Excess adsorption model isotherm parameter values and fit statistics.

Norit RX3	Langmuir	Freundlich	Toth
a	33.86	0.835	44.92
b	8.84E-7	0.469	1.65E-6
c	-	3.61	0.560
SSE	14.94	17.86	13.35
R_{adj}^2	0.999	0.999	0.999
RSME	0.082	0.09	0.078

Table 4-35: Excess adsorption model isotherm parameter values and fit statistics.

FM30K	Langmuir	Freundlich	Toth
a	26.81	0.320	43.27
b	1.085E-6	0.170	2.021E-6
c	-	2.535	0.467
SSE	278	610.9	12.99
R_{adj}^2	0.997	0.994	0.999
RSME	0.373	0.553	0.0807

Table 4-36: Excess adsorption model isotherm parameter values and fit statistics.

FM10	Langmuir	Freundlich	Toth
a	18.04	0.452	40.21
b	6.9E-7	0.231	2.31E-6
c	-	3.422	0.519
SSE	1316	802.1	12.99
R_{adj}^2	0.992	0.995	0.997
RSME	0.247	0.205	0.151

From the isotherm plots displayed above it is evident that all models fit the experimental data very well.

Based on the fit statistics displayed above in Tables 4-34 to 4-36 and a visual inspection of Figures 4-60 to 4-63, it is clear that the Toth model describes the adsorption data most accurately for the RX3, FM30K, and FM10 materials.

Effective Storage

Figures 4-63 to 4-68 presented below show fits of the isotherm models and modified isotherm models for the absolute effective storage isotherms for the carbon materials tested. The parameter values and fit statistics for the models are shown below in Tables 4-37 through 4-39. Differences in the goodness of fit between the original and modified isotherm models can be obtained from these tables.

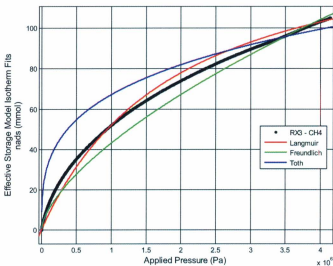


Figure 4-63: Norit RX3 - Absolute effective storage isotherm model fits.

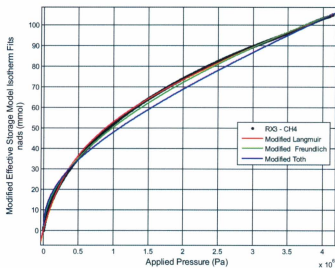


Figure 4-64: Norit RX3 - Absolute effective storage modified isotherm model fits.

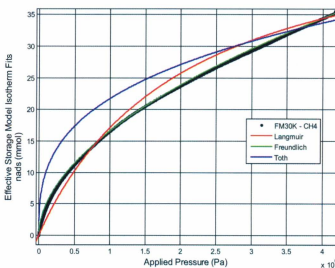


Figure 4-65: Zorflex FM30K - Absolute effective storage isotherm model fits.

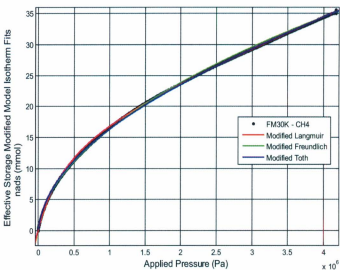


Figure 4-66: Zorflex FM30K - Absolute effective storage modified isotherm model fits.

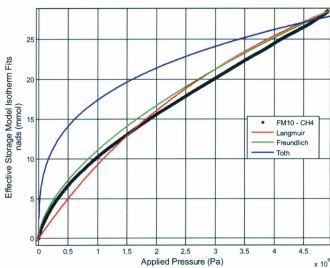


Figure 4-67: Zorflex FM10 - Absolute effective storage isotherm model fits.

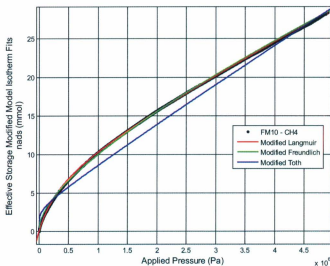


Figure 4-68: Zorflex FM10 - Absolute effective storage modified isotherm model fits.

Table 4-37: Excess adsorption model isotherm parameter values and fit statistics.

Norit RX3	Langmuir	Modified Langmuir	Freundlich	Modified Freundlich	Toth	Modified Toth
a	54.56	22.85	0.519	0.067	1.993E5	4.67E5
b	6E-7	1.902E-6	0.0214	0.076	363	79.01
c	-	4.677E-69	1.893	1.7	0.041	0.038
d	-	-	-	2.337E-6	-	5.074E-6
SSE	2168	79.56	316.8	314.5	23830	289.1
R_{adj}^2	0.995	0.998	0.999	0.999	0.942	0.999
RMSE	0.992	0.190	0.380	0.378	3.29	0.362

Table 4-38: Effective storage model isotherm parameter values and fit statistics.

FM30K	Langmuir	Modified Langmuir	Freundlich	Modified Freundlich	Toth	Modified Toth
a	51.76	17.21	0.129	0.0297	1.506E6	37.47
b	4.939E-7	2.327E-6	0.0906	0.159	2210	2.407E-6
c	-	4.716E-6	1.904	1.675	0.0348	0.477
d	-	-	-	1.132E-8	-	3.527E-6
SSE	1394	48.52	138.8	84.46	1.351E4	14.55
R _{adj} ²	0.995	0.999	0.999	0.999	0.956	1
RMSE	0.835	0.156	0.264	0.206	2.601	0.0854

Table 4-39: Effective storage model isotherm parameter values and fit statistics.

Parameter	Langmuir	Modified Langmuir	Freundlich	Modified Freundlich	Toth	Modified Toth
a	61.04	8.47	0.322	0.097	2.262E5	10.74
b	1.786E-7	2.516E-6	0.010	0.100	5330	31.7
c	-	4.235E-6	1.691	2.077	0.038	0.116
d	-	-	-	2.56E-6	-	4.98E-6
SSE	4465	152.3	3057	311	117200	5947
R _{adj} ²	0.995	0.999	0.997	0.999	0.871	0.993
RMSE	0.454	0.0839	0.376	0.120	2.327	0.524

Based on the model isotherm fits plot displayed above for the RX3 Extra, it is evident that the Langmuir and Freundlich models fit the storage data reasonably well, while the Toth equation provides a poor fit. Based on the fit statistics displayed in Table 4-37 for the modified isotherm models, it is clear that the Modified Langmuir model describes the effective storage data most accurately.

From the model isotherm fits plots displayed above for the Zorflex FM30K and FM10 materials, it is evident that the Langmuir and Freundlich models fit the data reasonably well, while the Toth equation provides a relatively poor fit for both

materials. Based on the fit statistics for the modified isotherm models is it clear that the Modified Langmuir model describes the adsorption data most accurately for both materials.

Based on the original and modified isotherm model plots and fit statistics presented above, it can be concluded that the modified isotherm models fit the effective storage data much better than the original models.

4.5.3 - Zeolites

4.5.3.1 - Introduction

Four types of zeolite materials were tested. These were 3A Zeolite, 4A Zeolite, 5A Zeolite, and 13X Zeolite. 3A through 5A zeolites are classified according to their average pore size. The average pore size of each of the zeolites along with a description and the material supplier are presented below in Table 4-40.

Table 4-40: Zeolite materials classification and supplier.

Material	Description	Average Pore Size	Supplier
3A	Molecular Sieve 3A	0.3 nm	Sigma Aldrich
4A	Molecular Sieve 4A	0.4 nm	Anachemia
5A	Matrix Molecular Sieve 5A	0.5 nm	Supelco / Sigma Aldrich
13X	Matrix Molecular Sieve 13X	0.8 nm	Supelco / Sigma Aldrich

4.5.3.2 - Material Properties

The physical properties for each of the zeolite materials tested are presented below in Table 4-41.

Table 4-41: Physical properties of zeolite materials. A_{sm} is the specific surface area, A_{sv} is the available surface area per packed volume, ρ_k is the bulk material density (not packed), ρ_{pak} is the packed material density, m_s is the total sample mass, V_p is the sample packed volume, and D_{pore} is the average material pore diameter.

	3A Zeolite	4A Zeolite	5A Zeolite	13X Zeolite
$A_{sm} \left(\frac{m^2}{g} \right)$	-	< 100	500	400
$A_{sv} \left(\frac{m^2}{cm^3} \right)$	-	320	355	360
D_{pore} (nm)	0.3	0.4	0.5	0.8
$\rho_b \left(\frac{g}{cm^3} \right)$	0.64	0.7	0.7	0.66
$\rho_{pak} \left(\frac{g}{cm^3} \right)$	0.75	0.8	0.71	0.6
m_s (g)	9.6	7.28	7.28	5.96
V_p (cm ³)	9.7	8.2	8.2	10
$Cost \left(\frac{\$}{kg} \right)$	1.30	1.02	1.05	1.10
$Cost \left(\frac{\$}{L} \right)$	0.98	0.82	0.75	0.66

The specific surface area of 3A Zeolite cannot be specified since its pores are too small for the adsorption of nitrogen, which is required for determining the specific surface area using the BET method. As previously stated, 3A zeolite has an average pore diameter of 0.3 nm, and the kinetic diameters of methane and nitrogen are approximately 0.38 and 0.37 respectively. Excess adsorption and effective storage tests conducted on the material using both methane and nitrogen gas confirms this property.

4A zeolite has an average pore diameter of 0.4 nm, and the kinetic diameters of methane and nitrogen are approximately 0.414 and 0.365 respectively. Thus, unlike 3A Zeolite the specific surface area of 4A zeolite can be determined via the BET method and the material should adsorb methane gas.

Prior to adsorption testing, the 3A and 4A zeolites were powdered using a mortar and pestle to maximize their packing densities since the particle size of the supplied materials were relatively large. The 5A and 13X zeolites consisted of particles having a 60 to 80 mesh size. Thus, no additional powdering process was required since any changes in the packing densities resulting from the process would be insignificant when considering the relatively small sample volumes used (≈ 10 ml). The powdering process increased the natural packing densities of the 3A and 4A zeolites from 0.75 and $0.71 \frac{\text{g}}{\text{cm}^3}$, to 0.99 and $0.89 \frac{\text{g}}{\text{cm}^3}$ respectively. This represents packing density increases of 32 % and 25 %, which is quite significant. Samples were also heated to approximately 120 °C for a period of at least 48 hours to remove any adsorbed moisture prior to gas adsorption testing, since zeolites are generally desiccants.

4.5.3.3 - Results

4.5.3.3.1 - Excess Adsorption

Excess Adsorption

Isotherm plots of the excess adsorption of methane on the 3A Zeolite, 4A Zeolite, 5A Zeolite, 13X Zeolite materials expressed in various commonly used evaluation unit parameters are presented below in Figures 4-69 through 4-81. Plots of the excess adsorption of nitrogen on 3A Zeolite is also presented. The excess adsorption capacities displayed by the isotherm plots have been tabulated and are displayed for each of the materials below in Tables 4-42 to 4-44. Excess adsorption isotherm plots measured in other less commonly used performance units are presented in Appendix A2.

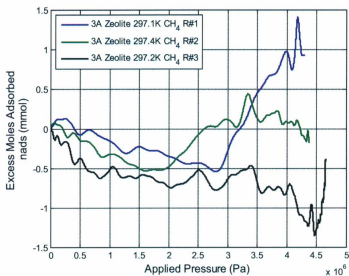


Figure 4-69: 3A Zeolite - Absolute Excess Molar Adsorption Capacity.

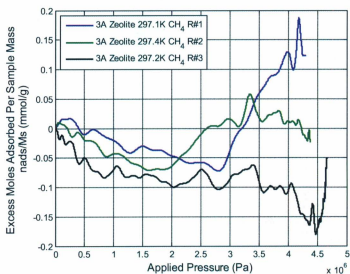


Figure 4-70: 3A Zeolite - Specific Excess Molar Adsorption Capacity.

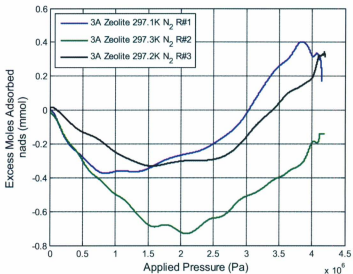


Figure 4-71: 3A Zeolite - Absolute Excess Molar Adsorption Capacity (N₂).

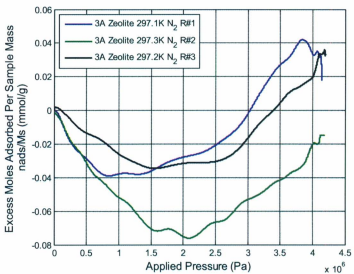


Figure 4-72: 3A Zeolite - Specific Excess Molar Adsorption Capacity (N₂).

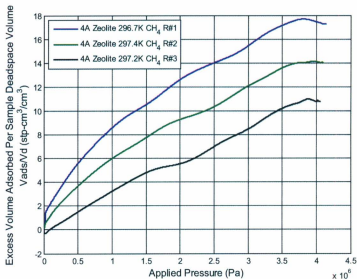


Figure 4-73: 4A Zeolite - Excess Volumetric Adsorption Capacity.

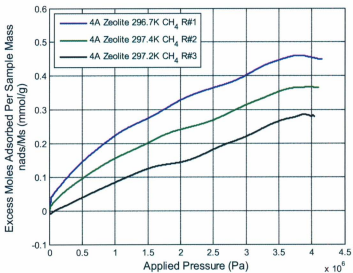


Figure 4-74: 4A Zeolite - Specific Excess Molar Adsorption Capacity.

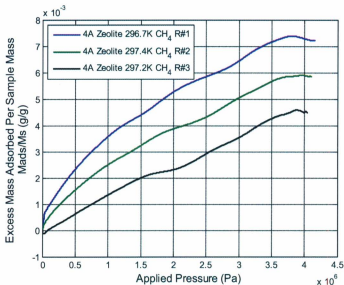


Figure 4-75: 4A Zeolite - Specific Excess Mass Adsorption Capacity.

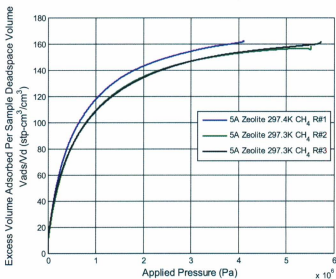


Figure 4-76: 5A Zeolite - Excess Volumetric Adsorption Capacity.

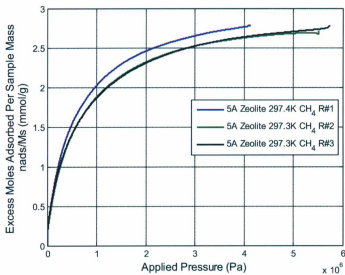


Figure 4-77: 5A Zeolite - Specific Excess Molar Adsorption Capacity.

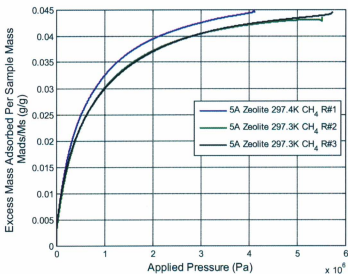


Figure 4-78: 5A Zeolite - Specific Excess Mass Adsorption Capacity.

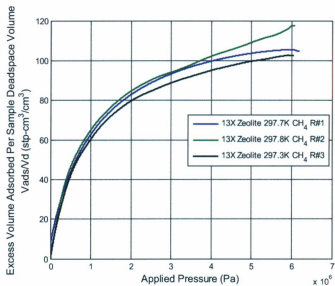


Figure 4-79: 13X Zeolite - Excess Volumetric Adsorption Capacity.

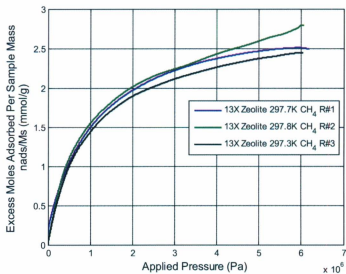


Figure 4-80: 13X Zeolite - Specific Excess Molar Adsorption Capacity.

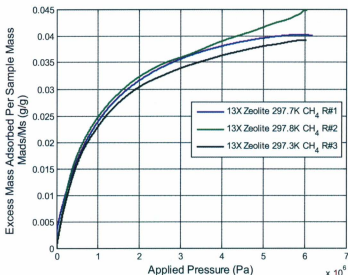


Figure 4-81: 13X Zeolite - Specific Excess Mass Adsorption Capacity.

Table 4-42: 4A Zeolite - Excess Adsorption Capacities ($T \approx 298$ K). $\rho_{n_a}^a$ is the excess molar adsorption density, $\rho_{V_a}^a$ is the excess volumetric adsorption density, $\rho_{m_a}^a$ is the excess mass adsorption density, $M_{n_a}^a$ is the excess specific molar adsorption capacity, $M_{V_a}^a$ is the excess specific volumetric adsorption capacity, and $M_{m_a}^a$ is the excess specific mass adsorption capacity.

P ± 0.01 MPa	$\rho_{n_a}^a$ ± 0.3 mmol/ml	$\rho_{V_a}^a$ ± 6 ml/ml	$\rho_{m_a}^a$ ± 4 mg/ml	$M_{n_a}^a$ ± 0.2 mmol/g	$M_{V_a}^a$ ± 4 ml/g	$M_{m_a}^a$ ± 3 mg/g
1.00	0.2	6.0	4	0.2	3.8	2
2.00	0.4	9.3	6	0.2	5.8	4
3.00	0.5	12.1	8	0.3	7.6	5
3.50	0.6	13.6	9	0.4	8.5	6
4.00	0.6	14.1	9	0.4	8.9	6

Table 4-43: 5A Zeolite - Excess Adsorption Capacities ($T \approx 298$ K). $\rho_{n_a}^a$ is the excess molar adsorption density, $\rho_{V_a}^a$ is the excess volumetric adsorption density, $\rho_{m_a}^a$ is the excess mass adsorption density, $M_{n_a}^a$ is the excess specific molar adsorption capacity, $M_{V_a}^a$ is the excess specific volumetric adsorption capacity, and $M_{m_a}^a$ is the excess specific mass adsorption capacity.

P	n_a^a	$\rho_{n_a}^a$	$\rho_{V_a}^a$	$\rho_{m_a}^a$	$M_{n_a}^a$	$M_{V_a}^a$	$M_{m_a}^a$
± 0.01	± 1.2	± 0.4	± 10	± 7	± 0.2	± 4	± 3
MPa	mmol	mmol/ml	ml/ml	mg/ml	mmol/g	ml/g	mg/g
1.00	13.5	4.6	112	74	1.9	46	31
2.00	16.5	5.6	136	90	2.3	56	37
3.00	18.0	6.1	148	99	2.5	61	41
3.50	18.4	6.3	152	101	2.6	63	42
4.00	18.5	6.3	154	103	2.6	64	43
4.50	19.0	6.5	156	104	2.7	65	43
5.00	19.2	6.6	158	105	2.7	65	44
5.50	19.5	6.6	160	107	2.7	66	44
5.83	19.5	6.7	161	107	2.8	66	44

Table 4-44: 13X Zeolite - Excess Adsorption Capacities ($T \approx 298$ K). $\rho_{n_a}^a$ is the excess molar adsorption density, $\rho_{V_a}^a$ is the excess volumetric adsorption density, $\rho_{m_a}^a$ is the excess mass adsorption density, $M_{n_a}^a$ is the excess specific molar adsorption capacity, $M_{V_a}^a$ is the excess specific volumetric adsorption capacity, and $M_{m_a}^a$ is the excess specific mass adsorption capacity.

P	n_a^a	$\rho_{n_a}^a$	$\rho_{V_a}^a$	$\rho_{m_a}^a$	$M_{n_a}^a$	$M_{V_a}^a$	$M_{m_a}^a$
± 0.01	± 1.2	± 0.4	± 8	± 6	± 0.2	± 5	± 3
MPa	mmol	mmol/ml	ml/ml	mg/ml	mmol/g	ml/g	mg/g
1.00	9.3	2.7	65	43	1.6	37	25
2.00	12.0	3.5	85	56	2.0	49	32
3.00	13.4	3.9	94	63	2.2	54	36
3.50	13.9	4.1	98	65	2.3	56	37
4.00	14.5	4.2	102	65	2.4	59	37
4.50	15.0	4.4	106	70	2.5	61	40
5.00	15.5	4.5	109	73	2.6	63	42
5.50	15.9	4.7	112	75	2.7	64	43
6.00	16.7	4.9	118	78	2.8	68	45

Adsorption/Desorption Cycle

Isotherm plots of an excess adsorption-desorption cycle for the 5A and 13X Zeolites expressed in various commonly used evaluation unit parameters are presented below in Figures 4-82 to 4-87. Tables 4-45 through 4-46 provides values for the excess amounts of gas remaining adsorbed for various discharge pressures for each of the materials.

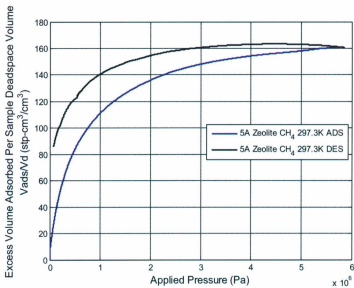


Figure 4-82: 5A Zeolite - Excess Volumetric Adsorption/Desorption Cycle.

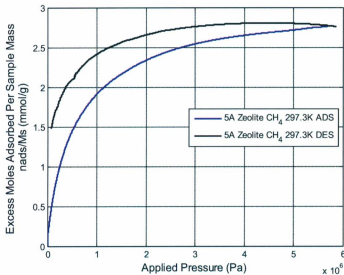


Figure 4-83: 5A Zeolite - Specific Excess Molar Adsorption/Desorption Cycle.

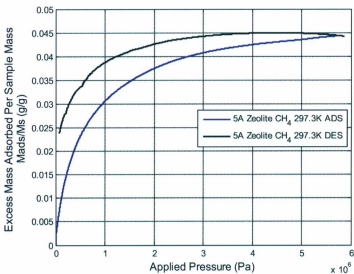


Figure 4-84: 5A Zeolite - Specific Excess Mass Adsorption/Desorption Cycle.

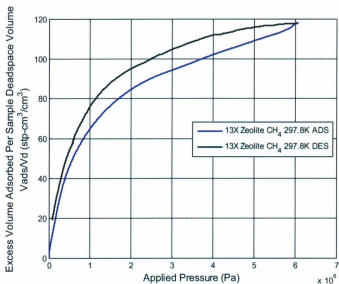


Figure 4-85: 13X Zeolite - Excess Volumetric Adsorption/Desorption Cycle.

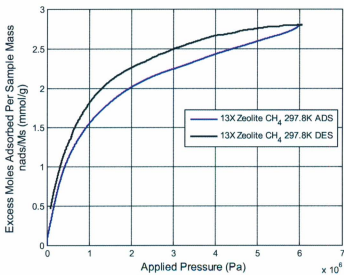


Figure 4-86: 13X Zeolite - Specific Excess Molar Adsorption/Desorption Cycle.

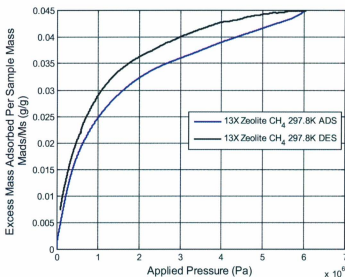


Figure 4-87: 13X Zeolite - Specific Excess Mass Adsorption/Desorption Cycle.

Table 4-45: 5A Zeolite - Excess adsorption capacities during desorption process ($T \approx 298$ K). $\rho_{n_d}^a$ is the excess molar desorption density, $\rho_{V_d}^a$ is the excess volumetric desorption density, $\rho_{m_d}^a$ is the excess mass desorption density, $M_{n_d}^a$ is the excess specific molar desorption capacity, $M_{V_d}^a$ is the excess specific volumetric desorption capacity, and $M_{m_d}^a$ is the excess specific mass desorption capacity.

P	n_d^a	$\rho_{n_d}^a$	$\rho_{V_d}^a$	$\rho_{m_d}^a$	$M_{n_d}^a$	$M_{V_d}^a$	$M_{m_d}^a$
± 0.01	± 1.2	± 0.4	± 10	± 7	± 0.2	± 4	± 3
MPa	mmol	mmol/ml	ml/ml	mg/ml	mmol/g	ml/g	mg/g
atm	11.1	3.8	91	61	1.6	38	25
1.00	17.1	5.8	141	94	2.4	58	39
2.00	18.8	6.4	155	103	2.7	64	43
3.00	19.5	6.7	161	107	2.8	66	44
3.50	19.7	6.7	162	108	2.8	67	45
4.00	19.8	6.8	163	109	2.8	67	45
4.50	19.8	6.8	163	109	2.8	68	45
5.00	19.8	6.8	163	108	2.8	67	45
5.50	19.7	6.7	162	108	2.8	67	45
5.83	19.5	6.7	161	107	2.8	66	44

Table 4-46: 13X Zeolite - Excess adsorption capacities during desorption process ($T \approx 298$ K). $\rho_{n_d}^a$ is the excess molar desorption density, $\rho_{V_d}^a$ is the excess volumetric desorption density, $\rho_{m_d}^a$ is the excess mass desorption density, $M_{n_d}^a$ is the excess specific molar desorption capacity, $M_{V_d}^a$ is the excess specific volumetric desorption capacity, and $M_{m_d}^a$ is the excess specific mass desorption capacity.

P ± 0.01 MPa	n_d^a ± 1.2 mmol	$\rho_{n_d}^a$ ± 0.4 mmol/ml	$\rho_{V_d}^a$ ± 8 ml/ml	$\rho_{m_d}^a$ ± 6 mg/ml	$M_{n_d}^a$ ± 0.2 mmol/g	$M_{V_d}^a$ ± 5 ml/g	$M_{m_d}^a$ ± 3 mg/g
atm	3.2	0.9	22	15	0.5	12.8	9
1.00	10.8	3.2	77	51	1.8	43.9	29
2.00	13.5	3.9	95	63	2.3	54.6	36
3.00	14.9	4.4	105	70	2.5	60.2	40
3.50	15.5	4.5	109	73	2.6	62.6	42
4.00	15.9	4.7	112	75	2.7	64.5	43
4.50	16.2	4.7	114	76	2.7	65.5	44
5.00	16.5	4.8	116	77	2.8	66.7	44
5.50	16.6	4.9	117	78	2.8	67.3	45
6.00	16.7	4.9	118	78	2.8	67.7	45

Effective Delivery

Isotherm plots of the excess amounts of gas that are effectively deliverable for the 5A and 13X Zeolite materials expressed in various commonly used unit parameters are presented below in Figures 4-88 to 4-93. Tables 4-47 and 4-48 provide values for the excess amounts effectively deliverable, along with the gas retention values for each of the materials.

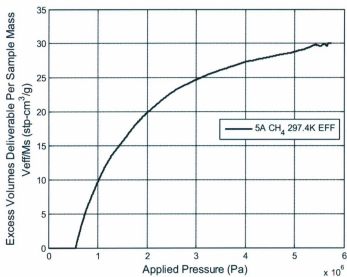


Figure 4-88: 5A Zeolite - Excess Volumetric Delivery Capacity.

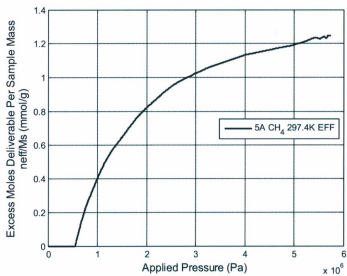


Figure 4-89: 5A Zeolite - Specific Excess Molar Delivery Capacity.

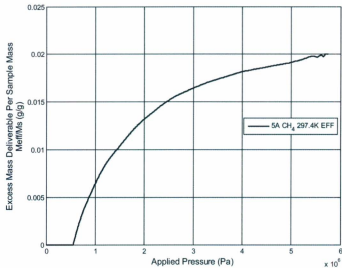


Figure 4-90: 5A Zeolite - Specific Excess Mass Delivery Capacity.

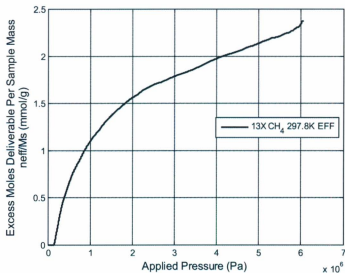


Figure 4-91: 13X Zeolite - Specific Excess Molar Delivery Capacity.

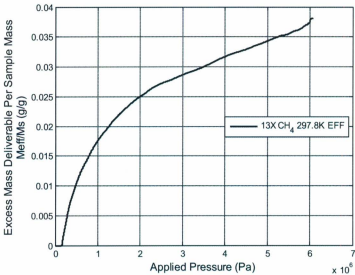


Figure 4-92: 13X Zeolite - Specific Excess Mass Delivery Capacity.

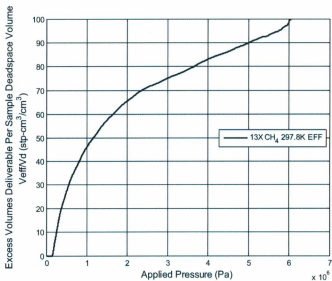


Figure 4-93: 13X Zeolite - Excess Volumetric Delivery Capacity.

Table 4-47: 5A Zeolite - Excess Adsorption - Effective Delivery Capacities ($T \approx 298$ K). $\rho_{n_e}^a$ is the excess molar delivery density, $\rho_{V_e}^a$ is the excess volumetric delivery density, $\rho_{m_e}^a$ is the excess mass delivery density, $M_{n_e}^a$ is the excess specific molar delivery capacity, $M_{V_e}^a$ is the excess specific volumetric delivery capacity, $M_{m_e}^a$ is the excess specific mass delivery capacity, and R^a is the excess adsorption gas retention.

P ± 0.01 MPa	n_e^a ± 1.2 mmol	$\rho_{n_e}^a$ ± 0.4 mmol/ml	$\rho_{V_e}^a$ ± 10 ml/ml	$\rho_{m_e}^a$ ± 7 mg/ml	$M_{n_e}^a$ ± 0.2 mmol/g	$M_{V_e}^a$ ± 4 ml/g	R^a (%)
1.00	0.8	20.4	13	0.3	8.4	6	82
2.00	1.9	45.1	30	0.8	18.7	12	67
3.00	2.4	57.0	38	1.0	23.6	16	62
3.50	2.5	60.6	40	1.0	25.1	17	60
4.00	2.5	63.2	42	1.0	26.2	17	60
4.50	2.7	65.2	43	1.1	27.0	18	58
5.00	2.8	67.1	44	1.1	27.7	18	58
5.50	2.9	69.2	46	1.2	28.6	19	57
5.83	2.9	69.6	46	1.2	28.8	19	57

Table 4-48: 13X Zeolite - Excess Adsorption - Effective Delivery Capacities ($T \approx 298$ K). $\rho_{n_e}^a$ is the excess molar delivery density, $\rho_{V_e}^a$ is the excess volumetric delivery density, $\rho_{m_e}^a$ is the excess mass delivery density, $M_{n_e}^a$ is the excess specific molar delivery capacity, $M_{V_e}^a$ is the excess specific volumetric delivery capacity, $M_{m_e}^a$ is the excess specific mass delivery capacity, and R^a is the excess adsorption gas retention.

P ± 0.01 MPa	$\rho_{n_e}^a$ ± 0.4 mmol/ml	$\rho_{V_e}^a$ ± 8 ml/ml	$\rho_{m_e}^a$ ± 6 mg/ml	$M_{n_e}^a$ ± 0.2 mmol/g	$M_{V_e}^a$ ± 5 ml/g	$M_{m_e}^a$ ± 3 mg/g	R^a (%)
1.00	1.8	43	28	1	25	16	34
2.00	2.6	62	42	1.5	36	24	26
3.00	3	72	48	1.7	41	28	24
3.50	3.1	76	50	1.8	43	29	23
4.00	3.3	80	53	1.9	46	31	22
4.50	3.5	83	55	2	48	32	21
5.00	3.6	87	58	2.1	50	33	21
5.50	3.7	90	60	2.1	52	34	20
6.00	4	96	63	2.3	55	36	19

4.5.3.3.2 - Effective Storage

Effective Storage

Isotherm plots of the effective storage of methane on 3A Zeolite, 4A Zeolite, 5A Zeolite, 13X Zeolite expressed in various commonly used evaluation unit parameters are presented below in Figures 4-94 through 4-106. Plots of the effective storage of nitrogen on 3A Zeolite is also presented. The storage capacities displayed by the isotherm plots have been tabulated and are displayed for each of the materials in Tables 4-49 to 4-51. Effective storage isotherm plots measured in other less commonly used performance units are also presented in Appendix A2.

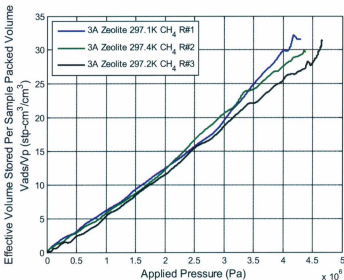


Figure 4-94: 3A Zeolite - Effective Volumetric Storage Capacity.

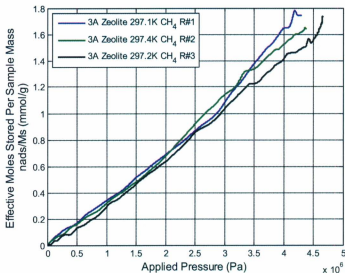


Figure 4-95: 3A Zeolite - Specific Effective Molar Storage Capacity.

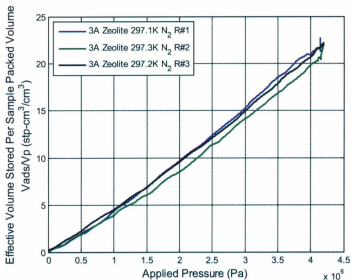


Figure 4-96: 3A Zeolite - Effective Volumetric Storage Capacity (N_2).

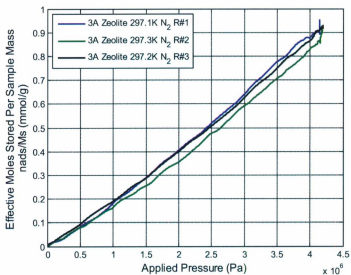


Figure 4-97: 3A Zeolite - Specific Effective Molar Charge/Discharge Cycle (N_2).

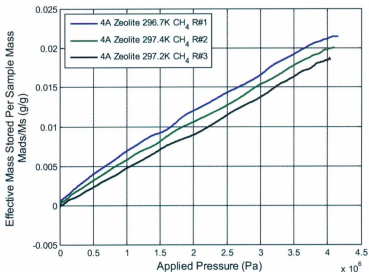


Figure 4-98: 4A Zeolite - Specific Effective Mass Storage Capacity.

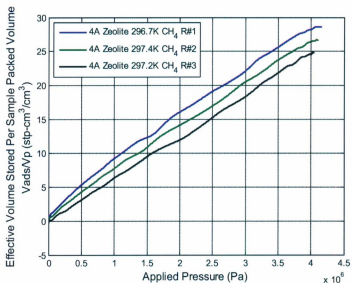


Figure 4-99: 4A Zeolite - Effective Volumetric Storage Capacity.

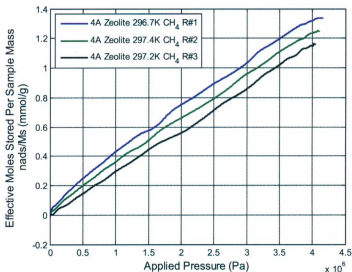


Figure 4-100: 4A Zeolite - Specific Effective Molar Storage Capacity.

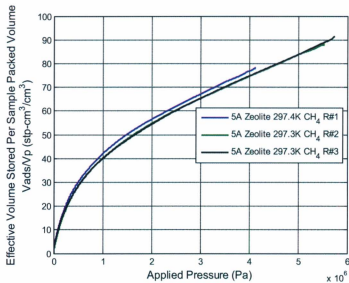


Figure 4-101: 5A Zeolite - Effective Volumetric Storage Capacity.

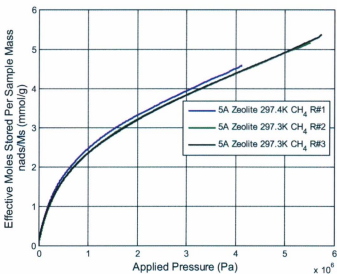


Figure 4-102: 5A Zeolite - Specific Effective Molar Storage Capacity.

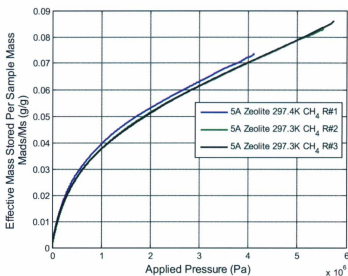


Figure 4-103: 5A Zeolite - Specific Effective Mass Storage Capacity.

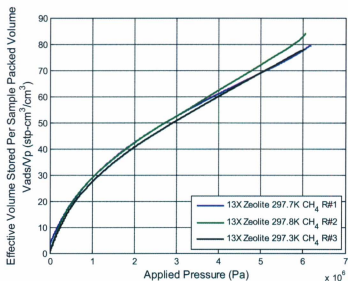


Figure 4-104: 13X Zeolite - Effective Volumetric Storage Capacity.

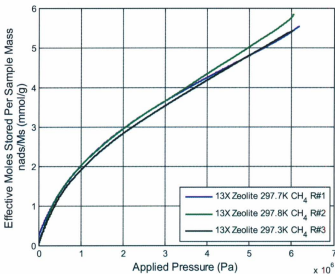


Figure 4-105: 13X Zeolite - Specific Effective Molar Storage Capacity.

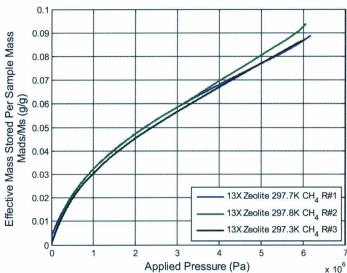


Figure 4-106: 13X Zeolite - Specific Effective Mass Storage Capacity.

Table 4-49: 4A Zeolite - Effective Storage Capacities ($T \approx 298$ K). $\rho_{n_a}^s$ is the effective molar storage density, $\rho_{V_a}^s$ is the effective volumetric storage density, $\rho_{m_a}^s$ is the effective mass storage density, $M_{n_a}^s$ effective specific molar storage capacity, $M_{V_a}^s$ is the effective specific volumetric storage capacity, and $M_{m_a}^s$ is the effective specific mass storage capacity.

P ± 0.01 MPa	$\rho_{n_a}^s$ ± 0.3 mmol/ml	$\rho_{V_a}^s$ ± 6 ml/ml	$\rho_{m_a}^s$ ± 4 mg/ml	$M_{n_a}^s$ ± 0.2 mmol/g	$M_{V_a}^s$ ± 4 ml/g	$M_{m_a}^s$ ± 3 mg/g
1.00	0.3	7.7	5	0.4	8.7	6
2.00	0.6	14.2	9	0.7	16.0	11
3.00	0.9	20.5	14	1.0	23.1	15
3.50	1.0	23.8	16	1.1	26.8	18
4.00	1.1	26.5	18	1.2	29.8	20

Table 4-50: 5A Zeolite - Effective Storage Capacities ($T \approx 298$ K). $\rho_{n_a}^s$ is the effective molar storage density, $\rho_{V_a}^s$ is the effective volumetric storage density, $\rho_{m_a}^s$ is the effective mass storage density, $M_{n_a}^s$ effective specific molar storage capacity, $M_{V_a}^s$ is the effective specific volumetric storage capacity, and $M_{m_a}^s$ is the effective specific mass storage capacity.

P ± 0.01 MPa	n_a^s ± 1.2 mmol	$\rho_{n_a}^s$ ± 0.1 mmol/ml	$\rho_{V_a}^s$ ± 3 ml/ml	$\rho_{m_a}^s$ ± 2 mg/ml	$M_{n_a}^s$ ± 0.2 mmol/g	$M_{V_a}^s$ ± 4 ml/g	$M_{m_a}^s$ ± 3 mg/g
1.00	16.5	1.6	40	27	2.3	56	37
2.00	22.5	2.3	54	36	3.2	77	51
3.00	27.1	2.7	65	43	3.8	92	61
3.50	29.0	2.9	70	47	4.1	99	66
4.00	30.9	3.1	75	50	4.4	105	70
4.50	32.8	3.3	79	53	4.6	112	74
5.00	34.7	3.5	84	56	4.9	118	79
5.50	36.7	3.7	89	59	5.2	125	83
5.83	38.1	3.8	92	61	5.4	130	86

Table 4-51: 13X Zeolite - Effective Storage Capacities ($T \approx 298$ K). $\rho_{n_a}^s$ is the effective molar storage density, $\rho_{v_a}^s$ is the effective volumetric storage density, $\rho_{m_a}^s$ is the effective mass storage density, $M_{n_a}^s$ effective specific molar storage capacity, $M_{v_a}^s$ is the effective specific volumetric storage capacity, and $M_{m_a}^s$ is the effective specific mass storage capacity.

P	n_a^s	$\rho_{n_a}^s$	$\rho_{v_a}^s$	$\rho_{m_a}^s$	$M_{n_a}^s$	$M_{v_a}^s$	$M_{m_a}^s$
± 0.01	± 1.2	± 0.1	± 3	± 2	± 0.2	± 5	± 3
MPa	mmol	mmol/ml	ml/ml	mg/ml	mmol/g	ml/g	mg/g
1.00	12.0	1.2	29.0	19	2.0	49	32
2.00	17.6	1.8	42.4	28	3.0	71	47
3.00	21.8	2.2	52.6	35	3.7	88	59
3.50	23.8	2.4	57.4	38	4.0	96	64
4.00	25.9	2.6	62.5	42	4.3	105	70
4.50	27.9	2.8	67.2	45	4.7	113	75
5.00	29.9	3.0	72.2	48	5.0	121	81
5.50	31.9	3.2	77.1	51	5.4	129	86
6.00	34.6	3.5	83.5	56	5.8	140	93

Adsorption/Desorption Cycle

Isotherm plots of an effective storage adsorption-desorption cycle for the 5A and 13X Zeolites expressed in various commonly used evaluation unit parameters are presented below in Figures 4-107 to 4-112. Tables 4-52 and 4-53 provide values for the effectively stored amounts of gas remaining adsorbed for various discharge pressures for each of the materials.

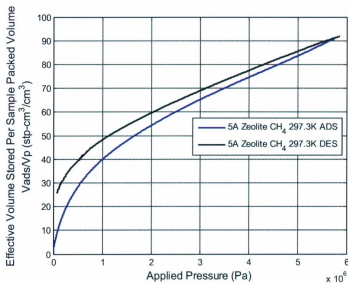


Figure 4-107: 5A Zeolite - Effective Volumetric Storage Charge/Discharge Cycle.

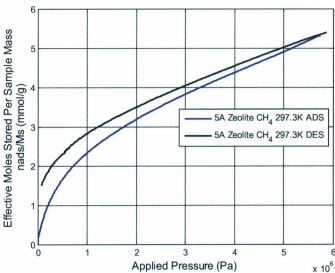


Figure 4-108: 5A Zeolite - Specific Effective Molar Charge/Discharge Cycle.

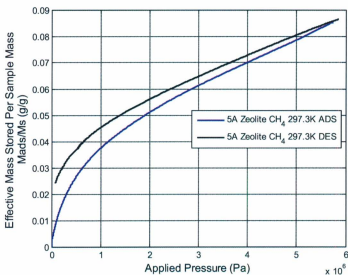


Figure 4-109: 5A Zeolite - Specific Effective Mass Charge/Discharge Cycle.

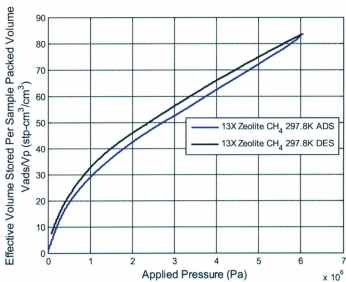


Figure 4-110: 13X Zeolite - Effective Volumetric Storage Charge/Discharge Cycle.

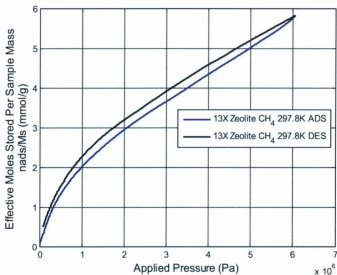


Figure 4-111: 13X Zeolite - Specific Effective Molar Charge/Discharge Cycle.

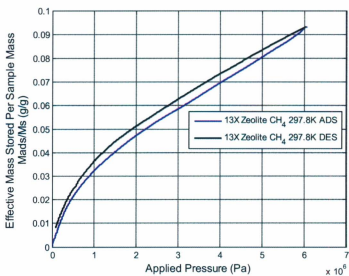


Figure 4-112: 13X Zeolite - Specific Effective Mass Charge/Discharge Cycle ($T \approx 298$ K).

Table 4-52: 5A Zeolite - Effective storage capacities during desorption process ($T \approx 298$ K). $\rho_{n_d}^s$ is the effective molar discharge density, $\rho_{V_d}^s$ is the effective volumetric discharge density, $\rho_{m_d}^s$ is the effective mass discharge density, $M_{n_d}^s$ is the effective specific molar discharge capacity, $M_{V_d}^s$ is the effective specific volumetric discharge capacity, and $M_{m_d}^s$ is the effective specific mass discharge capacity.

P	n_d^s	$\rho_{n_d}^s$	$\rho_{V_d}^s$	$\rho_{m_d}^s$	$M_{n_d}^s$	$M_{V_d}^s$	$M_{m_d}^s$
± 0.01	± 1.2	± 0.1	± 3	± 2	± 0.2	± 4	± 3
MPa	mmol	mmol/ml	ml/ml	mg/ml	mmol/g	ml/g	mg/g
atm	11.3	1.1	27	18	1.6	38	26
1.00	20.0	2.0	48	32	2.8	68	45
2.00	24.9	2.5	60	40	3.5	84	56
3.00	28.6	2.9	69	46	4.0	98	65
3.50	30.4	3.0	73	49	4.3	104	69
4.00	32.1	3.2	78	52	4.5	110	73
4.50	33.9	3.4	82	54	4.8	115	77
5.00	35.5	3.5	86	57	5.0	121	80
5.50	37.1	3.7	90	60	5.2	126	84
5.83	38.1	3.8	92	61	5.4	130	86

Table 4-53: 13X Zeolite - Effective storage capacities during desorption process ($T \approx 298$ K). $\rho_{n_d}^s$ is the effective molar discharge density, $\rho_{V_d}^s$ is the effective volumetric discharge density, $\rho_{m_d}^s$ is the effective mass discharge density, $M_{n_d}^s$ is the effective specific molar discharge capacity, $M_{V_d}^s$ is the effective specific volumetric discharge capacity, and $M_{m_d}^s$ is the effective specific mass discharge capacity.

P	n_d^s	$\rho_{n_d}^s$	$\rho_{V_d}^s$	$\rho_{m_d}^s$	$M_{n_d}^s$	$M_{V_d}^s$	$M_{m_d}^s$
± 0.01	± 1.2	± 0.1	± 3	± 2	± 0.2	± 5	± 3
MPa	mmol	mmol/ml	ml/ml	mg/ml	mmol/g	ml/g	mg/g
atm	3.6	0.4	7	6	0.6	14	10
1.00	13.6	1.4	33	22	2.3	55	36
2.00	19.1	1.9	46	31	3.2	77	51
3.00	23.4	2.3	56	38	3.9	95	63
3.50	25.5	2.5	62	41	4.3	103	69
4.00	27.5	2.7	66	44	4.6	111	74
4.50	29.3	2.9	71	47	4.9	119	79
5.00	31.2	3.1	75	50	5.2	126	84
5.50	32.9	3.3	79	53	5.5	133	89
6.00	34.5	3.5	8	56	5.8	140	93

Effective Delivery

Isotherm plots for the effectively stored amounts of gas that are effectively deliverable for the 5A and 13X Zeolite materials expressed in various commonly used unit parameters are presented below in Figures 4-113 to 4-118. Tables 4-54 and 4-55 displayed below provide values for the effectively stored amounts that are effectively deliverable, along with the gas retention values for each of the materials.

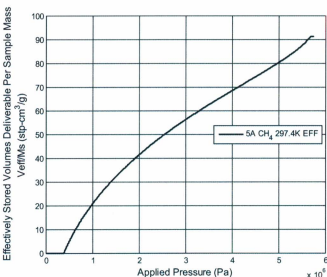


Figure 4-113: 5A Zeolite - Effective Volumetric Delivery Capacity.

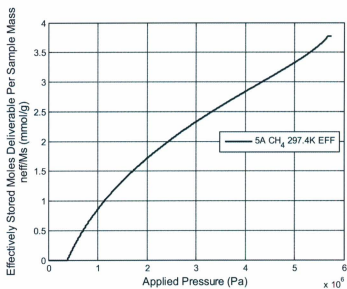


Figure 4-114: 5A Zeolite - Specific Effective Molar Delivery Capacity.

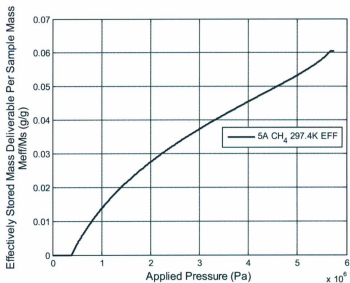


Figure 4-115: 5A Zeolite - Specific Effective Mass Delivery Capacity.

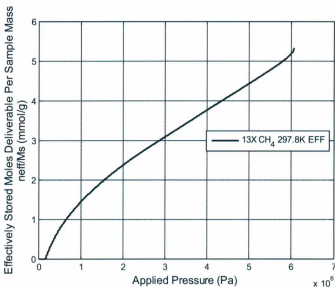


Figure 4-116: 13X Zeolite - Specific Effective Molar Delivery Capacity.

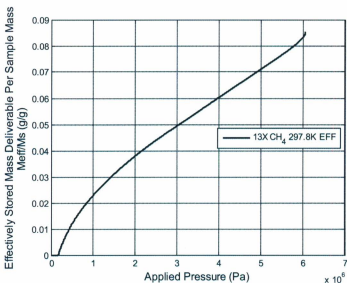


Figure 4-117: 13X Zeolite - Specific Effective Mass Delivery Capacity.

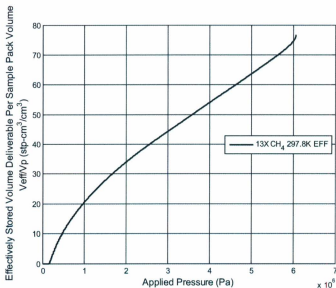


Figure 4-118: 13X Zeolite - Effective Volumetric Delivery Capacity.

Table 4-54: 5A Zeolite - Effective Storage - Effective Delivery Capacities ($T \approx 298$ K). $\rho_{n_e}^s$ is the effective molar delivery density, $\rho_{V_e}^s$ is the effective volumetric delivery density, $\rho_{m_e}^s$ is the effective mass delivery density, $M_{n_e}^s$ is the effective specific molar delivery capacity, $M_{V_e}^s$ is the effective specific volumetric delivery capacity, $M_{m_e}^s$ is the effective specific mass delivery capacity, and R^s is the effective adsorption gas retention.

P ± 0.01 MPa	n_e^s ± 1.2 mmol	$\rho_{n_e}^s$ ± 0.1 mmol/ml	$\rho_{V_e}^s$ ± 3 ml/ml	$\rho_{m_e}^s$ ± 2 mg/ml	$M_{n_e}^s$ ± 0.2 mmol/g	$M_{V_e}^s$ ± 4 ml/g	R^s (%)
1.00	0.5	12.7	8	0.7	18	12	68
2.00	1.1	27	18	1.6	38	26	50
3.00	1.6	38	25	2.2	54	36	42
3.50	1.8	43	29	2.5	61	40	39
4.00	2	47	32	2.8	67	44	37
4.50	2.1	52	35	3	73	49	34
5.00	2.3	56	38	3.3	80	53	33
5.50	2.5	61	41	3.6	87	58	31
5.83	2.7	65	43	3.8	91	61	30

Table 4-55: 13X Zeolite - Effective Storage - Effective Delivery Capacities ($T \approx 298$ K). $\rho_{n_e}^s$ is the effective molar delivery density, $\rho_{V_e}^s$ is the effective volumetric delivery density, $\rho_{m_e}^s$ is the effective mass delivery density, $M_{n_e}^s$ is the effective specific molar delivery capacity, $M_{V_e}^s$ is the effective specific volumetric delivery capacity, $M_{m_e}^s$ is the effective specific mass delivery capacity, and R^s is the effective adsorption gas retention.

P ± 0.01 MPa	$\rho_{n_e}^s$ ± 0.1 mmol/ml	$\rho_{V_e}^s$ ± 3 ml/ml	$\rho_{m_e}^s$ ± 2 mg/ml	$M_{n_e}^s$ ± 0.2 mmol/g	$M_{V_e}^s$ ± 5 ml/g	$M_{m_e}^s$ ± 3 mg/g	R^s (%)
1.00	0.8	20	14	1.4	34	23	1
2.00	1.4	34	23	2.4	57	38	2
3.00	1.8	44	29	3.1	74	49	3
3.50	2	49	33	3.4	82	55	3.5
4.00	2.2	54	36	3.7	90	60	4
4.50	2.4	59	39	4.1	98	65	4.5
5.00	2.6	64	42	4.4	107	71	5
5.50	2.8	69	46	4.8	115	77	5.5
6.00	3.1	75	50	5.2	126	84	6

4.5.3.4 - Analysis

4.5.3.4.1 - Excess Adsorption

From observation of the excess adsorption isotherms for the 3A Zeolite displayed above in Figures 4-69 to 4-72, it is evident that no statistically significant excess amount of methane or nitrogen gas has been adsorbed. Any adsorption values reported by the plots is essentially error due to the gas expansion process and temperature changes as previously described in Section 3.1.5.

Based on the excess adsorption isotherms for the 4A Zeolite displayed above in Figures 4-73 to 4-75, it is clear that the material did adsorb measureable amounts of methane gas. However, the amounts adsorbed are very small and the relative uncertainty of the values is fairly high. It is also apparent that significant deviations exist between the three test runs conducted. These can be directly attributed in part to temperature differences. Since consecutive runs produced succeeding lower

adsorption values, it may be possible that the material is being subject to severe cyclic loading damage. However, a more likely explanation is that all the residual adsorbed molecules from the previous test may not have been completely removed prior to conducting the next test. It is suspected that the very small porous network structure may also greatly inhibit gas diffusion compared to the other materials tested, and thus more time would have been required to remove any residual molecules.

From the excess adsorption isotherms of 5A Zeolite displayed above in Figures 4-76 to 4-78, it is evident that there is a deviation between the isotherm obtained from the first test run, and those obtained for the second and third runs. Since temperature differences are small and the isotherms do not merge to a common point, it is unknown why the deviation is present.

It is clear from the excess adsorption/desorption plots of the 5A and 13X zeolites displayed above in Figures 4-82 to 4-87 that hysteresis is present in for the cycles and its effect is very significant. A gas retention value of 60 % was obtained for a discharge pressure of 3.5 MPa for the 5A Zeolite which is very high. The 13X Zeolite produced a gas retention 23 % at 3.5 MPa which is also moderately high compared to some adsorbent materials presented in the literature. The plots also show a slight increase in the desorption portion of the isotherm when discharging from the maximum pressure region for the 5A Zeolite. This is simply an error caused by the gas expansion process associated with conducting the desorption portion of the test.

Based on the excess adsorption isotherms of 13X Zeolite displayed above in Figures 4-79 to 4-81, it is evident that there are deviations between isotherms obtained from the different test runs. Since temperature differences are not in agreement with the isotherm deviations, and the isotherms do not merge to a common point, it is unknown why the differences are present. The three isotherms are in good agreement up until approximately 3 MPa at which point one isotherm deviates largely from that of the other two. It is assumed that this deviation is an error and

that the isotherms obtained from runs 1 and 2 are correctly representative of the adsorbent material.

4.5.3.4.2 - Effective Storage

From the effective storage plots presented above in Figures 4-94 through 4-106 it is clear that significantly larger amounts of gas are effectively stored compared to the excess adsorption amounts obtained for each of the zeolite materials tested. For example, at a pressure of 3.5 MPa an excess adsorption value of $6 \frac{\text{mg}}{\text{g}}$ and an effective storage value of $18 \frac{\text{mg}}{\text{g}}$ were obtained for the 4A Zeolite. This represents a storage increase of approximately 200 %. The 5A Zeolite produced a storage increase of 57 % ($42 \frac{\text{mg}}{\text{g}}$ to $66 \frac{\text{mg}}{\text{g}}$), while the 13X Zeolite produced a storage increase of 73 % ($37 \frac{\text{mg}}{\text{g}}$ to $64 \frac{\text{mg}}{\text{g}}$). The 3A Zeolite did not adsorb any excess amounts of gas but did produce an effective storage capacity of $22 \frac{\text{mg}}{\text{g}}$. However, this storage value is due solely to the bulk compressive storage of gas located in the volumes between individual material particles since it is known that the material cannot adsorb any excess amounts of gas. This can also be somewhat concluded from the linear trends of the effective storage isotherms for the material.

It is evident that deviations between runs for effective storage isotherms are much less significant than that found with excess adsorption for all of the zeolite materials. This indicates that the adsorption process is much more temperature sensitive than the gas compression process.

For each of the materials, a rough calculation can be performed to determine the percentage of the effective storage capacity that can be attributed to the bulk gas compressive storage. The procedure for this calculation was previously discussed in Section 4.5.2.4.2 for the activated carbon materials.

For the 3A Zeolite it was determined that the effective storage capacity if no adsorption had taken place would be approximately $1.24 \frac{\text{mmol}}{\text{g}}$. This is in agreement with the values reported by Figure 4-95, which range from 1.2 to approximately $1.4 \frac{\text{mmol}}{\text{g}}$. Calculating the theoretical effective storage for nitrogen gas if no adsorption had taken place gives a storage value of $0.78 \frac{\text{mmol}}{\text{g}}$. This is again in good agreement with values reported by Figure 4-70, which range from 0.7 to approximately $0.8 \frac{\text{mmol}}{\text{g}}$. Thus, the compression process accounts for 100 % of the material's effective storage capacity when storing either methane or nitrogen gas.

The results of the bulk compression component analysis for each of the zeolite materials studied is presented below in Table 4-56.

Table 4-56: Bulk compression component fraction for effective storage of zeolites.

Material	Theoretical Effective Storage Without Adsorption	Effective Storage Value Obtained	Bulk Compression Component of Effective Storage
4A	0.7	1.1	68 %
5A	1.4	4.1	34 %
13X	1.7	3.9	44 %

From the effective adsorption/desorption cycle plots displayed above for the 5A and 13X Zeolite materials in Figures 4-82 through 4-87, it is evident that hysteresis is present but its effect is much less significant than that for excess adsorption. Since the amount of hysteresis present in the plots is greatly reduced, gas retention values are also greatly reduced when compared to excess adsorption. For example, the 13X Zeolite was found to have a gas retention value of 15 % when discharging from 3.5 MPa to atmospheric conditions. The 5A Zeolite was found to have a gas retention value of 39 %, which is very high compared to other materials reported in the literature.

4.5.3.4.3 - Model Isotherm Fits

Absolute excess amounts and effectively stored amounts were successfully described by the Langmuir, Freundlich, and Toth isotherm models for each of the zeolite materials tested. The modified versions of these models were also applied to the effective storage isotherms.

Excess Adsorption

Figures 4-119 to 4-121 presented below show fits of the isotherm models for the absolute excess adsorption isotherms of the 4A Zeolite, 5A Zeolite, and 13X Zeolite materials. The isotherm model parameter values and fit statistics are displayed below in Tables 4-57 through 4-59.

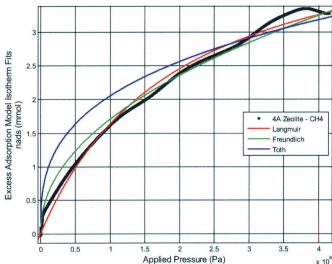


Figure 4-119: 4A Zeolite - Absolute excess adsorption Isotherm model fits.

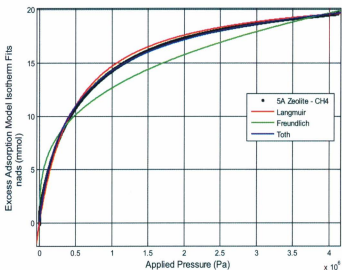


Figure 4-120: 5A Zeolite - Absolute excess adsorption isotherm model fits.

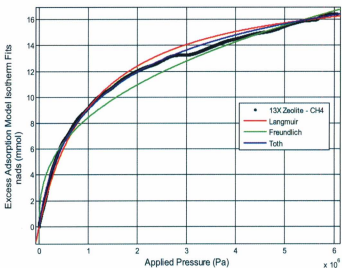


Figure 4-121: 13X Zeolite - Absolute excess adsorption isotherm model fits.

Table 4-57: Excess adsorption model isotherm parameter values and fit statistics.

4A Zeolite	Langmuir	Freundlich	Toth
a	4.856	0.282	219800
b	5.097E-7	0.010	5052
c	-	2.613	0.033
SSE	25.93	40.6	273.3
R ² _{adj}	0.994	0.991	0.938
RSME	0.072	0.090	0.234

Table 4-58: Excess adsorption model isotherm parameter values and fit statistics.

5A Zeolite	Langmuir	Freundlich	Toth
a	22.02	1.07	24.91
b	2.007E-6	0.147	2.97E-6
c	-	3.147	0.693
SSE	263.2	2273	82.8
R ² _{adj}	0.998	0.980	0.999
RSME	0.239	0.702	0.134

Table 4-59: Excess adsorption model isotherm parameter values and fit statistics.

13X Zeolite	Langmuir	Freundlich	Toth
a	19.08	1.169	25.08
b	9.31E-7	0.039	1.439E-6
c	-	2.648	0.583
SSE	560.5	1787	158.7
R ² _{adj}	0.995	0.983	0.999
RSME	0.360	0.642	0.191

From the model isotherm fit plots for the 4A and 5A Zeolites displayed above in Figures 4-119 and 4-120, it is evident that the Langmuir and Freundlich models both fit the experimental data very well but the Toth model does not. Based on the fit statistics it is clear that the Langmuir model describes the adsorption data most accurately for both materials.

From the model isotherm fits plot for the 13A Zeolite displayed above in Figure 4-121 it is evident that that all isotherm models fit the data very well. Based on the fit statistics is it clear that the Toth model describes the adsorption data most accurately.

Effective Storage

Figures 4-122 to 4-127 presented below show fits of the isotherm models and modified isotherm models for the absolute effective storage isotherms for the 4A, 5A, and 13X Zeolite materials. The parameter values and fit statistics for the models are shown below in Tables 4-60 through 4-62. Differences in the goodness of fit between the original and modified isotherm models can be obtained from these tables.

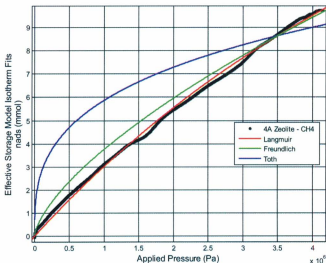


Figure 4-122: 4A Zeolite - Absolute effective storage isotherm model fits.

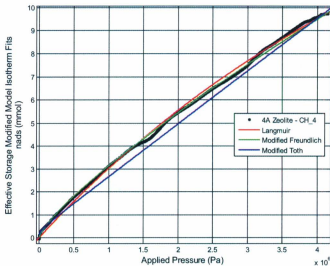


Figure 4-123: 4A Zeolite - Absolute effective storage modified isotherm model fits.

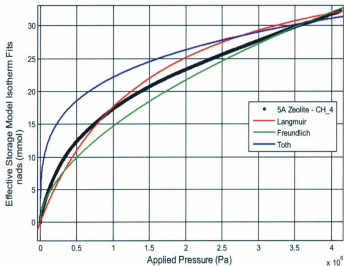


Figure 4-124: 5A Zeolite - Absolute effective storage isotherm model fits.

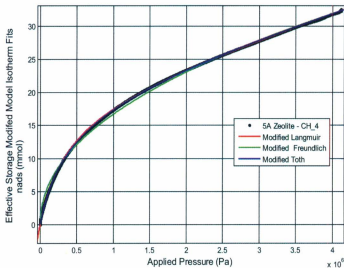


Figure 4-125: 5A Zeolite - Absolute effective storage modified isotherm model fits.

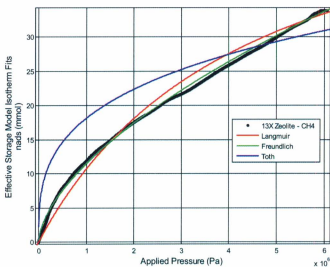


Figure 4-126: 13X Zeolite - Absolute effective storage isotherm model fits.

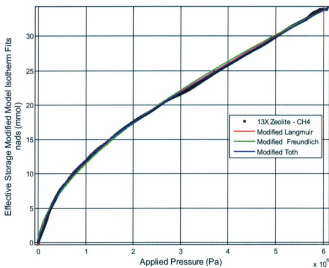


Figure 4-127: 13X Zeolite - Absolute effective storage modified isotherm model fits.

Table 4-60: Effective storage model isotherm parameter values and fit statistics.

4A Zeolite	Langmuir	Modified Langmuir	Freundlich	Modified Freundlich	Toth	Modified Toth
a	33.7	3.044	0.266	0.007	7047	0.612
b	9.839E-8	7.915E-7	0.009	0.016	3757	0.274
c	-	1.798E-6	1.839	1.395	0.0449	0.180
d	-	-	-	7.959E-7	-	2.277E-6
SSE	55.58	41.15	1665	33.67	11140	274.8
R ² _{adj}	0.999	0.999	0.967	0.999	0.780	0.995
RMSE	0.105	0.0907	0.577	0.082	1.493	0.235

Table 4-61: Effective storage model isotherm parameter values and fit statistics.

5A Zeolite	Langmuir	Modified Langmuir	Freundlich	Modified Freundlich	Modified Toth	Toth
a	43.77	19	0.450	0.165	21.89	7968
b	6.739E-7	2.674E-6	0.014	0.165	2.726E-6	4307
c	-	3.635E-6	1.782	2.151	0.822	0.049
d	-	-	-	5.163E-9	3.316E-6	-
SSE	2733	71.01	3568	486.2	87.29	32990
R _{adj} ²	0.993	0.999	0.991	0.999	0.999	0.915
RMSE	0.769	0.124	0.879	0.323	0.138	2.673

Table 4-62: Effective storage model isotherm parameter values and fit statistics.

13X Zeolite	Langmuir	Modified Langmuir	Freundlich	Modified Freundlich	Toth	Modified Toth
a	57.91	13.14	0.289	0.059	247000	11.89
b	2.266E-7	1.724E-6	0.010	0.060	2570	1.659E-6
c	-	3.633E-6	1.665	1.713	0.038	1.205
d	-	-	-	3.118E-7	-	3.745E-6
SSE	4528	105	520.5	515.9	73190	93.54
R _{adj} ²	0.992	0.999	0.999	0.999	0.874	0.999
RMSE	1.023	0.156	0.347	0.345	4.112	0.147

Based on the model isotherm fit plots displayed above for the 4A, 5A, and 13X Zeolites, it is evident that the Langmuir and Freundlich models fit the storage data reasonably well, while the Toth equation provides a poor fit.

Based on the fit statistics displayed above in Table 4-60 for the 4A Zeolite, it is clear that the Modified Freundlich model describes the effective storage data most accurately. The Modified Langmuir model was found to fit the effective storage data

for the 5A Zeolite most accurately, and was closely followed by the Modified Toth model. The large increase in the fit correlation for the Toth model clearly demonstrates the effectiveness of using the modified models for effective storage isotherms. From the fit statistics displayed above for the 13X Zeolite it is clear that the Modified Toth model describes the adsorption data most accurately.

Based on the original and modified isotherm model plots and fit statistics presented above, it can be concluded that the modified isotherm models fit the effective storage data much better than the original isotherm models. It should be noted however that Toth model did provide the best fit for the excess adsorption while also providing the worst fit for the effective storage of 13X Zeolite. This is simply due to the fact that none of the standard isotherm models are designed to facilitate effective storage. Thus, if a model were to provide the best fit characteristics for both the absolute adsorption and effective storage it would simply be coincidence.

4.5.4 - Silicates

4.5.4.1 - Introduction

In addition to the activated carbon and zeolite materials, a silica gel material was also studied since it is a relatively inexpensive and very common porous material. The silica gel used consisted of high grade chromatographic gel with a particle size between 74 to 37 μm , and was provided by Sigma Aldrich.

4.5.4.2 - Silica Gel

The physical properties for the silica gel are displayed in Table 4-63 below.

Table 4-63: Physical Properties - Silica Gel. A_{sm} is the specific surface area, A_{sv} is the available surface area per packed volume, ρ_b is the bulk material density (not packed), ρ_{pak} is the packed material density, m_s is the total sample mass, and V_p is the sample packed volume.

Silica Gel			
$A_{sm} \left(\frac{\text{m}^2}{\text{g}}\right)$	≈ 400	$m_s \text{ (g)}$	5.27
$A_{sv} \left(\frac{\text{m}^2}{\text{cm}^3}\right)$	265	$V_p \text{ (cm}^3\text{)}$	10
$D_{pore} \text{ (nm)}$	5 - 7	$Cost \left(\frac{\$}{\text{kg}}\right)$	0.73
$\rho_b \left(\frac{\text{g}}{\text{cm}^2}\right)$	0.4	$Cost \left(\frac{\$}{\text{L}}\right)$	0.39
$\rho_{pak} \left(\frac{\text{g}}{\text{cm}^2}\right)$	0.53		

4.5.4.2.1 - Results

Excess Adsorption

Isotherm plots of the excess adsorption of methane on silica gel expressed in various commonly used evaluation units are presented below in Figures 4-128 to 4-130. Table 4-64 provides the excess adsorption capacities obtained at various test pressures. Isotherm plots measured in other performance units are listed in Appendix A2.

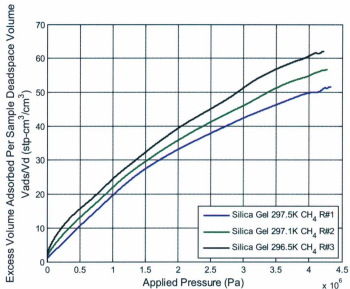


Figure 4-128: Silica Gel - Excess Volumetric Adsorption Capacity.

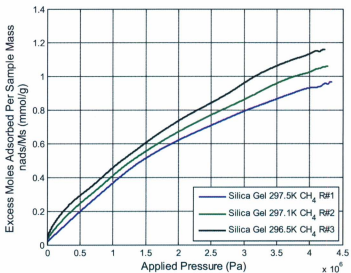


Figure 4-129: Silica Gel - Specific Excess Molar Adsorption Capacity.

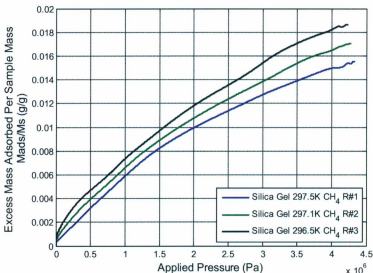


Figure 4-130: Silica Gel - Specific Excess Mass Adsorption Capacity.

Table 4-64: Silica Gel - Excess Adsorption Capacities ($T \approx 298$ K). $\rho_{n_a}^a$ is the excess molar adsorption density, $\rho_{V_a}^a$ is the excess volumetric adsorption density, $\rho_{m_a}^a$ is the excess mass adsorption density, $M_{n_a}^a$ is the excess specific molar adsorption capacity, $M_{V_a}^a$ is the excess specific volumetric adsorption capacity, and $M_{m_a}^a$ is the excess specific mass adsorption capacity.

P	n_a^a	$\rho_{n_a}^a$	$\rho_{V_a}^a$	$\rho_{m_a}^a$	$M_{n_a}^a$	$M_{V_a}^a$	$M_{m_a}^a$
± 0.01	± 1.2	± 0.5	± 12.2	± 8.1	± 0.2	± 5.5	± 4
MPa	mmol	mmol/ml	ml/ml	mg/ml	mmol/g	ml/g	mg/g
1.00	2.4	1.0	24.5	16	0.5	11.0	7
2.00	3.9	1.6	39.3	26	0.7	17.7	12
3.00	5.1	2.1	51.4	34	1.0	23.2	15
3.50	5.6	2.4	56.9	38	1.1	25.7	17
4.00	6.0	2.5	60.7	41	1.1	27.4	18

Since the adsorption performance of the material was so poor, no adsorption-desorption cycle testing was conducted on the material.

Effective Storage

Plots of the effective storage of methane on the silica gel expressed in various commonly used evaluation parameters are presented below in Figures 4-131 to 4-133. Table 4-65 provides the effective storage capacities obtained at various test pressures and is also displayed below. Effective storage isotherm plots measured in other performance units are listed in Appendix A2.

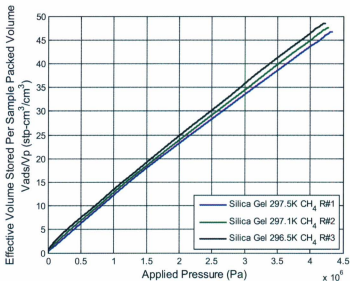


Figure 4-131: Silica Gel - Effective Volumetric Storage Capacity.

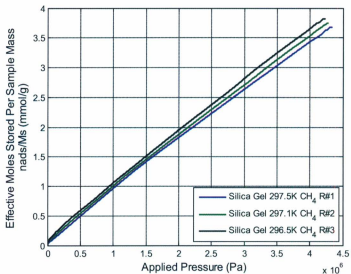


Figure 4-132: Silica Gel - Specific Effective Molar Storage Capacity.

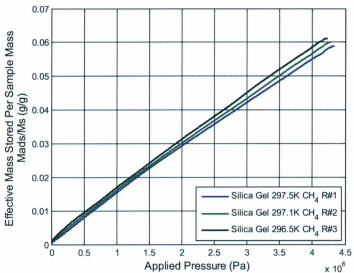


Figure 4-133: Silica Gel - Specific Effective Mass Storage Capacity.

Table 4-65: Silica Gel - Effective Storage Capacities ($T \approx 298$ K). $\rho_{n_a}^s$ is the effective molar storage density, $\rho_{V_a}^s$ is the effective volumetric storage density, $\rho_{m_a}^s$ is the effective mass storage density, $M_{n_a}^s$ effective specific molar storage capacity, $M_{V_a}^s$ is the effective specific volumetric storage capacity, and $M_{m_a}^s$ is the Effective specific mass storage capacity.

P	n_a^s	$\rho_{n_a}^s$	$\rho_{V_a}^s$	$\rho_{m_a}^s$	$M_{n_a}^s$	$M_{V_a}^s$	$M_{m_a}^s$
± 0.01	± 1.2	± 0.5	± 12.2	± 8.1	± 0.2	± 5.5	± 4
MPa	mmol	mmol/ml	ml/ml	mg/ml	mmol/g	ml/g	mg/g
1.00	5.6	0.6	13.4	9	1.1	25.5	17
2.00	10.3	1.0	24.8	17	2.0	47.1	31
3.00	14.8	1.5	35.7	24	2.8	67.8	45
3.50	17.1	1.7	41.3	28	3.2	78.4	52
4.00	19.3	1.9	46.4	31	3.7	88.1	59

4.5.4.2.2 - Analysis

Excess Adsorption

From the excess adsorption isotherms displayed in Figures 4-128 through 4-130 it is evident that there are deviations between all of the isotherms obtained from the different test runs. However, temperature differences between runs are in agreement with the trends in isotherm value deviations. It is therefore assumed that the values reported for each isotherm is correct.

Effective Storage

From the effective storage plots presented in Figures 4-131 through 4-133 it is evident that the relative deviations between runs are much less significant than that found with excess adsorption. Since the plot trend is essentially linear, it can be concluded that the storage process is dominated by the bulk gas pressure storage component. For example, at a pressure of 3.5 MPa an excess adsorption value of $17 \frac{\text{mg}}{\text{g}}$ and an effective storage value of $52 \frac{\text{mg}}{\text{g}}$ were obtained. This represents a storage

increase of approximately 200 %, which is very significant. A rough calculation reveals that the effective storage at 3.5 MPa if no adsorption had taken place would be approximately $2.0 \frac{\text{mmol}}{\text{g}}$. This value was obtained by the procedure previously discussed in Section 4.5.2.4.2 for the activated carbon materials. Since a value of approximately $3.2 \frac{\text{mmol}}{\text{g}}$ was obtained, $1.1 \frac{\text{mmol}}{\text{g}}$ would have been adsorbed which is in agreement with the results displayed by Figure 4-129. Thus, the compression process accounts for approximately 63% of the material's effective storage capacity.

Isotherm Fits

Absolute excess amounts adsorbed and absolute effectively stored amounts were successfully described by the Langmuir, Freundlich, and Toth isotherm models. The modified versions of these models were also applied to the effective storage isotherms.

Figure 4-134 presented below shows fits of the isotherm models for the absolute excess adsorption isotherm of the silica gel. From the plot it is evident that the Langmuir and Freundlich models fit the experimental very well but the Toth model does not. The model parameter values and fit statistics are shown below in Table 4-66. Based on the fit statistics it is clear that the Langmuir model describes the adsorption data most accurately.

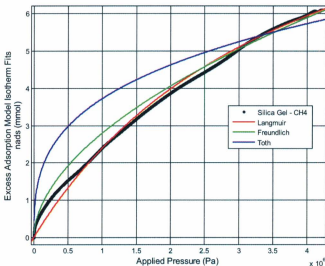


Figure 4-134: Silica Gel - Absolute excess adsorption isotherm model fits.

Table 4-66: Excess adsorption model isotherm parameter values and fit statistics.

Silica Gel	Langmuir	Freundlich	Toth
a	11.77	0.238	2.2745E5
b	2.556E-7	0.007	4377
c	-	1.863	0.035
SSE	77.2	194.5	2874
R_{adj}^2	0.997	0.992	0.881
RSME	0.1	0.159	0.612

Figure 4-135 presented below shows fits of the isotherm models to the absolute effective storage isotherm of methane on silica gel. From the plot it is again evident that the Langmuir and Freundlich models fit the data reasonably well while the Toth equation provides a very poor fit. Figure 4-136 displays the fits for the modified isotherm models. From the plot it is clear that the modified models fit much better

since all models fit the data extremely well. Differences in the goodness of fit for the models can be obtained from the model parameter values and fit statistics presented below in Table 4-67. Based on the fit statistics it is clear that the Modified Freundlich model describes the adsorption data most accurately.

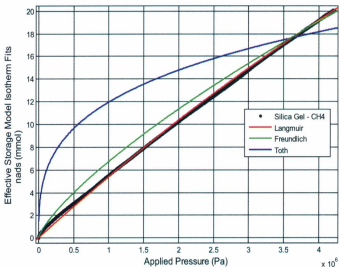


Figure 4-135: Silica Gel - Absolute effective storage isotherm model fits.

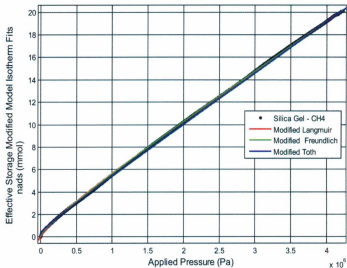


Figure 4-136: Silica Gel- Absolute effective storage modified isotherm model fits.

Table 4-67: Effective storage model isotherm parameter values and fit statistics.

Silica Gel	Langmuir	Modified Langmuir	Freundlich	Modified Freundlich	Toth	Modified Toth
a	130.5	1.715	0.077	0.0335	2.393E5	7.588
b	4.313E-8	2.546E-6	0.003	0.042	3305	71.31
c	-	4.401E-6	1.333	1.959	0.037	0.087
d	-	-	-	3.962E-6	-	4.52E-6
SSE	146.8	43.56	2275	22.87	71610	108.5
R ² _{adj}	0.999	0.999	0.993	0.999	0.779	0.999
RSME	0.138	0.075	0.545	0.055	3.055	0.119

4.5.5 - Porous Silicon

4.5.5.1 - Introduction

The porous silicon samples subject to adsorption testing consisted of thin porous films produced via electrochemical etching, and porous silicon particles produced via stain etching. The samples were produced during the experimental research production studies previously discussed. Film thicknesses were on the order of 30 μm , while particle sizes ranged from 88 to 37 μm . The results of the adsorption tests for these two material types are presented below.

4.5.5.2 - Porous Silicon Films

Three electrochemically etched porous film samples were tested. These samples are labeled PSi 3.11#1, PSi 3.12#1, and PSi 3.12#2. The fabrication parameters for each of these samples were previously presented in Table 4-1. Unlike other materials presented such as the porous carbons and zeolites, no information regarding material properties such as specific surface area, pore diameter, and packing density are known. The results of the adsorption tests for the samples are presented below.

4.5.5.2.1 - Individual Samples

Excess Adsorption

An isotherm plot of the absolute excess adsorption of methane on porous silicon samples PSi 3.11#1, PSi 3.12#1, and PSi 3.12#2 is presented below. Note that each of the samples was only tested once and the resulting three isotherms have been plotted together.

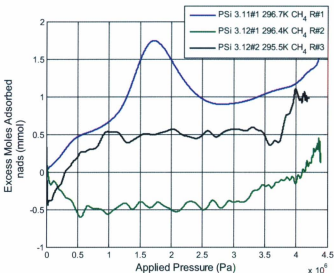


Figure 4-137: Electrochemical PSI- Absolute Excess Molar Adsorption Capacity.

From the above isotherm plot it is clear that no statistically significant amount of gas adsorption has occurred since absolute adsorption values range from 1.5 to -0.5 mmol, and the absolute uncertainty when measuring adsorption is ± 1.6 mmol. Data trends depicted by the plots are mostly experimental error resulting from the combination of signal noise and properties of the expansion process. The periodic fluctuations in the isotherm plots are evidence of this error. The negative adsorption values given by the isotherm of the second test run is also clear evidence that any values reported are essentially consumed entirely by error. Large relative deviations also appear to be present between experimental runs. However, the absolute value of these deviations is actually very small and can be considered insignificant.

It was suspected that the volumes of porous silicon possessed by each sample were not large enough to adsorb adequate amounts of gas. For example, the porous material volume for samples PSI 3.12#1 and PSI 3.12#2 was calculated to be approximately 0.014 cm^3 , and sample PSI 3.11#1 was calculated to be 0.004 cm^3 . In

comparison, most of the materials presented in this thesis had effective sample volumes of approximately 10 cm^3 .

Because the materials did not adsorb any significant excess amount of gas, no effective storage plots were generated.

4.5.5.2.2 - Combined Samples

Since the three electrochemically etched porous silicon samples failed to produce any measureable amount of gas adsorption, the three samples were tested together to effectively increase the total volume of porous silicon available.

Excess Adsorption

Plots of the excess adsorption of methane on the combined porous silicon samples PSI 3.11#1, PSI 3.12#1, and PSI 3.12#2 are presented below for various evaluation parameters.

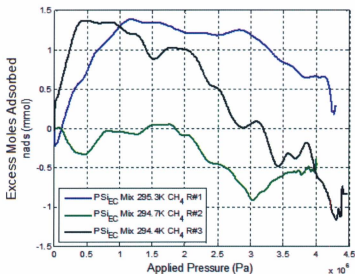


Figure 4-138: Electrochemical PSI - Absolute Excess Molar Adsorption Capacity.

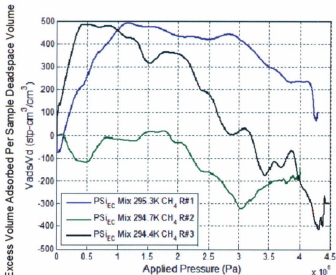


Figure 4-139: Electrochemical PSI – Excess Volumetric Adsorption Capacity.

From the plots it is again clear that no statistically significant amount of gas adsorption has taken place since adsorption values range from 1.4 to -1 mmol, and the uncertainty in adsorption measurement is ± 1.6 mmol. In fact, the absolute excess amounts adsorbed for the three combined samples are essentially equal to that obtained when testing the samples individually. This suggests that the isotherm trends are essentially the noise error inherent in the adsorption testing process.

An important feature of the isotherms to notice is the extremely large volumetric storage values obtained which is essentially all error. This is presumably due to the extremely small sample volume used. Thus, it is important to use large sample volumes to minimize the large errors that are possible when determining volumetric storage capacities.

Since the materials did not adsorb any significant excess amount of gas, no effective storage plots were generated.

4.5.5.3 - Porous Silicon Powder

Four stain etched porous silicon powder samples were tested. These samples have been labeled PSiPW_3, PSiPW_10, PSiPW_14, and PSiPW_15. Unlike the other materials presented such as the porous carbons and zeolites, no information regarding the specific surface area and average pore size of the porous silicon materials are known. The physical properties for the porous silicon powder samples are given in Table 4-68 below.

Table 4-68: Physical properties of porous silicon powder samples. m_s is the sample mass, d_p is the average particle size, V_p is the sample packed volume, ρ_{pak} is the sample packing density, and V_d is the sample dead space volume.

	PSiPW_3	PSiPW_10	PSiPW_14	PSiPW_15
m_s (g)	5.29	2.43	8.61	13
d_p (μm)	63 - 37	88 - 37	88 - 63	63 - 37
V_p ($\frac{\text{m}^2}{\text{cm}^3}$)	4.1	1.95	6.5	10
V_d (cm^2)	2.49	0.93	3.85	5.33
ρ_{pak} ($\frac{\text{g}}{\text{cm}^2}$)	1.29	1.25	1.32	1.3

The fabrication parameters for each of these samples were previously presented in the experimental stain etching studies section. The production parameters used to make sample PSiPW_3 were previously presented in Table 4-8. Sample PSiPW_10 consists of six different samples from experimental study #8 (runs 1 to 6) combined together. The samples were combined in order to produce a larger sample volume since the individual volumes were considered too small for adsorption testing. The fabrication parameters used in making the material has been previously presented in Table 4-9. Sample PSiPW_14 consists of three different samples from experimental study #9 (runs 3 to 5) combined together. The samples were again combined in order to produce a larger porous silicon volume. The fabrication parameters used in making the material has been previously presented in Table 4-10. The fabrication parameters

used in making sample PSiPW_15 have been previously presented in Table 4-11. The results of the adsorption tests for the porous silicon samples are presented below.

4.5.5.3.1 - Results

Excess Adsorption

Isotherm plots for the excess adsorption of methane on porous silicon powder samples PSiPW_3, PSiPW_10, PSiPW_14, and PSiPW_15 are presented below in Figures 4-140 to 4-143.

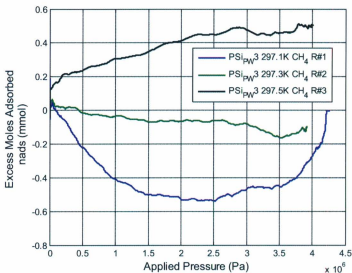


Figure 4-140: PSiPW3 - Absolute Excess Molar Adsorption Capacity.

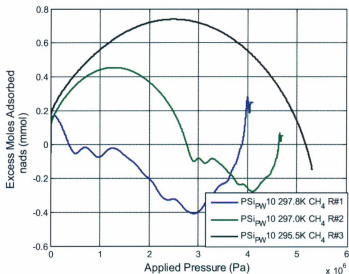


Figure 4-141: PSiPW10 – Absolute Excess Molar Adsorption Capacity.

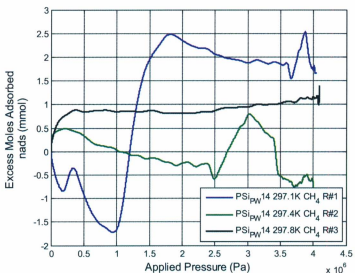


Figure 4-142: PSiPW14 – Absolute Excess Molar Adsorption Capacity.

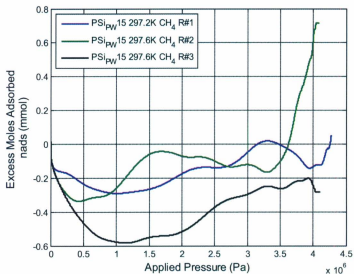


Figure 4-143: PSiPW15 – Absolute Excess Molar Adsorption Capacity.

Effective Storage

Isotherm plots for the effective storage of methane by porous silicon powder samples PSiPW_3, PSiPW_10, PSiPW_14, and PSiPW_15 are presented below in Figures 4-144 to 4-150.

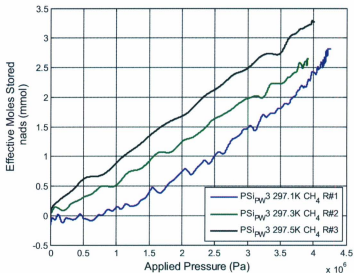


Figure 4-144: PSiPW3 – Absolute Effective Molar Storage Capacity.

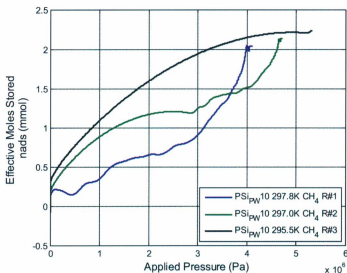


Figure 4-145: PSiPW10 – Effective Absolute Molar Storage Capacity.

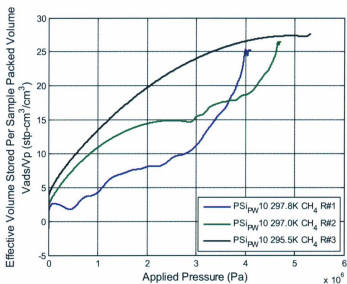


Figure 4-146: PSiPW10 - Effective Volumetric Storage Capacity.

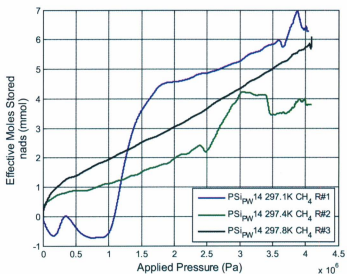


Figure 4-147: PSiPW14 - Effective Absolute Molar Storage Capacity.

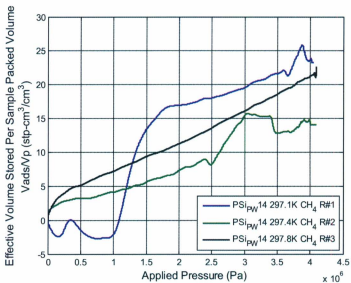


Figure 4-148: PSiPW14 - Effective Volumetric Storage Capacity.

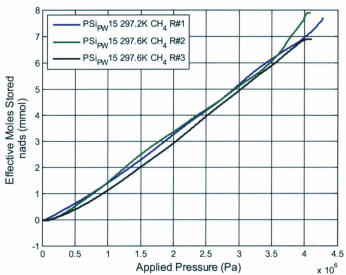


Figure 4-149: PSiPW15 - Effective Absolute Molar Storage Capacity.

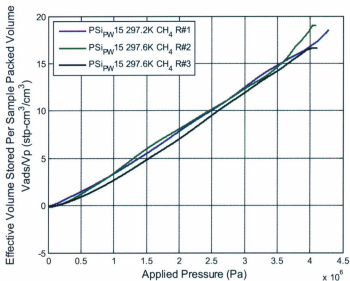


Figure 4-150: PSiPW15 – Effective Volumetric Storage Capacity.

4.5.5.3.2 - Analysis

Excess Adsorption

From the excess adsorption plots presented above in Figures 4-140 to 4-143 it is clear that no statistically significant amount of gas adsorption has taken place for any of the porous silicon samples. For each of the materials, the absolute number of excess moles of gas adsorbed was less than the experimental measurement uncertainty. Thus, any adsorption values reported cannot be considered reliable and must be classified entirely as random experimental error. The fact that all of the plots reported negative adsorption values is also clear evidence of this error.

Large deviations between isotherm values for different test runs are present for nearly all of the samples. However, the absolute value of these deviations is actually very small and can be considered insignificant. Also, most all of the adsorption

isotherms return to zero at the end of the gas expansion process. This also suggests that values reported by the isotherms at intermittent pressures of the process are essentially error from the gas expansion process. Since the materials did not adsorb any significant excess amount of gas, no desorption plots were generated.

Effective Storage

From the effective storage isotherm plots presented above in Figures 4-144 to 4-150 it is clear that the porous silicon samples all effectively store statistically significant amounts of methane gas. Deviations between experimental runs are greatly decreased for the effective storage isotherms compared to the excess adsorption isotherms, which provides an indication of the influence of bulk gas compressive storage. Since the effective storage plots for all of the samples are essentially linear, it can be concluded that the effective storage process is dominated by the bulk gas compressive storage component.

For each of the materials, a rough calculation can be performed to determine the percentage of the effective storage capacity that can be attributed to the bulk gas compressive storage component. This value was obtained by the procedure previously discussed in Section 4.5.2.4.2 for the activated carbon materials. Calculations are performed at a pressure of 4 MPa for each of the samples.

The results of the bulk compression component analysis for each of the porous silicon samples studied is presented below in Table 4-69.

Table 4-69: Bulk compression component fraction for effective storage of zeolites.

Material	Theoretical Effective Storage Without Adsorption	Effective Storage Value Obtained	Bulk Compression Component of Effective Storage
PSiPW_3	2.59	2.80	92 %
PSiPW_10	1.63	1.99	82 %
PSiPW_14	4.31	5.42	79 %
PSiPW_15	8.71	10.66	82 %

Since it was previously determined that the excess adsorption amounts reported by all of the samples are essentially entirely random error, it can be therefore assumed that the compression process accounts for approximately 100% of the effective storage capacity for all of the samples.

4.5.6 - All Materials

In order to gain a relative sense of the performance of the materials tested, the isotherms for each of the materials were plotted together to enable comparisons to be made easily. The combined isotherm plots for the materials are presented below in Figures 4-151 to 4-155.

4.5.6.1 - Results

4.5.6.1.1 - Excess Adsorption

Plots of the excess adsorption of methane on each of the tested materials expressed in two commonly used evaluation parameters are presented below in Figures 4-151 and 4-152.

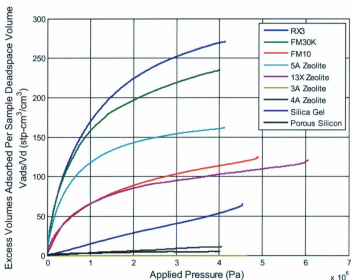


Figure 4-151: Combined Materials - Excess Volumetric Adsorption Capacity.

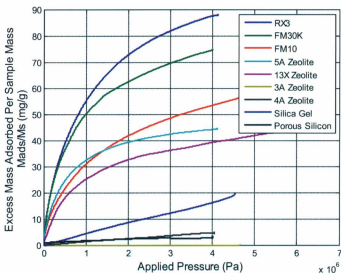


Figure 4-152: Combined Isotherms - Specific Excess Mass Adsorption Capacity.

4.5.6.1.2 - Effective Storage

Isotherm plots of the effective storage for each the tested materials expressed in two commonly used evaluation parameters are presented below in Figures 4-153 and 4-154.

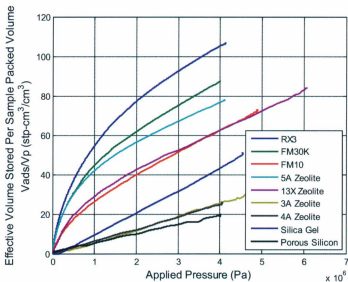


Figure 4-153: Combined Isotherms - Effective Volumetric Storage Capacity.

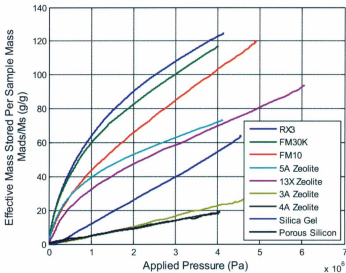


Figure 4-154: Combined Isotherms - Specific Effective Mass Storage Capacity.

A plot of the effectively stored amount of gas that can be effectively delivered is presented below in Figure 4-155 for the materials that produced reasonable storage values.

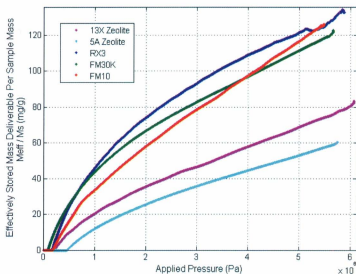


Figure 4-155: Combined Isotherms - Specific Effective Mass Delivery Capacity.

4.5.6.2 - Analysis

4.5.6.2.1 - Excess Adsorption

From the excess adsorption isotherms displayed in Figures 4-151 and 4-152 we can see that there is quite a large difference in the performance of the materials. Excess adsorption values were found to range from practically zero to almost $100 \left(\frac{\text{mg}}{\text{g}}\right)$. The Norit RX3 Extra produced the highest adsorption values, while the 3A zeolite produced the lowest. In fact, it is clear from the plots that the three activated carbon materials tested produced the largest specific (per mass) excess adsorption values. From a comparison of the three plots it is evident that the 5A zeolite produces higher volumetric storage values than the Zorflex FM10, but produces lower specific adsorption values.

4.5.6.2.2 - Effective Storage

From the effective storage plots presented in Figures 4-153 and 4-154 we can again see that there is quite a large difference in the storage performance of the materials. Effective storage values were found to range from approximately 20 to 120 ($\frac{\text{mg}}{\text{g}}$). In general, the effective storage isotherms produced higher values compared to the excess adsorption isotherms, and also exhibit more linearity due to the presence of the bulk pressure storage component. The Norit RX3 Extra again produced the highest storage values, while the porous silicon produced the lowest. The performance of both the FM30K and FM10 materials largely increase for the mass storage when compared to the volumetric storage, making them comparable to the RX3 Extra. The performance of the 5A Zeolite however, tends to reduce for mass storage when compared to volumetric storage. It is unknown what property of the material may cause this to occur.

From the effective delivery plot presented in Figure 4-155 we can see that the Norit RX3 Extra provides the best overall storage performance. However, the FM30K and FM10 both produce effective delivery capacities that are very close to the RX3. In fact, delivery capacities for the FM30K are actually higher than the RX3 Extra for pressures up to approximately 0.75 MPa. From a general comparison of the effective storage plots and the effective delivery plot, it is evident that the overall storage performance of the FM30K and FM10 increases relative to the other materials. It is also clear that the 13X Zeolite offers a higher delivery capacity than the 5A Zeolite, even though it has a lower storage capacity. This provides a clear example of how a material with a higher storage capacity may not necessarily be the overall higher performing adsorbent.

4.6 - Discussion & Literature Comparison

4.6.1 - General Discussion

Excess adsorption and effective storage isotherms given in common evaluation units were successfully generated for all of the materials tested. All of the excess adsorption plots resemble that of an IUPAC type-1 isotherm. No excess adsorption or effective storage isotherms were found to contain maxima with a subsequent change in slope to produce decreasing adsorption values for increasing pressures.

Effective storage values obtained for the materials were generally significantly larger than excess adsorption values. Gas retention values when the evaluating effective storage were found to always be lower than those for excess adsorption. The bulk gas compression component of the effective storage was found to represent anywhere from 28 % to 100 % of the total storage values obtained from the tested materials. It was also found that gas retention values generally decrease as storage pressures increase.

Deviations were generally obtained between the three experimental adsorption tests conducted for each material. However, these deviations could generally be attributed to differences in temperature and process expansion rates. Deviations between isotherms for different test runs were generally less for the effective storage isotherms compared to the excess adsorption isotherms. It was also found that hysteresis was generally less significant for effective storage when compared to excess adsorption. This is essentially due to the fact that the effective storage involves bulk gas compressive storage which is a reversible process that does not exhibit hysteresis.

A number of isotherms produced negative excess adsorption values. However, these values were simply error since the magnitude of the values reported by these isotherms were all less than the uncertainty of the measurement. This would imply

that the material being tested is incapable of adsorbing any statistically significant amount of gas.

As previously stated, the effective storage isotherms are essentially the superpositioning of the absolute adsorption and the bulk gas compressive storage components. Because of this, effective storage isotherms tend to resemble excess adsorption plots that approach a linear relationship instead of reaching a maximum limiting value. This trend can be observed for all materials tested shown in Figures 4-153 through 4-155.

All of the isotherms presented (with the exception of porous silicon and 3A Zeolite) were successfully modeled using the Langmuir, Freundlich, and Toth isotherm equations. The Langmuir model seemed to provide the overall best fit correlation for the materials tested. All of the models generally provided poor fits to the effective storage isotherms. However, all of the modified models fit the effective storage data extremely well.

From the isotherm plots presented for the 3A Zeolite and porous silicon materials, it is evident that neither material will adsorb any statistically significant amount of gas, since adsorption values reported were less than the minimum measurement uncertainty (1.2 mmol). It is believed the 3A Zeolite failed to adsorb methane gas because its average pore size (0.3 nm) is slightly smaller than the kinetic diameter of a methane molecule (0.38 nm). However, it is not known why the porous silicon material did not store any significant amount of gas. Initially it was presumed that porous material volumes produced were too small to facilitate an adequate amount of gas adsorption. This problem was later thought to be solved when stain etching was introduced as the primary method of porous material production. Based on the results of the stain etching wafer experiments previously presented, it was estimated that a 10 ml sample of stain etched silicon powder consisting of 37 to 63 μm sized particles would have a porous material volume on the order of 3 to 4 ml; which is a great deal larger than the electrochemically etched films which had volumes on the

order of 0.01 to 0.02 ml. However, it is unknown if the stain etching results obtained with the wafers can also be applied to produce porous silicon in particulate form having the same properties. Thus, actual porous material volumes obtained through the use of stain etching may still have been too small. It may also be possible that the average pore size of the porous silicon formed may have been too small to facilitate any gas adsorption. Based on the adsorption results obtained from the 3A and 4A zeolites, it can be observed that materials having pore sizes less than or equal to the diameter of the adsorbate molecule will not adsorb gas effectively. It may be the case that the porous silicon produced had an average pore diameter of less than 0.4 nm making it incapable of adsorbing methane gas, since it is also known that the production of porous silicon via stain etching generally produces a microporous material (less than 2 nm pore size) (Lehmann, 2002). The results of the KOH etching experiments and ultraviolet illumination tests also suggest that the porous silicon produced was in fact microporous.

Another possible explanation for the poor adsorption performance of the porous silicon is that the material may have an overall low adsorption affinity due to a low solid surface and/or interfacial layer surface energy. By letting the adsorption affinity (φ) be representative of the total adhesion energy (ϵ_{ad}) for a gas/solid system the following can be written using the Young-Dupré equation (Israelachvili, 1985):

Eq. 4-5

$$\varphi \propto \epsilon_{ad}$$

$$\epsilon_{ad} = \epsilon_{gas-surf} + \epsilon_{solid-surf} + \epsilon_{interfacial}$$

where $\epsilon_{gas-surf}$ is the surface energy of the gas phase, $\epsilon_{solid-surf}$ is the surface energy of the solid phase, and $\epsilon_{interfacial}$ is the surface energy of the phase dividing surface.

Carbon bonding exists in both activated carbon and methane which facilitates covalent bonding potential between the adsorbent and adsorbate. Also, during the

carbon activation process the material surface is modified to exhibit a graphitic like structure with short range order. This in turn creates large internal surface areas. These two properties generally cause activated carbons to have high solid surface energies and high interfacial layer energies, which makes them good adsorbents. The zeolites are metal-organic silicates with well-formed cage structure frameworks. These frameworks also contain additional metal ions that are free to bond and produce field potentials. These two properties generally cause the zeolites to have high surface energies and moderate interfacial layer energies, which also makes them good adsorbent materials. Porous silicon cannot mimic the bonding attributes of activated carbon nor does it possess the cage like structures of the zeolites and some activated carbons. Silicon and carbon however are quite chemically similar. Thus, one would expect that porous silicon would generally have a lower adhesion energy compared to the zeolites and activated carbons.

Effective storage and effective delivery storage capacities of 109 and 90 ($\frac{\text{ml}}{\text{ml}}$) at a pressure of 3.5 MPa were obtained for the Norit RX3 Extra GAC. Although these values are not in the high range for this type of material, significant increases in storage densities are still obtained when compared to CNG. Below Figure 4-156 displays a plot of the effective storage density of the Norit RX3 Extra compared to CNG.

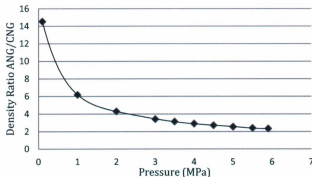


Figure 4-156: ANG/CNG Effective Storage Density Ratio for Norit RX3 Extra.

From the plot we can see that at lower pressures there is an extremely large relative density increase between ANG and CNG storage densities. However, this relative density increase greatly reduces as storage pressures increase. Thus, it is apparent that ANG produces the best performance characteristics at lower pressures. However, even as pressures approach 6 MPa the effective storage density of the RX3 is over twice that for CNG, which is still very significant.

4.6.2 - Literature Comparison

A comparison of the experimental results obtained with those found in the literature for similar materials is presented below for the porous activated carbon, zeolite, and silicate materials. These reported results can be used as a comparison, and to help verify that the adsorption values obtained from the experiments presented in this thesis are reasonable. All excess adsorption and effective storage values reported were obtained from adsorption experiments conducted at 298 K and 3.5 MPa using methane gas. Since the porous silicon samples failed to adsorb any significant amount of gas, the material was not compared to any reported in the literature.

4.6.2.1 - Porous Carbons

Excess adsorption and effective storage results that have been reported in the literature are presented below for various granulated activated carbons and activated carbon fibers with specific surface areas similar to those possessed by the tested carbon materials. No reports on the excess adsorption or effective storage of methane on the Norit RX3 Extra, Zorflex FM30K, or Zorflex FM10 were found in the literature.

4.6.2.1.1 - Excess Adsorption

Excess adsorption results that have been reported in the literature for materials very similar to the tested RX3 Extra, FM30K, and FM10 are presented below in Tables 4-71 through 4-73. A summary of the excess adsorption values obtained from the three carbon materials tested is presented below in Table 4-70.

Table 4-70: Excess adsorption capacity summary for carbon materials ($\text{CH}_4 - P = 3.5\text{MPa} - T \approx 298\text{K}$). A_{sp} is the specific surface area, n_a^a is the absolute excess molar adsorption capacity, $\rho_{n_a}^a$ is the excess molar adsorption density, $\rho_{V_a}^a$ is the excess volumetric adsorption density, $\rho_{m_a}^a$ is the excess mass adsorption density, $M_{n_a}^a$ is the excess specific molar adsorption capacity, $M_{V_a}^a$ is the excess specific volumetric adsorption capacity, $M_{m_a}^a$ is the excess specific mass adsorption capacity, n_e^a is the absolute excess molar delivery capacity, $\rho_{n_e}^a$ is the excess molar delivery density, $\rho_{V_e}^a$ is the excess volumetric delivery density, $\rho_{m_e}^a$ is the excess mass delivery density, $M_{n_e}^a$ is the excess specific molar delivery capacity, $M_{V_e}^a$ is the excess specific volumetric delivery capacity, $M_{m_e}^a$ is the excess specific mass delivery capacity, and R^a is the excess adsorption gas retention.

Material	A_{sp}	n_a^a	$\rho_{n_a}^a$	$\rho_{V_a}^a$	$\rho_{m_a}^a$	$M_{n_a}^a$	$M_{V_a}^a$	$M_{m_a}^a$
RX3	1370	27.8	13.1	315	210	5.9	144	96
FM30K	≈ 1300	20.4	9.0	217	145	4.3	104	69
FM10	≈ 800	14.8	5.5	132	88	3.9	93	62
	n_e^a	$\rho_{n_e}^a$	$\rho_{V_e}^a$	$\rho_{m_e}^a$	$M_{n_e}^a$	$M_{V_e}^a$	$M_{m_e}^a$	R^a
RX3	21.8	10.2	245	164	4.7	111	75	22%
FM30K	16.4	7.3	175	116	3.5	84	56	24%
FM10	10.7	3.9	95	63	2.8	67	45	28%

It is clear from the values presented below in Table 4-71 that the excess adsorption results obtained for the tested RX3 Extra agree with those obtained from the literature. An excess adsorption value of $96 \left(\frac{\text{mg}}{\text{g}}\right)$ was obtained, which is within the range of values presented in the table (82 to $103 \left(\frac{\text{mg}}{\text{g}}\right)$). It is interesting to note that the largest deviation between values in the table is from two of the same materials. Adsorption values reported for the Norit R1 GAC varied from 82 to $103 \left(\frac{\text{mg}}{\text{g}}\right)$, which is quite significant.

It is clear from the values presented in Table 4-72 that the excess adsorption results obtained for the tested Zorflex materials also agree with those obtained from the literature. Excess adsorption values of 69 and $62 \left(\frac{\text{mg}}{\text{g}}\right)$ were obtained for the FM30K and FM10 materials respectively, which is within the range of values presented in the

table (56 to $72\left(\frac{\text{mg}}{\text{g}}\right)$). It should be noted that the FM30K and FM10 materials produced adsorption values that were generally lower than most activated carbon fiber or cloth materials found in the literature.

It is evident from the above analysis that the excess adsorption values obtained from this work agree with those found in the literature for very similar materials. Additional activated carbon materials obtained from the literature that are less similar to the materials studied are presented below in Table 4-73.

Table 4-71: Excess adsorption values for materials similar to the Norit RX3 Extra found in the literature. A_{sp} is the specific surface area, $M_{n_a}^a$ is the excess specific molar adsorption capacity, and $M_{m_a}^a$ is the excess specific mass adsorption capacity.

Name	Type	A_{sp} $\left(\frac{\text{m}^2}{\text{g}}\right)$	$M_{n_a}^a$ $\left(\frac{\text{mmol}}{\text{g}}\right)$	$M_{m_a}^a$ $\left(\frac{\text{mg}}{\text{g}}\right)$	Reference
Norit RX3 Extra	GAC	1370	5.9	96	This Work
Norit R1	GAC	1450	5.9	95	(Himeno et al., 2005)
Norit R1	GAC	1450	6.4	103	(Dreisbach, Staudt, & Keller, 1999)
Norit R1	GAC	1240	5.1	82	(Menon & Komarneni, 1998)
Norit R1	GAC	1240	5.1	82	(Barton, Dacey, & Quinn, 1984)
Norit R3	GAC	1270	5.7	92	(Quinn, MacDonald, & Sosin, 1994)
Norit R3	GAC	1270	5.7	92	(Menon & Komarneni, 1998)
Kureha BAC	GAC	1350	6.2	99	(Menon & Komarneni, 1998)
Kureha BAC	GAC	1350	6.2	99	(Quinn et al., 1994)

Table 4-72: Excess adsorption values for materials similar to the Zorflex FM30K & FM10 found in the literature. A_{sp} is the specific surface area, $M_{n_a}^a$ is the excess specific molar adsorption capacity, and $M_{m_a}^a$ is the excess specific mass adsorption capacity.

Name	Type	A_{sp} ($\frac{m^2}{g}$)	$M_{n_a}^a$ ($\frac{mmol}{g}$)	$M_{m_a}^a$ ($\frac{mg}{g}$)	Reference
Zorflex FM30K	ACF	≈1300	4.3	69	This Work
Zorflex FM10	ACF	≈800	3.9	62	This Work
A10 Fiber	ACF	1200	4.5	72	(Tedesco et al., 2010)
CFS22	ACF	883	4.2	67	(Lozano et al., 2002)
CFS15	ACF	800	3.5	56	(Alcaniz-Monge et al., 1997)
CFS25	ACF	1050	4.1	66	(Alcaniz-Monge et al., 1997)
CFS36	ACF	1210	4.5	72	(Alcaniz-Monge et al., 1997)

The adsorption results obtained from the literature and displayed in Tables 4-71 and 4-72 were used to construct a plot of the specific excess mass adsorption versus specific area. The values for the carbon materials tested have also been included for verification. The plot is displayed below in Figure 4-157.

It has been previously determined that there is a linear relationship between excess mass adsorption and specific surface area (Sun et al., 2009; Yongjuni et al., 2010). From the plot it can be concluded that the values obtained from experiment are reliable since the materials follow data trends established from reports in the literature. It is also evident from this plot that values for the FM30K and FM10 are slightly lower for similar materials having similar specific surface areas as previously mentioned.

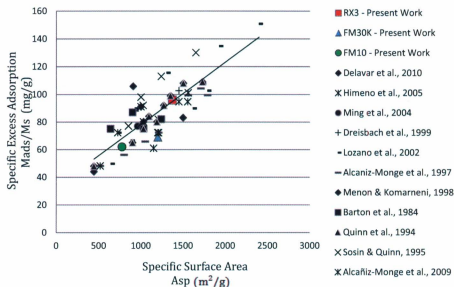


Figure 4-157: Comparison of specific mass adsorption capacity and specific surface area for carbon materials.

Table 4-73: Additional carbon material excess adsorption results. A_{sp} is the specific surface area, $M_{n_a}^a$ is the excess specific molar adsorption capacity, and $M_{m_a}^a$ is the excess specific mass adsorption capacity.

Name	Type	A_{sp} ($\frac{m^2}{g}$)	$M_{n_a}^a$ ($\frac{mmol}{g}$)	$M_{m_a}^a$ ($\frac{mg}{g}$)	Reference
GAC	GAC	907	6.6	106	(Delavar et al., 2010)
BPL	GAC	1150	3.8	61	(Tedesco et al., 2010)
AC-a	GAC	1207	5.1	82	
K02 AC	GAC	960	4.8	77	(Ming et al., 2004)
LFC14	ACF	520	3.0	48	(Lozano et al.,

						2002)
LFC30	ACF	930	5.6	90		
LFC47	ACF	1790	6.4	103		
LFC54	ACF	1930	8.4	135		
CFC19	ACF	647	3.1	50		
CFC49	ACF	1728	6.7	107		
CFS52	ACF	1618	5.6	90		
KUA11701	PAC	726	4.5	72		
KU21701- 200	PAC	1305	7.2	115		
CFC14	ACF	520	3.0	48	(Alcaniz-Monge et al., 1997)	
CFC30	ACF	930	5.5	88		
CFC47	ACF	1790	6.2	99		
CFS50	ACF	1560	6.2	99		
CFS60	ACF	1710	6.5	104		
MSC-5A	GAC	445	2.7	44	(Menon & Komarneni, 1998)	
Carbon Lorraine	GAC	640	4.7	75		
Saran (B)	GAC	900	5.4	87		
BPL	GAC	1030	4.7	75		
Norit WX6	GAC	445	3.0	48		
Calgon SGL	GAC	900	4.1	65		
Calgol BPL	GAC	1030	4.7	75		
Darco 1S4- 01	GAC	1095	5.2	84		
AC Carbone CNS196	GAC	1190	5.0	80		

California GMS-70	GAC	1502	6.7	108	
Baraebey MI	GAC	1730	6.8	109	
PVDC	GAC	1000	5.7	91	
BPL Calgon	GAC	1030	5.0	80	
KF 1500	ACF	1500	5.2	83	
A 10	ACF	1000	4.8	77	
Carbon Lorraine	GAC	640	4.7	75	(Barton, Dacey, & Quinn, 1984)
Saran (B)	GAC	900	5.4	87	
BPL	GAC	1030	4.7	75	
Norit WX6	GAC	445	3.0	48	(Quinn et al., 1994)
Calgon SGL	GAC	900	4.1	65	
Calgol BPL	GAC	1030	4.7	75	
Darco184- 01	GAC	1095	5.2	84	
AC carbone CNS196	GAC	1190	5.0	80	
California GMS-70	GAC	1502	6.7	108	
Baraebey MI	GAC	1730	6.8	109	
PVDC	GAC	1000	5.7	91	(Sosin & Quinn, 1995)
BPL Calgon	GAC	1030	5.0	80	

4-275

Saran A	ACM	1000	1.1	98	
Saran A 36X	ACM	1650	0.9	130	
Saran A 12X	ACM	1240	1.0	113	
Saran 415	ACM	852	0.9	77	
Saran 415 12X	ACM	1026	0.9	92	
CFC14	GAC	520	3	48	(Alcañiz-Monge et al., 2009)
CFC40	GAC	1555	5.9	95	
CFS36	GAC	1210	4.5	72	
CFS50	GAC	1560	6.3	101	
K1701	GAC	726	4.5	72	

4.6.2.1.2 - Effective Storage

Effective storage results that have been reported in the literature for materials very similar to the tested RX3 Extra, FM30K, and FM10 are presented below in Tables 4-75 and 4-76. As previously stated, no reports on the effective storage of methane by any of the carbon materials tested could be found in the literature. It should be noted that unlike excess adsorption, effective storage values reported for identical materials can vary largely since they greatly depend on the packing density used for the material. A summary of the effective storage values obtained from the three carbon materials tested is presented below in Table 4-74.

Table 4-74: Effective storage capacity summary for carbon materials ($\text{CH}_4 - P = 3.5\text{MPa} - T \approx 298\text{K}$). n_a^s is the absolute effective molar storage capacity, $\rho_{V_a}^s$ is the effective molar storage density, $\rho_{V_a}^s$ is the effective volumetric storage density, $\rho_{m_a}^s$ is the effective mass storage density, $M_{n_a}^s$ effective specific molar storage capacity, $M_{V_a}^s$ is the effective specific volumetric storage capacity, $M_{m_a}^s$ is the effective specific mass storage capacity. n_e^s is the absolute effective molar delivery capacity, $\rho_{n_e}^s$ is the effective molar delivery density, $\rho_{V_e}^s$ is the effective volumetric delivery density, $\rho_{m_e}^s$ is the effective mass delivery density, $M_{n_e}^s$ is the effective specific molar delivery capacity, $M_{V_e}^s$ is the effective specific volumetric delivery capacity, $M_{m_e}^s$ is the effective specific mass delivery capacity, and R^s is the effective storage gas retention.

Material	n_a^s	$\rho_{n_a}^s$	$\rho_{V_a}^s$	$\rho_{m_a}^s$	$M_{n_a}^s$	$M_{V_a}^s$	$M_{m_a}^s$
RX3	36.9	4.5	109	72	7.9	191	127
FM30K	31.3	3.3	80	53	6.6	160	106
FM10	25.2	2.6	64	42	6.6	159	105

	n_e^s	$\rho_{n_e}^s$	$\rho_{V_e}^s$	$\rho_{m_e}^s$	$M_{n_e}^s$	$M_{V_e}^s$	$M_{m_e}^s$	R^s
RX3	30.7	3.7	90	60	6.6	158	104	17 %
FM30K	27.0	2.8	68	45	5.7	138	91	14 %
FM10	20.8	2.2	53	35	5.4	131	87	17 %

It is clear from the values presented in Table 4-75 that the effective storage results obtained for the tested RX3 Extra agree with those obtained from the literature. A volumetric storage capacity of $109 \left(\frac{\text{stp ml}}{\text{ml}} \right)$ was obtained, which is within the range of values presented in the above table (61 to $127 \left(\frac{\text{stp ml}}{\text{ml}} \right)$). The effective storage, deliverability, and gas retention values obtained are very close to those reported for the KU21701-200, which has an approximately equal specific surface area.

It is evident from the values presented in Table 4-77 that the effective storage results obtained for the tested Zorflex materials also agree with those obtained from the literature for other similar materials. Volumetric storage capacities of 80 and $64 \left(\frac{\text{stp ml}}{\text{ml}} \right)$ were obtained for the FM30K and FM10 materials respectively, which is within the range of values presented by the table (60 to $127 \left(\frac{\text{stp ml}}{\text{ml}} \right)$). Other storage parameter values such as the effective delivery capacity and gas retention also agree

with those reported in the table. However, the volumetric effective storage capacities of the FM30K and FM10 materials are generally slightly lower than most activated carbon fiber and cloth materials found in the literature.

It is evident from the above analysis that the effective storage values obtained from this work agree with those found in the literature for very similar materials. Additional activated carbon materials obtained from the literature that are less similar to the materials studied are also presented below in Table 4-77.

Table 4-75: Effective storage values for materials similar to the Norit RX3 Extra found in the literature. A_{sp} is the specific surface area, $\rho_{V_a}^s$ is the effective volumetric storage density, $\rho_{V_e}^s$ is the effective volumetric delivery density, $M_{m_a}^s$ is the effective specific mass storage capacity, and R^s is the effective storage gas retention.

Name	Type	A_{sp} ($\frac{m^2}{g}$)	$\rho_{V_a}^s$ ($\frac{ml}{ml}$)	$\rho_{V_e}^s$ ($\frac{ml}{ml}$)	$M_{m_a}^s$ ($\frac{mg}{g}$)	R^s (%)	Reference
Norit RX3 Extra	GAC	1370	109	90	127	17	This Work
KU21701-200	GAC	1305	127	99	-	22	(Lozano-Castello et al., 2002)
C1	GAC	897	54	-	-	-	(Bastos-Neto et al., 2005)
C2	GAC	1037	73	-	-	-	
C3	GAC	1056	76	-	-	-	
C4	GAC	1478	68	-	-	-	
C5	GAC	945	67	-	-	-	
C6	GAC	826	61	-	-	-	
KUA11701	GAC	726	82	61	-	26	(Lozano-Castello et al., 2002)
KUA11701	GAC	726	82	61	-	26	
KUA11701	GAC	726	82	61	-	26	

Table 4-76: Effective storage values for materials similar to the Zorflex FM30K & FM10 found in the literature. A_{sp} is the specific surface area, $\rho_{V_a}^s$ is the effective volumetric storage density, $\rho_{V_e}^s$ is the effective volumetric delivery density, $M_{m_a}^s$ is the effective specific mass storage capacity, and R^s is the effective storage gas retention.

Name	Type	A_{sp} ($\frac{m^2}{g}$)	$\rho_{V_a}^s$ ($\frac{ml}{ml}$)	$\rho_{V_e}^s$ ($\frac{ml}{ml}$)	$M_{m_a}^s$ ($\frac{mg}{g}$)	R^s (%)	Reference
Zorflex FM30K	ACF	≈1300	80	68	106	14	This Work
Zorflex FM10	ACF	≈800	64	53	105	17	This Work
CFC11	ACF	283	60	49	-	18	(Lozano-Castello et al., 2002)
CFC50	ACF	1770	109	98	-	10	
CFS27	ACF	644	82	71	-	13	
LFC29	ACF	874	95	73	-	23	
LFC14	ACF	520	84	57	49	32	
LFC30	ACF	930	126	99	92	21	
LFC47	ACF	1790	127	103	105	19	

The adsorption results obtained from the literature and displayed in Tables 4-75 and 4-76 were used to construct a plot of the volumetric storage capacity versus specific surface area. The values for the carbon materials tested have also been included. The plot is displayed below in Figure 4-158. From the plot it can be concluded that the values obtained from experiment do deviate from data trends established from reports in the literature. However, as previously stated no one particular value for specific surface area was provided by the manufacturer of the FM30K and FM10 materials, but rather a range of values was given instead. Thus, the storage values obtained from these materials may actually produce a better data correlation if the actual specific surface areas for the tested samples were known.

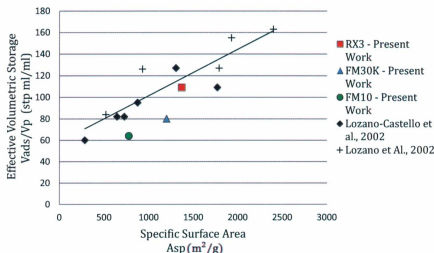


Figure 4-158: Comparison of effective volumetric storage capacity and specific surface area for carbon materials.

Table 4-77: Additional carbon material effective storage results. A_{sp} is the specific surface area, $\rho_{V_a}^s$ is the effective volumetric storage density, $\rho_{V_e}^s$ is the effective volumetric delivery density, $M_{m_a}^s$ is the effective specific mass storage capacity, and R^s is the effective storage gas retention.

Name	Type	A_{sp} ($\frac{m^2}{g}$)	$\rho_{V_a}^s$ ($\frac{ml}{ml}$)	$\rho_{V_e}^s$ ($\frac{ml}{ml}$)	$M_{m_a}^s$ ($\frac{mg}{g}$)	R^s (%)	Reference
LFC54	ACF	1930	155	135	136	13	(Lozano et al., 2002)
LFC73	ACF	2400	163	143	154	12	
LFS15	ACF	-	88	58	55	34	
LFS25	ACF	-	102	72	64	29	

LFS36	ACF	-	102	77	72	25	
LFS50	ACF	-	128	108	102	16	
LFS60	ACF	-	129	114	108	12	
CFC19	ACF	-	98	70	53	29	
CFC36	ACF	-	136	107	84	21	
CFC49	ACF	-	141	118	111	16	
CFC54	ACF	-	156	133	127	15	
CFC60	ACF	-	158	136	140	14	
CFC74	ACF	-	166	150	148	10	
CFS22	ACF	-	122	94	68	23	
CFS52	ACF	-	117	98	95	16	
CFS64	ACF	-	115	92	99	20	
Cloth 1	ACF	-	133	106	115	20	
Cloth 2	ACF	-	149	129	141	13	
Felt 1	ACF	-	151	131	133	13	
Felt 2	ACF	-	133	121	85	9	
A20	ACF	-	155	140	133	10	

4-281

KUA117 01	GAC	-	82	61	74	26	
KU21701 -200	GAC	-	127	99	119	22	
KUA217 51	GAC	-	143	124	149	13	
KUA218 01	GAC	-	160	126	164	21	
KUA416 51	GAC	-	153	134	166	12	
KUA417 01	GAC	-	166	142	191	14	
KUB417 01	GAC	-	165	140	166	15	
Maxsorb- A	GAC	-	152	138	197	9	
PVDC (AC)	GAC	-	154	-	-	-	(Cracknell et al., 1993)
AX21	GAC	-	113	-	-	-	
AX21-C	GAC	-	99	-	-	-	

4.6.2.2 - Zeolites

Excess adsorption and effective storage results that have been reported in the literature are presented below for various zeolite materials. No reports on the excess adsorption of methane gas at room temperature for the 3A and 4A zeolites could be found in the literature. Also, no reports on the effective storage of methane on any of the zeolites presented in this thesis could be found in the literature.

4.6.2.2.1 - Excess Adsorption

Excess adsorption results that have been reported in the literature for various zeolite materials with similar specific surface areas are presented below in Table 4-79. A summary of the excess adsorption values obtained from the four zeolite materials studied is also presented below in Table 4-78.

Table 4-78: Excess adsorption capacity summary for zeolite materials (CH₄ - P = 3.5MPa - T ≈ 298K). A_{sp} is the specific surface area, n_a^a is the absolute excess molar adsorption capacity, $\rho_{n_a}^a$ is the excess molar adsorption density, $\rho_{V_a}^a$ is the excess volumetric adsorption density, $\rho_{m_a}^a$ is the excess mass adsorption density, $M_{n_a}^a$ is the excess specific molar adsorption capacity, $M_{V_a}^a$ is the excess specific volumetric adsorption capacity, $M_{m_a}^a$ is the excess specific mass adsorption capacity, n_e^a is the absolute excess molar delivery capacity, $\rho_{n_e}^a$ is the excess molar delivery density, $\rho_{V_e}^a$ is the excess volumetric delivery density, $\rho_{m_e}^a$ is the excess mass delivery density, $M_{n_e}^a$ is the excess specific molar delivery capacity, $M_{V_e}^a$ is the excess specific volumetric delivery capacity, and $M_{m_e}^a$ is the excess specific mass delivery capacity.

Material	A_{sp}	n_a^a	$\rho_{n_a}^a$	$\rho_{V_a}^a$	$\rho_{m_a}^a$	$M_{n_a}^a$	$M_{V_a}^a$
3A	-	-	-	-	-	-	-
4A	≈200	2.6	0.6	14	9	0.4	6
5A	≈500	18.4	6.3	152	101	2.6	42
13X	≈400	13.9	4.1	98	65	2.3	37

	n_e^a	$\rho_{n_e}^a$	$\rho_{V_e}^a$	$\rho_{m_e}^a$	$M_{n_e}^a$	$M_{V_e}^a$	$M_{m_e}^a$
3A	-	-	-	-	-	-	-
4A	-	-	-	-	-	-	-
5A	7.3	2.5	61	40	1.0	17	60%
13X	10.7	3.1	76	50	1.8	29	23%

It is clear from the values presented in Table 4-79 that the excess adsorption results for the tested 5A Zeolite agree with those obtained from the literature. An excess adsorption value of 42 ($\frac{\text{mg}}{\text{g}}$) was obtained, which is within the range of values presented by the table for other 5A zeolites (35 to 50 ($\frac{\text{mg}}{\text{g}}$)). It is also clear that the excess adsorption values obtained for the tested 13X Zeolite agree with those found

in the literature. An excess adsorption value of $37 \left(\frac{\text{mg}}{\text{g}}\right)$ was obtained, which is within the range of values presented by the table for other 13X zeolites (12 to $82 \left(\frac{\text{mg}}{\text{g}}\right)$).

It is evident from the above analysis that the effective storage values obtained from this work agree with those found in the literature for very similar materials.

Table 4-79: Excess adsorption values for zeolite materials found in the literature. A_{sp} is the specific surface area, $M_{n_a}^a$ is the excess specific molar adsorption capacity, and $M_{m_a}^a$ is the excess specific mass adsorption capacity.

Material	$A_{sp} \left(\frac{\text{m}^2}{\text{g}}\right)$	$M_{n_a}^a \left(\frac{\text{mmol}}{\text{g}}\right)$	$M_{m_a}^a \left(\frac{\text{mg}}{\text{g}}\right)$	Reference
4A	≈ 200	0.4	6	This Work
13X	≈ 400	2.3	37	This Work
13X	600	5.1	82	(Cavenati et al., 2004)
13X	168	0.8	12	(Sun et al., 2009)
13X	-	3.3	53	(Rolniak & Kobayashi, 1980)
5A	≈ 500	2.6	42	This Work
5A	400	2.2	35	(Benard & Chahine, 1997)
5A	-	3.1	50	(Rolniak & Kobayashi, 1980)
5A	394	3.0	48	(Mentasty, Faccio, & Zgrablich, 1991)
5A	492	2.9	46	(Otto, 1981)
5A	-	2.6	42	(Wakasugi, Ozawa, & Ogino, 1981)
Na-ZSM-5	257	1.9	31	(Rolniak & Kobayashi, 1980)
NaX	-	4.1	66	(Sosin & Quinn, 1995)
MgX	-	4.1	66	
CaX	-	5.1	82	
SrX	-	3.9	62	
BaX	-	4.2	67	
NaY	-	3.5	56	(Talu et al., 1993)
MgY	-	3.9	62	
CaY	-	3.9	63	
SrY	-	3.8	61	
BaY	-	3.4	54	

The adsorption results displayed in Table 4-79 were used to construct a plot of the excess mass adsorption versus specific area, which is shown below in Figure 4-159. The zeolite materials tested have also been included to verify the values obtained. From the plot it can be concluded that the values obtained from experiment follow data trends established from reports in the literature. It should be noted however that the specific surface areas used for the tested zeolites are only an approximation based on reports in the literature.

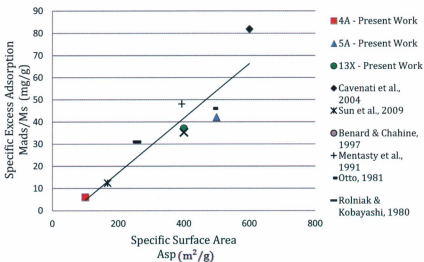


Figure 4-159: Comparison of specific mass adsorption capacity and specific surface area for zeolite materials.

4.6.2.2.2 - Effective Storage

Effective storage results that have been reported in the literature for two zeolite materials with unknown specific surface areas are presented below in Table 4-81. As previously stated, no reports on the effective storage of methane by any of the zeolite

materials tested could be found in the literature. A summary of the effective storage and effectively deliverable stored gas values for the materials tested is presented below in Table 4-80.

Table 4-80: Effective storage capacity summary for zeolite materials (CH₄ - P = 3.5MPa - T ≈ 298K). n_a^s is the absolute effective molar storage capacity, $\rho_{n_a}^s$ is the effective molar storage density, $\rho_{V_a}^s$ is the effective volumetric storage density, $\rho_{m_a}^s$ is the effective mass storage density, $M_{n_a}^s$ effective specific molar storage capacity, $M_{V_a}^s$ is the effective specific volumetric storage capacity, $M_{m_a}^s$ is the effective specific mass storage capacity. n_e^s is the absolute effective molar delivery capacity, $\rho_{n_e}^s$ is the effective molar delivery density, $\rho_{V_e}^s$ is the Effective volumetric delivery density, $\rho_{m_e}^s$ is the effective mass delivery density, $M_{n_e}^s$ is the effective specific molar delivery capacity, $M_{V_e}^s$ is the effective specific volumetric delivery capacity, $M_{m_e}^s$ is the effective specific mass delivery capacity, and R^s is the effective storage gas retention.

Material	n_a^s	$\rho_{n_a}^s$	$\rho_{V_a}^s$	$\rho_{m_a}^s$	$M_{n_a}^s$	$M_{V_a}^s$	$M_{m_a}^s$
3A	-	-	-	-	-	-	-
4A	8.1	1.0	24	16	1.1	27	18
5A	29.0	2.9	70	47	4.1	99	66
13X	23.8	2.4	57	38	4.0	96	64

	n_e^s	$\rho_{n_e}^s$	$\rho_{V_e}^s$	$\rho_{m_e}^s$	$M_{n_e}^s$	$M_{V_e}^s$	$M_{m_e}^s$	R^s
3A	-	-	-	-	-	-	-	-
4A	-	-	-	-	-	-	-	-
5A	17.7	1.8	43	29	2.5	61	40	39 %
13X	20.2	2.0	49	33	3.4	82	55	23 %

It is clear from the values presented in Table 4-81 that the effective storage results obtained for the tested zeolites are much less than those obtained from the literature. However, since the specific surface areas and packing densities of those materials are not known, they cannot be used as a direct and reliable comparison. Values reported can vary largely between materials and still remain correct since effective storage is dependent on the material packing density, which is often subject to processing to increase its value. Since the excess adsorption values obtained were found to agree with those reported in the literature, the effective storage values obtained for the tested zeolites can be assumed to be correct.

Table 4-81: Effective storage values for zeolite materials found in the literature. A_{sp} is the specific surface area, and $\rho_{V_a}^s$ is the effective volumetric storage density.

Material	A_{sp} $\left(\frac{\text{m}^2}{\text{g}}\right)$	$\rho_{V_a}^s$ $\left(\frac{\text{ml}}{\text{ml}}\right)$	Reference
4A	≈ 200	24	This Work
5A	≈ 500	70	This Work
13X	≈ 400	57	This Work
ZSM-5	-	99	(Dai, Liu, Qian, Qiao, & Yan, 2008)
NaX	-	158	(Dai et al., 2008)

4.6.2.3 - Silicates

Excess adsorption results that have been reported in the literature are presented below for various silica gel materials. No reports on the effective storage of methane on silica gel were found in literature

4.6.2.3.1 - Excess Adsorption

Excess adsorption results that have been reported in the literature for silica gel materials with similar specific surface areas are presented below in Table 4-83. A summary of the excess adsorption values obtained is also presented below in Table 4-82.

Table 4-82: Summary of excess adsorption and storage capacity for silica gel ($\text{CH}_4 - \text{P} = 3.5\text{MPa} - \text{T} \approx 298\text{K}$). A_{sp} is the specific surface area, n_a^a is the absolute excess molar adsorption capacity, $\rho_{n_a}^a$ is the excess molar adsorption density, $\rho_{V_a}^a$ is the excess volumetric adsorption density, $\rho_{m_a}^a$ is the excess mass adsorption density, $M_{n_a}^a$ is the excess specific molar adsorption capacity, $M_{V_a}^a$ is the excess specific volumetric adsorption capacity, $M_{m_a}^a$ is the excess specific mass adsorption capacity, $\rho_{n_a}^s$ is the effective molar storage density, $\rho_{V_a}^s$ is the effective volumetric storage density, $\rho_{m_a}^s$ is the effective mass storage density, $M_{n_a}^s$ effective specific molar storage capacity, $M_{V_a}^s$ is the effective specific volumetric storage capacity, $M_{m_a}^s$ is the effective specific mass storage capacity, and R^s is the effective storage gas retention.

Excess Adsorption							
Material	A_{sp}	n_a^a	$\rho_{n_a}^a$	$\rho_{V_a}^a$	$\rho_{m_a}^a$	$M_{n_a}^a$	$M_{V_a}^a$
Silica Gel	≈ 400	2.4	57	38	1.1	26	17
Effective Storage							
Material	$\rho_{n_a}^s$	$\rho_{V_a}^s$	$\rho_{m_a}^s$	$M_{n_a}^s$	$M_{V_a}^s$	$M_{m_a}^s$	R^s
Silica Gel	1.7	41	28	3.2	78	52	17%

It is clear from the values presented in Table 4-83 that the excess adsorption results obtained for the tested silica gel agree with those obtained from the literature. An excess adsorption value of $17 \left(\frac{\text{mg}}{\text{g}} \right)$ was obtained, which is within the range of values presented by the table for other silica gels (14 to $36 \left(\frac{\text{mg}}{\text{g}} \right)$). It is evident from the analysis that the excess adsorption values obtained from this work agree with those found in the literature.

Table 4-83: Excess adsorption values for various silica gel materials found in the literature. A_{sp} is the specific surface area, $M_{n_a}^a$ is the excess specific molar adsorption capacity, and $M_{m_a}^a$ is the excess specific mass adsorption capacity.

Material	A_{sp} ($\frac{m^2}{g}$)	$M_{n_a}^a$ ($\frac{mmol}{g}$)	$M_{m_a}^a$ ($\frac{mg}{g}$)	
Silica Gel	≈ 400	1.1	17	This Work
Silica Gel	377	0.9	14	(Sun et al., 2009)
Silica Gel 1	532	2.2	36	(Menon & Komarneni, 1998)
Silica Gel 2	803	2.0	32	(Menon & Komarneni, 1998)
Silica Gel	530	2.2	36	(Gilmer & Kobayashi, 1964)
Silica Gel	800	2.0	32	(Haydel & Kobayashi, 1967)

The adsorption results displayed above in Table 4-83 were used to construct a plot of the excess mass adsorption versus specific area. The values for the silica gel material tested have also been included. It should be noted that the specific surface area used for the tested silica gel is only an approximation based on reports found in the literature.

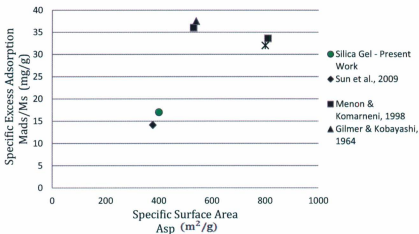


Figure 4-160: Comparison of specific mass adsorption capacity and specific surface area for silica gel.

4.6.3 - Materials Comparison

From the effective delivery isotherms for nearly all of the materials studied we can see that as the storage pressure increases, adsorbent performance generally decreases. The relative adsorption affinity of a material can be observed by the slope of the excess adsorption isotherm. For example, from Figures 4-151 and 4-152 shown above it is clear that the RX3 has a much larger adsorption affinity than the FM10 since its isotherm depicts a much higher attraction (larger slope) at the beginning of the adsorption process. A lower adsorption affinity is typically preferable since it leads to less gas retention upon discharge. However, most all materials with high adsorption capacities also have a high adsorption affinity. The three activated carbon materials presented are shown to have higher adsorption affinities compared to the zeolites and silicates. The 5A and 13X zeolites were found to have higher adsorption affinities compared to the silicate materials tested.

In general, the activated carbon materials produced the best performance characteristics compared to the zeolite and silicate materials. The Norit RX3 Extra was found to have the highest excess and effective storage capacities, followed by the FM30K. The 5A zeolite was found to have the third highest volumetric adsorption and effective storage capacities, while the Zorflex FM10 was found to have the third highest mass adsorption and storage characteristics. For applications where space is limited such as with natural gas vehicles, the 5A zeolite would therefore be a better suited adsorbent compared to the FM10.

The Norit RX3 Extra was found to have the best overall storage performance characteristics as determined from the effective delivery isotherms. It was however closely followed by the Zorflex FM30K and FM10. Unlike the excess and effective storage isotherms, the effective delivery capacity of the 13X Zeolite was higher than the 5A Zeolite. Due to the low gas retention properties of the FM30K and FM10, delivery capacities were very close to that obtained for the Norit RX3 Extra. The zeolite materials were generally found to have the highest gas retention values.

Ultimately, the optimum storage pressure for a material depends on the storage potential of the material and the cost of gas compression; at some point the cost of compressing the gas for ANG storage will exceed the benefit of the increased storage capacity created by the higher pressures. In any case, an adsorbent will not be economical if its cost is too high, and high performance materials are often expensive. However, in this study the highest performing material was one of the least expensive. The RX3 was found to have a bulk cost of approximately $5.9 \left(\frac{\$}{\text{kg}}\right)$ or $3.4 \left(\frac{\$}{\text{L}}\right)$, which is relatively low. The next highest performing material that was tested (FM30K) had a bulk cost of approximately $260 \left(\frac{\$}{\text{kg}}\right)$ or $125 \left(\frac{\$}{\text{L}}\right)$, which is relatively very high. The FM10 also has a high bulk cost with values on the order of $220 \left(\frac{\$}{\text{kg}}\right)$ or $85 \left(\frac{\$}{\text{L}}\right)$. The zeolite materials had the lowest bulk costs, with the price of 5A Zeolite being on the order of $1.05 \left(\frac{\$}{\text{kg}}\right)$ and 13X Zeolite being $1.10 \left(\frac{\$}{\text{kg}}\right)$. However, even with these low prices the zeolite materials are unlikely to serve as economical adsorbent materials due to their low overall performance. Cost values were provided by the material manufacturers for the above materials.

- 5 - Conclusions & Recommendations

5.1 - Conclusions

5.1.1 - Porous Silicon Production

Based on the experimental work conducted on the production of porous silicon, it can be concluded that electrochemical etching is not a viable method of economically producing large volumes of microporous silicon. However, the stain etching method of production is capable of efficiently producing large volumes of porous silicon in relatively short periods of time. Based on the results of the presented experimental stain etching studies, process parameter values were established that enable the production of microporous silicon films having thicknesses on the order of 4 to 5 μm and porosities on the order of 40 to 50%. Slightly modified values for these process conditions were also used to produce porous silicon powder. These conditions consisted of p^+ type silicon etched in a 1200:1 volumetric ratio solution of 49% HF and 70% HNO_3 for a time of 600 s.

5.1.2 - Adsorption Results

From the adsorption experiments conducted it can be concluded that current methods of porous silicon production are incapable of producing a material that will adsorb measureable amounts of methane gas. It is unknown whether the material pores are too small, if actual porous material volumes being produced are too small, or if surface layer and interfacial surface energies are too low for the material.

Overall, the Norit RX3 Extra granulated activated carbon produced the highest excess adsorption and effective storage capacities. Effective storage and delivery capacities of 109 and $90 \frac{\text{stp ml}}{\text{ml}}$ were obtained at a pressure of 3.5 MPa and temperature of approximately 298 K. This represents a volumetric energy density of 12% of that for gasoline. A gas retention value of 17% was also obtained, which is typical of activated

carbon materials. In general, the activated carbon materials provided the best performance characteristics.

It was found that the zeolite 3A material is incapable of storing methane gas because its average pore size is smaller than the average kinetic diameter of a methane molecule. The carbon materials were generally found to have better mass storage performance due to their decreased structural (dead space) densities compared to the zeolites or silica gel. In contrast, the zeolite materials were found to exhibit better volumetric storage performance. This is because zeolite materials generally produce higher packing densities than carbon materials.

All of the materials tested with the exception of porous silicon and 3A zeolite were successfully described using the Langmuir, Freundlich, and Toth isotherm models. Modification of these isotherm models was required in order for the models to accurately describe effective storage isotherms.

Excess adsorption and effective storage values reported in the literature were found to vary largely between similar (in some cases the same) materials. Effective storage values varied quite largely since their value greatly depends on the material packing density which can be changed.

5.1.3 - Summary of Contributions

An apparatus was successfully designed and constructed to conduct supercritical gas adsorption tests at room temperature. The apparatus was also proven to produce accurate and reliable results through extensive data error evaluation, and comparing adsorption results with those found in the literature. Supercritical adsorption tests of methane gas were successfully conducted on porous activated carbon, zeolite, and silicate materials at room temperature. None of the carbon materials tested had been previously reported in the literature. Also, no reports on the effective storage of any of the materials tested could be obtained from the literature. Based on reports found in the literature, an empirical model was presented to approximate a material's

specific surface area based on its specific excess mass adsorption capacity at 3.5 MPa and 298 K. Modified versions of the Langmuir, Freundlich, and Toth isotherm models were developed and presented to accurately describe effective storage isotherms. Stain etching process conditions that enable the production of porous silicon films of a much greater thickness than that currently reported in the literature were identified. A process method was also established to enable the production of porous silicon powder.

5.1.4 - Final Remarks

The RX3 GAC produced the highest adsorption and storage capacities but did not meet the target effective volumetric delivery capacity of $180 \frac{\text{stp ml}}{\text{ml}}$. However, the material was found to be relatively inexpensive with bulk purchasing costs being much less than the suggested maximum of 10 \$/kg. Thus, the material still may be economical for some adsorption applications.

In conclusion, no materials tested were found to possess the performance values generally thought to be required for an economical adsorbent. However, some of these values such the U.S. D.O.E. volumetric capacity are simply suggestions that reflect the economics of the technology at the time of their being established. The economics of utilizing ANG technology is also greatly affected by other factors such as mass capacity, material cost, and operation life. Thus, some ANG adsorbent materials may still be capable of facilitating the utilization of ANG as an economical energy storage technology even though they may not achieve traditional storage performance targets.

5.2 - Recommendations

Upon completion of the research project a number of areas that may be improved were identified. These areas were essentially regarding the gas adsorption apparatus developed for the tests. Since temperature changes were found to often occur during the course of a test, a better method of controlling the temperature of the apparatus

and contained gas during the testing process would lead to increased accuracy. It was found that gas expansion rates were a significant source of measurement error, and the control of such rates was somewhat unstable. It is recommended that a more appropriate valve such as a needle valve be fitted to the apparatus to enable better gas expansion control.

As previously stated, stain etching was successfully utilized to produce porous silicon powder. However more work is required to confirm the properties and volumes of the porous material samples created to establish why they did not adsorb any statistically significant amount of methane gas.

The reasons for using, benefits, and potential applications of ANG were previously discussed in Chapter 2. It was identified that ANG may be suitable for a wide variety of applications which would also often involve different operating conditions. These operating conditions would involve changes in pressure and temperature for the most part. However, the work presented in this thesis did not consider temperature as a variable and was thus held constant throughout all experiments. For many applications however such as natural gas vehicles, temperatures may vary throughout the adsorption and desorption processes. From the results of experiments presented in this thesis it was shown that slight changes in temperature can have a significant effect on the adsorption and desorption performance of a material. These temperature changes were essentially unintentional and were the result of an inadequate temperature control system. It is therefore recommended that future works on this topic consider temperature as a variable when studying the adsorption and desorption processes. This may involve conducting adsorption tests at different temperatures, conducting desorption tests at temperatures different from that used during the adsorption process, and varying temperatures throughout the adsorption and desorption processes. Such work may thus enable the development of adsorption models that can describe adsorption and desorption systems for both changing pressures and temperatures. Currently no such models exist.

- 6 - Bibliography

1. Ackley, M. W., Rege, S. U., & Saxena, H. (2003). Application of natural zeolites in the purification and separation of gases. *Microporous and Mesoporous Materials*, *61*, 25-42.
2. Akkimaradi, B. S., Prasad, M., Dutta, P., Saha, B. B., & Srinivasan, K. (2009). Adsorption of nitrogen on activated carbon-refit of experimental data and derivation of properties required for design of equipment. *Journal of Chemical Engineering Data*, *46*, 2291-2295.
3. Al Asheh, S., & Al Emadi, K. (2009). Sorptive storage of natural gas on molecular sieves: Dynamic investigation. *International Journal of Chemical and Biological Engineering*, *2*(1), 30-37.
4. Al-Baghli, N. A., & Loughlin, K. F. (2005). Adsorption of methane, ethane, and ethylene on titanosilicate ETS-10 zeolite. *Journal of Chemical Engineering Data*, *50*, 843-848.
5. Alcañiz-Monge, J., Casa-Lillo, M. A., Cazorla-Amoros, D., & Linares-Solano, A. (1997). Methane storage in activated carbon fibres. *Carbon*, *35*, 291-297.
6. Alcañiz-Monge, J., & Illán-Gómez, M. J. (2008). Modification of activated carbon porosity by pyrolysis under pressure of organic compounds. *Adsorption*, *14*, 93-100.
7. Alcañiz-Monge, J., Lozano-Castelló, D., Cazorla-Amorós, D., & Linares-Solano, A. (2009). Fundamentals of methane adsorption in microporous carbons. *Microporous and Mesoporous Materials*, *124*, 110-116.
8. Al-Muhtaseb, S. A., & Ritter, J. A. (1998). New virial-type model for predicting single- and multicomponent isosteric heats of adsorption. *Industrial & Engineering Chemistry Research*, *37*, 684-696.
9. Amankwah, K. A. G., & Schwarz, J. A. A. (1995). A modified approach for estimating pseudo-vapor pressures in the application of the dubinin-astakhov equation. *Carbon*, *33*(9), 1313-1319.
10. Angstore Technologies Ltd. (2011). *Adsorbed natural gas technology*. Retrieved from http://www.moregastech.com/index.php?option=com_content&task=view&id=13&Itemid=14
11. Aranovich, G., & Donahue, M. (1996). Adsorption of supercritical fluids. *Journal of Colloid Interface Science*, *180*, 537-541.

12. Aranovich, G., & Donohue, M. (1997). Determining surface areas from linear adsorption isotherms at supercritical conditions. *Journal of Colloid Interface Science*, *194*, 392-397.
13. Aranovich, G. L., & Donohue, M. D. (1996). Adsorption of supercritical fluids. *Journal of Colloid and Interface Science*, *180*, 537-541.
14. Aravamudhan, S., A.R.A. Rahman, and S. Bhansali. (2005). Porous silicon based orientation independent, self-priming micro direct ethanol fuel cell. *Sensors and Actuators a-Physical*, 497-504.
15. Arwin, H., Gavutis, M., & Gustafsson, J. (2000). Protein adsorption in this porous silicon film. *Physica Status Solidi (a)*, *182*, 515-520.
16. Arwin, H., Wang, G., & Jansson, R. (2003). Gas sensing based on ellipsometric measurement on porous silicon. *Physica Status Solidi (a)*, *197*(2), 518- 522.
17. Atkins, P., Paula J. (2009). Elements of Physical Chemistry: The Properties of Gases. W.H. Freeman
18. Balathanigaimani, M. S., Kang, H., Shim, W., Kim, C., Lee, J., & Moon, H. (2006). Preparation of powdered activated carbon from rice husk and its methane adsorption properties. *Korean Journal of Chemical Engineering*, *23*(4), 663-668.
19. Bari, H. A. A., Mohammed, A. H. A. K., & Shua'ab, A. K. M. Y., R.B.M. (2008). Equilibrium adsorption of hydrogen and methane on 5A molecular sieve. *American Journal of Engineering and Applied Sciences*, *1*(2), 157-160.
20. Barton, S. S., Dacey, J. R., & Quinn, D. F. (1984) High pressure adsorption of methane on porous carbons. *Proceedings of the first international conference on the fundamentals of adsorption*, 65-75.
21. Bastos-Neto, M., Torres, A. E. B., Azevedo, D. C. s., & Cavalcante, C. L. (2005). A theoretical and experimental study of charge and discharge cycles in a storage vessel for adsorbed natural gas. *Adsorption*, *11*, 147-157.
22. Belmabkhout, Y., De Weireld, G., & Frere, M. (2004). High-pressure adsorption isotherms of N₂, CH₄, O₂, and Ar on different carbonaceous adsorbents. *Journal of Chemical Engineering Data*, *49*, 1379-1391.
23. Benard, P., & Chahine, R. (1997). Modeling of high pressure adsorption isotherms above the critical temperature on microporous adsorbents: Application to methane. *Langmuir*, *13*, 808-813.

24. Biloe, S., Goetz, V., & Guillot, A. (2002). Optimal design of an activated carbon for an adsorbed natural gas storage system. *Carbon*, *40*, 1295-1308.
25. Biloea, S., Goetz, V., & Mauran, S. (2001). Characterization of adsorbent composite blocks for methane storage. *Carbon*, *39*, 1653-1662.
26. Bisi, O., Stefano, O., & Pavesi, L. (2000). Porous silicon: A quantum sponge structure for silicon based optoelectronics. *Surface Science Reports*, *98*.
27. Bjorklund, R. B., Zangoie, S., & Arwin, H. (1997). Planar pore-filling - adsorption in porous silicon. *Advanced Materials*, *9*(13), 1067-1070.
28. Bomchil, G., Herino, R., Barla, K., & Pfister, J. C. (1983). Pore size distribution in porous silicon studied by adsorption isotherms. *Journal of the Electrochemical Society*, *130*(7), 1611-1614.
29. Bruggeman, D. A. G. (1935). Berechnung verschiedener physikalischer konstanten von heterogenen substanzen. *Annalen der Physik (Leipzig)*, *(24)*, 636-679.
30. Brunauer, S., Emmett, P. H., & Teller, E. (1938). Adsorption of gases in multimolecular layers. *Journal of the American Chemical Society*, *60*, 309.
31. Burchell, T. D., Cook, T. L., Komodromos, C., Quinn, D. F., & Ragan, S. (1999). Adsorbent storage for natural gas vehicles. In *Carbon materials for advanced technologies* (pp. 269-302). Amsterdam: Elsevier.
32. Busch, A., Krooss, B. M., Gensterblum, Y., Van Bergen, F., & Pagnier, H. J. M. (2003). High-pressure adsorption of methane, carbon dioxide and their mixtures on coals with a special focus on the preferential sorption behaviour. *Geochemical Exploration*, *78-79*, 671-674.
33. Canada-Newfoundland and Labrador Offshore Petroleum Board. (2011). Retrieved, 2011, from <http://www.cnlopb.nl.ca/>
34. Canham, L. T. (2006). *Properties of porous silicon*. London, United Kingdom: The Institution of Electrical Engineers.
35. Cardenas, A. R., Lagoven, S. A., & Pilehvari, A. A. (1996). Is there a hope for adsorbed natural gas (ANG) vehicles? *Society of Petroleum Engineers*, (SPE 35581)
36. Cavenati, S., Grande, C., & Rodrigues, A. E. (2004). Adsorption equilibrium of methane, carbon dioxide, and nitrogen on zeolite 13X at high pressures. *Journal of Chemical Engineering Data*, *49*, 1095-1101.

37. Chaffee, A. L. (1990). Natural gas storage on high surface area carbons. Paris. 323-324.
38. Chart Ferox. (2011). *Cryogenic semi-trailer for liquid natural gas transport*. Retrieved, 2011, from <http://www.chart-ferox.com/bulk/bulk-mobile-units-lng-trailers.htm>
39. Chen, J. H., Wong, D. S. H., Tan, C. S., Subramanian, R., Lira, C. T., & Orth, M. (1997). Adsorption and desorption of carbon dioxide onto and from activated carbon at high pressures. *Industrial & Engineering Chemistry Research*, 36, 2808-2815.
40. Choi, B. K., Choi, D. K., Lee, Y. W., Lee, B. K., & Kim, S. H. (2003). Adsorption equilibria of methane, ethane, ethylene, nitrogen and hydrogen onto activated carbon. *Journal of Chemical Engineering Data*, 48, 603-607.
41. Cisneros, R., Peiffer, H., & Wang, C. (2010). Adsorption in free-standing porous silicon: A structural, optical and kinetic analysis. *Nanoscale Research Letters*, 5, 686-691.
42. Coasne, B., Grosman, A., Ortega, C., & Simon, M. (2005). Adsorption in non interconnected pores open at one or at both ends: A reconsideration of the origin of the hysteresis phenomenon. *Physical Review Letters*, 25, 1-5.
43. Cracknell, R., Gordon, P., & Gubbins, K. (1993). Influence of pore geometry on the design of microporous materials for methane storage. *Journal of Physical Chemistry*, 97, 494-499.
44. Crittenden, B., & Thomas, W. J. (1998). *Adsorption technology and design*. Oxford: Butterworth - Heinemann.
45. Dai, X. D., Liu, X. M., Qian, L., Qiao, K., & Yan, Z. F. (2008). Pilot preparation of activated carbon for natural gas storage. *Energy & Fuels*, 22, 3420-3423.
46. David, F. (2002). Supercritical adsorption of "permanent" gases under corresponding states on various carbons. *Carbon*, 40, 2767-2773.
47. Delavar, M., Ghoreyshi, A. A., Jahanshahi, M., & Irannejad, M. (2010). Experimental evaluation of methane adsorption on granular activated carbon (GAC) and determination of model isotherm. *World Academy of Science, Engineering, and Technology*, 62, 47-50.
48. Dimova-Malinovska, D., Sendova-Vassileva, M., Tzenov, N., & Kamenova, M. (1997). Preparation of thin porous silicon layers by stain etching. *Thin Solid Films*, 297, 9-12.

49. Ding, T., Ozawa, S., Yamazaki, T., Watanuki, I., Ogino, Y. (1988). A generalized treatment of adsorption of methane onto various zeolites. *Langmuir*, *4*(2), 392-396.
50. Do, D. D., & Wang, K. (1998). Predictions of adsorption equilibria of nonpolar hydrocarbons onto activated carbon. *Langmuir*, *14*, 7271-7277.
51. Do, D. D., & Do, H. D. (2003). Adsorption of supercritical fluids in non-porous and porous carbons: Analysis of adsorbed phase volume and density. *Carbon*, *41*, 1777-1791.
52. Dobruskin, V. K. (1998). Micropore volume filling. A condensation approximation approach as a foundation to the Dubinin-Astakhov equation. *Langmuir*, *14*, 3840-3846.
53. Dolino, G., Bellet, D., & Faivre, C. (1996). Adsorption strains in porous silicon. *Physical Review B*, *54*(24), 919-929.
54. Donohue, M. D., & Aranovich, G. L. (1998). Classification of gibbs adsorption isotherms. *Advances in Colloid and Interface Science*, *76-77*, 137-152.
55. Dreisbach, F., Staudt, R., & Keller, J. U. (1999). High pressure adsorption data of methane, nitrogen, carbon dioxide and their binary and ternary mixtures on activated carbon. *Adsorption*, *5*, 215-227.
56. Duren, T., Sarkisov, L., Yaghi, O. M., & Snurr, R. Q. (2004). Design of new materials for methane storage. *Langmuir*, *20*, 2683-2689.
57. Economides, J. M., Kai, S., Subero, G. (2005). Compressed Natural Gas (CNG): An Alternative To Liquid Natural Gas (LNG). *SPE Production & Operations*, *21*, 318-324.
58. Emmett, P. H. (1942). *Advanced Colloid Science*, *1*, 3-9.
59. Emmett, P. H., & Brunauer, S. (1934). The adsorption of nitrogen by iron synthetic ammonia catalysts. *Journal of the American Chemical Society*, *56*, 35.
60. Fathauer, R. W., George, T., Ksendzov, A., & Vasquez, R. P. (1991). Visible luminescence from silicon wafers subjected to stain etches. *Applied Physics Letters*, *60*(8), 995-997.
61. Fischer, J., Bohn, M., Korner, B., & Findenegg, G. H. (1986). Supercritical gas adsorption in porous materials. II. prediction of adsorption isotherms. *German Chemical Engineering*, *6*, 84-91.

62. Fitzgerald, J. E., Pan, Z., Sudibandriyo, M., Rohinson, R. J. J., Gasema, K. A. M., & Reeves, S. (2005). Adsorption of methane, nitrogen, carbon dioxide and their mixtures on wet tiffany coal. *Fuel*, *18*, 2351-2363.
63. Foll, H., Christophersen, M., Carstensen, J., & Hasse, G. (2002). Formation and application of porous silicon. *Materials Science and Engineering R*, 93-141.
64. Fontana, F. (1777). Memorie di Matematica e Fisica della Società Italiana, 1, 679.
65. Foucaran, A., Pascal-Delannoy, F., Giani, A., Sackda, A., Combette, P., Boyer, A. (1997). Porous silicon layers used for gas sensor applications. *Thin Solid Films*, *297*, 317-320.
66. Frere, M. G., & Weireld, G. F. D. (2002). High-pressure and high temperature excess adsorption isotherms of N₂, CH₄ and C₃H₈ on activated carbon. *Journal of Chemical and Engineering Data*, *47*, 823-829.
67. Freundlich, H. (1906). Über die adsorption in losungen. *Zeitschrift für Physikalische Chemie*, *57*, 385-470.
68. G-Tec. (2011). *Adsorbed Natural Gas Cylinders*, Retrieved, 2011, from <http://www.gas-tec.com/Cylinder%20Brochure.pdf>
69. Galeazzo, E., Peres, H. E. M., Santos, G., Peixoto, N., & Ramirez-Fernandez, F. J. (2003). Gas sensitive porous silicon devices: Responses to organic vapours. *Sensors and Actuators B*, *93*, 384-390.
70. Germanischer Lloyd Industrial Services. (2011). *Low pressure adsorbed natural gas for vehicle*. Retrieved from http://www.glnobledenton.com/assets/downloads/ANG_for_Vehicle_moped_DS.pdf;
71. Gilmer, H. B., & Kobayashi, R. (1964). The study of gas-solid equilibrium at high-pressures by gas-chromatography: Part I. *AIChE Journal*, *10*(6), 797-803.
72. Goodman, A. L., Busch, A., Duffy, O. J., Fitzgerald, I. E., Gasem, K. M., Gensterblum, Y., White, C. M. (2004). An inter-laboratory comparison of CO₂ isotherms measured on argonne premium coal samples. *Energy and Fuel*, *18*, 1175-1182.
73. Graham, S., & Szczepanski, R. (1982). Methane-based equations of state for a corresponding states reference substance. *Chemical Engineering Science*, *37*(5), 719-725.
74. Gregg, S. J., & Sing, K. S. W. (1982). *Adsorption, surface area and porosity* (Second Edition). London, UK: Academic Press.

75. Hammond, K., Tompsett, G., Auerbach, S., & Conner, W. (2007). Apparatus for measuring physical adsorption on intact supported porous membranes. *Journal of Porous Matter*, 14, 409.
76. Haydel, J. J., & Kobayashi, R. (1967). Adsorption equilibria in the methane-propane—Silica gel system at high pressures. *I & EC Fundamentals*, 6(4), 546-554.
77. Himeno, S., Komatsu, T., & Fujita, S. (2005). High-pressure adsorption equilibria of methane and carbon dioxide on several activated carbons. *Journal of Chemical Engineering Data*, 50, 369-376.
78. Israelachvili, J.N. (1985) Intermolecular and Surface Forces. *Academic Press, New York*.
79. Jalkanena, T., Tuuraa, J., Mäkilä, E., & Salonen, J. (2010). Electro-optical porous silicon gas sensor with enhanced selectivity. *Sensors and Actuators B*, 147, 100-104.
80. Jarvis, K. L., Barnes, T. J., Badalyan, A., Pendleton, P., & Prestidge, C. A. (2008). Impact of thermal oxidation on the adsorptive properties and structure of porous silicon particles. *Journal of Physical Chemistry C*, 112, 9717-9722.
81. Jenkins, M. W. (1977). A new preferential etch for defects in silicon crystals. *Journal of The Electrochemical Society*, 124(5), 757-762.
82. Jensen, C. R. C., & Seaton, N. A. (1996). An isotherm equation for adsorption to high pressures in microporous adsorbents. *Langmuir*, 12(11), 2866-2867.
83. Jiang, S. Y., Zollweg, J. A., & Gubbins, K. E. (1994). High-pressure adsorption of methane and ethane in activated carbon and carbon fibers. *Journal of Physical Chemistry*, 98(22), 5709-5713.
84. Jiang, T. (2007). Preparation and characterization of silicon-based three-dimensional. *Electrochemistry*, 9(5) 930-934.
85. Kaneko, K., Cracknell, R., & Nicholson, D. (1994). Nitrogen adsorption in slit pores at ambient temperatures: Comparison of simulation and experiments. *Langmuir*, 10, 4606-4609.
86. Kaneko, K., & Murata, K. (1997). An analytical method of micropore filling of a supercritical gas. *Adsorption*, 3, 197-208.
87. Kaneko, K., Shimizu, K., & Suzuki, T. (1992). Intra-pore field dependent micropore filling of supercritical nitrogen in slit shaped micropores. *Journal of Chemical Physics*, 97, 8705-8711.

88. Kang, S. P., & Lee, J. W. (2010). Formation characteristics of synthesized natural gas hydrates in meso- and macroporous silica gels. *Journal of Physical Chemistry B*, *114*, 6973–6978.
89. Karge, H. G., & Weitkamp, J. (2008). *Adsorption and diffusion*. Berlin, Germany: Springer.
90. Kayser, H. (1881). *Annalen der Physik*, *14*, 451.
91. Krooss, B. M., Bergen, F. V., Gensterblum, Y., Siemon, N., Pagnier, H. J. M., & David, P. (2002). High-pressure methane and carbon dioxide adsorption on dry and moisture-equilibrate Pennsylvanian coals. *International Journal of Coal Geology*, *23*, 69–92.
92. Keller, J. U., Staudt, R., & Siegen, U. (2005). *Gas adsorption equilibria - experimental methods and adsorptive isotherms*. Boston, U.S.A: Springer.
93. Kim, M., Holste, J., Hall, K., & Slattery, J. (1993). Supercritical adsorption in small pores. *Journal of Colloid Interface Science*, *158*, 488–501.
94. Langmuir, I. (1916). The constitution and fundamental properties of solids and liquids. *Journal of the American Chemical Society*, *38*(11), 2221–2295.
95. Lehmann, V. (2002). *Electrochemistry of silicon: Instrumentation, science, materials and applications*. Wiley.
96. Li, C., Yan, W., Xin, Q. (1993). Interaction of methane with surface of alumina studied by FT-IR spectroscopy. *Catalysis Letters*, *24*, 249–256.
97. Li, Z., Ming, L., & Yaping, Z. (2000). Measurement and theoretical analysis of the adsorption of supercritical methane on super activated carbon. *Science in China (Series B)*, *43*(2), 143–153.
98. Litvinenko, S., Alekseev, S., Lysenko, V., Venturello, A., Geobaldo, F., Gulina, L., Barbier, D. (2010). Hydrogen production from nano-porous Si powder formed by stain etching. *International Journal of Hydrogen Energy*, *35*, 6773–6778.
99. Lozano, D., De la Casa, M.A., Alcañiz, J., Cazorla, D., & Linares, A. (2002). Advances in the study of methane storage in porous carbonaceous materials. *Fuel*, *81*, 1777–1803.
100. Lozano-Castello, D., Cazorla-Amoros, D., & Linares-Solano, A. (2002). Powdered activated carbons and activated carbon fibers for methane storage: A comparative study. *Energy Fuels*, *16*, 1321–1328.

101. Ma, S., Sun, D., Simmons, J. M., Collier, C. D., Yuan, D., & Zhou, H. (2008). Metal-organic framework from an anthracene derivative containing nanoscopic cages exhibiting high methane uptake. *Journal of the American Chemical Society*, *130*, 1012-1016.
102. Malbrunot, P., Vidal, D., & Vermesse, J. (1997). Adsorbent helium density measurement and its effect on adsorption isotherms at high pressure. *Langmuir*, *13*, 539-544.
103. Malbrunot, P., Vidal, D., Vermesse, J., Chahine, R., & Bose, T. K. (1992). Adsorption measurements of argon, neon, krypton, nitrogen, and methane on activated carbon up to 650 MPa. *Langmuir*, *8*, 577-580.
104. Manocha, S. M. (2003). Porous carbons. *Sadhana*, *28*, 335-348.
105. Mat, H., Zakaria, Z., & Paou, T. (2006). The development of adsorbent based natural gas storage for vehicle application. *University Teknologi Malaysia*.
106. Matranga, K. R., Myers, A. L., & Glandt, E. D. (1992). Storage of natural gas by adsorption on activated carbon. *Chemical Engineering Science*, *47*(7), 1569-1579.
107. Menon, V. C., & Komarneni, S. (1998). Porous adsorbents for vehicular natural gas storage: A review. *Journal of Porous Materials*, *5*, 43-58.
108. Mentasty, L., Faccio, R. J., & Zgrablich, G. (1991). High-pressure methane adsorption in 5A zeolite and the nature of gas-solid interactions. *Adsorption Science & Technology*, *8*(2), 105-113.
109. Meunier, F. (1998a). Adsorption for environment. In B. Crittenden, & W. J. Thomas (Eds.), *Adsorption technology and design* (pp. 1-12). Oxford: Butterworth - Heinemann.
110. Meunier, F. (1998b). Solid sorption heat powered cycles for cooling and heat pumping applications. *Applied Thermal Engineering*, *18*, 715-729.
111. Ming, L., Anzhong, G., Xuesheng, L., & Rongshun, W. (2004). Supercritical methane adsorption equilibrium data on activated carbon with prediction by the adsorption by the adsorption potential theory. *Journal of Chemical and Engineering Data*, *49*, 73-76.
112. Miyawaki, J., & Kanedo, K. (2001). Pore width dependence of the temperature change of the confined methane density in slit-shaped micropores. *Chemical Physics Letters*, *337*, 243-247.

113. Mkhitarian, Z. H., Shatveryan, A. A., & Aroutiounian, V. M. (2007). Current-voltage characteristics of structures with a porous silicon layer at adsorption of carbon monoxide. *Journal of Contemporary Physics*, 42(4), 158-161.
114. Moffat, D. H., & Weale, K. E. (1955). Sorption by coal of methane at high pressure. *Fuel*, 34, 449-460.
115. Monuko du, P. (2007). Properties of porous silicon nano-explosive devices. *Sensors and Actuators A*, 666-674.
116. Mota, J. P., & Lyubchik, S. (2008). Adsorbed natural gas technology. In *Recent advances in adsorption processes for environmental protection and security* (pp. 177-192). Netherlands: Springer.
117. Munson, R. A., & Clifton, R. A. J. (1971). Natural gas storage with zeolites. *Bureau of Mines Nonmetallic Minerals Program, U.S. Department of Interior*, 38, 12.
118. Murata, K., & Kaneko, K. (2000). Nano-range interfacial layer upon high pressure adsorption of supercritical gases. *Chemical Physics Letters*, 321, 342-348.
119. Natural Gas Supply Association. (2010). Retrieved from <http://www.naturalgas.org/>
120. Neimark, A. V., & Ravikovitch, P. I. (1998) Calibration of adsorption theories. *Fundamentals of Adsorption* 6, 159-164.
121. Nguyen, C., & Do, D. D. (1999). Adsorption of supercritical gases in porous media: Determination of micropore size distribution. *Journal of Physical Chemistry*, 103, 6900-6908.
122. Notaro, F., Ackley, M. W., & Smolarek, J. (1999). Recover industrial gases via adsorption. *Chem. Eng.*, 106, 104-108.
123. Otto, K. (1981). Adsorption of methane on active carbons and zeolites. *Proceedings of the 4th International Conference of Alternative Energy Sources*, Ford Motor Company, Miami, FL., 241-260)
124. Ozawa, S., Kusumi, S., & Ogino, Y. (1976). Physical adsorption of gases at high pressure. an improvement of the dubinin-astakhov equation. *Journal of Colloid Interface Science*, 56, 83-91.
125. Parbukov, A. N., Beklemyshev, V. I., Gontar, V. M., Makhonin, I. I., Gavrilov, S. A., & Bayliss, S. C. (2001). The production of a novel stain-etched porous silicon,

- metallization of the porous surface and application in hydrocarbon sensors. *Materials Science and Engineering C*, 15, 121-123.
126. Patrick, J. W. (1995). *Porosity in carbons: Characterization and applications*. Great Britain: Halsted Press.
 127. Peckham, J., & Andrews, G.T. (2011). *Thin Solid Films*, 520 (7), 2526-2531.
 128. Pérez, E. X. (2007). Design, fabrication and characterization of porous silicon multilayer optical devices. Department of Electrical Engineering, Universitat Rovira I Virgili.
 129. Quinn, D. F., MacDonald, J. A., & Sosin, K. (1994). Microporous carbons as adsorbents for methane storage. *American Chemical Society, American Chemical Society (Division of Fuel Chemistry)*, 39, 451-455.
 130. Rangarajan, B., Lira, C., & Subramanian, R. (1995). Simplified local density model for adsorption over large pressure ranges. *AIChE Journal*, 41(4), 838-845.
 131. Rieger, M.M., Kohl, P.A. (1995). Mechanism of (111) Silicon Etching in HF-Acetonitrile. *Journal of Electrochemical Society*, 142(5), 1490-1495.
 132. Rolniak, P. D., & Kobayashi, R. (1980). Adsorption of methane and several mixtures and carbon dioxide at elevated pressures and near ambient temperatures on 5A and 13X molecular sieves by tracer perturbation chromatography. *AIChE J.*, 26(4), 616-625.
 133. Rouquerol, F., Rouquerol, L., & Sing, K. (1999). *Adsorption by powders and porous solids*. London, UK: Academic Press.
 134. Russell Communications Group. (2011). *Natural gas vehicles for america*. Retrieved from <http://www.ngvc.org>
 135. Ruthven, D. M. (1984). *Principles of adsorption and adsorption processes*. New York: Jon Wiley & Sons.
 136. Saha, D., & Deng, S. (2010). Hydrogen adsorption on metal-organic framework MOF-177. *Tsinghua Science and Technology*, 15(4), 363-376.
 137. Salehi, E., Taghikhani, V., Ghotbi, C., Nemati Lay, E., & Shojaei, A. (2007). Theoretical and experimental study on the adsorption and desorption of methane by granular activated carbon at 25 °C. *Journal of Natural Gas Chemistry*, 16, 415-422.

138. Salem, M. M. K., Braeuer, P., Szombathely, M., Henschel, M., Harting, P., & Quitzsch, K. (1998). Thermodynamics of high pressure adsorption of argon, nitrogen, and methane on microporous adsorbents. *Langmuir*, *14*, 3376-3389.
139. Salonen, J., Björkqvist, M., & Laine, E. (2000). Comparison of different methods in microstructural characterization of porous silicon. *Journal of Applied Crystallography*, *33*, 504-506.
140. Schamp, H. W., Mason, E. A., Richardson, A. C. B., & Altman, A. (1954). Compressibility and intermolecular forces in gases: Methane. *The Physics of Fluids*, *1*(4), 329-337.
141. Scheele, C. W. (1780). Chemical observations on air and fire., London, 182-197.
142. Schneider, M. S., Grunwaldt, J. D., & Baiker, A. (2004). Near-critical CO₂ in mesoporous silica studied by in situ FTIR spectroscopy. *Langmuir*, *20*, 2890-2899.
143. Senkovska, I., & Kaskel, S. (2008). High pressure methane adsorption in the metal-organic frameworks Cu₃(btc)₂, Zn₂(bdc)₂dabco, and Cr₃F(H₂O)₂O(bdc)₃. *Microporous and Mesoporous Materials*, *112*, 108-115.
144. Shethna, H. K., & Bhatia, S. K. (1994). Interpretation of adsorption isotherms at above-critical temperatures using a modified micropore filling model. *Langmuir*, *10*, 870-876.
145. Shih, S., Jung, K. H., Hsieh, T. Y., Sarathy, J., Campbell, J. C., & Kwong, D. L. (1992). Photoluminescence and formation mechanism of chemically etched silicon. *Applied Physics Letters*, *60*(15), 1863-1865.
146. Siemons, N., & Busch, A. (2007). Measurement and interpretation of supercritical CO₂ sorption on various coals. *International Journal of Coal Geology*, *69*, 229-242.
147. Sievers, U., & Schulz, S. (1980). An equation of state in the form of bender's equation for temperatures between 91 K and 625 K and pressures up to 500 bar. *Fluid Phase Equilibria*, *5*, 35-54.
148. Sing, K. (1985). Reporting physisorption data for gas/solid systems with special reference to the determination of surface area and porosity. *Pure and Applied Chemistry*, *57*(4), 603-619.
149. Skryshevsky, V. A., Zinchuk, V. M., Benilov, A. I., Milovanov, Y. S., & Tretyak, O. V. (2006). Overcharging of porous silicon localized states at gas adsorption. *Semiconductor Science & Technology*, *21*, 1605-1608.

150. Solara, C., Sardellab, F., Deianab, C., Lagoc, R. M., Vallonea, A., & Sapag, K. (2008). Natural gas storage in microporous carbon obtained from waste of the olive oil production. *Materials Research*, *11*(4), 409-414.
151. Solntsev, V. S., Litovchenko, V. G., Gorbanyuk, T. I., & Evtukh, A. A. (2008). Influence of H₂S and H₂ adsorption on characteristics of MIS structures with si porous layers. *Semiconductor Physics, Quantum Electronics & Optoelectronics*, *11*(4), 381-384.
152. Sosin, K. A., & Quinn, D. F. (1995). Using the high-pressure methane isotherm for determination of pore size distribution of carbon adsorbents. *Journal of Porous Materials*, *1*(1)
153. Soule, A. D., Sntith, C.A., Yang, X.N., & Lira, C.T. (2001). Adsorption modeling with the ESD equation of state. *Langmuir*, *17*, 2950-2957.
154. Spangler, C. V. (1953). *Method of storing gases*. U.S. Patent: 2663626
155. Subramanian, R., Pyada, H., & Lira, C. T. (1995). An engineering model for adsorption of gases onto flat surfaces and clustering in supercritical fluids. *Industrial & Engineering Chemistry Research*, *34*(11), 3830-3837.
156. Sun, J., Brady, T. A., Rood, M. J., & Lehmann, C. M. (1997). Adsorbed natural gas storage with activated carbons made from illinois coals and scrap tires. *Energy & Fuels*, *11*, 316-322.
157. Sun, J., Jarvi, T. D., Conopask, L. F., & Satyapal, S. (2001). Direct measurements of volumetric gas storage capacity and some new insight into adsorbed natural gas storage. *Energy & Fuels*, *15*, 1241-1246.
158. Sun, Y., Liu, C. M., Su, W., Zhou, Y. P., & Zhou, L. (2009). Principles of methane adsorption and natural gas storage. *Adsorption*, *15*, 133-137.
159. Suzuki, M. (1990). *Adsorption engineering*. Tokyo: Kodansha-Elsevier.
160. Ding, T., Ozawa, S., Yamazaki, T., Watanuki, I., Ogino, Y. (1988). A generalized treatment of adsorption of methane onto various zeolites. *Langmuir*, *4*(2), 392-396.
161. Talu, O., & Myers, A. L. (2001). Molecular simulation of adsorption: Gibbs dividing surface and comparison with experiment. *AIChE Journal*, *47*(5), 1160.
162. Talu, O., Zhang, S. Y., & Hayhurst, D. T. (1993). Effect of cations on methane adsorption by NaY, MgY, CaY, SrY, and BaY zeolites. *Journal of Physical Chemistry*, *97*, 894-898.

163. Tan, Z. G., K. (1990). Adsorption in carbon micropores at supercritical temperatures. *Journal of Physical Chemistry*, *94*, 6061-6069.
164. Tedesco, C., Erra, L., & Brunelli, M. (2010). Methane adsorption in a supramolecular organic zeolite. *Chemistry - A European Journal*, *16*, 2371 - 2374.
165. Toth, J. (1971). State equations of the solid-gas interface layers. *Acta Chimica Academiae Scientiarum Hungaricae*, *69*, 311-328.
166. Triebe, R. W., Tezel, F. H., & Khulbe, K. C. (1996). Adsorption of methane, ethane and ethylene on molecular sieve zeolites. *Gas Separation and Purification*, *10*(1), 81-84.
167. Turner, D.R. (1958). Electropolishing silicon in hydrofluoric acid solutions. *Journal of the Electrochemical Society*, *105*(7), 402-408.
168. Turner, D.R. (1960). On the mechanism of chemically etching germanium and silicon *Journal of the Electrochemical Society*, *107*(10), 810-816.
169. U.S. Department of Energy. (2011). *Energy information agency*. Retrieved, 2011, from www.eia.doe.gov
170. *Ullmann's encyclopaedia of industrial chemistry* (2001). (6th Edition ed.). Weinheim: Wiley - VHC.
171. Ustinov, E. A., Do, D. D., Herbst, A., Staudt, R., & Harting, P. (2002). Modeling of gas adsorption equilibrium over a wide range of pressure: A thermodynamic approach based on equation of state. *Journal of Colloid Interface Science*, *250*(1), 49-62.
172. Valladares, A. A., Valladares, A., Valladares, R. M., & Calles, A. G. (2007). The energetics of hydrogen adsorbed in nanoporous silicon. *Materials Research Society*, *971*
173. Vashpanov, Y., Jung, J. I., & Kwack, K. D. (2011). Photo-EMF sensitivity of porous silicon thin Layer-Crystalline silicon hetero-junction to ammonia adsorption. *Sensors*, *11*, 1321-1327.
174. Vashpanov, Y., Son, J., Kwack, K., & Shin, S. (2008). Electronic parameters of mesoporous silicon upon adsorption of plant viruses. *Japanese Journal of Applied Physics*, *47*(6), 5100-5102.
175. Vasiliev, L. L. (2001). Solar-gas solid sorption refrigerator. *Adsorption*, *7*, 149-161.

176. Vazsonyi, E., Szilagyi, E., Petrik, P., Horvath, Z. E., Lohner, T., Fried, M., & Jalsovszky, G. (2001). Porous silicon formation by stain etching. *Thin Solid Films*, 388, 295-302.
177. Ventura, S.C., Hum, G.P., Narang, S.C. (1992). Novel strategies for the synthesis of methane adsorbents with controlled porosity and high surface area. No. PB-93-189967/XAB. SRI International.
178. Wakasugi, Y., Ozawa, S., & Ogino, Y. (1981). Physical adsorption of gases at high pressure: V. an extension of a generalized adsorption equation to systems with polar adsorbents. *Journal of Colloid and Interface Science*, 79(2), 399-409.
179. Wakasugi, Y., Ozawa, S., & Yoshtsada, O. (1981). Physical adsorption of gases at high pressure. an extension of a generalized adsorption equation to systems with polar adsorbents. *Journal of Colloid and Interface Science*, 79(2), 399-409.
180. Wang, D., Wei, F., & Wang, J. (2006). Method and apparatus to measure gas amounts adsorbed on a powder sample . U.S. Patent: 6981426
181. Wang, X., French, J., Kandadai, S., & Chua, H. (2010). Adsorption measurements of methane on activated carbon in the temperature range (281 to 343) K and pressures to 1.2 MPa. *Journal of Chemical Engineering Data*, 55, 2700-2706.
182. Wegrzyn, J. (1996). Adsorbent storage of natural gas. *Applied Energy*, 55(2), 71-83.
183. Whitlock, W. H., Wzell, E.F., & Hwang, S.C. (2000). High purity gases. In Kirk-Othmer Encyclopaedia of Chemical Technology (pp. 455-469) John Wiley & Sons, Inc.
184. Winton, M. J., Russell, S. D., & Gronsky, R. (1997). Observation of competing etches in chemically etched porous silicon. *Journal of Applied Physics*, (1), 436-441.
185. Xiao-dong, Y., Wen-sheng, L., Qing-rong, Z., An-zhong, G., Xue-sheng, L., & Yan, S. (2002). Thermodynamic study of high-pressure adsorption of methane and heats of methane adsorption on microporous carbons. *Journal of Shanghai Jiaotong University*, E-7(2), 152-157.
186. Yang, R. T. (1997). *Gas separation by adsorption processes*. London: Imperial College Press.

187. Yongjun, C. (1999). Discussion on the volume correction method in the isothermal adsorption measurement of coal. *Coal Geology and Exploration*, 23, 131-133.
188. Yongjuni, C., Dengfeng, Z., Qun, Z., Weigang, L., Wenli, S., Yuhui, L., & Wenping, J. (2010). Features of the excess adsorption isotherms of high-pressure methane adsorption on coal and simulation model. *Acta Geologica Sinica*, 84(6), 1547-1554.
189. Zhang, X. G. (2004). Morphology and formation mechanisms of porous silicon. *Journal of the Electrochemical Society*, 151, C69-C80.
190. Zhou, L. (2009). Fundamentals of high pressure adsorption. *Langmuir*, 25(23), 13461-13466.
191. Zhou, L., Chen, L. P., Li, M., Sun, Y., & Zhou, Y. (2000). Prying the nature of supercritical adsorption via isotherm space transformation. *Adsorption Science and Technology - Proceedings of the Second Pacific Basin Conference*, 717-721. Brisbane, Australia
192. Zhou, L., Liu, J., Su, W., Sun, Y., & Zhou, Y. (2010). Progress in studies of natural gas storage with wet adsorbents. *Energy Fuels*, 24, 3789-3795.
193. Zhou, L., & Zhou, Y. (1996). A comprehensive model for the adsorption of supercritical hydrogen on activated carbon. *Industrial & Engineering Chemistry Research*, 35, 4166-4168.
194. Zhou, L., & Zhou, Y. (1998). Linearization of adsorption isotherms for high pressure applications. *Chemical Engineering Science*, 53, 2531-2536.
195. Zhou, L., & Zhou, Y. (2000). Experiment and modeling study of the supercritical methane on a high surface activated carbon. *Langmuir*, 16, 5955-5959.
196. Zhou, L., Zhou, Y. P., Bai, S. P., & Yang, B. (2002). Studies on the transition behaviour of physical adsorption from the sub- to the supercritical region: Experiments on silica gel. *Journal of Colloid Interface Science*, 253(1), 9-15.
197. Zhou, W. (2010). Methane storage in porous Metal-Organic frameworks: Current records and future perspectives. *The Chemical Record*, 10, 200-204.
198. Zouadi, N., Gabouze, N., Bradai, D., & Dahmane, D. (2009). A FET gas sensor device based on porous silicon. *Materials Science Forum*, 609, 261-264.

- 7 - Appendix A1

Appendix A1 provides the MATLAB code utilized to calculate the presented isotherm plots.
MATLAB Programs

7.1 - Helium Dead Space Volume Measurement

The MATLAB code utilized to make dead space volume measurements is shown below.

```
%----This program finds the deadspace volume of vessel 2-----
clear all
close all
clc
%----All units in Base Metric---%
%----1-Supply, 2-Samp-----%
%----Rem Change SSQ Plot Save Dir!!!-----%
[T1,T2,P1,P2] = textread('L:\MEng\Experimentation\New folder\Adsorption
Studies\PSiPW_15\Vol_Exp_SiPW_15_He_1.txt', '%f%f%f%f', 'bufsize', 15000');
%----He Redlich-Kwong Constants-----%
%--Critical Temp & Pressure for He----%
Tc = 5.20; %K
Pc = 229000; %Pa
%--Modified R-K Equation---
R = 8.3144;
a = 0.4224*R^2*Tc^2.5/Pc;
b = 0.0852*R*Tc/Pc;
%----CC to Cubic Meters-----%
V1 = 325/1000000;
%----Volume of Sample-----%
Vs = 0.0/1000000;
%----Effective Sample Cham. Vol-----&
%V2 = 1.0/1000000;
%----Set V2 test bounds-----%
V2=linspace(.000025,0.000032,10000);
s = length(P1);
%----Number of Initial data points-----%
ini = 25;
%----Number of final Data Points-----%
fin = 25;
errorr = 1;
n = 1;
```

```

for(j=1:10000)
for(i=1:s)
    while(error >= 0.0000001)
        %----R-K-----
        rho1(1) = 0;
        rho2(1) = 0;
        %----RK Function-----
        f1(i) = -P1(i) - (R*T1(i)*rho1(n))/(b*rho1(n) - 1) - (a*rho1(n))/(T1(i)^(1/2)*(b*rho1(n) + 1));
        f2(i) = -P2(i) - (R*T2(i)*rho2(n))/(b*rho2(n) - 1) - (a*rho2(n))/(T2(i)^(1/2)*(b*rho2(n) + 1));
        %----RK Function derivative wrt rho----
        fp1(i)=(a*b*rho1(n))/(T1(i)^(1/2)*(b*rho1(n) + 1)^2) - (R*T1(i))/(b*rho1(n) - 1) - a/(T1(i)^(1/2)*(b*rho1(n) + 1)) + (R*T1(i)*b*rho1(n))/(b*rho1(n) - 1)^2;
        fp2(i)=(a*b*rho2(n))/(T2(i)^(1/2)*(b*rho2(n) + 1)^2) - (R*T2(i))/(b*rho2(n) - 1) - a/(T2(i)^(1/2)*(b*rho2(n) + 1)) + (R*T2(i)*b*rho2(n))/(b*rho2(n) - 1)^2;

        %----Newton Raphson to obtain rho-----
        rho1(n+1) = rho1(n) - f1(i)/fp1(i);
        rho2(n+1) = rho2(n) - f2(i)/fp2(i);
        error1 = abs(rho1(n+1) - rho1(n))/rho1(n+1);
        error2 = abs(rho2(n+1) - rho2(n))/rho2(n+1);
        error = error1 + error2;
        %----Values of molar density that satisfy MBWR given P & T-----
        rhoa1(i) = rho1(n);
        rhoa2(i) = rho2(n);
        %---Number of Moles Present in each chamber-----
        n1(i) = rhoa1(i)*V1;
        n2(i) = rhoa2(i)*V2(j);
        nt(i) = n1(i)+n2(i);
        Vt(i) = nt(i)*(R*293/101000)*1000000;
        n = n+1;
        Pe(i) = P2(i)/Pc;
    end
    n=1;
    error = 1;
end
%----Average Initial and Final moles in supply chamber----%
n1ini = sum(n1(1:ini))/ini;
n1fin = sum(n1((s-fin):s))/fin;
%----Average Initial and Final moles in sample chamber----%
n2ini = sum(n2(1:ini))/ini;
n2fin = sum(n2((s-fin):s))/fin;
%-----Average temperature-----%

```

```

Tavg = (sum(T1{1:s})+ sum(T2{1:s}))/ (2*s);
for(i=1:s)
%---moles in 2 based on conditions in 1----%
n2t(i) = n1ini-n1(i)+n2ini;
dum(i) = i;
f(i) = (n2ini + n1ini - n1(i) - n2(i));
%----Square of diff b/t theory n2 and actual n2-----%
SQ(i) = (n2t(i)-n2(i))^2;
SQ(i) = (f(i))^2;
%---moles adsorbed-----%
nads(i) = n2t(i) - n2(i);
end
%----Total sum of diff. squares for each V2-----%
SS(j) = sum(SQ{1:s});
end
%----Output deadspace volume (ml)-----%
Vexp = V2(find(SS == min(SS)))
figure(1)
plot(dum,n2t,dum,n2)
xlabel('Mes. Pt. #')
ylabel('n2theory, n2actual')
grid on
figure(2)
plot(dum,f)
xlabel('Mes. Pt. #')
ylabel('f')
grid on
figure(3)
plot(dum, nads)
xlabel('Mes. Pt. #')
ylabel('nads')
grid on
figure(4)
plot(dum, nt)
xlabel('Mes. Pt. #')
ylabel('ntotal')
grid on
figure(5)
plot(V2,SS, 'k', 'LineWidth',2)
xlabel('V2')
ylabel('Sum SQ Error n2t & n2')
title('SS Err vs V2')
grid on

```

7.2 - Methane Excess Adsorption & Effective Storage

The MATLAB program from calculating the excess adsorption and effective storage isotherms is presented below. It consists of one master or main function and two called sub-functions (excess adsorption sub-function and effective storage sub-function).

7.2.1 - Master control program

```

clear all
close all
clc
%------%
%---This program calculates the excess adsorption and effective---%
%---storage isotherms using the Modified BWR equation of state---%
%---for methane gas------%
%-----Variables to change!!------%
% EXS & EFF file Dir
% Clipping Value C x6
% M, Vs, Vp
% Save Fig Dir and Names
% T values in legends
% Same name in legends
%---All units in Base Metric------%
%---Number of Initial data points------%
ini = 25;
%---Number of final Data Points------%
fin = 25;
%-----Ideal Gas Constant------%
R = 8.3144;
%---Supply Vessel Volume (ml)------%
V1 = 325/1000000;
%---Sample Vessel Volume + Container Volume (ml)------%
Vcc = 32.52/1000000;
%------%
%---Sample Info------%
%------%
%---Dead Volume of Sample (He Exp.)------%
Vs = 2.28/1000000;
%---Powder Packed Volume------%
Vp = 8.19/1000000;
%-----Mass of Sample (g)------%
Msam = 4.67;
%---Effective Sample Cham. Vol------%
V2 = Vcc - Vs ;

```

```

%----Clip Isotherm Values at C (0 is default value ie No Clipping)-----%
C = 0;
%----Enter File Directory of Data .txt file-----%
%----Run #1-----%
[t1,T1,T2,P1,P2] = textread('L:\MEng\Experimentation\New folder\Adsorption
Studies\RX3\ADS_RX3_2_2.txt', '%f%f%f%f%f', 'bufsize', 15000);
s1=length(T1);
for(i=1:s1)
    dum1(i)=i;
end
%----Call Excess Adsorption Function-----%
%----Make sure this file and the function file are in the same Dir!---%
[n1, n2, f, nads, Vads, Mads, nadsg, Vadsg, Madsg, nadsv, Vadvsv, Madsv, dum, n2t, Vhr, Tavg] =
MBWR_ADS_FCN_EXS(P1, T1, P2, T2, V1, V2, Vs, Vp, Msam, t1, C);
%----Assign function values-----%
P21 = P2;
n11 = n1;
n21 = n2;
f1 = f;
nads1 = nads*1000;
Vads1 = Vads;
Mads1 = Mads*1000;
nadsg1 = nadsg*1000;
Vadsg1 = Vadsg;
Madsg1 = Madsg*1000;
nadsv1 = nadsv*1000;
Vadvsv1 = Vadvsv;
Madsv1 = Madsv*1000;
dum1 = dum;
n2t1 = n2t;
Vhr1=Vhr;
navg1 = sum(nads1)/s1;
%----Average adsorption test temperature-----%
Tavg=sum(T2)/s1
%----Run #2-----%
%----Clip ADS Values at C-----%
C = 0;
[t1,T1,T2,P1,P2] = textread('L:\MEng\Experimentation\New folder\Adsorption
Studies\Zorflex\FM30K_2\ADS_FM30K_2_CH4_3.txt', '%f%f%f%f%f', 'bufsize', 15000);
s2=length(T1);
for(i=1:s2)
    dum1(i)=i;
end

```

```

[n1, n2, f, nads, Vads, Mads, nadsg, Vadsg, Madsg, nadsv, Vadsv, Madsv, dum, n2t, Vhr, Tavg] =
MBWR_ADS_FCN_EXS(P1 ,T1 ,P2 ,T2, V1, V2, Vs, Vp, Msam, t1, C);
P22 = P2;
n12 = n1;
n22 = n2;
f2 = f;
nads2 = nads*1000;
Vads2 = Vads;
Mads2 = Mads*1000;
nadsg2 = nadsg*1000;
Vadsg2 = Vadsg;
Madsg2 = Madsg*1000;
nadsv2 = nadsv*1000;
Vadsv2 = Vadsv;
Madsv2 = Madsv*1000;
dum2 = dum;
n2t2 = n2t;
Vhr2=Vhr;
navg2 = sum(nads2)/s1;
Tavg=sum(T2)/s2
%----Run #3-----%
%---Clip ADS Values at C-----%
C = 0;
[t1,T1,T2,P1,P2] = textread('L:\MEng\Experimentation\New folder\Adsorption
Studies\Zorflex\FM10_2\ADS_CH4_FM10_2_2.txt', '%f %f %f %f %f', 'bufsize',15000');
s3=length(T1);
for(i=1:s3)
    dum1(i)=i;
end
[n1, n2, f, nads, Vads, Mads, nadsg, Vadsg, Madsg, nadsv, Vadsv, Madsv, dum, n2t, Vhr, Tavg] =
MBWR_ADS_FCN_EXS(P1 ,T1 ,P2 ,T2, V1, V2, Vs, Vp, Msam, t1, C);
P23 = P2;
n13 = n1;
n23 = n2;
f3 = f;
nads3 = nads*1000;
Vads3 = Vads;
Mads3 = Mads*1000;
nadsg3 = nadsg*1000;
Vadsg3 = Vadsg;
Madsg3 = Madsg*1000;
nadsv3 = nadsv*1000;
Vadsv3 = Vadsv;
Madsv3 = Madsv*1000;

```

```

dum3 = dum;
n2t3 = n2t;
Vhr3=Vhr;
navg3 = sum(nads3)/s1;
Tavg=sum(T2)/s3
%---Run #4-----%
%---Clip ADS Values at C-----%
    C =0;
[t1,T1,T2,P1,P2] = textread('L:\MEng\Experimentation\New folder\Adsorption
Studies\Zeolite 5A\ADS_ZEO_5A_CH4_1.txt', '%f%f%f%f%f', 'bufsize',15000');
s1=length(T1);
for(i=1:s1)
    dum1(i)=i;
end
[n1, n2, f, nads, Vads, Mads, nads, Vads, Madsg, nads, Vads, Mads, dum, n2t, Vhr, Tavg] =
MBWR_ADS_FCN_EXS(P1 ,T1 ,P2 ,T2, V1, V2, Vs, Vp, Msam, t1, C);
P24 = P2;
n14 = n1;
n24 = n2;
f4 = f;
nads4 = nads*1000;
Vads4 = Vads;
Mads4 = Mads*1000;
nads4 = nads*1000;
Vads4 = Vads;
Madsg4 = Madsg*1000;
nads4 = nads*1000;
Vads4 = Vads;
Mads4 = Mads*1000;
nads4 = nads*1000;
Vads4 = Vads;
Mads4 = Mads*1000;
dum4 = dum;
n2t4 = n2t;
Vhr4=Vhr;
navg4 = sum(nads4)/s1;
%---Run #5-----%
%---Clip ADS Values at C-----%
    C =0;
[t1,T1,T2,P1,P2] = textread('L:\MEng\Experimentation\New folder\Adsorption
Studies\Zeolite 13X\ADS_ZEO_13X_CH4_4.txt', '%f%f%f%f%f', 'bufsize',15000');
s1=length(T1);
for(i=1:s1)
    dum1(i)=i;
end
[n1, n2, f, nads, Vads, Mads, nads, Vads, Madsg, nads, Vads, Mads, dum, n2t, Vhr, Tavg] =
MBWR_ADS_FCN_EXS(P1 ,T1 ,P2 ,T2, V1, V2, Vs, Vp, Msam, t1, C);

```

```

P25 = P2;
n15 = n1;
n25 = n2;
f5 = f;
nads5 = nads*1000;
Vads5 = Vads;
Mads5 = Mads*1000;
nadsg5 = nadsg*1000;
Vadsg5 = Vadsg;
Madsg5 = Madsg*1000;
nadsv5 = nadsv*1000;
Vadsv5 = Vadsv;
Madsv5 = Madsv*1000;
dum5 = dum;
n2t5 = n2t;
Vhr5=Vhr;
navg5 = sum(nads5)/s1;
%---Run #6-----%
%---Clip ADS Values at C-----%
C = 0;
[t1,T1,T2,P1,P2] = textread('L:\MEng\Experimentation\New folder\Adsorption
Studies\Zeolite 3A\ADS_ZEO_3A_1_CH4_3.txt', '%f%f%f%f%f', 'bufsize', 15000');
s1=length(T1);
for(i=1:s1)
    dum1(i)=i;
end
[n1, n2, f, nads, Vads, Mads, nadsg, Vadsg, Madsg, nadsv, Vadsv, Madsv, dum, n2t, Vhr, Tavg] =
MBWR_ADS_FCN_EXS(P1 ,T1 ,P2 ,T2, V1, V2, Vs, Vp, Msam, t1, C);
P26 = P2;
n16 = n1;
n26 = n2;
f6 = f;
nads6 = nads*1000;
Vads6 = Vads;
Mads6 = Mads*1000;
nadsg6 = nadsg*1000;
Vadsg6 = Vadsg;
Madsg6 = Madsg*1000;
nadsv6 = nadsv*1000;
Vadsv6 = Vadsv;
Madsv6 = Madsv*1000;
dum6 = dum;
n2t6 = n2t;
Vhr6=Vhr;

```

```

navg6 = sum(nads6)/s1;
%---Run #7-----%
%---Clip ADS Values at C-----%
  C = 0;
[t1,T1,T2,P1,P2] = textread('L:\MEng\Experimentation\New folder\Adsorption
Studies\Zeolite 4A\ADS_ZEO_4A_2_CH4_3.txt', '%f%f%f%f%f', 'bufsize', 15000);
s1=length(T1);
for(i=1:s1)
  dum1(i)=i;
end
[n1, n2, f, nads, Vads, Mads, nadsg, Vadsg, Madsg, nadsv, Vadsv, Madsv, dum, n2t, Vhr, Tavgl] =
MBWR_ADS_FCN_EXS(P1, T1, P2, T2, V1, V2, Vs, Vp, Msam, t1, C);
P27 = P2;
n17 = n1;
n27 = n2;
f7 = f;
nads7 = nads*1000;
Vads7 = Vads;
Mads7 = Mads*1000;
nadsg7 = nadsg*1000;
Vadsg7 = Vadsg;
Madsg7 = Madsg*1000;
nadsv7 = nadsv*1000;
Vadsv7 = Vadsv;
Madsv7 = Madsv*1000;
dum7 = dum;
n2t7 = n2t;
Vhr7=Vhr;
navg7 = sum(nads7)/s1;
%---Run #8-----%
%---Clip ADS Values at C-----%
  C = 0;
[t1,T1,T2,P1,P2] = textread('L:\MEng\Experimentation\New folder\Adsorption Studies\Silica
Gel\ADS_GEL_1_CH4_1.txt', '%f%f%f%f%f', 'bufsize', 15000);
s1=length(T1);
for(i=1:s1)
  dum1(i)=i;
end
[n1, n2, f, nads, Vads, Mads, nadsg, Vadsg, Madsg, nadsv, Vadsv, Madsv, dum, n2t, Vhr, Tavgl] =
MBWR_ADS_FCN_EXS(P1, T1, P2, T2, V1, V2, Vs, Vp, Msam, t1, C);
P28 = P2;
n18 = n1;
n28 = n2;
f8 = f;

```

```

nads8 = nads*1000;
Vads8 = Vads;
Mads8 = Mads*1000;
nads8 = nads*1000;
Vads8 = Vads;
Mads8 = Mads*1000;
nads8 = nads*1000;
Vads8 = Vads;
Mads8 = Mads*1000;
dum8 = dum;
n2t8 = n2t;
Vhr8=Vhr;
navg8 = sum(nads8)/s1;
%----Run #9-----%
%---Clip ADS Values at C-----%
C = 0;
[t1,T1,T2,P1,P2] = textread('L:\MEng\Experimentation\New folder\Adsorption
Studies\PSiPW_3\ADS_PSiPW_3_CH4_3.txt', '%f%f%f%f%f', 'bufsize',15000');
s1=length(T1);
for(i=1:s1)
    dum1(i)=i;
end
[n1, n2, f, nads, Vads, Mads, nads8, Vads8, Mads8, nads9, Vads9, Mads9, dum, n2t, Vhr, Tavg] =
MBWR_ADS_FCN_EXS(P1 ,T1 ,P2 ,T2, V1, V2, Vs, Vp, Msam, t1, C);
P29 = P2;
n19 = n1;
n29 = n2;
f9 = f;
nads9 = nads*1000;
Vads9 = Vads;
Mads9 = Mads*1000;
nads9 = nads*1000;
Vads9 = Vads;
Mads9 = Mads*1000;
nads9 = nads*1000;
Vads9 = Vads;
Mads9 = Mads*1000;
dum9 = dum;
n2t9 = n2t;
Vhr9=Vhr;
navg9 = sum(nads9)/s1;
%----Run #10-----%
%---Clip ADS Values at C-----%
C = 0;

```

```

[t1,T1,T2,P1,P2] = textread('L:\MEng\Experimentation\New folder\Calibration\ADS
ERR\MBWR ADS_ERR_CH4_10.txt', '%f%f%f%f%f', 'bufsize', 15000);
s1=length(T1);
for(i=1:s1)
    dum1(i)=i;
end
[n1, n2, f, nads, Vads, Mads, nadsg, Vadsg, Madsg, nadsv, Vadsv, Madsv, dum, n2t, Vhr, Tav] =
MBWR_ADS_FCN_EXS(P1, T1, P2, T2, V1, V2, Vs, Vp, Msam, t1, C);
P210 = P2;
n110 = n1;
n210 = n2;
f10 = f;
nads10 = nads*1000;
Vads10 = Vads;
Mads10 = Mads;
nadsg10 = nadsg*1000;
Vadsg10 = Vadsg;
Madsg10 = Madsg;
nadsv10 = nadsv*1000;
Vadsv10 = Vadsv;
Madsv10 = Madsv;
dum10 = dum;
n2t10 = n2t;
Vhr10 = Vhr;
navg10 = sum(nads10)/s1;
figure(1)
plot(P21,Vads1,P22,Vads2,P23,Vads3,P24,Vads4,P25,Vads5,P26,Vads6,P27,Vads7,P28,Vads8,
P29,Vads9,'k', 'LineWidth',2)
legend('RX3','FM30K', 'FM10','5A Zeolite', '13X Zeolite','3A Zeolite','4A Zeolite','Silica
Gel','Porous Silicon','Location','NorthEast')
title({'Excess Volumes Adsorbed'},FontSize,14)
xlabel('Applied Pressure (Pa)',FontSize,12)
ylabel('Vads (stp-cm^3)',FontSize,12)
grid on
figure(2)
plot(P21,nads1,P22,nads2,P23,nads3,P24,nads4,P25,nads5,P26,nads6,P27,nads7,P28,nads8,P
29,nads9,'k', 'LineWidth',2)
legend('RX3','FM30K', 'FM10','5A Zeolite', '13X Zeolite','3A Zeolite','4A Zeolite','Silica
Gel','Porous Silicon','Location','NorthEast')
title({'Excess Moles Adsorbed'},FontSize,14)
xlabel('Applied Pressure (Pa)',FontSize,12)
ylabel('nads (mmol)',FontSize,12)
grid on
figure(3)

```

```

plot(P21,Mads1,P22,Mads2,P23,Mads3,P24,Mads4,P25,Mads5,P26,Mads6,P27,Mads7,P28,Ma
ds8,P29,Mads9,'k', 'LineWidth',2)
legend('RX3','FM30K','FM10','5A Zeolite','13X Zeolite','3A Zeolite','4A Zeolite','Silica
Gel','Porous Silicon','Location','NorthEast')
title({'Excess Mass Adsorbed'},'FontSize',14)
xlabel('Applied Pressure (Pa)','FontSize',12)
ylabel('Mads (mg)','FontSize',12)

```

```
grid on
```

```
figure(4)
```

```

plot(P21,Vadsv1,P22,Vadsv2,P23,Vadsv3,P24,Vadsv4,P25,Vadsv5,P26,Vadsv6,P27,Vadsv7,P2
8,Vadsv8,P29,Vadsv9,'k', 'LineWidth',2)
legend('RX3','FM30K','FM10','5A Zeolite','13X Zeolite','3A Zeolite','4A Zeolite','Silica
Gel','Porous Silicon','Location','NorthEast')
title({'Excess Volumes Adsorbed Per Sample Deadspace Volume'},'FontSize',14)
xlabel('Applied Pressure (Pa)','FontSize',12)
ylabel('Vads/Vd (stp-cm^3/cm^3)','FontSize',12)

```

```
grid on
```

```
figure(5)
```

```

plot(P21,nadsv1,P22,nadsv2,P23,nadsv3,P24,nadsv4,P25,nadsv5,P26,nadsv6,P27,nadsv7,P28,
nadsv8,P29,nadsv9,'k', 'LineWidth',2)
legend('RX3','FM30K','FM10','5A Zeolite','13X Zeolite','3A Zeolite','4A Zeolite','Silica
Gel','Porous Silicon','Location','NorthEast')
title({'Excess Moles Adsorbed Per Sample Deadspace Volume'},'FontSize',14)
xlabel('Applied Pressure (Pa)','FontSize',12)
ylabel('nads/Vd (mmol/cm^3)','FontSize',12)

```

```
grid on
```

```
figure(6)
```

```

plot(P21,Madsv1,P22,Madsv2,P23,Madsv3,P24,Madsv4,P25,Madsv5,P26,Madsv6,P27,Madsv7,
P28,Madsv8,P29,Madsv9,'k', 'LineWidth',2)
legend('RX3','FM30K','FM10','5A Zeolite','13X Zeolite','3A Zeolite','4A Zeolite','Silica
Gel','Porous Silicon','Location','NorthEast')
title({'Excess Mass Adsorbed Per Sample Deadspace Volume'},'FontSize',14)
xlabel('Applied Pressure (Pa)','FontSize',12)
ylabel('Mads/Vd (mg/cm^3)','FontSize',12)

```

```
grid on
```

```
figure(7)
```

```

plot(P21,Vadsg1,P22,Vadsg2,P23,Vadsg3,P24,Vadsg4,P25,Vadsg5,P26,Vadsg6,P27,Vadsg7,P2
8,Vadsg8,P29,Vadsg9,'k', 'LineWidth',2)
legend('RX3','FM30K','FM10','5A Zeolite','13X Zeolite','3A Zeolite','4A Zeolite','Silica
Gel','Porous Silicon','Location','NorthEast')
title({'Excess Volumes Adsorbed Per Sample Mass'},'FontSize',14)
xlabel('Applied Pressure (Pa)','FontSize',12)
ylabel('Vads/Ms (stp-cm^3/g)','FontSize',12)

```

```
grid on
```

```

figure(8)
plot(P21,nadsg1,P22,nadsg2,P23,nadsg3,P24,nadsg4,P25,nadsg5,P26,nadsg6,P27,nadsg7,P28,
nadsg8,P29,nadsg9,'k','LineWidth',2)
legend('RX3','FM30K','FM10','5A Zeolite','13X Zeolite','3A Zeolite','4A Zeolite','Silica
Gel','Porous Silicon','Location','NorthEast')
title({'Excess Moles Adsorbed Per Sample Mass'},FontSize,14)
xlabel('Applied Pressure (Pa)',FontSize,12)
ylabel('nads/Ms (mmol/g)',FontSize,12)
grid on
figure(9)
plot(P21,Madsg1,P22,Madsg2,P23,Madsg3,P24,Madsg4,P25,Madsg5,P26,Madsg6,P27,Madsg7,
P28,Madsg8,P29,Madsg9,'k','LineWidth',2)
legend('RX3','FM30K','FM10','5A Zeolite','13X Zeolite','3A Zeolite','4A Zeolite','Silica
Gel','Porous Silicon','Location','NorthEast','FontSize',8)
title({'Excess Mass Adsorbed Per Sample Mass'},FontSize,14)
xlabel('Applied Pressure (Pa)',FontSize,12)
ylabel('Mads/Ms (mg/g)',FontSize,12)
grid on
%-----Save figures to a directory-----%
saveas(1,'L:\MEng\Thesis\Figures\Experimental Plots\ADS
plots\Combined\COM_Vads_EXS.fig')
saveas(1,'L:\MEng\Thesis\Figures\Experimental Plots\ADS
Plots\Combined\COM_Vads_EXS.emf')
saveas(2,'L:\MEng\Thesis\Figures\Experimental Plots\ADS
Plots\Combined\COM_nads_EXS.fig')
saveas(2,'L:\MEng\Thesis\Figures\Experimental Plots\ADS
Plots\Combined\COM_nads_EXS.emf')
saveas(3,'L:\MEng\Thesis\Figures\Experimental Plots\ADS
Plots\Combined\COM_Mads_EXS.fig')
saveas(3,'L:\MEng\Thesis\Figures\Experimental Plots\ADS
Plots\Combined\COM_Mads_EXS.emf')
saveas(4,'L:\MEng\Thesis\Figures\Experimental Plots\ADS Plots\Combined\COM_Vads-
Vd_EXS.fig')
saveas(4,'L:\MEng\Thesis\Figures\Experimental Plots\ADS Plots\Combined\COM_Vads-
Vd_EXS.emf')
saveas(5,'L:\MEng\Thesis\Figures\Experimental Plots\ADS Plots\Combined\COM_nads-
Vd_EXS.fig')
saveas(5,'L:\MEng\Thesis\Figures\Experimental Plots\ADS Plots\Combined\COM_nads-
Vd_EXS.emf')
saveas(6,'L:\MEng\Thesis\Figures\Experimental Plots\ADS Plots\Combined\COM_Mads-
Vd_EXS.fig')
saveas(6,'L:\MEng\Thesis\Figures\Experimental Plots\ADS Plots\Combined\COM_Mads-
Vd_EXS.emf')

```



```

n21 = n2;
f1 = f;
nads1 = nads*1000;
Vads1 = Vads;
Mads1 = Mads;
nadsg1 = nadsg*1000;
Vadsg1 = Vadsg;
Madsg1 = Madsg;
nadsv1 = nadsv*1000;
Vadsv1 = Vadsv;
Madsv1 = Madsv;
dum1 = dum;
n2t1 = n2t;
Vhr1=Vhr;
navg1 = sum(nads1)/s1;
Tavg=sum(T2)/s1
%----Run #2-----%
%---Clip ADS Values at C-----%
    C =0;
[t1,T1,T2,P1,P2] = textread('L:\MEng\Experimentation\New folder\Adsorption
Studies\PSiPW_3\ADS_PSiPW_3_CH4_2.txt', '%f %f %f %f %f', 'bufsize',15000');
s2=length(T1);
for(i=1:s2)
    dum1(i)=i;
end
[n1, n2, f, nads, Vads, Mads, nadsg, Vadsg, Madsg, nadsv,Vadsv,Madsv, dum, n2t, Vhr, Tavg] =
MBWR_ADS_FCN_EFF(P1 ,T1 ,P2 ,T2, V1, V2, Vs, Vp, Msam, t1, C);
P22 = P2;
n12 = n1;
n22 = n2;
f2 = f;
nads2 = nads*1000;
Vads2 = Vads;
Mads2 = Mads;
nadsg2 = nadsg*1000;
Vadsg2 = Vadsg;
Madsg2 = Madsg;
nadsv2 = nadsv*1000;
Vadsv2 = Vadsv;
Madsv2 = Madsv;
dum2 = dum;
n2t2 = n2t;
Vhr2=Vhr;
navg2 = sum(nads2)/s1;

```

```

Tavg=sum(T2)/s2
%---Run #3-----%
%---Clip ADS Values at C-----%
    C = 0;
[t1,T1,T2,P1,P2] = textread('L:\MEng\Experimentation\New folder\Adsorption
Studies\PSiPW_3\ADS_PSiPW_3_CH4_3.txt','%f%f%f%f%f','bufsize',15000);
s3=length(T1);
for(i=1:s3)
    dum1(i)=i;
end
[n1, n2, f, nads, Vads, Mads, nadsg, Vadsg, Madsg, nadsv,Vadsv,Madsv, dum, n2t, Vhr, Tavg] =
MBWR_ADS_FCN_EFF(P1 ,T1 ,P2 ,T2, V1, V2, Vs, Vp, Msam, t1, C);
P23 = P2;
n13 = n1;
n23 = n2;
f3 = f;
nads3 = nads*1000;
Vads3 = Vads;
Mads3 = Mads;
nadsg3 = nadsg*1000;
Vadsg3 = Vadsg;
Madsg3 = Madsg;
nadsv3 = nadsv*1000;
Vadsv3 = Vadsv;
Madsv3 = Madsv;
dum3 = dum;
n2t3 = n2t;
Vhr3=Vhr;
navg3 = sum(nads3)/s1;
Tavg=sum(T2)/s3
figure(10)
plot(P21,Vads1,P22,Vads2,P23,Vads3,P24,Vads4,P25,Vads5,P26,Vads6,P27,Vads7,P28,Vads8,
P29,Vads9,'k','LineWidth',2)
legend('RX3','FM30K','FM10','5A Zeolite','13X Zeolite','3A Zeolite','4A Zeolite','Silica
Gel','Porous Silicon','Location','SouthEast')
%legend('Zorflex 3A 297.1K CH_4 R#1','Zorflex 3A 297.4K CH_4 R#2','Zorflex 3A 297.2K
CH_4 R#3','Location','NorthWest')
title({'Effective Volume Stored'},'FontSize',14)
xlabel('Applied Pressure (Pa)','FontSize',12)
ylabel('Vads (stp-cm^3)','FontSize',12)
grid on
figure(11)
plot(P21,nads1,P22,nads2,P23,nads3,P24,nads4,P25,nads5,P26,nads6,P27,nads7,P28,nads8,P
29,nads9,'k','LineWidth',2)

```

```

legend('RX3','FM30K','FM10','5A Zeolite','13X Zeolite','3A Zeolite','4A Zeolite','Silica
Gel','Porous Silicon','Location','SouthEast')
title({'Effective Moles Stored'},'FontSize',14)
xlabel('Applied Pressure (Pa)','FontSize',12)
ylabel('nads (mmol)','FontSize',12)
grid on
figure(12)
plot(P21,Mads1,P22,Mads2,P23,Mads3,P24,Mads4,P25,Mads5,P26,Mads6,P27,Mads7,P28,Ma
ds8,P29,Mads9,'k','LineWidth',2)
legend('RX3','FM30K','FM10','5A Zeolite','13X Zeolite','3A Zeolite','4A Zeolite','Silica
Gel','Porous Silicon','Location','SouthEast')
title({'Effective Mass Stored'},'FontSize',14)
xlabel('Applied Pressure (Pa)','FontSize',12)
ylabel('Mads (g)','FontSize',12)
grid on
figure(13)
plot(P21,Vadsv1,P22,Vadsv2,P23,Vadsv3,P24,Vadsv4,P25,Vadsv5,P26,Vadsv6,P27,Vadsv7,P2
8,Vadsv8,P29,Vadsv9,'k','LineWidth',2)
legend('RX3','FM30K','FM10','5A Zeolite','13X Zeolite','3A Zeolite','4A Zeolite','Silica
Gel','Porous Silicon','Location','SouthEast')
title({'Effective Volume Stored Per Sample Packed Volume'},'FontSize',14)
xlabel('Applied Pressure (Pa)','FontSize',12)
ylabel('Vads/Vp (stp-cm^3/cm^3)','FontSize',12)
grid on
figure(14)
plot(P21,nadsv1,P22,nadsv2,P23,nadsv3,P24,nadsv4,P25,nadsv5,P26,nadsv6,P27,nadsv7,P28,
nadsv8,P29,nadsv9,'k','LineWidth',2)
legend('RX3','FM30K','FM10','5A Zeolite','13X Zeolite','3A Zeolite','4A Zeolite','Silica
Gel','Porous Silicon','Location','SouthEast')
title({'Effective Moles Stored Per Sample Packed Volume'},'FontSize',14)
xlabel('Applied Pressure (Pa)','FontSize',12)
ylabel('nads/Vp (mmol/cm^3)','FontSize',12)
grid on
figure(15)
plot(P21,Madsv1,P22,Madsv2,P23,Madsv3,P24,Madsv4,P25,Madsv5,P26,Madsv6,P27,Madsv7,
P28,Madsv8,P29,Madsv9,'k','LineWidth',2)
legend('RX3','FM30K','FM10','5A Zeolite','13X Zeolite','3A Zeolite','4A Zeolite','Silica
Gel','Porous Silicon','Location','SouthEast')
title({'Effective Mass Stored Per Sample Packed Volume'},'FontSize',14)
xlabel('Applied Pressure (Pa)','FontSize',12)
ylabel('Mads/Vp (g/cm^3)','FontSize',12)
grid on
figure(16)

```

```

plot(P21,Vadsg1,P22,Vadsg2,P23,Vadsg3,P24,Vadsg4,P25,Vadsg5,P26,Vadsg6,P27,Vadsg7,P28,Vadsg8,P29,Vadsg9,'k','LineWidth',2)
legend('RX3','FM30K','FM10','5A Zeolite','13X Zeolite','3A Zeolite','4A Zeolite','Silica Gel','Porous Silicon','Location','SouthEast')
title({'Effective Volume Stored Per Sample Mass'},'FontSize',14)
xlabel('Applied Pressure (Pa)','FontSize',12)
ylabel('Vads/Ms (satp-cm^3/g)','FontSize',12)
grid on
figure(17)
plot(P21,nadsg1,P22,nadsg2,P23,nadsg3,P24,nadsg4,P25,nadsg5,P26,nadsg6,P27,nadsg7,P28,nadsg8,P29,nadsg9,'k','LineWidth',2)
legend('RX3','FM30K','FM10','5A Zeolite','13X Zeolite','3A Zeolite','4A Zeolite','Silica Gel','Porous Silicon','Location','SouthEast')
title({'Effective Moles Stored Per Sample Mass'},'FontSize',14)
xlabel('Applied Pressure (Pa)','FontSize',12)
ylabel('nads/Ms (mmol/g)','FontSize',12)
grid on
figure(18)
plot(P21,Madsg1,P22,Madsg2,P23,Madsg3,P24,Madsg4,P25,Madsg5,P26,Madsg6,P27,Madsg7,P28,Madsg8,P29,Madsg9,'k','LineWidth',2)
legend('RX3','FM30K','FM10','5A Zeolite','13X Zeolite','3A Zeolite','4A Zeolite','Silica Gel','Porous Silicon','Location','SouthEast')
title({'Effective Mass Stored Per Sample Mass'},'FontSize',14)
xlabel('Applied Pressure (Pa)','FontSize',12)
ylabel('Mads/Ms (g/g)','FontSize',12)
grid on
saveas(10,'L:\MEng\Thesis\Figures\Experimental Plots\ADS Plots\Combined\COM_Vads_EFF.emf')
saveas(11,'L:\MEng\Thesis\Figures\Experimental Plots\ADS Plots\Combined\COM_nads_EFF.fig')
saveas(11,'L:\MEng\Thesis\Figures\Experimental Plots\ADS Plots\Combined\COM_nads_EFF.emf')
saveas(12,'L:\MEng\Thesis\Figures\Experimental Plots\ADS Plots\Combined\COM_Mads_EFF.fig')
saveas(12,'L:\MEng\Thesis\Figures\Experimental Plots\ADS Plots\Combined\COM_Mads_EFF.emf')
saveas(13,'L:\MEng\Thesis\Figures\Experimental Plots\ADS Plots\Combined\COM_Vads-Vp_EFF.fig')
saveas(13,'L:\MEng\Thesis\Figures\Experimental Plots\ADS Plots\Combined\COM_Vads-Vp_EFF.emf')
saveas(14,'L:\MEng\Thesis\Figures\Experimental Plots\ADS Plots\Combined\COM_nads-Vp_EFF.fig')
saveas(14,'L:\MEng\Thesis\Figures\Experimental Plots\ADS Plots\Combined\COM_nads-Vp_EFF.emf')

```

```

saveas(15,'L:\MEng\Thesis\Figures\Experimental Plots\ADS Plots\Combined\COM_Mads-
Vp_EFF.fig')
saveas(15,'L:\MEng\Thesis\Figures\Experimental Plots\ADS Plots\Combined\COM_Mads-
Vp_EFF.emf')
saveas(16,'L:\MEng\Thesis\Figures\Experimental Plots\ADS Plots\Combined\COM_Vads-
Ms_EFF.fig')
saveas(16,'L:\MEng\Thesis\Figures\Experimental Plots\ADS Plots\Combined\COM_Vads-
Ms_EFF.emf')
saveas(17,'L:\MEng\Thesis\Figures\Experimental Plots\ADS Plots\Combined\COM_nads-
Ms_EFF.fig')
saveas(17,'L:\MEng\Thesis\Figures\Experimental Plots\ADS Plots\Combined\COM_nads-
Ms_EFF.emf')
saveas(18,'L:\MEng\Thesis\Figures\Experimental Plots\ADS Plots\Combined\COM_Mads-
Ms_EFF.fig')
saveas(18,'L:\MEng\Thesis\Figures\Experimental Plots\ADS Plots\Combined\COM_Mads-
Ms_EFF.emf')

```

7.2.2 - Excess Adsorption Function

```

function [n1, n2, f, nads, Vads, Mads, nadsg, Vadsg, Madsg, nadvsv, Madsv, dum, n2t, Vhr,
Tavg] = MBWR_ADS_FCN_EXS(P1 ,T1 ,P2, T2, V1, V2, Vs, Vp, Msam, t1, C)
%---This function calculates excess adsorption values using the MBWR---%
%---equation of state for methane gas------%
%---MBWR equation constants------%
A1 = 8.98183102418E-5;
A2 = 1.88570883291E-2;
A3 = -5.07334853102E-1;
A4 = 2.42440372451E1;
A5 = -2.75937243281E3;
A6 = 6.67706377937E-9;
A7 = 6.59554690590E-6;
A8 = -4.75099859428E-3;
A9 = 9.41749168525E-1;
A10 = 2.03123055432E-13;
A11 = -8.82991375776E-11;
A12 = 2.69841136359E-7;
A13 = 1.63105161849E-14;
A14 = -9.65840913441E-16;
A15 = -4.97527927565E-14;
A16 = 3.88068765783E-20;
A17 = -4.47156684621E-25;
A18 = 2.80554989023E-23;
A19 = -4.96671746902E-29;

```

```

A20 = 4.27414662506E-1;
A21 = -1.25241753250E2;
A22 = -1.02133310576E-8;
A23 = 7.88608202448E-5;
A24 = -3.74931459167E-18;
A25 = 1.27111849576E-15;
A26 = -2.3634400069E-25;
A27 = -1.23455321379E-21;
A28 = 2.04715659218E-34;
A29 = 4.06242840085E-32;
A30 = -8.73417429883E-43;
A31 = -3.81661132665E-41;
A32 = 5.32641296927E-40;
GAMMA = 9.70E-9;
%---Ideal Gas Constant-----%
R = 8.3144;
%---Use an avering process to smooth out sensor data-----%
for(i=1000)
    P1 = smooth(P1);
    T1 = smooth(T1);
    P2 = smooth(P2);
    T2 = smooth(T2);
end
s1=length(T1);
%---Number of Initial data points-----%
ini = 25;
%---Number of final Data Points-----%
fin = 25;
%---Ads Start & Finish Time-----%
ti = t1(1);
tf = t1(s1);
tads = (tf-ti)/(60*60);
Pi = sum(P1{1:ini})/ini;
Pf = sum(P1{(s1-fin):s1})/fin;
n = (Pi-Pf)*V1/(R*293);
Vstp = n*R*293/101000*1000000;
%---Avg STP Expansion Rate-----%
Vhr = Vstp/tads;
Tavg=sum(T2)/s1;
errorr = 1;
n = 1;
h = 1;
for(i=1:s1)
    while(errorr >= 0.0000001)

```

%----Modified BWR-----%

$$\text{rho1}(1) = 0;$$

$$\text{rho2}(1) = 0;$$

%----MBWR Function-----%

$$\begin{aligned} f1(i) = & -P1(i) + \text{rho1}(n)^R * T1(i) + (\text{rho1}(n)^2) * (A1^*T1(i) + A2^*(T1(i)^{0.5}) + A3 + A4/T1(i) + \\ & A5/(T1(i)^2)) + (\text{rho1}(n)^3) * (A6^*T1(i) + A7 + A8/T1(i) + A9/(T1(i)^2)) + \\ & (\text{rho1}(n)^4) * (A10^*T1(i) + A11 + A12/T1(i)) + (\text{rho1}(n)^5) * A13 + (\text{rho1}(n)^6) * (A14/T1(i) + \\ & A15/(T1(i)^2)) + (\text{rho1}(n)^7) * A16/T1(i) + (\text{rho1}(n)^8) * (A17/T1(i) + A18/(T1(i)^2)) + \\ & (\text{rho1}(n)^9) * A19/(T1(i)^2) + (\text{rho1}(n)^3) * \exp(-\text{GAMMA} * (\text{rho1}(n)^2)) * ((A20/(T1(i)^2) + \\ & A21/(T1(i)^3)) + (\text{rho1}(n)^2) * (A22/(T1(i)^2) + A23/(T1(i)^4)) + \\ & (\text{rho1}(n)^4) * (A24/(T1(i)^2) + A25/(T1(i)^3)) + (\text{rho1}(n)^6) * (A26/(T1(i)^2) + \\ & A27/(T1(i)^4)) + (\text{rho1}(n)^8) * (A28/(T1(i)^2) + A29/(T1(i)^3)) + \\ & (\text{rho1}(n)^{10}) * (A30/(T1(i)^2) + A31/(T1(i)^3) + A32/(T1(i)^4))); \end{aligned}$$

$$\begin{aligned} f2(i) = & -P2(i) + \text{rho2}(n)^R * T2(i) + (\text{rho2}(n)^2) * (A1^*T2(i) + A2^*(T2(i)^{0.5}) + A3 + A4/T2(i) + \\ & A5/(T2(i)^2)) + (\text{rho2}(n)^3) * (A6^*T2(i) + A7 + A8/T2(i) + A9/(T2(i)^2)) + \\ & (\text{rho2}(n)^4) * (A10^*T2(i) + A11 + A12/T2(i)) + (\text{rho2}(n)^5) * A13 + (\text{rho2}(n)^6) * (A14/T2(i) + \\ & A15/(T2(i)^2)) + (\text{rho2}(n)^7) * A16/T2(i) + (\text{rho2}(n)^8) * (A17/T2(i) + A18/(T2(i)^2)) + \\ & (\text{rho2}(n)^9) * A19/(T2(i)^2) + (\text{rho2}(n)^3) * \exp(-\text{GAMMA} * (\text{rho2}(n)^2)) * ((A20/(T2(i)^2) + \\ & A21/(T2(i)^3)) + (\text{rho2}(n)^2) * (A22/(T2(i)^2) + A23/(T2(i)^4)) + \\ & (\text{rho2}(n)^4) * (A24/(T2(i)^2) + A25/(T2(i)^3)) + (\text{rho2}(n)^6) * (A26/(T2(i)^2) + \\ & A27/(T2(i)^4)) + (\text{rho2}(n)^8) * (A28/(T2(i)^2) + A29/(T2(i)^3)) + \\ & (\text{rho2}(n)^{10}) * (A30/(T2(i)^2) + A31/(T2(i)^3) + A32/(T2(i)^4))); \end{aligned}$$

%----MBWR Function Derivative-----%

$$\begin{aligned} fp1(i) = & R^*T1(i) + 4^*\text{rho1}(n)^3 * (A11 + A12/T1(i) + A10^*T1(i)) + 6^*\text{rho1}(n)^5 * (A14/T1(i) + \\ & A15/T1(i)^2) + 8^*\text{rho1}(n)^7 * (A17/T1(i) + A18/T1(i)^2) + 2^*\text{rho1}(n)^9 * (A3 + A2^*T1(i)^{1/2}) \\ & + A4/T1(i) + A5/T1(i)^2 + A1^*T1(i) + 3^*\text{rho1}(n)^2 * (A7 + A8/T1(i) + A9/T1(i)^2 + A6^*T1(i)) \\ & + 5^*A13^*\text{rho1}(n)^4 + (7^*A16^*\text{rho1}(n)^6)/T1(i) + (9^*A19^*\text{rho1}(n)^8)/T1(i)^2 + \\ & (\text{rho1}(n)^3 * (4^*\text{rho1}(n)^3 * (A24/T1(i)^2 + A25/T1(i)^3) + 6^*\text{rho1}(n)^5 * (A26/T1(i)^2 + \\ & A27/T1(i)^4) + 8^*\text{rho1}(n)^7 * (A28/T1(i)^2 + A29/T1(i)^3) + 10^*\text{rho1}(n)^9 * (A30/T1(i)^2 + \\ & A31/T1(i)^3 + A32/T1(i)^4) + 2^*\text{rho1}(n)^9 * (A22/T1(i)^2 + \\ & A23/T1(i)^4)) / \exp(\text{GAMMA} * \text{rho1}(n)^2) + (3^*\text{rho1}(n)^2 * (\text{rho1}(n)^2 * (A22/T1(i)^2 + \\ & A23/T1(i)^4) + \text{rho1}(n)^4 * (A24/T1(i)^2 + A25/T1(i)^3) + \text{rho1}(n)^6 * (A26/T1(i)^2 + \\ & A27/T1(i)^4) + \text{rho1}(n)^8 * (A28/T1(i)^2 + A29/T1(i)^3) + A20/T1(i)^2 + A21/T1(i)^3 + \\ & \text{rho1}(n)^{10} * (A30/T1(i)^2 + A31/T1(i)^3 + A32/T1(i)^4)) / \exp(\text{GAMMA} * \text{rho1}(n)^2) - \\ & (2^*\text{GAMMA} * \text{rho1}(n)^4 * (\text{rho1}(n)^2 * (A22/T1(i)^2 + A23/T1(i)^4) + \text{rho1}(n)^4 * (A24/T1(i)^2 \\ & + A25/T1(i)^3) + \text{rho1}(n)^6 * (A26/T1(i)^2 + A27/T1(i)^4) + \text{rho1}(n)^8 * (A28/T1(i)^2 + \\ & A29/T1(i)^3) + A20/T1(i)^2 + A21/T1(i)^3 + \text{rho1}(n)^{10} * (A30/T1(i)^2 + A31/T1(i)^3 + \\ & A32/T1(i)^4)) / \exp(\text{GAMMA} * \text{rho1}(n)^2); \end{aligned}$$

$$\begin{aligned} fp2(i) = & R^*T2(i) + 4^*\text{rho2}(n)^3 * (A11 + A12/T2(i) + A10^*T2(i)) + 6^*\text{rho2}(n)^5 * (A14/T2(i) + \\ & A15/T2(i)^2) + 8^*\text{rho2}(n)^7 * (A17/T2(i) + A18/T2(i)^2) + 2^*\text{rho2}(n)^9 * (A3 + A2^*T2(i)^{1/2}) \\ & + A4/T2(i) + A5/T2(i)^2 + A1^*T2(i) + 3^*\text{rho2}(n)^2 * (A7 + A8/T2(i) + A9/T2(i)^2 + A6^*T2(i)) \\ & + 5^*A13^*\text{rho2}(n)^4 + (7^*A16^*\text{rho2}(n)^6)/T2(i) + (9^*A19^*\text{rho2}(n)^8)/T2(i)^2 + \\ & (\text{rho2}(n)^3 * (4^*\text{rho2}(n)^3 * (A24/T2(i)^2 + A25/T2(i)^3) + 6^*\text{rho2}(n)^5 * (A26/T2(i)^2 + \\ & A27/T2(i)^4) + 8^*\text{rho2}(n)^7 * (A28/T2(i)^2 + A29/T2(i)^3) + 10^*\text{rho2}(n)^9 * (A30/T2(i)^2 + \end{aligned}$$

$$\frac{A31/T2(i)^3 + A32/T2(i)^4 + 2*\rho2(n)*(A22/T2(i)^2 + A23/T2(i)^4))}{\exp(\text{GAMMA}*\rho2(n)^2) + (3*\rho2(n)^2*(\rho2(n)^2*(A22/T2(i)^2 + A23/T2(i)^4) + \rho2(n)^4*(A24/T2(i)^2 + A25/T2(i)^3) + \rho2(n)^6*(A26/T2(i)^2 + A27/T2(i)^4) + \rho2(n)^8*(A28/T2(i)^2 + A29/T2(i)^3) + A20/T2(i)^2 + A21/T2(i)^3 + \rho2(n)^{10}*(A30/T2(i)^2 + A31/T2(i)^3 + A32/T2(i)^4)))} / \frac{\exp(\text{GAMMA}*\rho2(n)^2) - (2*\text{GAMMA}*\rho2(n)^4*(\rho2(n)^2*(A22/T2(i)^2 + A23/T2(i)^4) + \rho2(n)^4*(A24/T2(i)^2 + A25/T2(i)^3) + \rho2(n)^6*(A26/T2(i)^2 + A27/T2(i)^4) + \rho2(n)^8*(A28/T2(i)^2 + A29/T2(i)^3) + A20/T2(i)^2 + A21/T2(i)^3 + \rho2(n)^{10}*(A30/T2(i)^2 + A31/T2(i)^3 + A32/T2(i)^4)))}{\exp(\text{GAMMA}*\rho2(n)^2)}$$

```
%----Newton Raphson to obtain rho-----%
rho1(n+1) = rho1(n) - f1(i)/fp1(i);
rho2(n+1) = rho2(n) - f2(i)/fp2(i);
error1 = abs(rho1(n+1) - rho1(n))/rho1(n+1);
error2 = abs(rho2(n+1) - rho2(n))/rho2(n+1);
error = error1 + error2;

%----Values of molar density that satisfy MBWR given P & T-----%
rhoa1(i) = rho1(n);
rhoa2(i) = rho2(n);

%---Number of Moles Present in each chamber-----%
n1(i) = rhoa1(i)*V1;
n2(i) = rhoa2(i)*V2;
n = n+1;
Pe(i) = P2(i)/Pc;
end
n = 1;
error = 1;
end
for(i=1:s1)
%----Average Initial and Final moles in supply chamber-----%
n1ini = sum(n1(1:ini))/ini;
n1fin = sum(n1((s1-fin):s1))/fin;
%----Average Initial and Final moles in sample chamber-----%
n2ini = sum(n2(1:ini))/ini;
n2fin = sum(n2((s1-fin):s1))/fin;
%---moles in Sample Vessel based on conditions in Supply Vessel-----%
n2t(i) = n1ini-n1(i) + n2ini;
dum(i) = i;
f(i) = (n2ini + n1ini - n1(i) - n2(i));
%----moles adsorbed-----%
nads(i) = n1ini + n2ini - n1(i) - n2(i);
%---Clip ADS Values at C-----%
if (i > (s1 - C))
nads(i) = nads(s1 - C);
```

```

end
%---Set negative adsorption values to zero-----%
if(nads(i) <= 0)
    nads(i) = 0;
end
Vads(i) = (nads(i)*R*293/101000)*1000000;
Mads(i) = nads(i)*16.04;
%-----Normalized Plotting Variables-----%
nads(i) = nads(i)/Msam;
Vadsg(i) = Vads(i)/Msam;
Madsg(i) = Mads(i)/Msam;
nadsv(i) = nads(i)/(Vs*1000000);
Vadsv(i) = Vads(i)/(Vs*1000000);
Madsv(i) = Mads(i)/(Vs*1000000);
deln1(i) = (0.0008/P1(i)) + (0.005/T1(i)) + (0.01/(V1*1000000))*n1(i);
deln2(i) = (0.0008/P2(i)) + (0.005/T2(i)) + (0.01/(V2*1000000))*n2(i);
delnads(i) = (2*deln1(i)+2*deln2(i));
delVstp(i) = (delnads(i)/nads(i))*nads(i)*R*293/101000*1000000;
mmads(i,1) = Mads(i)*1000;
mnads(i,1) = nads(i)*1000;
Vstp(i,1) = Vads(i);
mnsys(i,1) = f(i)*1000;
Vsys(i,1) = f(i)*(R*293/101000)*1000000;
end
end

```

7.2.3 - Effective Storage Function

```

function [n1, n2, f, nads, Vads, Mads, nadsg, Vadsg, Madsg, nadsv, Vadsv, Madsv, dum, n2t, Vhr,
Tavg] = MBWR_ADS_FCN_EFF(P1 ,T1 ,P2 ,T2, V1, V2, Vs, Vp, Msam, t1, C)
%---This function calculates effective storage values using the MBWR---%
%---equation of state for methane gas-----%
%---MBWR equation constants-----%
A1 = 8.98183102418E-5;
A2 = 1.88570883291E-2;
A3 = -5.07334853102E-1;
A4 = 2.42440372451E1;
A5 = -2.75937243281E3;
A6 = 6.67706377937E-9;
A7 = 6.59554690590E-6;
A8 = -4.75099859428E-3;
A9 = 9.41749168525E-1;
A10 = 2.03123055432E-13;

```

```

A11 = -8.82991375776E-11;
A12 = 2.69841136359E-7;
A13 = 1.63105161849E-14;
A14 = -9.65840913441E-16;
A15 = -4.97527927565E-14;
A16 = 3.88068765783E-20;
A17 = -4.47156684621E-25;
A18 = 2.80554989023E-23;
A19 = -4.96671746902E-29;
A20 = 4.27414662506E-1;
A21 = -1.25241753250E2;
A22 = -1.02133310576E-8;
A23 = 7.88608202448E-5;
A24 = -3.74931459167E-18;
A25 = 1.27111849576E-15;
A26 = -2.3634400069E-25;
A27 = -1.23455321379E-21;
A28 = 2.04715659218E-34;
A29 = 4.06242840085E-32;
A30 = -8.73417429883E-43;
A31 = -3.81661132665E-41;
A32 = 5.32641296927E-40;
GAMMA = 9.70E-9;
%----Ideal Gas Constant-----%
R = 8.3144;
%----Use an averaging process to smooth out sensor data-----%
for(i=1:1000)
    P1 = smooth(P1);
    T1 = smooth(T1);
    P2 = smooth(P2);
    T2 = smooth(T2);
end
s1=length(T1);
%----Number of Initial data points-----%
ini = 25;
%----Number of final Data Points-----%
fin = 25;
%--Ads Start & Finish Time-----%
ti = t1(1);
tf = t1(s1);
tads = (tf-ti)/(60*60);
Pi = sum(P1(1:ini))/ini;
Pf = sum(P1((s1-fin):s1))/fin;
n = (Pi-Pf)*V1/(R*293);

```

```

Vstp = n*R*293/101000*1000000;
%----Avg STP Expansion Rate-----%Vhr = Vstp/tads;
Tavg=sum(T2)/s1;
errorr = 1;
n = 1;
h = 1;
for(i=1:s1)
    while(errorr >= 0.0000001)
%----Modified BWR-----%
    rho1(1) = 0;
    rho2(1) = 0;
%----MBWR Function-----%
    f1(i) = -P1(i) + rho1(n)*R*T1(i) + (rho1(n)^2)*(A1*T1(i) + A2*(T1(i)^0.5) + A3 + A4/T1(i) +
A5/(T1(i)^2)) + (rho1(n)^3)*(A6*T1(i) + A7 + A8/T1(i) + A9/(T1(i)^2)) +
(rho1(n)^4)*(A10*T1(i) + A11 + A12/T1(i)) + (rho1(n)^5)*A13 + (rho1(n)^6)*(A14/T1(i) +
A15/(T1(i)^2)) + (rho1(n)^7)*A16/T1(i) + (rho1(n)^8)*(A17/T1(i) + A18/(T1(i)^2)) +
(rho1(n)^9)*A19/(T1(i)^2) + (rho1(n)^3)*exp(-GAMMA*(rho1(n)^2))*(A20/(T1(i)^2) +
A21/(T1(i)^3)) + (rho1(n)^2)*(A22/(T1(i)^2) + A23/(T1(i)^4)) +
(rho1(n)^4)*(A24/(T1(i)^2) + A25/(T1(i)^3)) + (rho1(n)^6)*(A26/(T1(i)^2) +
A27/(T1(i)^4)) + (rho1(n)^8)*(A28/(T1(i)^2) + A29/(T1(i)^3)) +
(rho1(n)^10)*(A30/(T1(i)^2) + A31/(T1(i)^3) + A32/(T1(i)^4));
    f2(i) = -P2(i) + rho2(n)*R*T2(i) + (rho2(n)^2)*(A1*T2(i) + A2*(T2(i)^0.5) + A3 + A4/T2(i) +
A5/(T2(i)^2)) + (rho2(n)^3)*(A6*T2(i) + A7 + A8/T2(i) + A9/(T2(i)^2)) +
(rho2(n)^4)*(A10*T2(i) + A11 + A12/T2(i)) + (rho2(n)^5)*A13 + (rho2(n)^6)*(A14/T2(i) +
A15/(T2(i)^2)) + (rho2(n)^7)*A16/T2(i) + (rho2(n)^8)*(A17/T2(i) + A18/(T2(i)^2)) +
(rho2(n)^9)*A19/(T2(i)^2) + (rho2(n)^3)*exp(-GAMMA*(rho2(n)^2))*(A20/(T2(i)^2) +
A21/(T2(i)^3)) + (rho2(n)^2)*(A22/(T2(i)^2) + A23/(T2(i)^4)) +
(rho2(n)^4)*(A24/(T2(i)^2) + A25/(T2(i)^3)) + (rho2(n)^6)*(A26/(T2(i)^2) +
A27/(T2(i)^4)) + (rho2(n)^8)*(A28/(T2(i)^2) + A29/(T2(i)^3)) +
(rho2(n)^10)*(A30/(T2(i)^2) + A31/(T2(i)^3) + A32/(T2(i)^4));
%----MBWR Function derivative-----%
    fp1(i) = R*T1(i) + 4*rho1(n)^3*(A11 + A12/T1(i) + A10*T1(i)) + 6*rho1(n)^5*(A14/T1(i) +
A15/T1(i)^2) + 8*rho1(n)^7*(A17/T1(i) + A18/T1(i)^2) + 2*rho1(n)^9*(A3 + A2*T1(i)^0.5) +
A4/T1(i) + A5/T1(i)^2 + A1*T1(i) + 3*rho1(n)^2*(A7 + A8/T1(i) + A9/T1(i)^2) + A6*T1(i)) +
5*A13*rho1(n)^4 + (7*A16*rho1(n)^6)/T1(i) + (9*A19*rho1(n)^8)/T1(i)^2 +
(rho1(n)^3*(4*rho1(n)^3*(A24/T1(i)^2 + A25/T1(i)^3) + 6*rho1(n)^5*(A26/T1(i)^2 +
A27/T1(i)^4) + 8*rho1(n)^7*(A28/T1(i)^2 + A29/T1(i)^3) + 10*rho1(n)^9*(A30/T1(i)^2 +
A31/T1(i)^3 + A32/T1(i)^4) + 2*rho1(n)^11*(A22/T1(i)^2 +
A23/T1(i)^4))/exp(GAMMA*rho1(n)^2) + (3*rho1(n)^2*(rho1(n)^2*(A22/T1(i)^2 +
A23/T1(i)^4) + rho1(n)^4*(A24/T1(i)^2 + A25/T1(i)^3) + rho1(n)^6*(A26/T1(i)^2 +
A27/T1(i)^4) + rho1(n)^8*(A28/T1(i)^2 + A29/T1(i)^3) + A20/T1(i)^2 + A21/T1(i)^3 +
rho1(n)^10*(A30/T1(i)^2 + A31/T1(i)^3 + A32/T1(i)^4))/exp(GAMMA*rho1(n)^2) -
(2*rho1(n)^4*(rho1(n)^2*(A22/T1(i)^2 + A23/T1(i)^4) + rho1(n)^4*(A24/T1(i)^2 +
A25/T1(i)^3) + rho1(n)^6*(A26/T1(i)^2 + A27/T1(i)^4) + rho1(n)^8*(A28/T1(i)^2 +

```

```

A29/T1(i)^3) + A20/T1(i)^2 + A21/T1(i)^3 + rho1(n)^10*(A30/T1(i)^2 + A31/T1(i)^3 +
A32/T1(i)^4))/exp(GAMMA*rho1(n)^2);
    fp2(i)= R*T2(i) + 4*rho2(n)^3*(A11 + A12/T2(i) + A10*T2(i)) + 6*rho2(n)^5*(A14/T2(i) +
A15/T2(i)^2) + 8*rho2(n)^7*(A17/T2(i) + A18/T2(i)^2) + 2*rho2(n)^9*(A3 + A2*T2(i)^(1/2)
+ A4/T2(i) + A5/T2(i)^2 + A1*T2(i)) + 3*rho2(n)^2*(A7 + A8/T2(i) + A9/T2(i)^2 + A6*T2(i))
+ 5*A13*rho2(n)^4 + (7*A16*rho2(n)^6)/T2(i) + (9*A19*rho2(n)^8)/T2(i)^2 +
(rho2(n)^3*(4*rho2(n)^3*(A24/T2(i)^2 + A25/T2(i)^3) + 6*rho2(n)^5*(A26/T2(i)^2 +
A27/T2(i)^4) + 8*rho2(n)^7*(A28/T2(i)^2 + A29/T2(i)^3) + 10*rho2(n)^9*(A30/T2(i)^2 +
A31/T2(i)^3 + A32/T2(i)^4) + 2*rho2(n)*(A22/T2(i)^2 +
A23/T2(i)^4)))/exp(GAMMA*rho2(n)^2) + (3*rho2(n)^2*(rho2(n)^2*(A22/T2(i)^2 +
A23/T2(i)^4) + rho2(n)^4*(A24/T2(i)^2 + A25/T2(i)^3) + rho2(n)^6*(A26/T2(i)^2 +
A27/T2(i)^4) + rho2(n)^8*(A28/T2(i)^2 + A29/T2(i)^3) + A20/T2(i)^2 + A21/T2(i)^3 +
rho2(n)^10*(A30/T2(i)^2 + A31/T2(i)^3 + A32/T2(i)^4)))/exp(GAMMA*rho2(n)^2) -
(2*(GAMMA*rho2(n)^4*(rho2(n)^2*(A22/T2(i)^2 + A23/T2(i)^4) + rho2(n)^4*(A24/T2(i)^2
+ A25/T2(i)^3) + rho2(n)^6*(A26/T2(i)^2 + A27/T2(i)^4) + rho2(n)^8*(A28/T2(i)^2 +
A29/T2(i)^3) + A20/T2(i)^2 + A21/T2(i)^3 + rho2(n)^10*(A30/T2(i)^2 + A31/T2(i)^3 +
A32/T2(i)^4)))/exp(GAMMA*rho2(n)^2);
%----Newton Raphson to obtain rho-----%
rho1(n+1) = rho1(n) - f1(i)/fp1(i);
rho2(n+1) = rho2(n) - f2(i)/fp2(i);
error1 = abs(rho1(n+1) - rho1(n))/rho1(n+1);
error2 = abs(rho2(n+1) - rho2(n))/rho2(n+1);
error = error1 + error2;
%----Values of molar density that satisfy MBWR given P & T-----%
rhoa1(i) = rho1(n);
rhoa2(i) = rho2(n);
%---Number of Moles Present in each chamber-----%
n1(i) = rhoa1(i)*V1;
n2(i) = rhoa2(i)*V2;
n = n+1;
Pe(i) = P2(i)/Pc;
end
n=1;
errorr = 1;
end
for(i=1:s1)
%----Average Initial and Final moles in supply chamber-----%
n1ini = sum(n1(1:ini))/ini;
n1fin = sum(n1((s1-fin):s1))/fin;
%----Average Initial and Final moles in sample chamber-----%
n2ini = sum(n2(1:ini))/ini;
n2fin = sum(n2((s1-fin):s1))/fin;
%---moles in Sample Vessel based on conditions in Supply Vessel-----%
n2t(i) = n1ini-n1(i) + n2ini;

```

```

dum(i) = i;
f(i) = (n2ini + n1ini - n1(i) - n2(i));
%----moles adsorbed-----%
nads(i) = n1ini + n2ini - n1(i) - n2(i);
%---Clip ADS Values at C-----%
if (i > (s1 - C))
    nads(i) = nads(s1 - C);
end
%---Set negative adsorption values to zero-----%
if(nads(i) <= 0)
    nads(i) = 0;
end
Vads(i) = (nads(i)*R*293/101000)*1000000;
Mads(i) = nads(i)*16.04;
%----Normalized Plotting Variables-----%
nadsg(i) = nads(i)/Msam;
Vadsg(i) = Vads(i)/Msam;
Madsg(i) = Mads(i)/Msam;
nadsv(i) = nads(i)/(Vp*1000000);
Vadsv(i) = Vads(i)/(Vp*1000000);
Madsv(i) = Mads(i)/(Vp*1000000);
deln1(i) = (0.0008/P1(i)) + (0.005/T1(i)) + (0.01/(V1*1000000))*n1(i);
deln2(i) = (0.0008/P2(i)) + (0.005/T2(i)) + (0.01/(V2*1000000))*n2(i);
delnads(i) = (2*deln1(i) + 2*deln2(i));
delVstp(i) = (delnads(i)/nads(i))*nads(i)*R*293/101000*1000000;
mmads(i,1) = Mads(i)*1000;
mnads(i,1) = nads(i)*1000;
Vstp(i,1) = Vads(i);
mnsys(i,1) = f(i)*1000;   Vsys(i,1) = f(i)*(R*293/101000)*1000000;
end
end

```

7.3 - Methane Excess Adsorption & Effective Storage Cycle

7.3.1 - Master control program

```

clear all
close all
clc
%-----%
%----This program calculates the excess adsorption and effective-----%
%----storage charge/discharge cycle isotherms using the Modified-----%
%----BWR equation of state for methane gas-----%

```

```

%-----Variables to change!!-----%
% EXS & EFF file Dir
% Clipping Value C x6
% M, Vs, Vp
% Save Fig Dir and Names
% T values in legends
% Same name in legends
%----All units in Base Metric-----%
%----Number of Initial data points-----%
ini = 25;
%----Number of final Data Points-----%
fin = 25;
%-----Ideal Gas Constant-----%
R = 8.3144;
%----Sample Info-----%
%----CC to Cubic Meters-----%
V1 = 325/1000000;
%----Vol of Cont + Chamber-----%
Vcc = 32.52/1000000;
%----Dead Volume of Sample (He Exp.)-----%
Vs = 3.42/1000000;
%---Powder Packed Volume-----%
Vp = 10/1000000;
%-----Mass of Sample (g)-----%
Msam = 5.96;
%----Effective Sample Cham. Vol-----%
V2 = Vcc - Vs;
%---Adsorption Part of Cycle-----%
%---Clip ADS Values at C-----%
C = 0;
[t1,T1,T2,P1,P2] = textread('L:\MEng\Experimentation\New folder\Adsorption
Studies\Zeolite 13X\ADS_ZEO_13X_CH4_4.txt', '%f%f%f%f%f', 'bufsize',15000);
s1=length(T1);
for(i=1:s1)
    dum1(i)=i;
end
%----Call Excess Adsorption Function-----%
%----Make sure this file and the function file are in the same Dir!---%
[n1, n2, f, nads, Vads, Mads, nadsg, Vadsg, Madsg, nadv, Vadsv, Madsv, dum, n2t, Vhr, Tavgl] =
MBWR_ADS_FCN_EXS(P1 ,T1 ,P2 ,T2, V1, V2, Vs, Vp, Msam, t1, C);
%----Assign function values-----%
P21 = P2;
n11 = n1;
n21 = n2;

```

```

f1 = f;
nads1 = nads*1000;
Vads1 = Vads;
Mads1 = Mads;
nads1 = nads*1000;
Vads1 = Vads;
Mads1 = Mads;
nads1 = nads*1000;
Vads1 = Vads;
Mads1 = Mads;
dum1 = dum;
n2t1 = n2t;
Vhr1=Vhr;
navg1 = sum(nads1)/s1;
Tavg=sum(T2)/s1
%-----Desorption Part 1-----%
ndesi = (sum(nads1((s1-fin):s1))/fin)/1000;
[t1,T2,T1,P2,P1] = textread('L:\MEng\Experimentation\New folder\Adsorption
Studies\Zeolite 13X\DES_ZEO_13X_CH4_4_1.txt', '%f %f %f %f %f', 'bufsize',15000');
s1 = length(T1);
%---Offset moles DES initial Value-----%
SCL= -0.000;
%----Section Volume Adjustment-----%
V1 = V2 - 1.65/1000000;
V2 = 325/1000000 + 1.65/1000000;
[n1, n2, ndes, Vdes, Mdes, ndesg, Vdesg, Mdesg, ndesv, Vdesv, Mdesv, n2t] =
MBWR_DES_FCN_EXS(P1 ,T1 ,P2 ,T2, V1, V2, Vs, Vp, Msam, ndesi, SCL);
Pd11 = P1;
Pd21 = P2;
nd11 = n1;
nd21 = n2;
ndes1 = ndes*1000;
Vdes1 = Vdes;
Mdes1 = Mdes;
ndesg1 = ndesg*1000;
Vdesg1 = Vdesg;
Mdesg1 = Mdesg;
ndesv1 = ndesv*1000;
Vdesv1 = Vdesv;
Mdesv1 = Mdesv;
%-----Desorption Part 2-----%
ndesi = (sum(ndes1((s1-fin):s1))/fin)/1000;
[t1,T2,T1,P2,P1] = textread('L:\MEng\Experimentation\New folder\Adsorption
Studies\Zeolite 13X\DES_ZEO_13X_CH4_4_2.txt', '%f %f %f %f %f', 'bufsize',15000');

```

```

s1 = length(T1);
%---Offset moles DES initial Value-----%
SCL= -0.000;
[n1, n2, ndes, Vdes, Mdes, ndesg, Vdesg, Mdesg, ndesv, Vdesv, Mdesv, n2t] =
MBWR_DES_FCN_EXS(P1 ,T1 ,P2 ,T2, V1, V2, Vs, Vp, Msam, ndesi, SCL);
Pd12 = P1;
Pd22 = P2;
nd12 = n1;
nd22 = n2;
ndes2 = ndes*1000;
Vdes2 = Vdes;
Mdes2 = Mdes;
ndesg2 = ndesg*1000;
Vdesg2 = Vdesg;
Mdesg2 = Mdesg;
ndesv2 = ndesv*1000;
Vdesv2 = Vdesv;
Mdesv2 = Mdesv;
for(i=1:length(Pd12))
    if(100500<Pd12<101500)
        j=i;
    end
    ndesg2m = ndesg2(j);
    Vdesg2m = Vdesg2(j);
    Mdesg2m = Mdesg2(j);
    Vdesv2m = Vdesv2(j);
end
for(i=1:length(nads1))
    neffg(i) = nads1(i)-ndesg2m;
    Veffg(i) = Vads1(i)-Vdesg2m;
    Meffg(i) = Madsg1(i)-Mdesg2m;
    Veffv(i) = Vads1(i)-Vdesv2m;
    if(neffg(i)<0)
        neffg(i)=0;
    end
    if(Veffg(i)<0)
        Veffg(i)=0;
    end
    if(Meffg(i)<0)
        Meffg(i)=0;
    end
    if(Veffv(i)<0)
        Veffv(i)=0;
    end
end

```

```

end
figure(1)
plot(P21,Vads1,Pd11,Vdes1,'k',Pd12,Vdes2,'k','LineWidth',2)
legend('FM10 CH_4 296.5K ADS','FM30K CH_4 296.5K DES','Location','East')
title({'Excess Volume Adsorbed'},'FontSize',14)
xlabel('Applied Pressure (Pa)','FontSize',12)
ylabel('Vads (stp-cm^3)','FontSize',12)
grid on
figure(2)
plot(P21,nads1,Pd11,ndes1,'k',Pd12,ndes2,'k','LineWidth',2)
legend('FM30K CH_4 296.5K ADS','FM30K CH_4 296.5K DES','Location','East')
title({'Excess Moles Adsorbed'},'FontSize',14)
xlabel('Applied Pressure (Pa)','FontSize',12)
ylabel('nads (mmol)','FontSize',12)
grid on
figure(3)
plot(P21,Mads1,Pd11,Mdes1,'k',Pd12,Mdes2,'k','LineWidth',2)
legend('FM30K CH_4 296.5K ADS','FM30K CH_4 296.5K DES','Location','East')
title({'Excess Mass Adsorbed'},'FontSize',14)
xlabel('Applied Pressure (Pa)','FontSize',12)
ylabel('Mads (g)','FontSize',12)
grid on
figure(4)
plot(P21,Vadsv1,Pd11,Vdesv1,'k',Pd12,Vdesv2,'k','LineWidth',2)
legend('FM30K CH_4 296.5K ADS','FM30K CH_4 296.5K DES','Location','East')
title({'Excess Volume Adsorbed Per Sample Deadspace Volume'},'FontSize',14)
xlabel('Applied Pressure (Pa)','FontSize',12)
ylabel('Vads/Vd (stp-cm^3/cm^3)','FontSize',12)
grid on
figure(5)
plot(P21,nadsv1,Pd11,ndesv1,'k',Pd12,ndesv2,'k','LineWidth',2)
legend('FM30K CH_4 296.5K ADS','FM30K CH_4 296.5K DES','Location','East')
title({'Excess Moles Adsorbed Per Sample Deadspace Volume'},'FontSize',14)
xlabel('Applied Pressure (Pa)','FontSize',12)
ylabel('nads/Vd (mmol/cm^3)','FontSize',12)
grid on
figure(6)
plot(P21,Madsv1,Pd11,Mdesv1,'k',Pd12,Mdesv2,'k','LineWidth',2)
legend('FM30K CH_4 296.5K ADS','FM30K CH_4 296.5K DES','Location','East')
title({'Excess Mass Adsorbed Per Sample Deadspace Volume'},'FontSize',14)
xlabel('Applied Pressure (Pa)','FontSize',12)
ylabel('Mads/Vd (g/cm^3)','FontSize',12)
grid on
figure(7)

```

```

plot(P21,Vadsg1,Pd11,Vdesg1,'k',Pd12,Vdesg2,'k', 'LineWidth',2)
legend('FM30K CH_4 296.5K ADS','FM30K CH_4 296.5K DES','Location','East')
title({'Excess Volume Adsorbed Per Sample Mass'},'FontSize',14)
xlabel('Applied Pressure (Pa)','FontSize',12)
ylabel('Vads/Ms (stp-cm^3/g)','FontSize',12)
grid on
figure(8)
plot(P21,nadsg1,Pd11,ndesg1,'k',Pd12,ndesg2,'k', 'LineWidth',2)
legend('FM30K CH_4 296.5K ADS','FM30K CH_4 296.5K DES','Location','East')
title({'Excess Moles Adsorbed Per Sample Mass'},'FontSize',14)
xlabel('Applied Pressure (Pa)','FontSize',12)
ylabel('nads/Ms (mmol/g)','FontSize',12)
grid on
figure(9)
plot(P21,Madsg1,Pd11,Mdesg1,'k',Pd12,Mdesg2,'k', 'LineWidth',2)
legend('FM30K CH_4 296.5K ADS','FM30K CH_4 296.5K DES','Location','East')
title({'Excess Mass Adsorbed Per Sample Mass'},'FontSize',14)
xlabel('Applied Pressure (Pa)','FontSize',12)
ylabel('Mads/Ms (g/g)','FontSize',12)
grid on
figure(10)
plot(P21,neffg,'k', 'LineWidth',2)
legend('13X CH_4 297.8K EFF','Location','East')
title({'Excess Moles Deliverable Per Sample Mass'},'FontSize',14)
xlabel('Applied Pressure (Pa)','FontSize',12)
ylabel('neff/Ms (mmol/g)','FontSize',12)
grid on
figure(11)
plot(P21,Veffg,'k', 'LineWidth',2)
legend('13X CH_4 297.8K EFF','Location','East')
title({'Excess Volumes Deliverable Per Sample Mass'},'FontSize',14)
xlabel('Applied Pressure (Pa)','FontSize',12)
ylabel('Veff/Ms (stp-cm^3/g)','FontSize',12)
grid on
figure(12)
plot(P21,Meffg,'k', 'LineWidth',2)
legend('13X CH_4 297.8K EFF','Location','East')
title({'Excess Mass Deliverable Per Sample Mass'},'FontSize',14)
xlabel('Applied Pressure (Pa)','FontSize',12)
ylabel('Meff/Ms (g/g)','FontSize',12)
grid on
figure(13)
plot(P21,Veffv,'k', 'LineWidth',2)
legend('13X CH_4 297.8K EFF','Location','East')

```

```
title({'Excess Volumes Deliverable Per Sample Deadspace Volume'}, 'FontSize', 14)
xlabel('Applied Pressure (Pa)', 'FontSize', 12)
ylabel('Veff/Vd (stp-cm^3/cm^3)', 'FontSize', 12)
grid on
saveas(1, 'L:\MEng\Thesis\Figures\Experimental Plots\ADS
Plots\13X\CH4\EXS\13X_Vdes_EXS.fig')
saveas(1, 'L:\MEng\Thesis\Figures\Experimental Plots\ADS
Plots\13X\CH4\EXS\13X_Vdes_EXS.emf')
saveas(2, 'L:\MEng\Thesis\Figures\Experimental Plots\ADS
Plots\13X\CH4\EXS\13X_ndes_EXS.fig')
saveas(2, 'L:\MEng\Thesis\Figures\Experimental Plots\ADS
Plots\13X\CH4\EXS\13X_ndes_EXS.emf')
saveas(3, 'L:\MEng\Thesis\Figures\Experimental Plots\ADS
Plots\13X\CH4\EXS\13X_Mdes_EXS.fig')
saveas(3, 'L:\MEng\Thesis\Figures\Experimental Plots\ADS
Plots\13X\CH4\EXS\13X_Mdes_EXS.emf')
saveas(4, 'L:\MEng\Thesis\Figures\Experimental Plots\ADS Plots\13X\CH4\EXS\13X_Vdes-
Vd_EXS.fig')
saveas(4, 'L:\MEng\Thesis\Figures\Experimental Plots\ADS Plots\13X\CH4\EXS\13X_Vdes-
Vd_EXS.emf')
saveas(5, 'L:\MEng\Thesis\Figures\Experimental Plots\ADS Plots\13X\CH4\EXS\13X_ndes-
Vd_EXS.fig')
saveas(5, 'L:\MEng\Thesis\Figures\Experimental Plots\ADS Plots\13X\CH4\EXS\13X_ndes-
Vd_EXS.emf')
saveas(6, 'L:\MEng\Thesis\Figures\Experimental Plots\ADS Plots\13X\CH4\EXS\13X_Mdes-
Vd_EXS.fig')
saveas(6, 'L:\MEng\Thesis\Figures\Experimental Plots\ADS Plots\13X\CH4\EXS\13X_Mdes-
Vd_EXS.emf')
saveas(7, 'L:\MEng\Thesis\Figures\Experimental Plots\ADS Plots\13X\CH4\EXS\13X_Vdes-
Ms_EXS.fig')
saveas(7, 'L:\MEng\Thesis\Figures\Experimental Plots\ADS Plots\13X\CH4\EXS\13X_Vdes-
Ms_EXS.emf')
saveas(8, 'L:\MEng\Thesis\Figures\Experimental Plots\ADS Plots\13X\CH4\EXS\13X_ndes-
Ms_EXS.fig')
saveas(8, 'L:\MEng\Thesis\Figures\Experimental Plots\ADS Plots\13X\CH4\EXS\13X_ndes-
Ms_EXS.emf')
saveas(9, 'L:\MEng\Thesis\Figures\Experimental Plots\ADS Plots\13X\CH4\EXS\13X_Mdes-
Ms_EXS.fig')
saveas(9, 'L:\MEng\Thesis\Figures\Experimental Plots\ADS Plots\13X\CH4\EXS\13X_Mdes-
Ms_EXS.emf')
saveas(10, 'L:\MEng\Thesis\Figures\Experimental Plots\ADS Plots\13X\CH4\EXS\13X_neff-
Ms_EXS.fig')
saveas(10, 'L:\MEng\Thesis\Figures\Experimental Plots\ADS Plots\13X\CH4\EXS\13X_neff-
Ms_EXS.emf')
```

```

saveas(11,'L:\MEng\Thesis\Figures\Experimental Plots\ADS Plots\13X\CH4\EXS\13X_Veff-
Ms_EXS.fig')
saveas(11,'L:\MEng\Thesis\Figures\Experimental Plots\ADS Plots\13X\CH4\EXS\13X_Veff-
Ms_EXS.emf')
saveas(12,'L:\MEng\Thesis\Figures\Experimental Plots\ADS Plots\13X\CH4\EXS\13X_Meff-
Ms_EXS.fig')
saveas(12,'L:\MEng\Thesis\Figures\Experimental Plots\ADS Plots\13X\CH4\EXS\13X_Meff-
Ms_EXS.emf')
saveas(13,'L:\MEng\Thesis\Figures\Experimental Plots\ADS Plots\13X\CH4\EXS\13X_Veff-
Vd_EXS.fig')
saveas(13,'L:\MEng\Thesis\Figures\Experimental Plots\ADS Plots\13X\CH4\EXS\13X_Veff-
Vd_EXS.emf')

%------%
%------%
%-----Effective Storage------%
%------%
%------%
clear all
clc
R = 8.3144;
%---Number of Initial data points------%
ini = 25;
%---Number of final Data Points------%
fin = 25;
%---Sample Info------%
%---CC to Cubic Meters------%
V1 = 325/1000000;
%---Vol of Cont + Chamber------%
Vcc = 32.52/1000000;
%---Dead Volume of Sample (He Exp.)------%
Vs = 3.42/1000000;
%---Powder Packed Volume------%
Vp = 10/1000000;
%---Mass of Sample (g)------%
Msam = 5.96;
%-----Effective Sample Cham. Vol------%
V2 = Vcc - Vp;
%---Clip ADS Values at C------%
C = 0;
[t1,T1,T2,P1,P2] = textread('L:\MEng\Experimentation\New folder\Adsorption
Studies\Zeolite 13X\ADS_ZEO_13X_CH4_4.txt', '%f%f%f%f%f', 'bufsize',15000');
s1 = length(T1);

```

```

[n1, n2, f, nads, Vads, Mads, nadsg, Vadsg, Madsg, nadsv, Vadsv, Madsv, dum, n2t, Vhr] =
MBWR_ADS_FCN_EFF(P1, T1, P2, T2, V1, V2, Vs, Vp, Msam, t1, C);
P21 = P2;
n11 = n1;
n21 = n2;
f1 = f;
nads1 = nads*1000;
Vads1 = Vads;
Mads1 = Mads;
nadsg1 = nadsg*1000;
Vadsg1 = Vadsg;
Madsg1 = Madsg;
nadsv1 = nadsv*1000;
Vadsv1 = Vadsv;
Madsv1 = Madsv;
dum1 = dum;
n2t1 = n2t;
%-----Desorption-----%
ndesi = (sum(nads1((s1-fin):s1))/fin)/1000;
[t1, T2, T1, P2, P1] = textread('L:\MEng\Experimentation\New folder\Adsorption
Studies\Zeolite 13X\DES_ZEO_13X_CH4_4_1.txt', '%f %f %f %f %f', 'bufsize', 15000');
s1 = length(T1);
%---Offset moles DES initial Value-----%
SCL= -0.000;
%----Section Volume Adjustment-----%
V1 = V2 - 1.65/1000000;
V2 = 325/1000000 + 1.65/1000000;
[n1, n2, ndes, Vdes, Mdes, ndesg, Vdesg, Mdesg, ndesv, Vdesv, Mdesv, n2t] =
MBWR_DES_FCN_EFF(P1, T1, P2, T2, V1, V2, Vs, Vp, Msam, ndesi, SCL);
Pd11 = P1;
Pd21 = P2;
nd11 = n1;
nd21 = n2;
ndes1 = ndes*1000;
Vdes1 = Vdes;
Mdes1 = Mdes;
ndesg1 = ndesg*1000;
Vdesg1 = Vdesg;
Mdesg1 = Mdesg;
ndesv1 = ndesv*1000;
Vdesv1 = Vdesv;
Mdesv1 = Mdesv;
ndesi= (sum(ndes1((s1-fin):s1))/fin)/1000;

```

```

[t1,T2,T1,P2,P1] = textread('L:\MEng\Experimentation\New folder\Adsorption
Studies\Zeolite 13X\DES_ZEO_13X_CH4_4_2.txt', '%f%f%f%f%f', 'bufsize',15000');
s1 = length(T1);
%---Offset moles 2nd DES part-----%
SCL=-0.000;
[n1, n2, ndes, Vdes, Mdes, ndesg, Vdesg, Mdesg, ndesv, Vdesv, Mdesv, n2t] =
MBWR_DES_FCN_EFF(P1 ,T1 ,P2 ,T2, V1, V2, Vs, Vp, Msam, ndesi, SCL);
Pd12 = P1;
Pd22 = P2;
nd12 = n1;
nd22 = n2;
ndes2 = ndes*1000;
Vdes2 = Vdes;
Mdes2 = Mdes;
ndesg2 = ndesg*1000;
Vdesg2 = Vdesg;
Mdesg2 = Mdesg;
ndesv2 = ndesv*1000;
Vdesv2 = Vdesv;
Mdesv2 = Mdesv;
for(i=1:length(Pd12))
    if(100500<Pd12<101500)
        j=i;
        end
        ndesg2m = ndesg2(j);
        Vdesg2m = Vdesg2(j);
        Mdesg2m = Mdesg2(j);
        Vdesv2m = Vdesv2(j);
    end
for(i=1:length(nads1))
    neffg(i) = nadsg1(i)-ndesg2m;
    Veffg(i) = Vadsg1(i)-Vdesg2m;
    Meffg(i) = Madsg1(i)-Mdesg2m;
    Veffv(i) = Vadsv1(i)-Vdesv2m;
    if(neffg(i)<0)
        neffg(i)=0;
    end
    if(Veffg(i)<0)
        Veffg(i)=0;
    end
    if(Meffg(i)<0)
        Meffg(i)=0;
    end
    if(Veffv(i)<0)

```

```

    Veffv(i)=0;
end
figure(14)
plot(P21,Vads1,Pd11,Vdes1,'k',Pd12,Vdes2,'k','LineWidth',2)
legend('FM30K CH_4 296.5K ADS','FM30K CH_4 296.5K DES','Location','East')
title({'Effective Volume Stored'},'FontSize',14)
xlabel('Applied Pressure (Pa)','FontSize',12)
ylabel('Vads (stp-cm^3)','FontSize',12)
grid on
figure(15)
plot(P21,nads1,Pd11,ndes1,'k',Pd12,ndes2,'k','LineWidth',2)
legend('FM30K CH_4 296.5K ADS','FM30K CH_4 296.5K DES','Location','East')
title({'Effective Moles Stored'},'FontSize',14)
xlabel('Applied Pressure (Pa)','FontSize',12)
ylabel('nads (mmol)','FontSize',12)
grid on
figure(16)
plot(P21,Mads1,Pd11,Mdes1,'k',Pd12,Mdes2,'k','LineWidth',2)
legend('FM30K CH_4 296.5K ADS','FM30K CH_4 296.5K DES','Location','East')
title({'Effective Mass Stored'},'FontSize',14)
xlabel('Applied Pressure (Pa)','FontSize',12)
ylabel('Mads (g)','FontSize',12)
grid on
figure(17)
plot(P21,Vadsv1,Pd11,Vdesv1,'k',Pd12,Vdesv2,'k','LineWidth',2)
legend('FM30K CH_4 296.5K ADS','FM30K CH_4 296.5K DES','Location','East')
title({'Effective Volume Stored Per Sample Packed Volume'},'FontSize',14)
xlabel('Applied Pressure (Pa)','FontSize',12)
ylabel('Vads/Vp (stp-cm^3/cm^3)','FontSize',12)
grid on
figure(18)
plot(P21,nadsv1,Pd11,ndesv1,'k',Pd12,ndesv2,'k','LineWidth',2)
legend('FM30K CH_4 296.5K ADS','FM30K CH_4 296.5K DES','Location','East')
title({'Effective Moles Stored Per Sample Packed Volume'},'FontSize',14)
xlabel('Applied Pressure (Pa)','FontSize',12)
ylabel('nads/Vp (mmol/cm^3)','FontSize',12)
grid on
figure(19)
plot(P21,Madsv1,Pd11,Mdesv1,'k',Pd12,Mdesv2,'k','LineWidth',2)
legend('FM30K CH_4 296.5K ADS','FM30K CH_4 296.5K DES','Location','East')
title({'Effective Mass Stored Per Sample Packed Volume'},'FontSize',14)
xlabel('Applied Pressure (Pa)','FontSize',12)

```

```

ylabel('Mads/Vp (g/cm^3)','FontSize',12)
grid on
figure(20)
plot(P21,Vadsg1,Pd11,Vdesg1,'k',Pd12,Vdesg2,'k','LineWidth',2)
legend('FM30K CH_4 296.5K ADS','FM30K CH_4 296.5K DES','Location','East')
title('Effective Volume Stored Per Sample Mass'),'FontSize',14)
xlabel('Applied Pressure (Pa)','FontSize',12)
ylabel('Vads/Ms (stp-cm^3/g)','FontSize',12)
grid on
figure(21)
plot(P21,nadsg1,Pd11,ndesg1,'k',Pd12,ndesg2,'k','LineWidth',2)
legend('FM30K CH_4 296.5K ADS','FM30K CH_4 296.5K DES','Location','East')
title('Effective Moles Stored Per Sample Mass'),'FontSize',14)
xlabel('Applied Pressure (Pa)','FontSize',12)
ylabel('nads/Ms (mmol/g)','FontSize',12)
grid on
figure(22)
plot(P21,Madsg1,Pd11,Mdesg1,'k',Pd12,Mdesg2,'k','LineWidth',2)
legend('FM30K CH_4 296.5K ADS','FM30K CH_4 296.5K DES','Location','East')
title('Effective Mass Stored Per Sample Mass'),'FontSize',14)
xlabel('Applied Pressure (Pa)','FontSize',12)
ylabel('Mads/Ms (g/g)','FontSize',12)
grid on
figure(23)
plot(P21,neffg,'k','LineWidth',2)
legend('13X CH_4 297.8K EFF','Location','East')
title('Effectively Stored Moles Deliverable Per Sample Mass'),'FontSize',14)
xlabel('Applied Pressure (Pa)','FontSize',12)
ylabel('neff/Ms (mmol/g)','FontSize',12)
grid on
figure(24)
plot(P21,Veffg,'k','LineWidth',2)
legend('13X CH_4 297.8K EFF','Location','East')
title('Effectively Stored Volumes Deliverable Per Sample Mass'),'FontSize',14)
xlabel('Applied Pressure (Pa)','FontSize',12)
ylabel('Veff/Ms (stp-cm^3/g)','FontSize',12)
grid on
figure(25)
plot(P21,Meffg,'k','LineWidth',2)
legend('13X CH_4 297.8K EFF','Location','East')
title('Effectively Stored Mass Deliverable Per Sample Mass'),'FontSize',14)
xlabel('Applied Pressure (Pa)','FontSize',12)
ylabel('Meff/Ms (g/g)','FontSize',12)
grid on

```

```
figure(26)
plot(P21,Veffv,'k','LineWidth',2)
legend('13X CH_4 297.8K EFF','Location','East')
title('Effectively Stored Volume Deliverable Per Sample Pack Volume'),'FontSize',14)
xlabel('Applied Pressure (Pa)','FontSize',12)
ylabel('Veff/Vp (stp-cm^3/cm^3)','FontSize',12)
grid on
saveas(14,'L:\MEng\Thesis\Figures\Experimental Plots\ADS
Plots\13X\CH4\EFF\13X_Vdes_EFF.fig')
saveas(14,'L:\MEng\Thesis\Figures\Experimental Plots\ADS
Plots\13X\CH4\EFF\13X_Vdes_EFF.emf')
saveas(15,'L:\MEng\Thesis\Figures\Experimental Plots\ADS
Plots\13X\CH4\EFF\13X_ndes_EFF.fig')
saveas(15,'L:\MEng\Thesis\Figures\Experimental Plots\ADS
Plots\13X\CH4\EFF\13X_ndes_EFF.emf')
saveas(16,'L:\MEng\Thesis\Figures\Experimental Plots\ADS
Plots\13X\CH4\EFF\13X_Mdes_EFF.fig')
saveas(16,'L:\MEng\Thesis\Figures\Experimental Plots\ADS
Plots\13X\CH4\EFF\13X_Mdes_EFF.emf')
saveas(17,'L:\MEng\Thesis\Figures\Experimental Plots\ADS
Plots\13X\CH4\EFF\13X_Vdes-Vp_EFF.fig')
saveas(17,'L:\MEng\Thesis\Figures\Experimental Plots\ADS
Plots\13X\CH4\EFF\13X_Vdes-Vp_EFF.emf')
saveas(18,'L:\MEng\Thesis\Figures\Experimental Plots\ADS Plots\13X\CH4\EFF\13X_ndes-
Vp_EFF.fig')
saveas(18,'L:\MEng\Thesis\Figures\Experimental Plots\ADS Plots\13X\CH4\EFF\13X_ndes-
Vp_EFF.emf')
saveas(19,'L:\MEng\Thesis\Figures\Experimental Plots\ADS
Plots\13X\CH4\EFF\13X_Mdes-Vp_EFF.fig')
saveas(19,'L:\MEng\Thesis\Figures\Experimental Plots\ADS
Plots\13X\CH4\EFF\13X_Mdes-Vp_EFF.emf')
saveas(20,'L:\MEng\Thesis\Figures\Experimental Plots\ADS
Plots\13X\CH4\EFF\13X_Vdes-Ms_EFF.fig')
saveas(20,'L:\MEng\Thesis\Figures\Experimental Plots\ADS
Plots\13X\CH4\EFF\13X_Vdes-Ms_EFF.emf')
saveas(21,'L:\MEng\Thesis\Figures\Experimental Plots\ADS Plots\13X\CH4\EFF\13X_ndes-
Ms_EFF.fig')
saveas(21,'L:\MEng\Thesis\Figures\Experimental Plots\ADS Plots\13X\CH4\EFF\13X_ndes-
Ms_EFF.emf')
saveas(22,'L:\MEng\Thesis\Figures\Experimental Plots\ADS
Plots\13X\CH4\EFF\13X_Mdes-Ms_EFF.fig')
saveas(22,'L:\MEng\Thesis\Figures\Experimental Plots\ADS
Plots\13X\CH4\EFF\13X_Mdes-Ms_EFF.emf')
```

```

saveas(23,'L:\MEng\Thesis\Figures\Experimental Plots\ADS Plots\13X\CH4\EFF\13X_neff-
Ms_EFF.fig')
saveas(23,'L:\MEng\Thesis\Figures\Experimental Plots\ADS Plots\13X\CH4\EFF\13X_neff-
Ms_EFF.emf')
saveas(24,'L:\MEng\Thesis\Figures\Experimental Plots\ADS Plots\13X\CH4\EFF\13X_Veff-
Ms_EFF.fig')
saveas(24,'L:\MEng\Thesis\Figures\Experimental Plots\ADS Plots\13X\CH4\EFF\13X_Veff-
Ms_EFF.emf')
saveas(25,'L:\MEng\Thesis\Figures\Experimental Plots\ADS Plots\13X\CH4\EFF\13X_Meff-
Ms_EFF.fig')
saveas(25,'L:\MEng\Thesis\Figures\Experimental Plots\ADS Plots\13X\CH4\EFF\13X_Meff-
Ms_EFF.emf')
saveas(26,'L:\MEng\Thesis\Figures\Experimental Plots\ADS Plots\13X\CH4\EFF\13X_Veff-
Vp_EFF.fig')
saveas(26,'L:\MEng\Thesis\Figures\Experimental Plots\ADS Plots\13X\CH4\EFF\13X_Veff-
Vp_EFF.emf')

```

7.3.2 - Excess Desorption Function

```

function [n1, n2, ndes, Vdes, Mdes, ndesg, Vdesg, Mdesg, ndesv, Vdesv, Mdesv, n2t] =
MBWR_DES_FCN_EXS(P1 ,T1 ,P2 ,T2, V1, V2, Vs, Vp, Msam, ndesi, SCL)
%---This function calculates excess desorption values using the MBWR---%
%---equation of state for methane gas------%
%---MBWR equation constants------%
A1 = 8.98183102418E-5;
A2 = 1.88570883291E-2;
A3 = -5.07334853102E-1;
A4 = 2.42440372451E1;
A5 = -2.75937243281E3;
A6 = 6.67706377937E-9;
A7 = 6.59554690590E-6;
A8 = -4.75099859428E-3;
A9 = 9.41749168525E-1;
A10 = 2.03123055432E-13;
A11 = -8.82991375776E-11;
A12 = 2.69841136359E-7;
A13 = 1.63105161849E-14;
A14 = -9.65840913441E-16;
A15 = -4.97527927565E-14;
A16 = 3.88068765783E-20;
A17 = -4.47156684621E-25;
A18 = 2.80554989023E-23;
A19 = -4.96671746902E-29;

```

```

A20 = 4.27414662506E-1;
A21 = -1.25241753250E2;
A22 = -1.02133310576E-8;
A23 = 7.88608202448E-5;
A24 = -3.74931459167E-18;
A25 = 1.27111849576E-15;
A26 = -2.3634400069E-25;
A27 = -1.23455321379E-21;
A28 = 2.04715659218E-34;
A29 = 4.06242840085E-32;
A30 = -8.73417429883E-43;
A31 = -3.81661132665E-41;
A32 = 5.32641296927E-40;
GAMMA = 9.70E-9;
%---Ideal Gas Constant-----%
R = 8.3144;
%---Use an avering process to smooth out sensor data-----%
for(i=1:100)
    P1 = smooth(P1);
    T1 = smooth(T1);
    P2 = smooth(P2);
    T2 = smooth(T2);
end
s1=length(T1);
%---Number of Initial data points-----%
ini = 25;
%---Number of final Data Points-----%
fin = 25;
errorr = 1;
n = 1;
h = 1;
for(i=1:s1)
    while(errorr >= 0.0000001)
%---Modified BWR-----%
        rho1(1) = 0;
        rho2(1) = 0;
%---MBWR Function-----%
        f1(i) = -P1(i) + rho1(n)*R*T1(i) + (rho1(n)^2)*(A1*T1(i) + A2*(T1(i)^0.5) + A3 + A4/T1(i) +
A5/(T1(i)^2)) + (rho1(n)^3)*(A6*T1(i) + A7 + A8/T1(i) + A9/(T1(i)^2)) +
(rho1(n)^4)*(A10*T1(i) + A11 + A12/T1(i)) + (rho1(n)^5)*A13 + (rho1(n)^6)*(A14/T1(i) +
A15/(T1(i)^2)) + (rho1(n)^7)*A16/T1(i) + (rho1(n)^8)*(A17/T1(i) + A18/(T1(i)^2)) +
(rho1(n)^9)*A19/(T1(i)^2) + (rho1(n)^3)*exp(-GAMMA*(rho1(n)^2))*(A20/(T1(i)^2) +
A21/(T1(i)^3)) + (rho1(n)^2)*(A22/(T1(i)^2) + A23/(T1(i)^4)) +
(rho1(n)^4)*(A24/(T1(i)^2) + A25/(T1(i)^3)) + (rho1(n)^6)*(A26/(T1(i)^2) +

```

```

A27/(T1(i)^4) ) + (rho1(n)^8)*(A28/(T1(i)^2) + A29/(T1(i)^3)) +
(rho1(n)^10)*(A30/(T1(i)^2) + A31/(T1(i)^3) + A32/(T1(i)^4));
f2(i) = -P2(i) + rho2(n)*R*T2(i) + (rho2(n)^2)*(A1*T2(i) + A2*(T2(i)^0.5) + A3 + A4/T2(i) +
A5/(T2(i)^2)) + (rho2(n)^3)*(A6*T2(i) + A7 + A8/T2(i) + A9/(T2(i)^2)) +
(rho2(n)^4)*(A10*T2(i) + A11 + A12/T2(i)) + (rho2(n)^5)*A13 + (rho2(n)^6)*(A14/T2(i) +
A15/(T2(i)^2)) + (rho2(n)^7)*A16/T2(i) + (rho2(n)^8)*(A17/T2(i) + A18/(T2(i)^2)) +
(rho2(n)^9)*A19/(T2(i)^2) + (rho2(n)^3)*exp(-GAMMA*(rho2(n)^2))*((A20/(T2(i)^2) +
A21/(T2(i)^3)) + (rho2(n)^2)*(A22/(T2(i)^2) + A23/(T2(i)^4)) +
(rho2(n)^4)*(A24/(T2(i)^2) + A25/(T2(i)^3)) + (rho2(n)^6)*(A26/(T2(i)^2) +
A27/(T2(i)^4)) + (rho2(n)^8)*(A28/(T2(i)^2) + A29/(T2(i)^3)) +
(rho2(n)^10)*(A30/(T2(i)^2) + A31/(T2(i)^3) + A32/(T2(i)^4)));
%----MBWR Function derivate-----%
fp1(i) = R*T1(i) + 4*rho1(n)^3*(A11 + A12/T1(i) + A10*T1(i)) + 6*rho1(n)^5*(A14/T1(i) +
A15/T1(i)^2) + 8*rho1(n)^7*(A17/T1(i) + A18/T1(i)^2) + 2*rho1(n)^9*(A3 + A2*T1(i)^(1/2)
+ A4/T1(i) + A5/T1(i)^2 + A1*T1(i)) + 3*rho1(n)^2*(A7 + A8/T1(i) + A9/T1(i)^2 + A6*T1(i))
+ 5*A13*rho1(n)^4 + (7*A16*rho1(n)^6)/T1(i) + (9*A19*rho1(n)^8)/T1(i)^2 +
(rho1(n)^3*(4*rho1(n)^3*(A24/T1(i)^2 + A25/T1(i)^3) + 6*rho1(n)^5*(A26/T1(i)^2 +
A27/T1(i)^4) + 8*rho1(n)^7*(A28/T1(i)^2 + A29/T1(i)^3) + 10*rho1(n)^9*(A30/T1(i)^2 +
A31/T1(i)^3 + A32/T1(i)^4) + 2*rho1(n)^*(A22/T1(i)^2 +
A23/T1(i)^4))/exp(GAMMA*rho1(n)^2) + (3*rho1(n)^2*(rho1(n)^2*(A22/T1(i)^2 +
A23/T1(i)^4) + rho1(n)^4*(A24/T1(i)^2 + A25/T1(i)^3) + rho1(n)^6*(A26/T1(i)^2 +
A27/T1(i)^4) + rho1(n)^8*(A28/T1(i)^2 + A29/T1(i)^3) + A20/T1(i)^2 + A21/T1(i)^3 +
rho1(n)^10*(A30/T1(i)^2 + A31/T1(i)^3 + A32/T1(i)^4))/exp(GAMMA*rho1(n)^2) -
(2*GAMMA*rho1(n)^4*(rho1(n)^2*(A22/T1(i)^2 + A23/T1(i)^4) + rho1(n)^4*(A24/T1(i)^2
+ A25/T1(i)^3) + rho1(n)^6*(A26/T1(i)^2 + A27/T1(i)^4) + rho1(n)^8*(A28/T1(i)^2
+ A29/T1(i)^3) + A20/T1(i)^2 + A21/T1(i)^3 + rho1(n)^10*(A30/T1(i)^2 + A31/T1(i)^3 +
A32/T1(i)^4))/exp(GAMMA*rho1(n)^2);
fp2(i) = R*T2(i) + 4*rho2(n)^3*(A11 + A12/T2(i) + A10*T2(i)) + 6*rho2(n)^5*(A14/T2(i) +
A15/T2(i)^2) + 8*rho2(n)^7*(A17/T2(i) + A18/T2(i)^2) + 2*rho2(n)^9*(A3 + A2*T2(i)^(1/2)
+ A4/T2(i) + A5/T2(i)^2 + A1*T2(i)) + 3*rho2(n)^2*(A7 + A8/T2(i) + A9/T2(i)^2 + A6*T2(i))
+ 5*A13*rho2(n)^4 + (7*A16*rho2(n)^6)/T2(i) + (9*A19*rho2(n)^8)/T2(i)^2 +
(rho2(n)^3*(4*rho2(n)^3*(A24/T2(i)^2 + A25/T2(i)^3) + 6*rho2(n)^5*(A26/T2(i)^2 +
A27/T2(i)^4) + 8*rho2(n)^7*(A28/T2(i)^2 + A29/T2(i)^3) + 10*rho2(n)^9*(A30/T2(i)^2 +
A31/T2(i)^3 + A32/T2(i)^4) + 2*rho2(n)^*(A22/T2(i)^2 +
A23/T2(i)^4))/exp(GAMMA*rho2(n)^2) + (3*rho2(n)^2*(rho2(n)^2*(A22/T2(i)^2 +
A23/T2(i)^4) + rho2(n)^4*(A24/T2(i)^2 + A25/T2(i)^3) + rho2(n)^6*(A26/T2(i)^2 +
A27/T2(i)^4) + rho2(n)^8*(A28/T2(i)^2 + A29/T2(i)^3) + A20/T2(i)^2 + A21/T2(i)^3 +
rho2(n)^10*(A30/T2(i)^2 + A31/T2(i)^3 + A32/T2(i)^4))/exp(GAMMA*rho2(n)^2) -
(2*GAMMA*rho2(n)^4*(rho2(n)^2*(A22/T2(i)^2 + A23/T2(i)^4) + rho2(n)^4*(A24/T2(i)^2
+ A25/T2(i)^3) + rho2(n)^6*(A26/T2(i)^2 + A27/T2(i)^4) + rho2(n)^8*(A28/T2(i)^2 +
A29/T2(i)^3) + A20/T2(i)^2 + A21/T2(i)^3 + rho2(n)^10*(A30/T2(i)^2 + A31/T2(i)^3 +
A32/T2(i)^4))/exp(GAMMA*rho2(n)^2);
%----Newton Raphson to obtain rho-----%
rho1(n+1) = rho1(n) - f1(i)/fp1(i);

```

```

rho2(n+1) = rho2(n) - f2(i)/fp2(i);
error1 = abs(rho1(n+1) - rho1(n))/rho1(n+1);
error2 = abs(rho2(n+1) - rho2(n))/rho2(n+1);
error = error1 + error2;
%----Values of molar density that satisfy MBWR given P & T-----%
rhoa1(i) = rho1(n);
rhoa2(i) = rho2(n);
%---Number of Moles Present in each chamber-----%
n1(i) = rhoa1(i)*V1;
n2(i) = rhoa2(i)*V2;
n = n+1;
end
n=1;
error = 1;
end
%-----Part 1 of Run 1-----%
for(i=1:s1)
%----Average Initial and Final moles in supply chamber-----%
n1ini = sum(n1(1:ini))/ini;
n1fin = sum(n1((s1-fin):s1))/fin;
%----Average Initial and Final moles in sample chamber-----%
n2ini = sum(n2(1:ini))/ini;
n2fin = sum(n2((s1-fin):s1))/fin;
%----moles in 2 based on conditions in 1-----%
n2t(i) = n1ini + n2ini - n1(i);
%----moles desorbed-----%
ndes(i) = ndesi + n1ini + n2ini - n1(i)-n2(i) + SCL;
Vdes(i) = (ndes(i)*R*293/101000)*1000000;
Mdes(i) = ndes(i)*16.04;
%----Normalized Plotting Variables-----%
ndesg(i) = ndes(i)/Msam;
Vdesg(i) = Vdes(i)/Msam;
Mdesg(i) = Mdes(i)/Msam;
ndesv(i) = ndes(i)/(Vs*1000000);
Vdesv(i) = Vdes(i)/(Vs*1000000);
Mdesv(i) = Mdes(i)/(Vs*1000000);
end
end

```

7.3.3 - Effective Storage Discharge Function

```

function [n1, n2, ndes, Vdes, Mdes, ndesg, Vdesg, Mdesg, ndesv, Vdesv, Mdesv, n2t] =
MBWR_DES_FCN_EFF(P1 ,T1 ,P2 ,T2, V1, V2, Vs, Vp, Msam, ndesi, SCL)

```

```

%---This function calculates effective storage discharge values using -%
%---the MBWR equation of state for methane gas------%
%---MBWR equation constants------%
A1 = 8.98183102418E-5;
A2 = 1.88570883291E-2;
A3 = -5.07334853102E-1;
A4 = 2.42440372451E1;
A5 = -2.75937243281E3;
A6 = 6.67706377937E-9;
A7 = 6.59554690590E-6;
A8 = -4.75099859428E-3;
A9 = 9.41749168525E-1;
A10 = 2.03123055432E-13;
A11 = -8.82991375776E-11;
A12 = 2.69841136359E-7;
A13 = 1.63105161849E-14;
A14 = -9.65840913441E-16;
A15 = -4.97527927565E-14;
A16 = 3.88068765783E-20;
A17 = -4.47156684621E-25;
A18 = 2.80554989023E-23;
A19 = -4.96671746902E-29;
A20 = 4.27414662506E-1;
A21 = -1.25241753250E2;
A22 = -1.02133310576E-8;
A23 = 7.88608202448E-5;
A24 = -3.74931459167E-18;
A25 = 1.27111849576E-15;
A26 = -2.3634400069E-25;
A27 = -1.23455321379E-21;
A28 = 2.04715659218E-34;
A29 = 4.06242840085E-32;
A30 = -8.73417429883E-43;
A31 = -3.81661132665E-41;
A32 = 5.32641296927E-40;
GAMMA = 9.70E-9;
%---Ideal Gas Constant------%
R = 8.3144;
%---Use an avering process to smooth out sensor data------%
for(i=1:10)
    T2 = smooth(T2);
    T1 = smooth(T1);
    P2 = smooth(P2);
    P1 = smooth(P1);

```

```

end
s1=length(T1);
%----Number of Initial data points-----%
ini = 25;
%----Number of final Data Points-----%
fin = 25;
error = 1;
n = 1;
h = 1;
for(i=1:s1)
    while(error >= 0.0000001)
%----Modified BWR-----%
        rho1(1) = 0;
        rho2(1) = 0;
%----MBWR Function-----%
        f1(i) = -P1(i) + rho1(n)*R*T1(i) + (rho1(n)^2)*(A1*T1(i) + A2*(T1(i)^0.5) + A3 + A4/T1(i) +
A5/(T1(i)^2)) + (rho1(n)^3)*(A6*T1(i) + A7 + A8/T1(i) + A9/(T1(i)^2)) +
(rho1(n)^4)*(A10*T1(i) + A11 + A12/T1(i)) + (rho1(n)^5)*A13 + (rho1(n)^6)*(A14/T1(i) +
A15/(T1(i)^2)) + (rho1(n)^7)*A16/T1(i) + (rho1(n)^8)*(A17/T1(i) + A18/(T1(i)^2)) +
(rho1(n)^9)*A19/(T1(i)^2) + (rho1(n)^3)*exp(-GAMMA*(rho1(n)^2))*(A20/(T1(i)^2) +
A21/(T1(i)^3) + (rho1(n)^2)*(A22/(T1(i)^2) + A23/(T1(i)^4)) +
(rho1(n)^4)*(A24/(T1(i)^2) + A25/(T1(i)^3)) + (rho1(n)^6)*(A26/(T1(i)^2) +
A27/(T1(i)^4) + (rho1(n)^8)*(A28/(T1(i)^2) + A29/(T1(i)^3)) +
(rho1(n)^10)*(A30/(T1(i)^2) + A31/(T1(i)^3) + A32/(T1(i)^4));
        f2(i) = -P2(i) + rho2(n)*R*T2(i) + (rho2(n)^2)*(A1*T2(i) + A2*(T2(i)^0.5) + A3 + A4/T2(i) +
A5/(T2(i)^2)) + (rho2(n)^3)*(A6*T2(i) + A7 + A8/T2(i) + A9/(T2(i)^2)) +
(rho2(n)^4)*(A10*T2(i) + A11 + A12/T2(i)) + (rho2(n)^5)*A13 + (rho2(n)^6)*(A14/T2(i) +
A15/(T2(i)^2)) + (rho2(n)^7)*A16/T2(i) + (rho2(n)^8)*(A17/T2(i) + A18/(T2(i)^2)) +
(rho2(n)^9)*A19/(T2(i)^2) + (rho2(n)^3)*exp(-GAMMA*(rho2(n)^2))*(A20/(T2(i)^2) +
A21/(T2(i)^3) + (rho2(n)^2)*(A22/(T2(i)^2) + A23/(T2(i)^4)) +
(rho2(n)^4)*(A24/(T2(i)^2) + A25/(T2(i)^3)) + (rho2(n)^6)*(A26/(T2(i)^2) +
A27/(T2(i)^4) + (rho2(n)^8)*(A28/(T2(i)^2) + A29/(T2(i)^3)) +
(rho2(n)^10)*(A30/(T2(i)^2) + A31/(T2(i)^3) + A32/(T2(i)^4));
%----MBWR Function derivative-----%
        fp1(i) = R*T1(i) + 4*rho1(n)^3*(A11 + A12/T1(i) + A10*T1(i)) + 6*rho1(n)^5*(A14/T1(i) +
A15/T1(i)^2) + 8*rho1(n)^7*(A17/T1(i) + A18/T1(i)^2) + 2*rho1(n)^9*(A3 + A2*T1(i)^(1/2)
+ A4/T1(i) + A5/T1(i)^2 + A1*T1(i)) + 3*rho1(n)^2*(A7 + A8/T1(i) + A9/T1(i)^2 + A6*T1(i))
+ 5*A13*rho1(n)^4 + (7*A16*rho1(n)^6)/T1(i) + (9*A19*rho1(n)^8)/T1(i)^2 +
(rho1(n)^3*(4*rho1(n)^3*(A24/T1(i)^2 + A25/T1(i)^3) + 6*rho1(n)^5*(A26/T1(i)^2 +
A27/T1(i)^4) + 8*rho1(n)^7*(A28/T1(i)^2 + A29/T1(i)^3) + 10*rho1(n)^9*(A30/T1(i)^2 +
A31/T1(i)^3 + A32/T1(i)^4) + 2*rho1(n)^2*(A22/T1(i)^2 +
A23/T1(i)^4))/exp(GAMMA*rho1(n)^2) + (3*rho1(n)^2*(rho1(n)^2*(A22/T1(i)^2 +
A23/T1(i)^4) + rho1(n)^4*(A24/T1(i)^2 + A25/T1(i)^3) + rho1(n)^6*(A26/T1(i)^2 +
A27/T1(i)^4) + rho1(n)^8*(A28/T1(i)^2 + A29/T1(i)^3) + A20/T1(i)^2 + A21/T1(i)^3 +

```

```
rho1(n)^10*(A30/T1(i)^2 + A31/T1(i)^3 + A32/T1(i)^4))/exp(GAMMA*rho1(n)^2) -
(2*GAMMA*rho1(n)^4*(rho1(n)^2*(A22/T1(i)^2 + A23/T1(i)^4) + rho1(n)^4*(A24/T1(i)^2
+ A25/T1(i)^3) + rho1(n)^6*(A26/T1(i)^2 + A27/T1(i)^4) + rho1(n)^8*(A28/T1(i)^2 +
A29/T1(i)^3) + A20/T1(i)^2 + A21/T1(i)^3 + rho1(n)^10*(A30/T1(i)^2 + A31/T1(i)^3 +
A32/T1(i)^4))/exp(GAMMA*rho1(n)^2);
```

```
fp2(i) = R*T2(i) + 4*rho2(n)^3*(A11 + A12/T2(i) + A10*T2(i)) + 6*rho2(n)^5*(A14/T2(i) +
A15/T2(i)^2) + 8*rho2(n)^7*(A17/T2(i) + A18/T2(i)^2) + 2*rho2(n)*(A3 + A2*T2(i)^(1/2)
+ A4/T2(i) + A5/T2(i)^2 + A1*T2(i)) + 3*rho2(n)^2*(A7 + A8/T2(i) + A9/T2(i)^2 + A6*T2(i))
+ 5*A13*rho2(n)^4 + (7*A16*rho2(n)^6)/T2(i) + (9*A19*rho2(n)^8)/T2(i)^2 +
(rho2(n)^3*(4*rho2(n)^3*(A24/T2(i)^2 + A25/T2(i)^3) + 6*rho2(n)^5*(A26/T2(i)^2 +
A27/T2(i)^4) + 8*rho2(n)^7*(A28/T2(i)^2 + A29/T2(i)^3) + 10*rho2(n)^9*(A30/T2(i)^2 +
A31/T2(i)^3 + A32/T2(i)^4) + 2*rho2(n)*(A22/T2(i)^2 +
A23/T2(i)^4))/exp(GAMMA*rho2(n)^2) + (3*rho2(n)^2*(rho2(n)^2*(A22/T2(i)^2 +
A23/T2(i)^4) + rho2(n)^4*(A24/T2(i)^2 + A25/T2(i)^3) + rho2(n)^6*(A26/T2(i)^2 +
A27/T2(i)^4) + rho2(n)^8*(A28/T2(i)^2 + A29/T2(i)^3) + A20/T2(i)^2 + A21/T2(i)^3 +
rho2(n)^10*(A30/T2(i)^2 + A31/T2(i)^3 + A32/T2(i)^4))/exp(GAMMA*rho2(n)^2) -
(2*GAMMA*rho2(n)^4*(rho2(n)^2*(A22/T2(i)^2 + A23/T2(i)^4) + rho2(n)^4*(A24/T2(i)^2
+ A25/T2(i)^3) + rho2(n)^6*(A26/T2(i)^2 + A27/T2(i)^4) + rho2(n)^8*(A28/T2(i)^2 +
A29/T2(i)^3) + A20/T2(i)^2 + A21/T2(i)^3 + rho2(n)^10*(A30/T2(i)^2 + A31/T2(i)^3 +
A32/T2(i)^4))/exp(GAMMA*rho2(n)^2);
```

```
%----Newton Raphson to obtain rho-----%
```

```
rho1(n+1) = rho1(n) - f1(i)/fp1(i);
rho2(n+1) = rho2(n) - f2(i)/fp2(i);
error1 = abs(rho1(n+1) - rho1(n))/rho1(n+1);
error2 = abs(rho2(n+1) - rho2(n))/rho2(n+1);
error = error1 + error2;
```

```
%----Values of molar density that satisfy MBWR given P & T-----%
```

```
rhoa1(i) = rho1(n);
rhoa2(i) = rho2(n);
```

```
%---Number of Moles Present in each chamber-----%
```

```
n1(i) = rhoa1(i)*V1;
n2(i) = rhoa2(i)*V2;
n = n+1;
```

```
end
n=1;
error = 1;
```

```
end
```

```
%-----Part 1 of Run 1-----%
```

```
for(i=1:s1)
```

```
%----Average Initial and Final moles in supply chamber-----%
```

```
n1ini = sum(n1(1:ini))/ini;
n1fin = sum(n1((s1-fin):s1))/fin;
```

```
%----Average Initial and Final moles in sample chamber-----%
```

```
n2ini = sum(n2(1:ini))/ini;
```

```
n2fin = sum(n2((s1-fin):s1))/fin;
%----moles in 2 based on conditions in 1-----%
n2t(i) = n1ini + n2ini - n1(i);
%----moles desorbed-----%
ndes(i) = ndesi + n1ini + n2ini - n1(i)-n2(i) + SCL;
Vdes(i) = (ndes(i)*R*293/101000)*1000000;
Mdes(i) = ndes(i)*16.04;
%----Normalized Plotting Variables-----%
ndesg(i) = ndes(i)/Msam;
Vdesg(i) = Vdes(i)/Msam;
Mdesg(i) = Mdes(i)/Msam;
ndesv(i) = ndes(i)/(Vp*1000000);
Vdesv(i) = Vdes(i)/(Vp*1000000);
Mdesv(i) = Mdes(i)/(Vp*1000000);
end
end
```

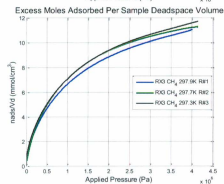
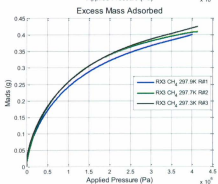
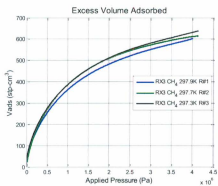
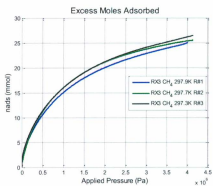
- 8 - Appendix A2

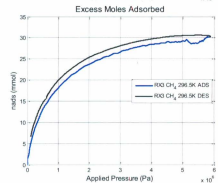
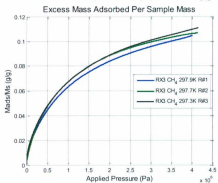
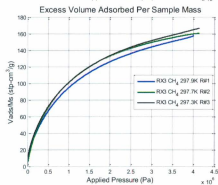
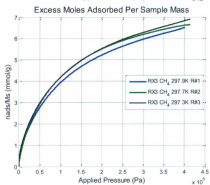
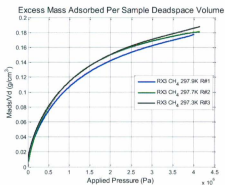
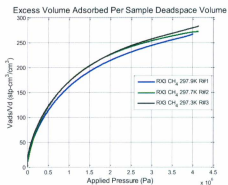
8.1 - Adsorption Plots

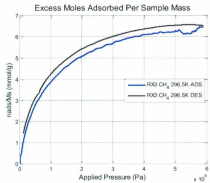
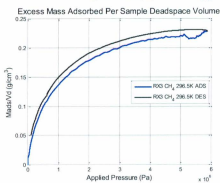
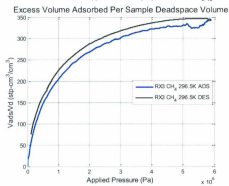
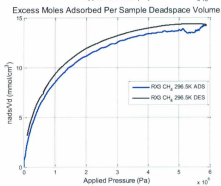
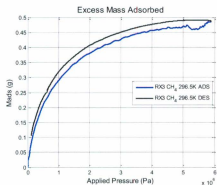
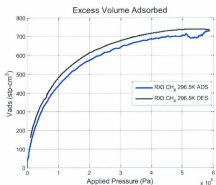
The adsorption isotherms for all of the materials tested are presented below for each of the evaluation unit parameters previously discussed.

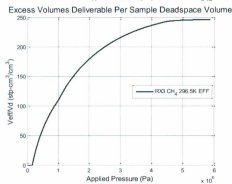
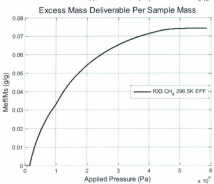
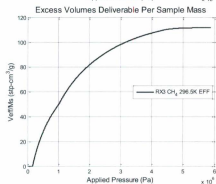
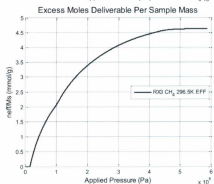
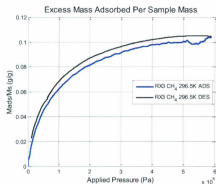
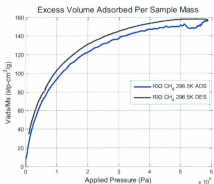
8.1.1 - RX3

8.1.1.1 - Excess Adsorption

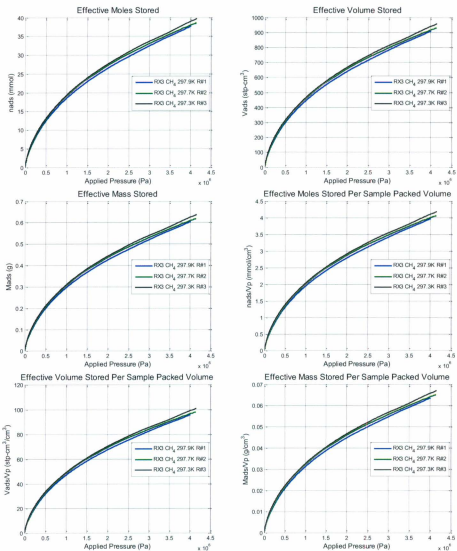


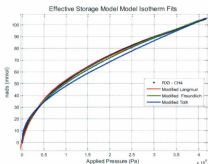
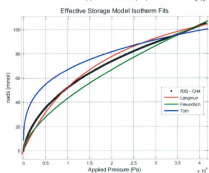
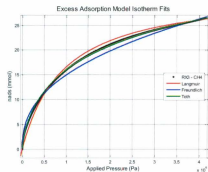
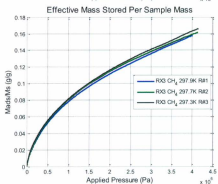
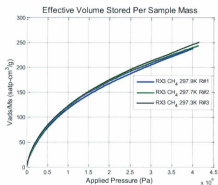
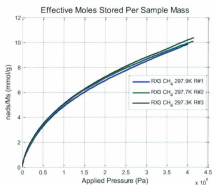


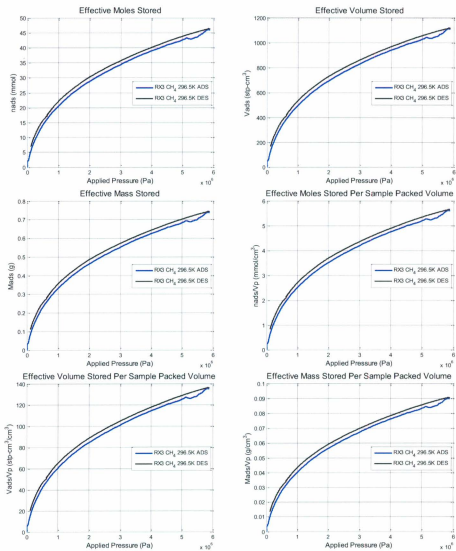


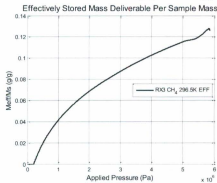
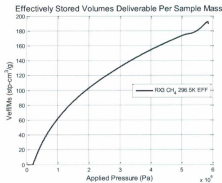
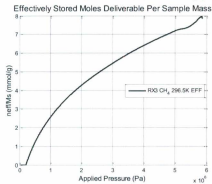
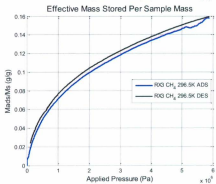
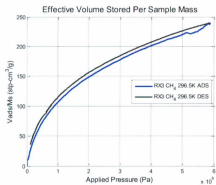
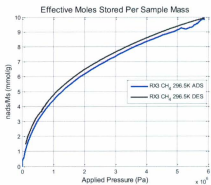


8.1.1.2 - Effective Storage

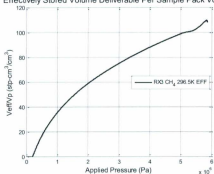






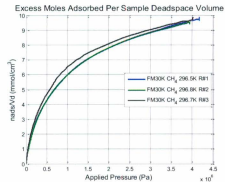
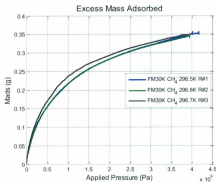
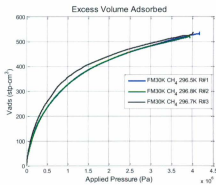
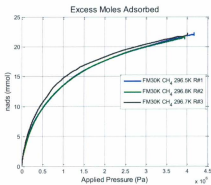


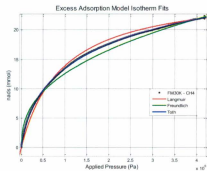
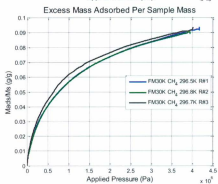
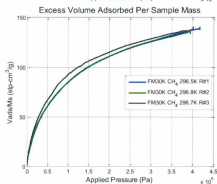
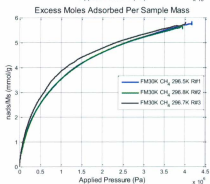
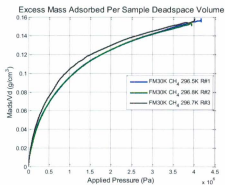
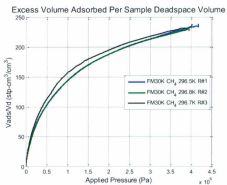
Effectively Stored Volume Deliverable Per Sample Pack Volume

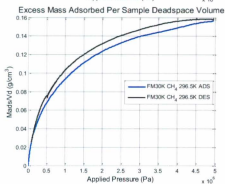
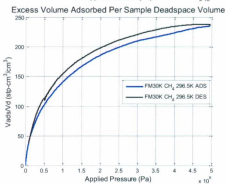
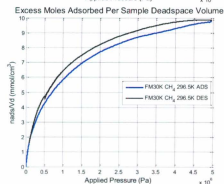
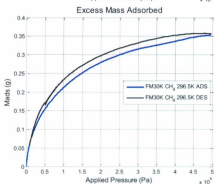
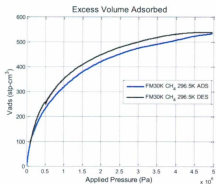
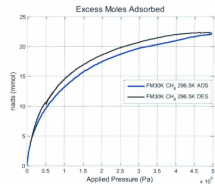


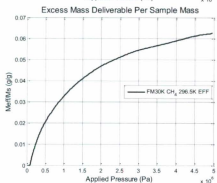
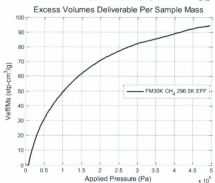
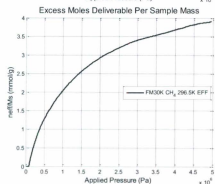
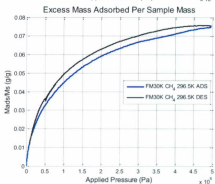
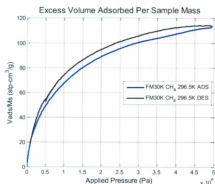
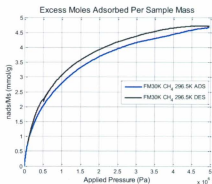
8.1.2 - FM30K

8.1.2.1 - Excess Adsorption

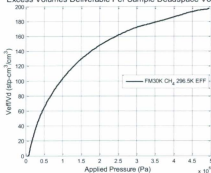




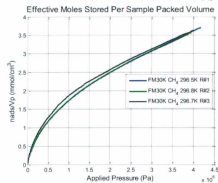
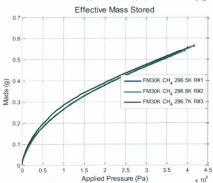
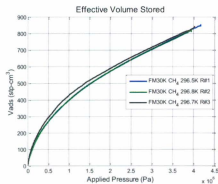
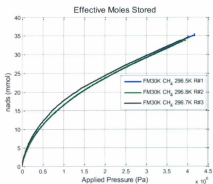


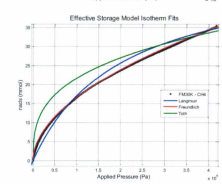
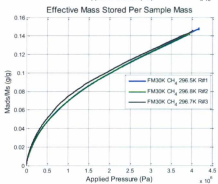
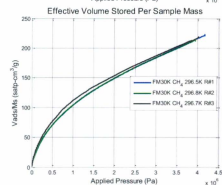
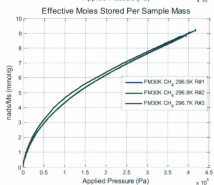
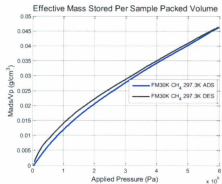
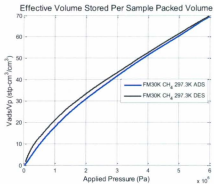


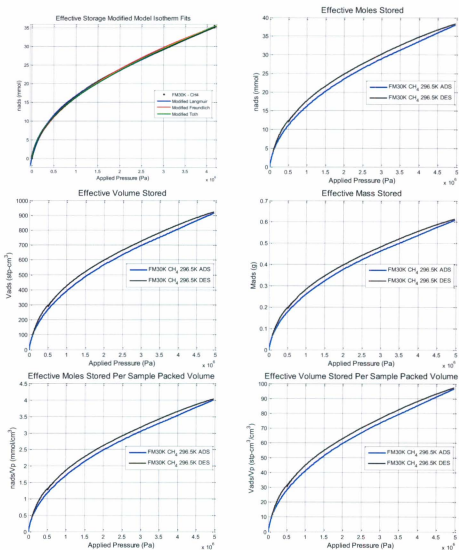
Excess Volumes Deliverable Per Sample Deadspace Volume

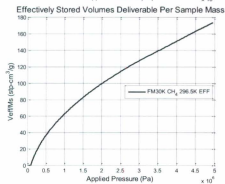
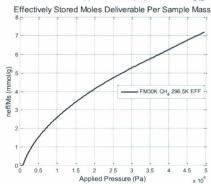
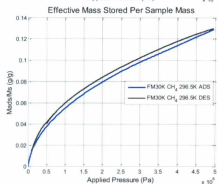
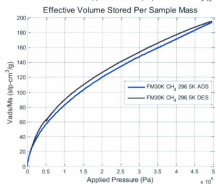
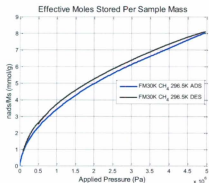
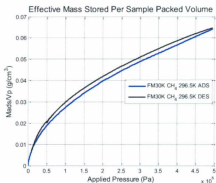


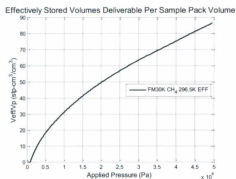
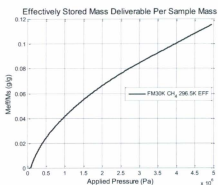
8.1.2.2 - Effective Storage





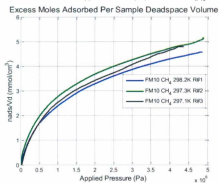
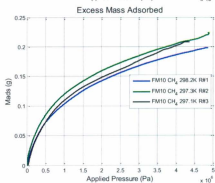
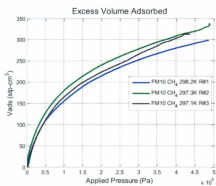
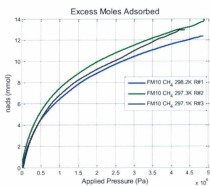


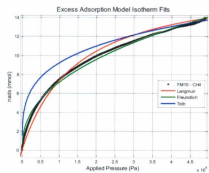
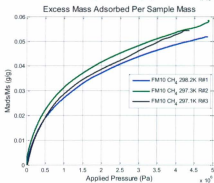
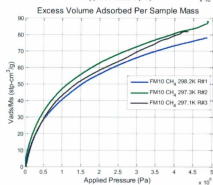
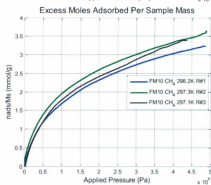
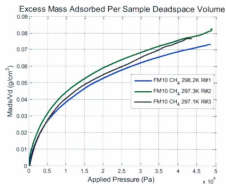
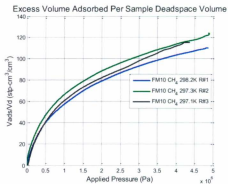


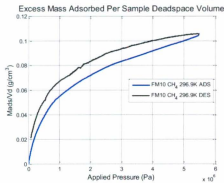
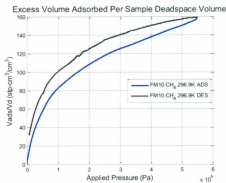
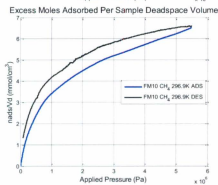
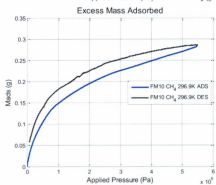
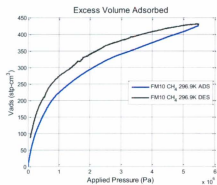
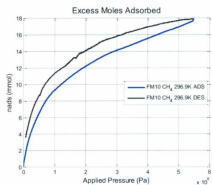


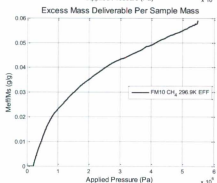
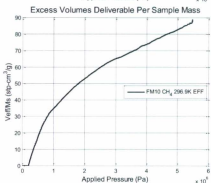
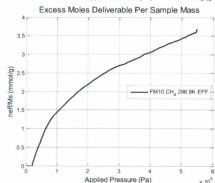
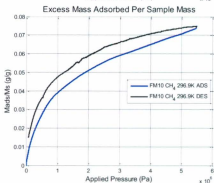
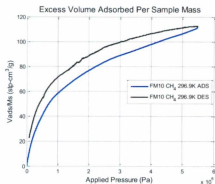
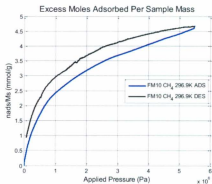
8.1.3 - FM10

8.1.3.1 - Excess Adsorption

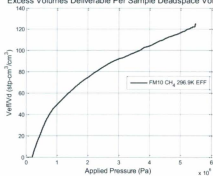




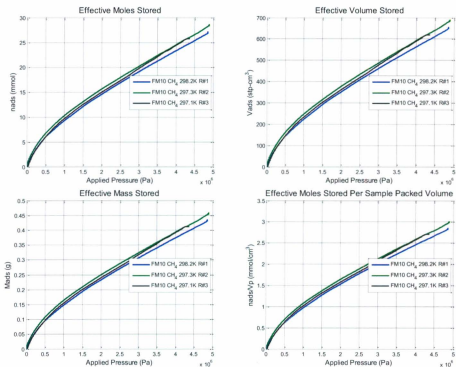


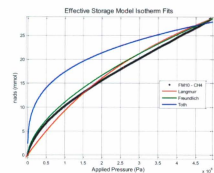
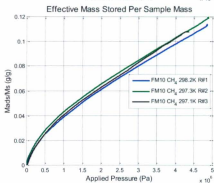
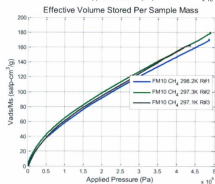
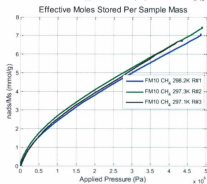
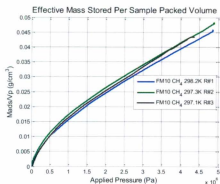
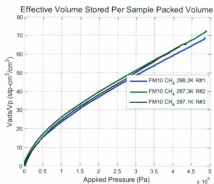


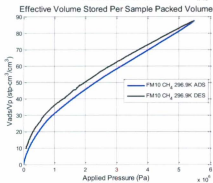
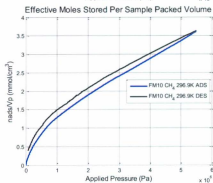
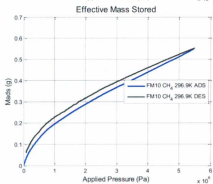
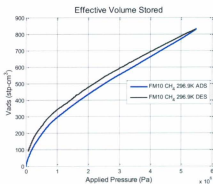
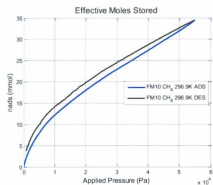
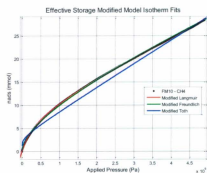
Excess Volumes Deliverable Per Sample Deadspace Volume

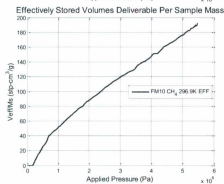
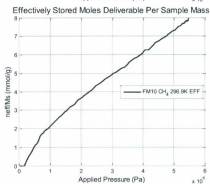
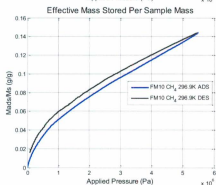
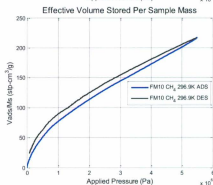
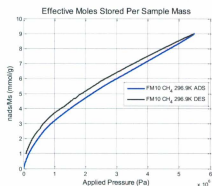
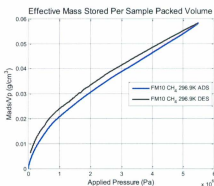


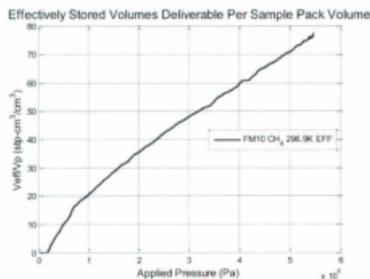
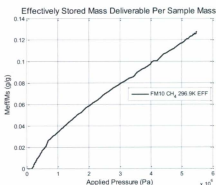
8.1.3.2 - Effective Storage





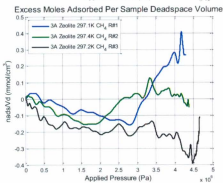
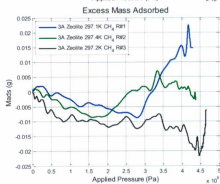
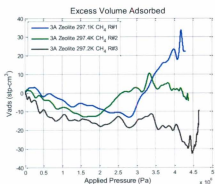
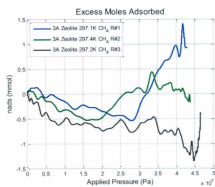


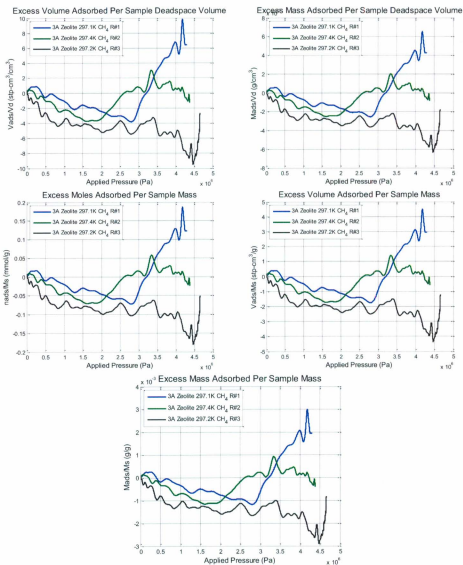


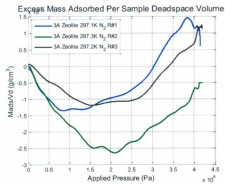
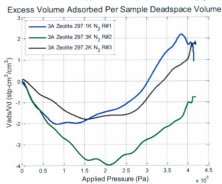
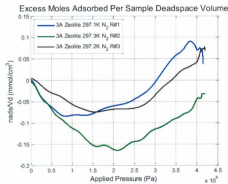
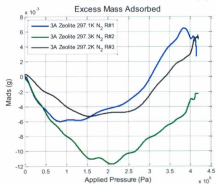
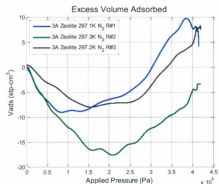
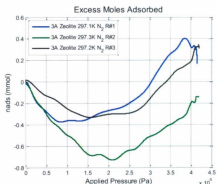


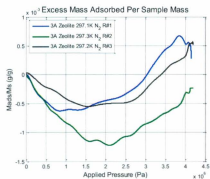
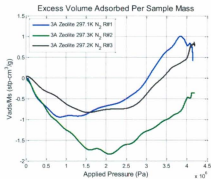
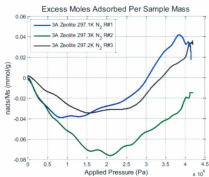
8.1.4 - 3A Zeolite

8.1.4.1 - Excess Adsorption

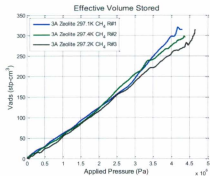
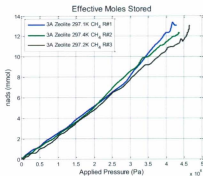


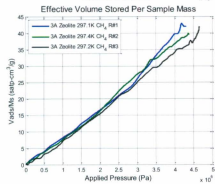
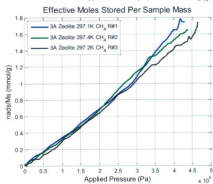
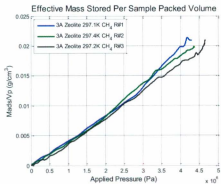
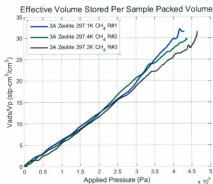
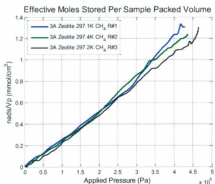
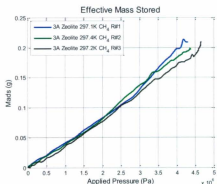
8.1.4.1.1 - Adsorption (N₂)

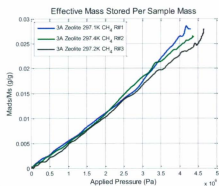
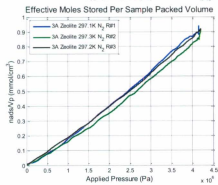
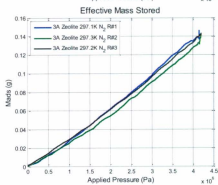
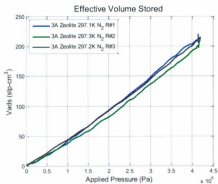
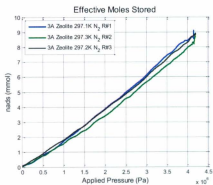


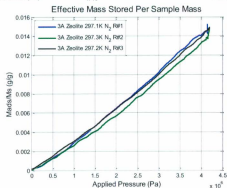
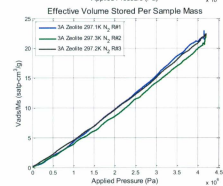
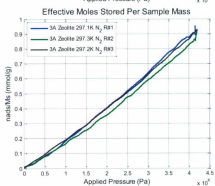
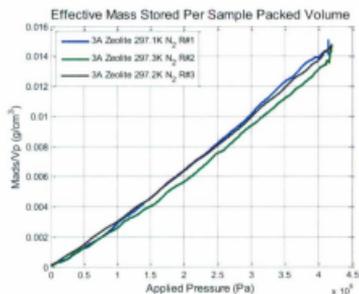
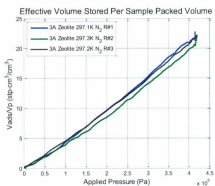


8.1.4.2 - Effective Storage



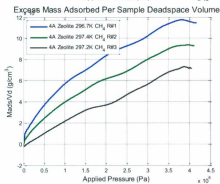
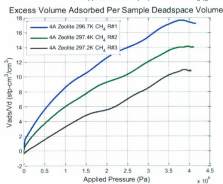
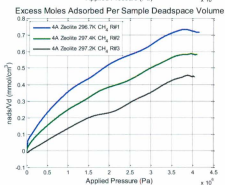
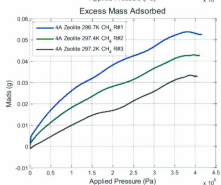
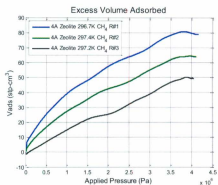
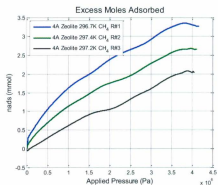


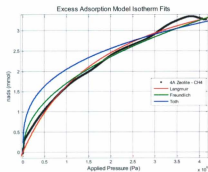
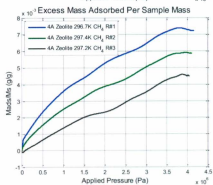
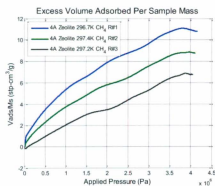
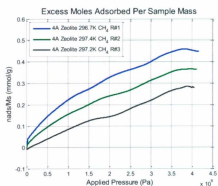
8.1.4.2.1 - Adsorption (N₂)



8.1.5 - 4A Zeolite

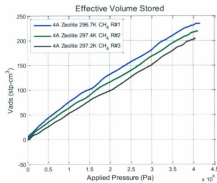
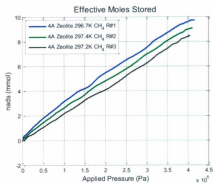
8.1.5.1 - Excess Adsorption

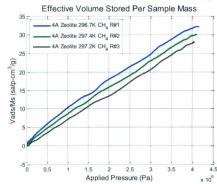
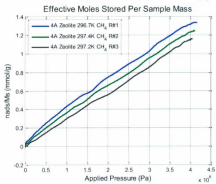
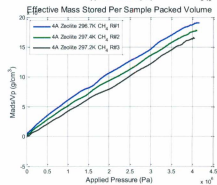
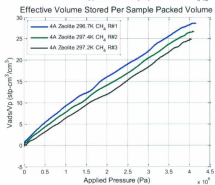
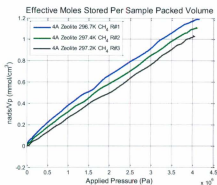
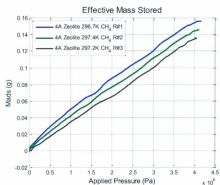


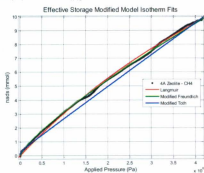
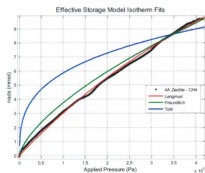
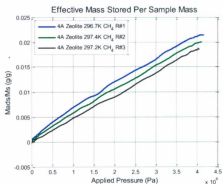


8.1.5.2 - Effective Storage

8.1.5.2.1 - Adsorption

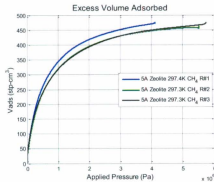
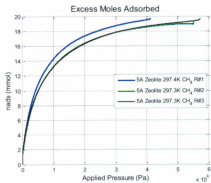


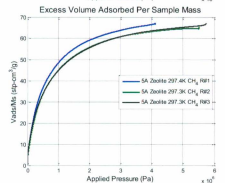
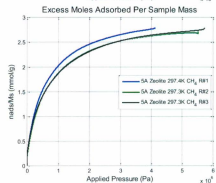
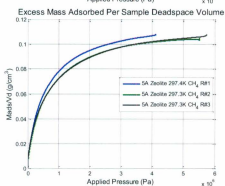
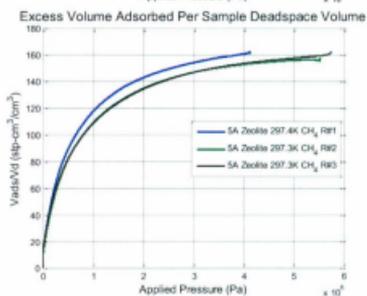
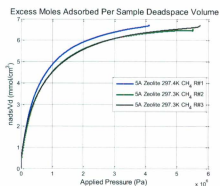
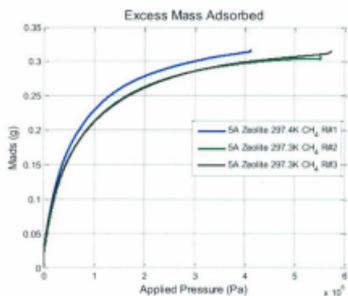


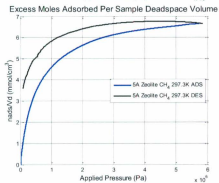
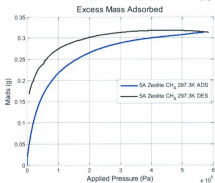
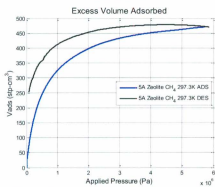
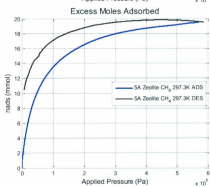
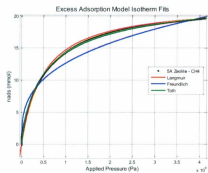
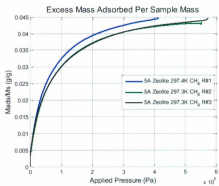


8.1.6 - 5A Zeolite

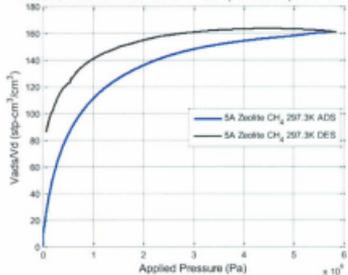
8.1.6.1 - Excess Adsorption



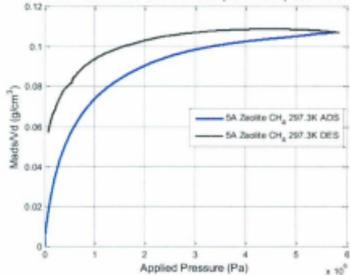




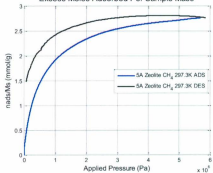
Excess Volume Adsorbed Per Sample Deadspace Volume



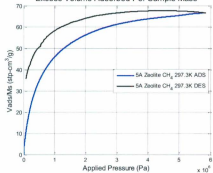
Excess Mass Adsorbed Per Sample Deadspace Volume



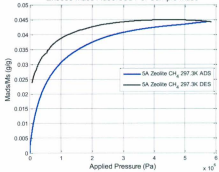
Excess Moles Adsorbed Per Sample Mass



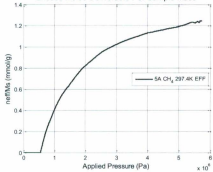
Excess Volume Adsorbed Per Sample Mass

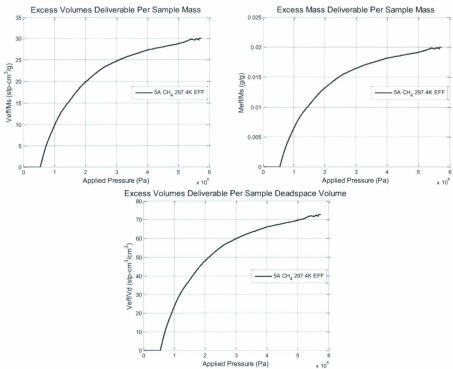


Excess Mass Adsorbed Per Sample Mass

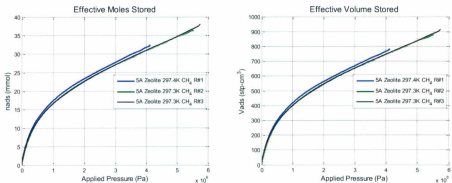


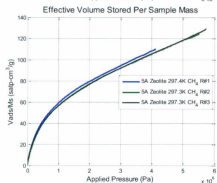
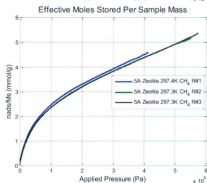
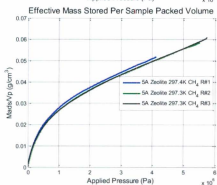
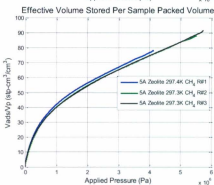
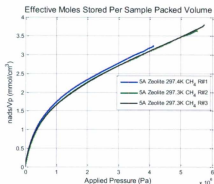
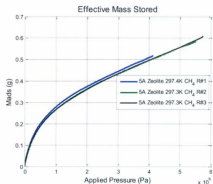
Excess Moles Deliverable Per Sample Mass

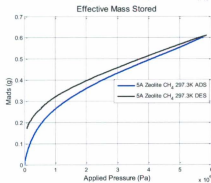
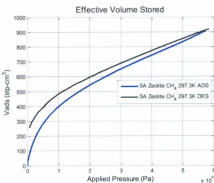
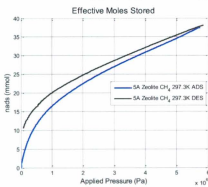
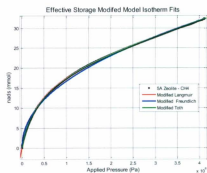
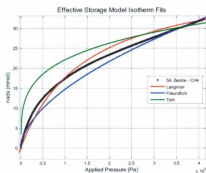
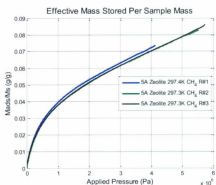


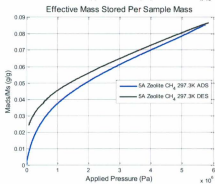
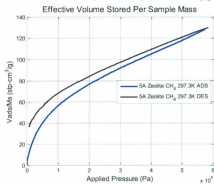
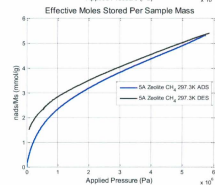
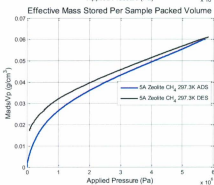
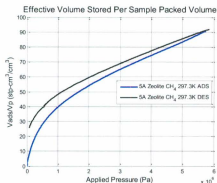
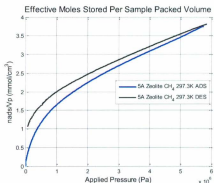


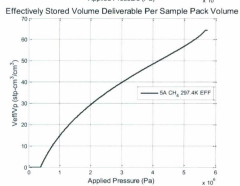
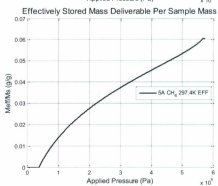
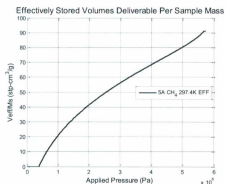
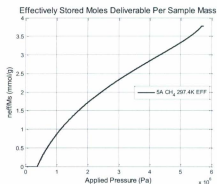
8.1.6.2 - Effective Storage





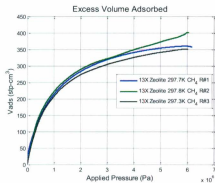
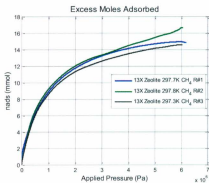


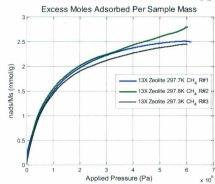
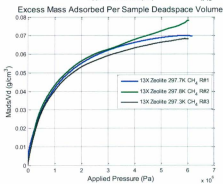
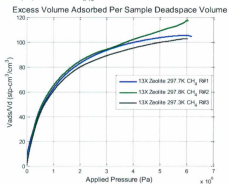
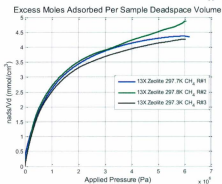
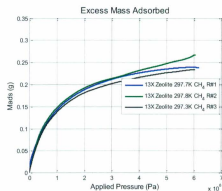


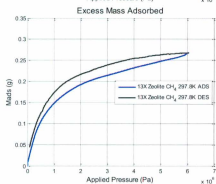
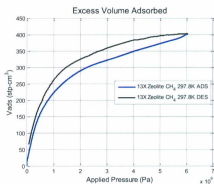
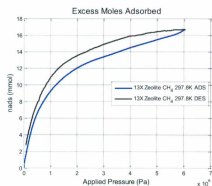
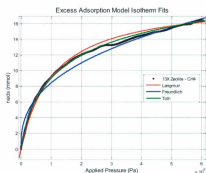
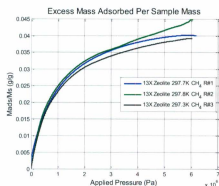
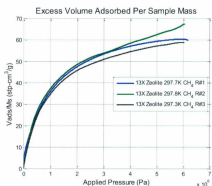


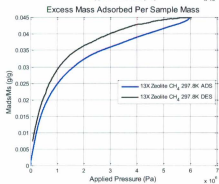
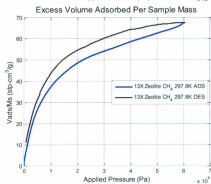
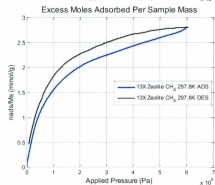
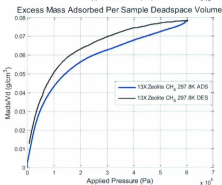
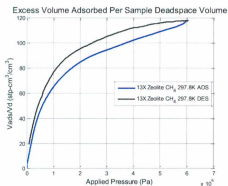
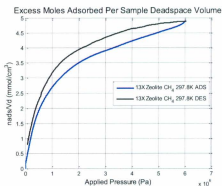
8.1.7 - 13X Zeolite

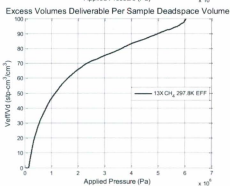
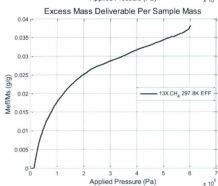
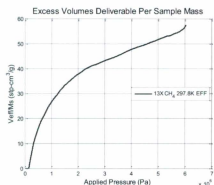
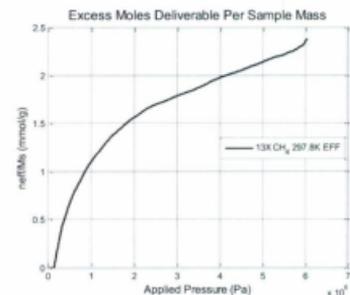
8.1.7.1 - Excess Adsorption



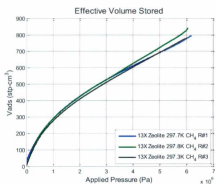
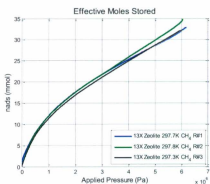


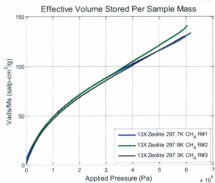
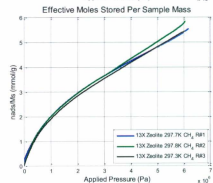
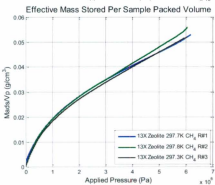
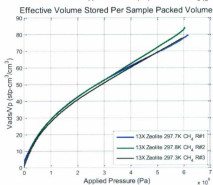
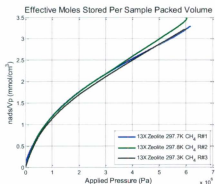
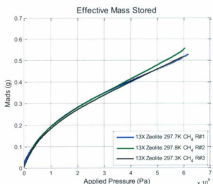


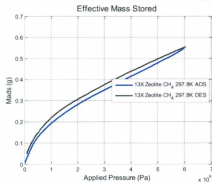
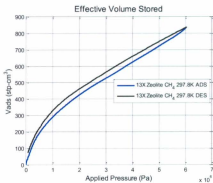
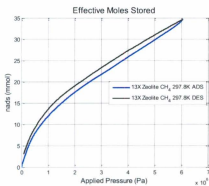
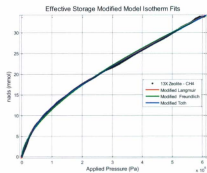
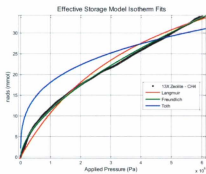
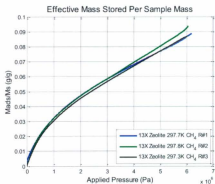


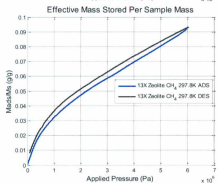
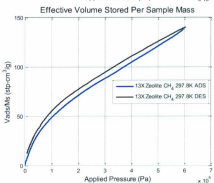
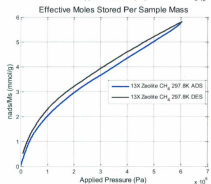
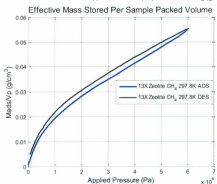
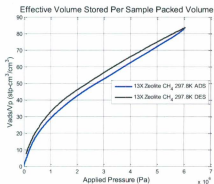
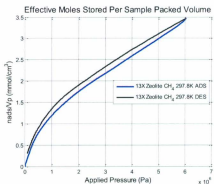


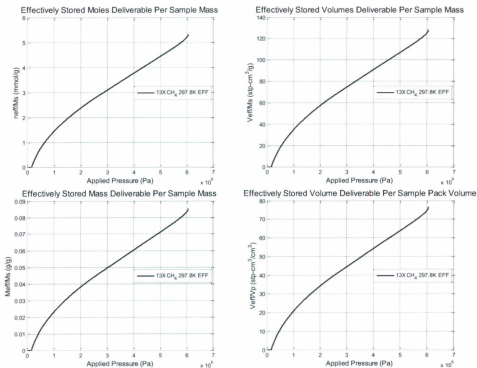
8.1.7.2 - Effective Storage





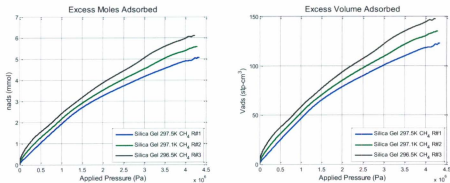


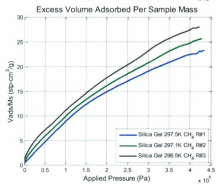
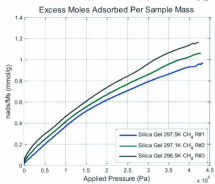
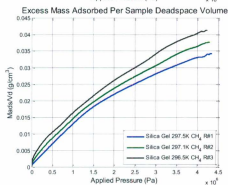
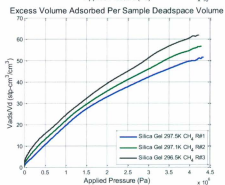
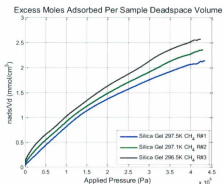
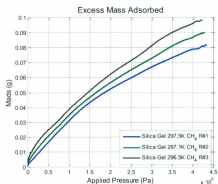


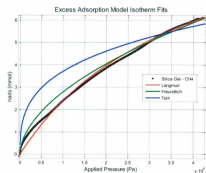
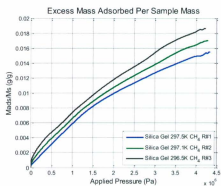


8.1.8 - Silica Gel

8.1.8.1 - Excess Adsorption

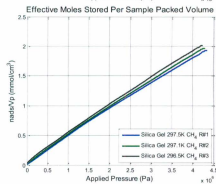
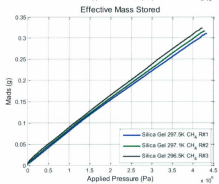
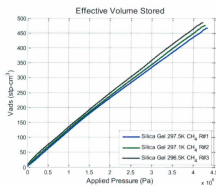
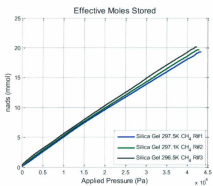


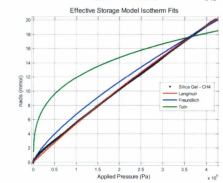
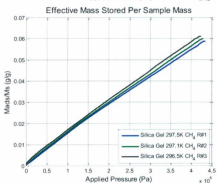
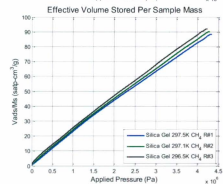
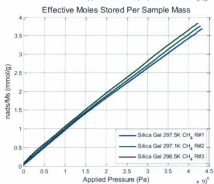
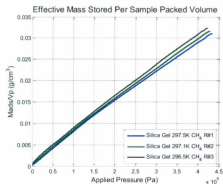
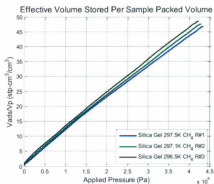


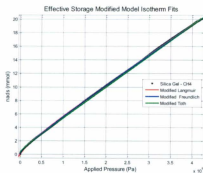


8.1.8.2 - Effective Storage

8.1.8.2.1 - Adsorption



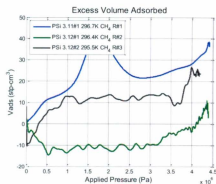
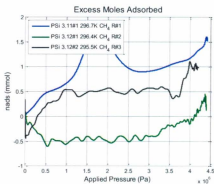


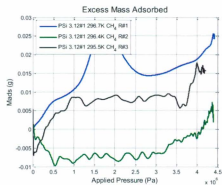


8.2 - Porous Silicon

8.2.1 - PSiEC_Mix

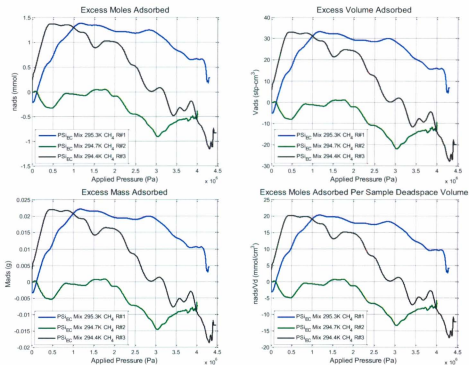
8.2.1.1 - Excess Adsorption

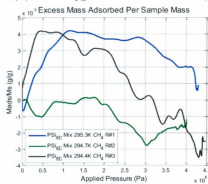
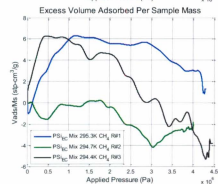
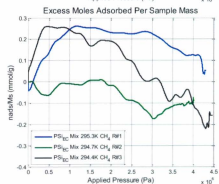
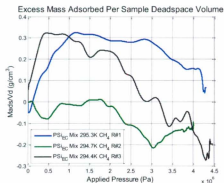
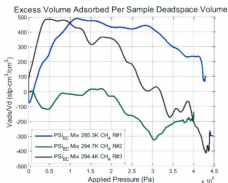




8.2.2 - PSIEC_Mix_2

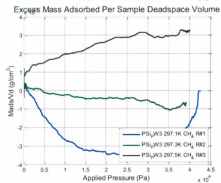
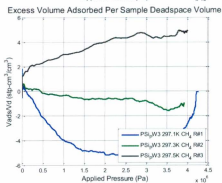
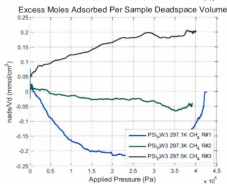
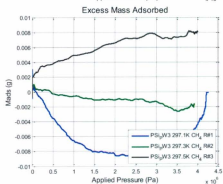
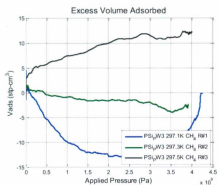
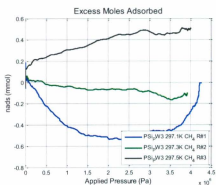
8.2.2.1 - Excess Adsorption

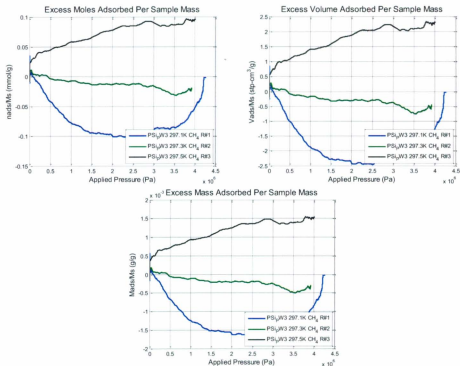




8.2.3 - PSiPW_3

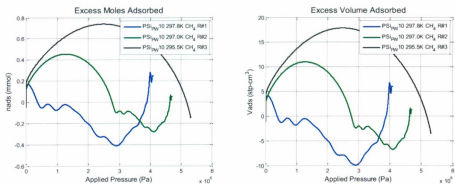
8.2.3.1 - Excess Adsorption

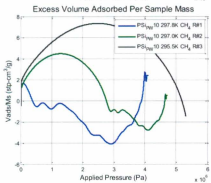
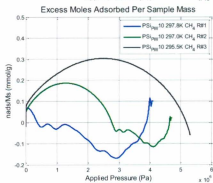
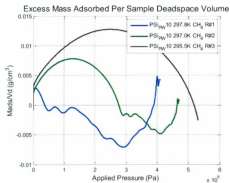
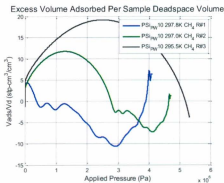
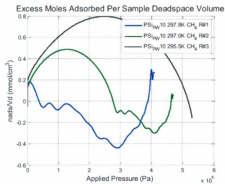
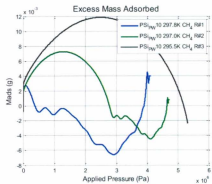


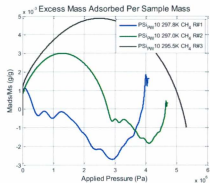


8.2.4 - PSiPW₁₀

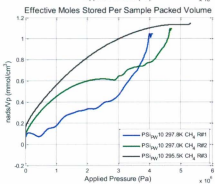
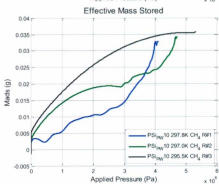
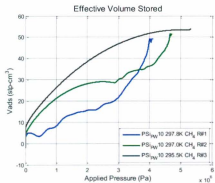
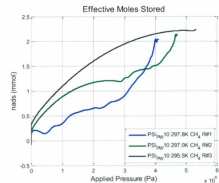
8.2.4.1 - Excess Adsorption

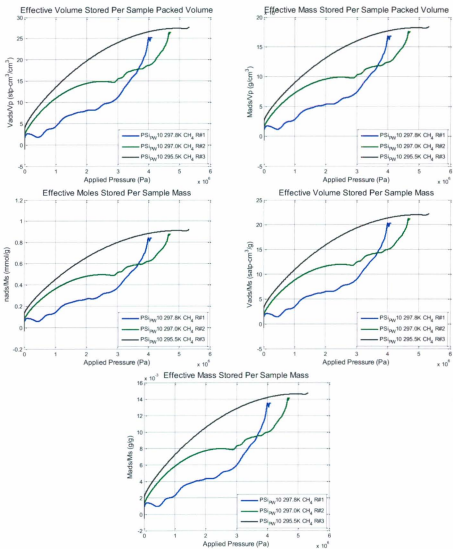






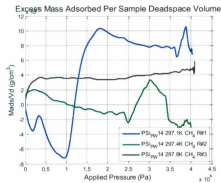
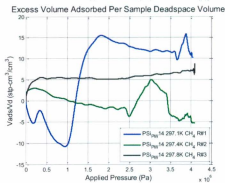
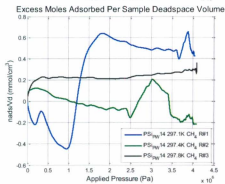
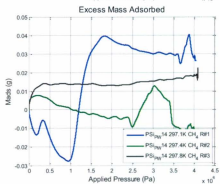
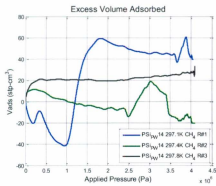
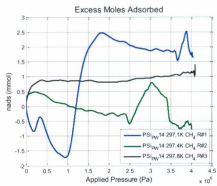
8.2.4.2 - Effective Storage

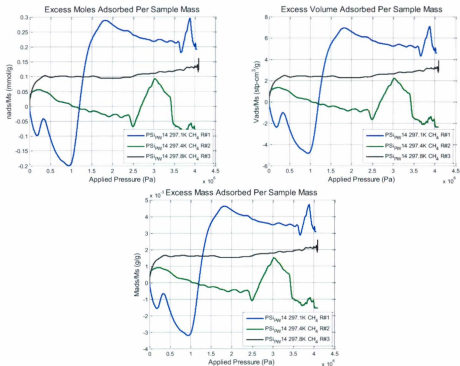




8.2.5 - PSiPW₁₄

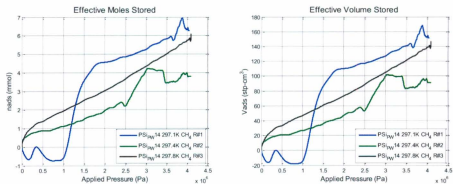
8.2.5.1 - Excess Adsorption

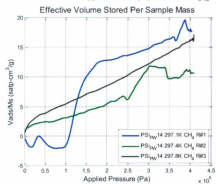
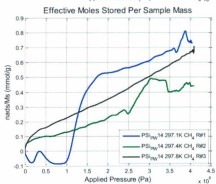
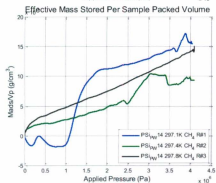
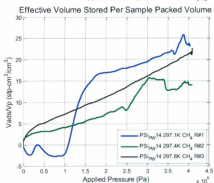
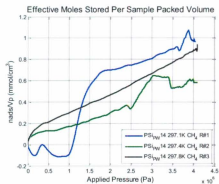
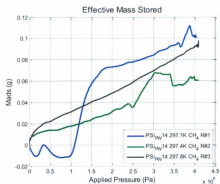


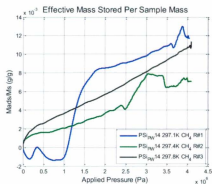


8.2.5.2 - Effective Storage

8.2.5.2.1 - Adsorption

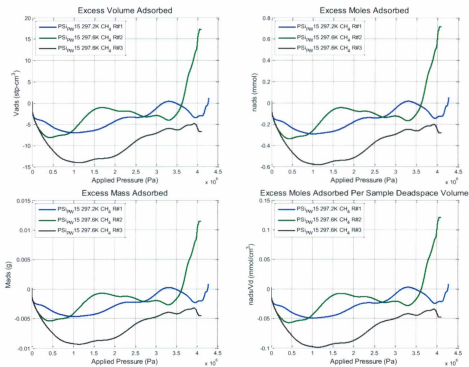


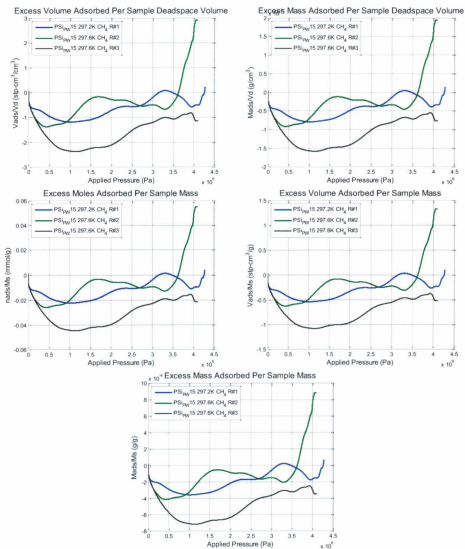




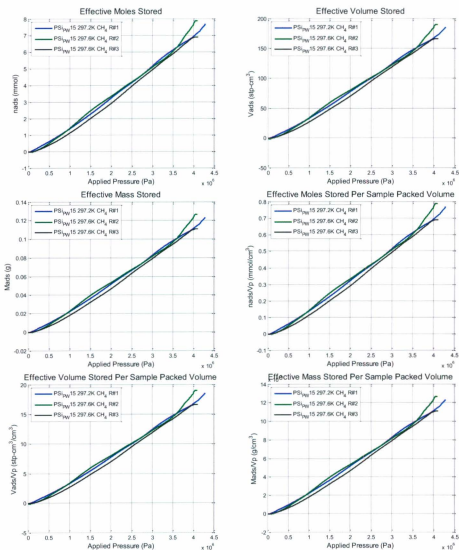
8.2.6 - PSiW₁₅

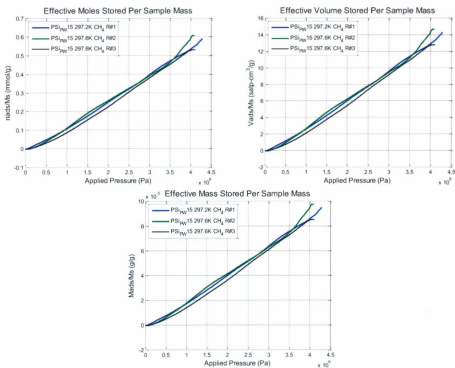
8.2.6.1 - Excess Adsorption





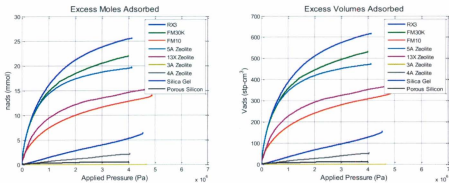
8.2.6.2 - Effective Storage

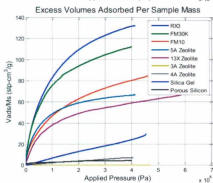
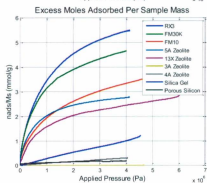
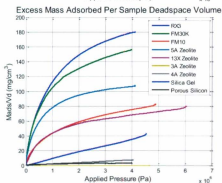
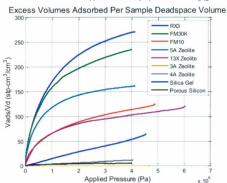
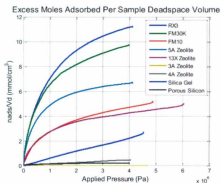
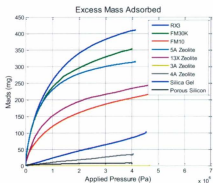


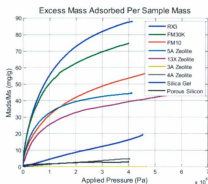


8.2.7 - Adsorption Isotherms

8.2.7.1 - Excess Adsorption







8.2.7.2 - Effective Storage

